NASA Conference Publication 2355

Landsat-4 Science Characterization Early Results

Volume I—Multispectral Scanner (MSS)

John L. Barker, *Editor*
NASA Goddard Space Flight Center
Greenbelt, Maryland

Proceedings of the Landsat-4 Science Characterization
Early Results Symposium, February 22–24, 1983
held at NASA Goddard Space Flight Center
Greenbelt, Maryland

National Aeronautics
and Space Administration

**Scientific and Technical
Information Branch**

1985

Foreword

One of the objectives and responsibilities of the Landsat-D Project at NASA's Goddard Space Flight Center (GSFC) was to characterize the performance of the imaging systems on Landsats-4 and -5. Additional objectives included assessment of the whole Landsat system, platform and ground processing, as evidenced in the resulting image data quality. In order to accomplish these objectives, staff scientists have enlisted the participation of nearly a hundred 'nternationally recognized members of the Landsat commercial, academic and governmental communities. These proceedings are part of their report.

The first public presentation of results from this group was at the Landsat-4 Scientific Characterization Early Results Symposium held 22-24 February, 1983 at NASA/GSFC under the sponsorship of the Landsat Project Scientists. It was attended by over four hundred investigators. The reports represented early results in the sense that many investigators had had access to Landsat-4 data for only a brief period following its launch on 16 July 1982. The symposium and resulting proceedings are an interim means of informing the Landsat user community of the direction in which these continuing investigations are moving, especially in terms of reporting initial assessments of the Thematic Mapper (TM) sensor which was orbited for the first time on Landsat-4.

Two summary volumes were derived in large part from this four volume set of proceedings. The summary volumes are entitled "Landsat-4 Science Investigations Summary, Including December 1983 Workshop Results" (NASA Conference Publication 2326). Since publication of the proceedings was delayed, the summary volumes include some results reached during post-symposium period up to and including the Investigators' Workshop of 6 December 1983.

Material within represents work-in-progress. In general, it dates from a period of up to a few months following the symposium. One exception is the relative radiometry (R&R) paper by John Barker, Landsat Associate Project Scientist, which was revised to include some initial results from Landsat-5, which was launched on 1 March 1984.

Several of the investigators have reported on their results elsewhere. The most complete documation to date is a volume entitled "Special Issue on Landsat-4", which appeared in IEEE Transactions on Geoscience and Remote Sensing in May, 1984 (Volume GE-22, ISSN 0196-2892). A final public presentation of the results of this scientific characterization of the system performance is currently planned for September, 1985, and will be co-ordinated by Brian Markham from GSFC.

The four volumes in these proceedings are arranged as follows:

Vol. I: Multispectral Scanner (MSS)

Vol. II and III: Thematic Mapper (TM)

Vol. IV: Applications

Each of these three sections is introduced by an overview prepared by the scientific staff: William Alford and Marc Inhoff for MSS, John Barker and Brian Markham for TM, and Darrel Williams for Applications. The few colored prints are reproduced here in black and white. The Table of Contents for all four volumes is repeated at the front of each volume.

Vincent V. Salomonson
Landsat Project Scientist

LANDSAT-4 SCIENCE CHARACTERIZATION EARLY RESULTS

CONTENTS

Volume I: MULTISPECTRAL SCANNER

CONTENTS (Continued)

CONTENTS (Continued)

CONTENTS (Continued)

CONTENTS (Continued)

Volume IV: APPLICATIONS

CONTENTS (Continued)

CONTENTS (Continued)

CONTENTS (Continued)

SUMMARY OF MSS CHARACTERIZATION INVESTIGATIONS

by

William L. Alford

Marc L. Imhoff

NASA's investigations to characterize the Landsat-4 Multispectral Scanner System data are nearing completion. Some of these results were presented at the Landsat-4 Scientific Characterization Early Results Symposium in February 1983 and at the Landsat-4 Workshop in December 1983. The reports in the volume - which describe most of the results presented at the February Symposium - are summarized in this paper.

The characterization results have been divided into two major categories: geometry and radiometry. These two categories have been divided into the nine subcategories plus a category called "Description of CCRS Processing" (See Table 1). This descriptive paper documents the geometric and radiometric processing performed at the Canada Centre for Remote Sensing (CCRS), and thus adds to the characterization of CCRS derived data. All other papers describe results from data processed through the NASA Multispectral Image Processing System (MIPS) and the EROS Data Center system.

GEOMETRIC CHARACTERIZATION

Geometric characterization spans many different aspects from spacecraft attitude performance to ground processing performance and the selection of geodetic control points. The studies summarized in this section, however, deal primarily with the geometric quality of the MSS data processed by the MSS Image Processing System (MIPS). All of these studies have examined P-format data which are rectified to conform to a true representation of the earth's surface defined by a cartographic projection. P-format MSS data are available in Universal Transverse Mercator (UTM), Polar Stereographic, and Space Oblique Mercator (SOM) projections. Regardless of projection, all P-format data fall into one of two categories: systematic and geodetic corrections. Systematic geometric corrections are based on spacecraft attitude and ephemeris data only. Geodetically corrected data, on the other hand, have been rectified to fit a set of geodetic control points, which are usually derived from 1:24,000 scale topographic maps.

During the early period of Landsat-4 data acquisition, the spacecraft attitude control system experienced some problems. Errors in the

initial star catalog and star progression software caused conflicting measurements between star trackers. This conflict caused attitude swings in the spacecraft which delayed fine tuning the systematic correction parameters in the MIPS. As a result, the MIPS generated data sets with systematic corrections that were not fully refined. These data sets were expected to contain larger than specified location errors. Since the development of the geodetic correction parameters build upon refined systematic corrections, few MSS data sets with geodetic corrections were available to investigators in a timely manner.

In general, the subject matter addressed in this section can be divided into 5 catagories: geodetic registration accuracy, systematic correction accuracy, temporal registration accuracy, band to band registration accuracy, and Landsat 4 to Landsats-2/3 registration accuracy. Table 1 defines the categories covered by each paper.

Systematic and Geodetic (Scene to Map) Registration Accuracy

Four investigations examined the accuracy of the systematic and geodetic corrections. Brooks et. al. (General Electric Space Division) and Imhoff and Alford (Goddard Space Flight Center) analyzed data processed with geodetic corrections. Both investigations examined the same data sets using different methods. Brooks et al. present results from their development of the systematic correction and ensuing geodetic correction algorithms which are currently used in the MIPS. Imhoff and Alford analyzed the data using independent ground verification points. Thormodsgard and DeVries, (USGS) and Welch and Usery (University of Georgia) investigated data processed through the MIPS that computed only the systematic corrections. Thormodsgard and DeVries tested the acuracy of systematically corrected MSS scenes (UTM Projection) and one geodetically corrected scene (SOM Projection) against a geodetic data base defined from 1:24,000 scale USGS topographic quadrangles. Welch and Usery examined two scenes (UTM projection) of northern Georgia and characterized the systematic correction accuracy and internal geometric integrity.

Brooks et al. used the online MIPS process and the Control Point Library Build (CPLB) process to provide the tools necessary for the verification, calibration, and evaluation of the Landsat-4 geometric correction process. A problem with the initial scan profile correction model was defined and corrected, and the MIPS system performance was evaluated for both temporal and geodetic registration. The geodetic registration performance was evaluated by correcting two MSS scenes: a November 2, 1982, scene and November 18, 1982, scene of Washington, DC. Both scenes were corrected using geodetic control points selected from the November 2 scene. With 20 control points used in the MAG correction and 32 control points designated in the CPLB, the November 2 scene had 90% errors of 0.35 IFOV cross track and 0.26 IFOV along track. Because of cloud cover, only 13 control points were used in the MAG to correct the November 18 scene with 14 control points designated in the CPLB. The 90% errors for the November 18 scene were 0.63 IFOV cross track and 0.43 IFOV along track. The system specifications was 0.5 IFOV or less 90% of the time, both cross and along track.

Imhoff and Alford made an independent examination of the geodetic accuracy of the data processed by the MIPS using the same Washington, D.C. scenes described above. Geodetic verification points (GVPs) were defined for the area using 7.5 minute topographic quadrangle maps. The digitized GVP map locations were compared to the image locations as defined by the MSS header record information. For this comparison, a zoom transfer scope was used which visually overlayed the map and the TV display of the image. Mean offsets for the line and sample directions were 0.06 and 0.08 pixels respectively. The combined RMS error for geodetic registration accuracy was 0.43 pixel (24.51 meters), well within specifications.

Thormodsgard and DeVries compared two systematically corrected MSS scenes and one partially geodetically corrected scene to a map control base. The latitude and longitude coordinates of 5 to 20 distinct features on 1:24,000-scale topographic maps were converted to line and sample coordinates using geodetic referencing algorithms. The line and sample coordinates of these features were located also in the image, and the pixel offsets from the calculated image locations were computed. Accuracy of the visual selection of the image features was estimated to be 1.5 pixels. The systematically corrected MSS scene over Los Angeles, California (UTM projection), had measured mean line and sample coordinates offset from the computed coordinates by 53.9 pixels and 19.9 pixels respectively. The second systematically corrected scene over Washington, D.C. (SOM projection), showed mean line and sample offsets of 14.1 pixels and 54.7 pixels respectively. The overall RMS error measurements for the two scenes were similar with RMS errors of 57.49 pixels for the Los Angeles scene and 56.97 pixels for the Washington, D.C. scene. A third systematically corrected scene (Central Alabama) with a partial geodetic correction yielded mean line and sample offsets of 4.2 pixels and 2.3 pixels respectively, and an RMS error of 5.73 pixels.

Welch and Usery examined two scenes (UTM projection) over northern Georgia in an effort to characterize the systematic correction accuracy and internal geometry. Using a series of first, second, and third degree polynomials for least squared fitting of image data to a geodetic base, RMS error values of approximately 80m were attained for a first degree polynomial and 57m for second or third degree polynomials. Subscene areas of 1024 X 1024 and 256 X 256 pixels were rectified with a first order polynomial to produce RMS error values of 40 to 45m.

Work to-date indicates the geometric quality of Landsat-4 MSS data is very good, reflecting the advantages of the improved pointing accuracy and attitude control of the platform. Rectification accuracies were found to be limited by the resolution of the MSS data, by map and digitizing errors, and by displacements due to terrain relief.

In general, the analyses of geodetically corrected image data show that the data appears to meet or nearly meet spectifications. It should be noted that no specifications for systematically corrected data exist at the time of this writing and that the nature of systematic corrections is such that it is almost wholly dependent upon accurate attitude and ephemeris data and attitude control. As such, it is expected that systematic-to-geodetic control offsets will exist. Systematic-to-geodetic offsets in the future, however, should become significantly smaller as improvements in the attitude and ephemeris control and measurement systems become available.

Temporal Registration Accuracy

Two investigations address temporal registration accuracy. Although these two investigations were independent in terms of their analytical procedures, they both utilized the same data sets.

Brooks et al. performed a temporal registration analysis on Washington, D.C. data sets. Control points selected from the Washington scene of November 2, 1982, were used in the correction of the Washington scene of November 18, 1982. The registration error was determined from the MAG control point residuals (a measure of random error) and a theoretical model bias between the model surface in the MAG and the CPLB. The 90% errors were computed to be 0.36 IFOV (Instantaneous Field Of View = 82.7 meters) cross track, and 0.29 IFOV along track.

Imhoff and Alford utilized a cross-correlation procedure to check the temporal registration accuracy between the two Washington, D.C. scenes. Registration accuracy assessment was made on a band-by-band basis which showed the maximum RSS offset for line and sample for all bands to be 0.31 pixel. The 90% error figure was 0.68 pixel.

Band to Band Registration

Only one study characterized the band to band registration accuracy. Imhoff and Alford used cross-correlation between bands for the November 2 Washington, D.C. scene. The best case registration errors between bands 1 and 2, and 3 and 4 were 0.173 pixel and 0.167 pixel respectively, both within specifications (Figures 3 and 4). The worst case registration error was 0.464 pixel between bands 2 and 3 (Figure 5). The lower statistical correlation between the information content represented by bands 2 and 3 is believed to be the cause of the higher registration error.

Landsat 4 to Landsat 2/3 Comparison

One paper examines scene to scene registration accuracies achievable within the Landsat-2/3 series with those between Landsat-4 and the Landsat-2/3 series.

J. Anderson (NASA/Earth Resources Laboratory) characterized the geometric accuracies of systematically corrected Landsat-3 and Landsat-4 MSS data by comparing them both to a common geodetic control base defined by Landsat-2 data. Results showed that definite differences in achievable registration accuracies are encountered in registering Landsat-2 and 3 to Landsat-4 data. The Landsat-3 to Landsat-2 registration yielded line and sample errors of 26.7m and 20.4m while the Landsat-4 to Landsat-2 registration yielded line and sample errors of 27.0m and 40.3m respectively. Anderson also noted a scan profile defect in his Landsat-4 data. It should be noted that while larger registration errors between Landsat 4 and Landsats 2/3 may be expected due to altitude differences, a portion of the error noted by Anderson may be due to the scan profile problems which have since been eliminated in the MIPS.

RADIOMETRIC CHARACTERIZATION

At the time the data was acquired and processed for the radiometric characterization studies, relevant system parameters had stabilized. Therefore the early radiometric characterization results more nearly represent the expected long term characteristics - unlike the geometric characterization where the processing parameters had not yet stablized.

The radiometric results are grouped into four categories: spectral characteristics, banding characteristics, Landsat-4 to Landsat-2 and 3 comparisons, and woodgrain noise patterns. Table 1 shows the studies performed relevant to each category.

Spectral Characteristics

Markham and Barker performed a comprehensive analysis and tabulation of spectral characteristics based on prelaunch acquired data. They examined data from the protoflight and flight instruments. Relative spectral response graphs were plotted for each of the twenty-four channels for both instruments. From these graphs, parameters (e.g. bandwidth and band edges) were derived, tabulated, and compared with similar parameters from Landsats-1, 2, and 3. Channel by channel outputs for soybean and soil targets were simulated and compared within each band and between instruments. The Landsat-4 scanners were generally more uniform from channel to channel within bands than were previous scanners. In Appendix A of this report, there is a brief description of the relative spectral response measurement procedure.

Banding Characteristics

The MIPS uses a new histogram radiometric calibration algorithm for Landsat-4. This algorithm has not been used before in the production process of Landsat data. It was anticipated that this process would remove the residual radiometric errors (commonly called banding) present in many MSS images of previous Landsats. Two studies examined banding in a variety of qualitative and quantitative methods.

Rice and Malila noted banding visually only in nearly uniform areas such as water bodies. They performed quantitative analysis on uniform areas and observed a maximum deviation between band means of 0.88 quantum units. For a different point of view, they also used an along track Fourier transform technique to quantify the banding. Alford and Imhoff analyzed a scene processed with both the new histogram technique as well as with the calibration wedge only technique. The improvements using the new technique are shown.

Landsat-4 to Landsat-2 and 3 Comparisons

Rice and Malila, Likens and Wrigley, and Alford and Imhoff compared Landsat-4 MSS signal levels to those of Landsat-3. In all three investigations, data was obtained from near simultaneous overpasses of the two satellites. For each band, Rice and Malila and Alford and Imhoff regressed average signal values of uniform areas common to both data sets. Likens and Wrigley used 512 X 512 areas that were registered. The results showed well defined relationships between the satellites, although the nominal signal values from the two satellites may differ by as much as 10 percent as shown by Alford and Imhoff. Likens and Wrigley also compared Landsat-4 with Landsat-2.

Woodgrain Noise Pattern

A woodgrain or diagonal pattern was observed in all MSS images. It is especially visible over uniform areas such as water. Rice and Malila used Fourier analysis on individual lines to quantify the noise. Alford and Imhoff used a resequencing technique to order the pixels of all bands into the time sequence in which they were originally sampled. Fourier analysis was then used on the resequenced data. Both investigations showed distinct frequencies that were stable over the time period of a scene. Alford and Imhoff discuss two possible sources of the noise.

SUMMARY

Most of the studies concerning Landsat-4 MSS image geometry showed positive conclusions despite the variable nature of the attitude control system during part of the acquisition period. Those studies, carried out using systematically corrected data, showed location offsets between 130 to 3,200 meters (2.3 - 56.1 pixels). This range was at least partially due to the attitude control problems mentioned above. Those same studies, however, also indicated that although the offsets seemed large, the internal geometry of the system corrected data was quite good, allowing for accurate warping of the data to user defined control points.

The two papers which dealt with geodetically corrected scene data also showed positive results. The analysis by Brooks et al. showed geodetically corrected scene data (included temporal registration) either meeting or exceeding the specifications. An independent analysis of the same data also showed that the correction exceeded, met, or very nearly met the specification.

The radiometric studies confirmed the expectation that the new histogram calibration method would eliminate most of the banding observed in previous Landsat images. Qualitatively and quantatively, the data showed very close agreement between channels within each band.

The comparions between the MSS's of Landsats-2, 3, and 4 showed consistent differences. Consequently, the relative radiometric values can be related between the three satellites. However, determining absolute radiometric values using the preflight calibration values Rmax and Rmin is questionable since each satellite will produce different results.

The observed woodgrain noise pattern was quantified. The effect on the results of applications was not considered and will generally depend on the application. However, modifications have been implemented in the flight instrument (Landsat-5) which should considerably decrease this type noise.

	Geodetic Registration	Systematic Correction	Temporal Registration	Band-to-Band Registration	Landsat-4 to Landsat-2&3 Registration	Spectral Characteristics	Banding Characteristics	Landsat-4 to Landsat-2&3 Radiometric Comparison	Woodgrain Noise Pattern	Description of CCRS Processing
Anderson					x					
Brooks	x	x	x							
Imhoff	x	x	x	x						
Thomodsgard	x	x								
Welch	x	x								
Markham						x				
Rice							x	x	x	
Likens								x		
Alford							x	x	x	
Murphy										x

185
0498

UNCLAS

N85-20498

RADIOMETRIC ACCURACY ASSESSMENT OF LANDSAT-4 MULTISPECTRAL SCANNER DATA

William L. Alford and Marc. L. Imhoff
NASA/Goddard Space Flight Center, Greenbelt, Maryland 20771

INTRODUCTION

The Landsat-4 mission has unique characteristics relative to previous Landsat missions. The spacecraft is new; the orbit is lower with a more frequent repeat cycle; and the ground processing facility consists of new hardware with different algorithms being applied. This study explored how some of these changes have effected the character of the Multispectural Scanner (MSS) radiometric data quality. This study examined the standard digital MSS products to describe quantitatively the radiometric data quality as well as the radiometric differences between the Landsat-4 MSS and previous MSS systems.

This investigation used standard production MSS digital products that were distributed from the EROS Data Center (EDC) as well as data obtained directly from the Multispectral Image Processing System (MIPS) at the Goddard Space Flight Center.

OBJECTIVES

The objective of this study was to characterize the radiometric quality of the MSS data based on a few early scenes. Continuing radiometric consistency will depend on the quality control of the production system as well as the hardware continuing to operate properly. The specific objectives were to:

1. Measure the channel to channel offsets within each band. Images from previous MSS missions have had various degrees of banding caused by channel offsets. The Landsat-4 Multispectral Image Processing System (MIPS) uses a new histogram calibration process.

2. Compare the radiometric responses between Landsats-3 and 4. The different orbits of Landsats 3 and 4 provide an opportunity not available in previous missions, simultaneous overpasses.

3. Quantify the woodgrain looking pattern that has been observed in many Landsat-4 MSS scenes.

INTERNAL CONSISTENCY

Background

One radiometric calibration process uses calibration lamps and a variable density filter in the MSS to generate calibration values for each channel every twelve lines (two scans of the MSS). In MIPS, these calibration values are used to establish offset and gain values for each channel which are applied to all image data values. This process, similar to that used for previous Landsat missions, is commonly called the cal-wedge calibration.

The usual radiometric calibration process in MIPS includes an additional step. The channel offsets and gains are adjusted so that the channel means and standard diviations within each band become the same as the average band value. The image is divided into segments for this process with offset and

gain values derived for each segment. These values are blended between segments before they are applied. This process, not used in the production processing of previous Landsat satellites, is commonly called histogram calibration.

Approach

At the time of this analysis near the end of 1982, all data processed for distribution by EDC had only histogram calibrations applied. By special request, one scene of Utah was produced using cal-wedge calibrations.

Scene ID	Path	Row	Date
40087717302	37	30	October 11, 1982

This scene was also processed with the usual histogram calibrations. These two data sets were processed to produce B format tapes (radiometric corrections only, no geometric corrections) and delivered directly from MIPS. Since EDC does no additional radiometric calibrations for B tape products, the image data used for this analysis is the same as that which would have been delivered by EDC.

Both data sets were analyzed identically. Data subsets consisting of 400 lines each were created from each of the 24 channels. These were subsequently divided into four 100-line segments in order to look for any significant trends throughout the image. For each segment, the channel means within each band were compared to the band means as shown in Figure 1. Histograms of each detector in band 1 for one segment are shown in Figure 2.

Results and Discussion

The plots in Figure 1 clearly demonstrate the improvement that histogram calibrations make over cal-wedge calibrations for this evaluation criteria. Form the graphs the peak to peak range is typically 0.4 quantization levels with a worst case of 0.62 for the cal-wedge calibrated data, whereas the histogram calibrated data is typically 0.1 peak to peak with the worst case being 0.24.

The Band 1 histograms in Figure 2 resemble those of previous Landsat's. The gaps are caused by the decompression processes which performs a nonlinear radiometric stretch followed by an offset and gain correction unique for each channel. In previous Landsats, the offsets and gains were updated every 12 lines, consequently the gaps could shift in position every 12 lines. In the Landsat-4 histogram calibration process, new offset and gain values are updated typically every 200 lines.

COMPARISON WITH LANDSAT-3

Approach

An absolute in-flight calibration of Landsat-4 had not been performed during the time of this investigation. This would involve measurements of ground truth with compensations for atmospheric effects. A direct comparison between Landsats 3 and 4 was possible, however, with a near simultaneous

overpass of both satellites.

An area in Vermont was selected where Landsats 3 and 4 passed within two minutes of each other with scene centers separated by about 10 minutes latitude and 14 minutes longitude. Standard B format tapes from EDC were used.

Satellite	Scene ID	Path	Row	Date
Landsat-3	31753148591	14	30	December 22, 1982
Landsat-4	40159150l0	13	30	December 22, 1982

Interacting with a television display, nine uniform polygonal areas were selected from each image that corresponded approximately to the same ground scene. The differences in the ground area covered were due primarily to (1) the rotated and shifted sampling grids relative to the two MSS instruments and (2) the line length variations in the Landsat-4 MSS. The line lengths between adjacent scans can vary by as much as eight pixels causing obvious six-line shifts in scenes derived from B format tapes. However, the polygon boundaries were selected well within the edges of uniform areas to minimize these geometric effects.

The means and standard deviations of each area have been tabulated and are listed in Table 1. To determine the relationship between the two MSS data sites, linear regressions were calculated for each band as shown in Table 2.

Prelaunch calibrations combined with post-launch data were used by the Landsat-D Project to derive values known as R_{max} and R_{min}. These are the radiance values associated with quantization levels 127 and 0 respectively. R_{max} and R_{min} values from both the Landsat-3 and 4 MSS's were also used to derive a linear relationship between the two instruments. These coefficients are shown in Table 3.

Results and Discussion

The relationships between the Landsat-3 and 4 MSS radiometry are significantly different using the two sets of coefficients in Tables 2 and 3. For example, a Landsat-3, Band 1 value of 50 maps into a Landsat-4 value of 52.3 using Table 2 and into 57.1 using Table 3.

Since most of the residuals in the fit to the linear model are much less than ±0.5, we might assume that the coefficients in Table 2 are reasonable. However, this leads to the conclusion that the R_{max} and R_{min} values are inaccurate for one or both satellites. For absolute radiometric calibrations to be assured, Rmax and Rmin values need to be redetermined, possibly by using calibrated radiometric targets.

QUANTIFICATION OF THE WOODGRAIN PATTERN

Approach

A woodgrain or diagonal pattern was observed in all the MSS images as shown in Figure 3. This pattern was especially visible over uniform areas such as

water. It appears visually to be the same whether the Thematic Mapper instrument was on or off. This type pattern or noise is typically caused by one or more spurious sine waves interacting with the analog to digital converter. One assumption fundamental to the analysis is that the noise is the same for all analog channels at the input to the multiplexer/analog-to-digital converter subsystem. This assumption was supported later by noise measurements made in July 1983, on the Landsat-D prime satellite before its launch. There was a significant increase in noise between the output of the scanner and the input to the multiplexer, probably caused by a common grounding problem.

Based on this assumption, pixels from the 24 channels were reordered into a single sequence in the order the pixels were sampled on the spacecraft. An interpolated 25th sample was included in this resequenced data since the format allowed space for thermal band samples. Before resequencing, the pixel values in each band were offset to a common mean. The effect of resequencing was to provide a time sequence that was sampled 25 times higher than any one channel.

Fourier analysis performed on resequenced data of several scenes from Landsat-D, including prelaunch test data, produced similar patterns in the frequency amplitude domain. The results from the analysis of one scene of North Carolina is reported herein.

ID	Path	Row	Date
4007015081	14	35	September 24, 1982

The test area is a fairly uniform region over water 170 pixels long and six pixels wide covering one scan of the MSS. This provides slightly more than 4,096 resequenced pixels required for the fast Fourier transform (FFT). A plot of the Fourier amplitudes is shown in Figure 4. The harmonics caused by the resequencing process are numbered 1 through 12 and can be ignored. With a channel sampling rate about 100,418 kilocycles, the highest component (2048 cycles) in Figure 4 represents 1,255,255 Hz. The amplitude values represent one-fourth the peak-to-peak amplitude of the corresponding sine wave.

Frequency components with amplitudes that exceed 0.037 are listed in Table 4. Since each channel is sampled one twenty-fifth as often as the resequenced data, the Nyquist frequency for any one channel is one twenty-fifth of 2,048 cycles/T which is 81.92 cycles/T (T is 1.63158 milliseconds). Consequently, most of the frequencies in the image domain are aliases of a much higher frequency in the resequenced data domain. The periods of these frequencies are given as they would appear in the image domain. See column 3 in Figure 4.

Results and Discussion

Most of the image domain periods lie between 2.0 and 5.1 pixels. Even though any one amplitude is small, the composite effect of all components causes the distinct diagonal pattern. Although the pattern shifts, fades, and wanders, a period between 2 to 5 pixels prevails. Two other strong components have periods of 11.6 and 14.5 pixels. Upon close observation of the image, one can discern a more subtle diagonal pattern with these approximate periods.

Filtering these components in the resequenced frequency domain removed the patterns in the image domain once the pixels were reassembled back into images.

Most of the frequency components form a pattern in the frequency domain and appear to originate from a common source with a fundamental frequency of 114,504 Hz. (A drifting voltage supply oscillator operates at about 115 KHz.) The 114,504 Hz translates into 186.823 cycles/T for the spectrum in Figure 4 where T is 1.63158 milliseconds.

Excepting three frequency components, each component can be accounted for by one of the first 35 harmonics of 186.823 cycles/T taking into account aliasing effects. However, this may not be the physical source for these frequencies. Two frequencies with intermodulation products can also account for these components.

CONCLUSIONS

The histogram calibration process made a significant reduction of the channel differences within a band. If this improvement proves consistent over a wide radiometric range and persists over time, Landsat-4 MSS may not have the banding problems that plagued previous MSS instruments.

For a simultaneous overpass of Landsat-3 and 4, uniform test areas were selected that were common in both data sets. Significant differences in radiance values between the two satellites were observed when R_{max} and R_{min} were used to compute absolute radiance values. Ground truth should be used to determine new values.

A woodgrain appearing pattern is apparent in the MSS images that was not apparent in previous MSS's. It is believed to be caused by many different frequency components, most of which originate from a common source. Efforts are being made to reduce this noise on the MSS of Landsat-D-prime before launch.

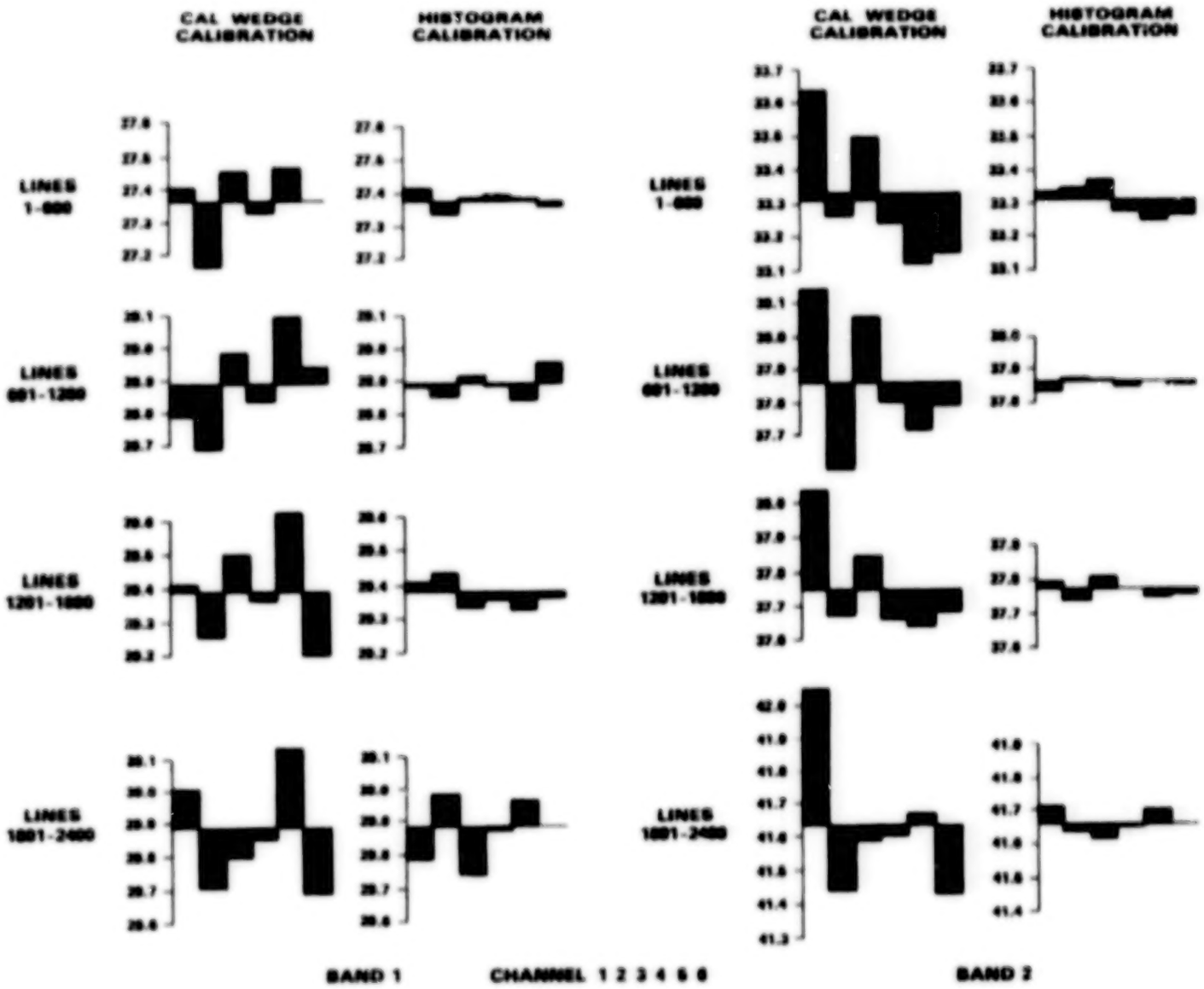

Figure 1 (a). Differences Between Band Means and Each Detector for Bands 1 and 2. Scene ID 4008717302; Utah; October 11, 1982.

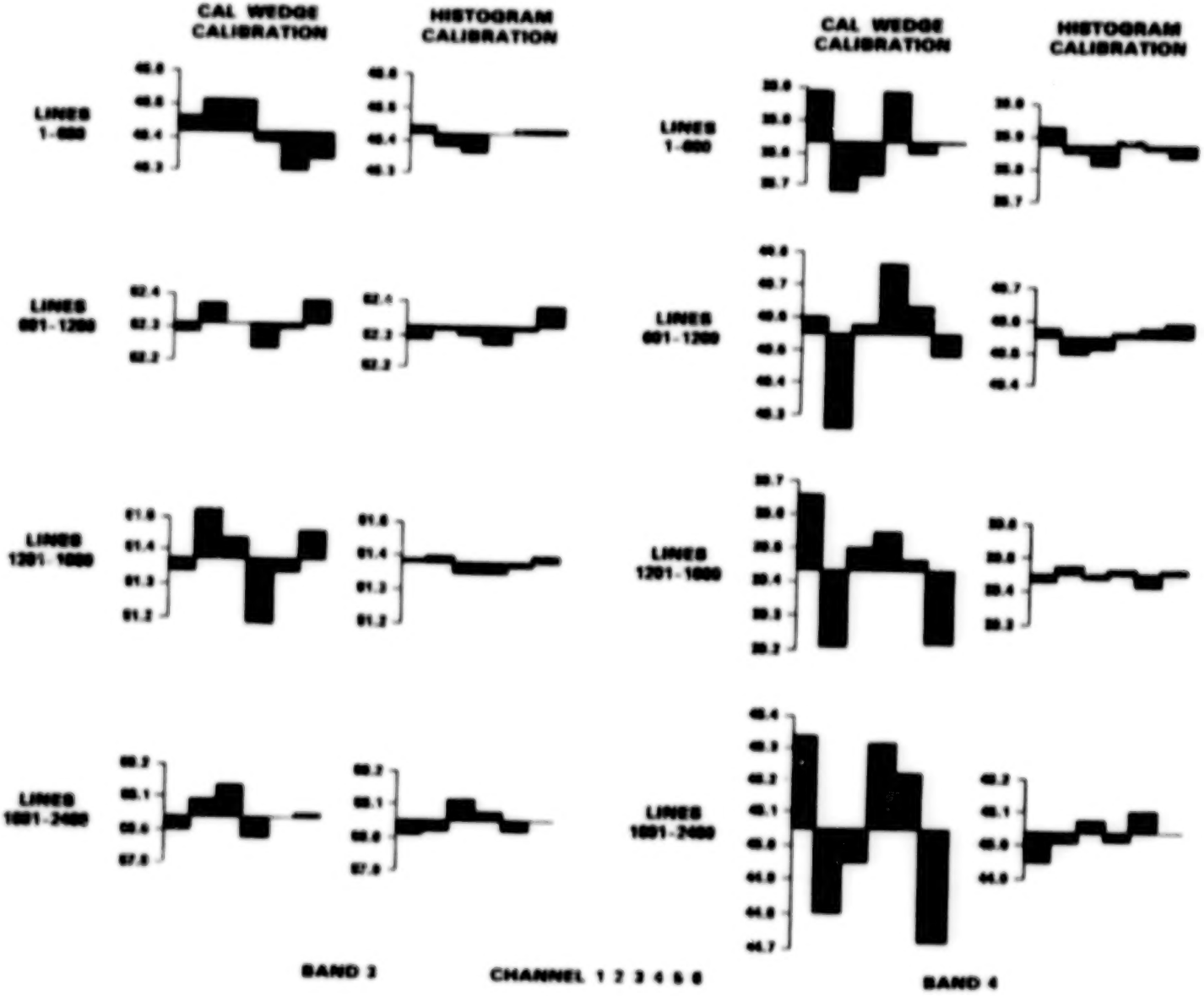

Figure 1 (b). Differences Between Band Means and Each Detector for Bands 3 and 4. Scene ID 4008717302; Utah; October 11, 1982.

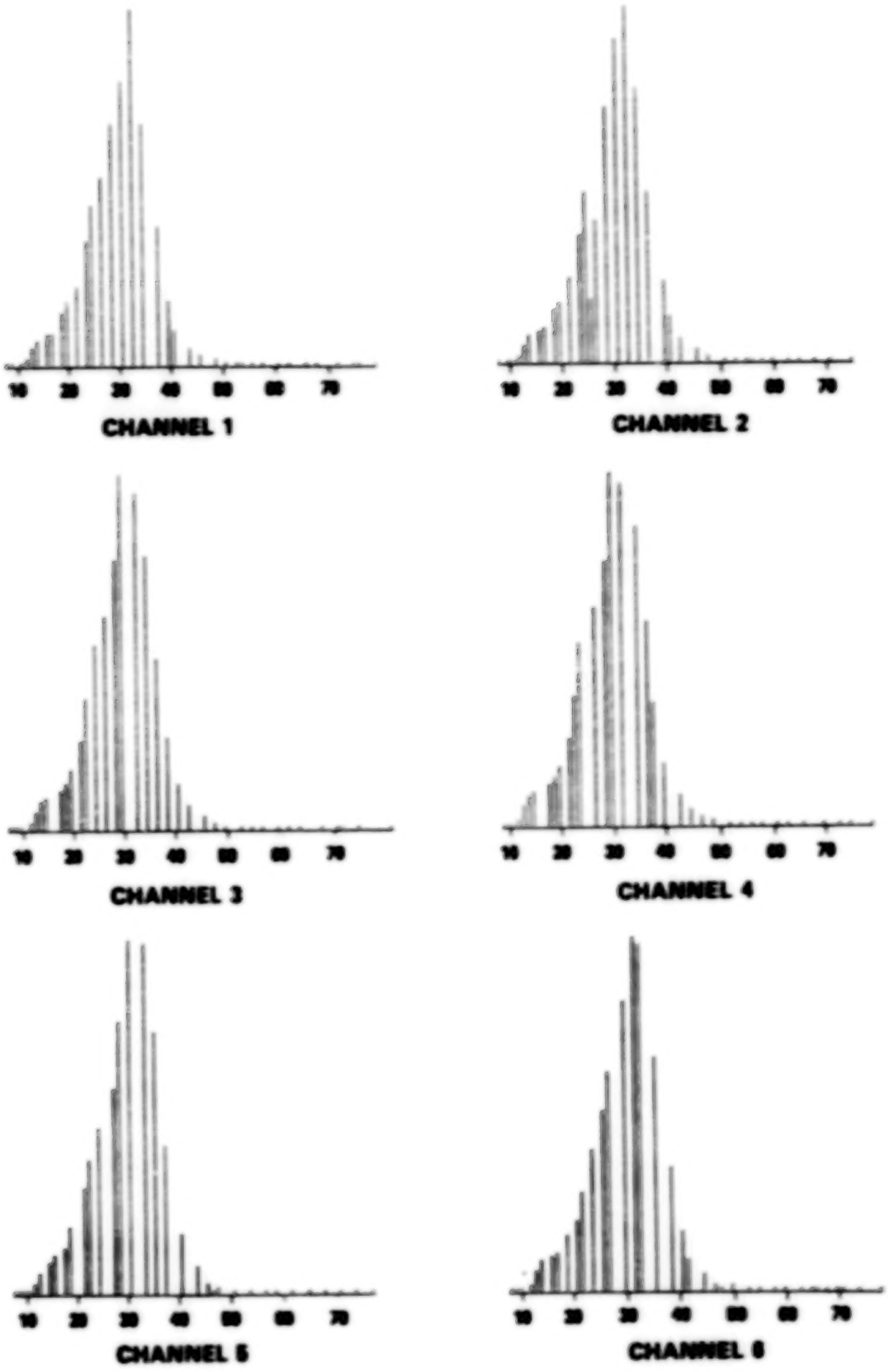

Figure 2. Histograms of Individual Detectors for Band 1, Lines 1801 - 2400. Scene ID 4008717302; Utah; October 11, 1982.

Figure 3. Band 1 with the Intensity Stretched to Emphasize the Woodgrain Pattern. Scene ID 4006215591; Louisiana; September 16, 1982.

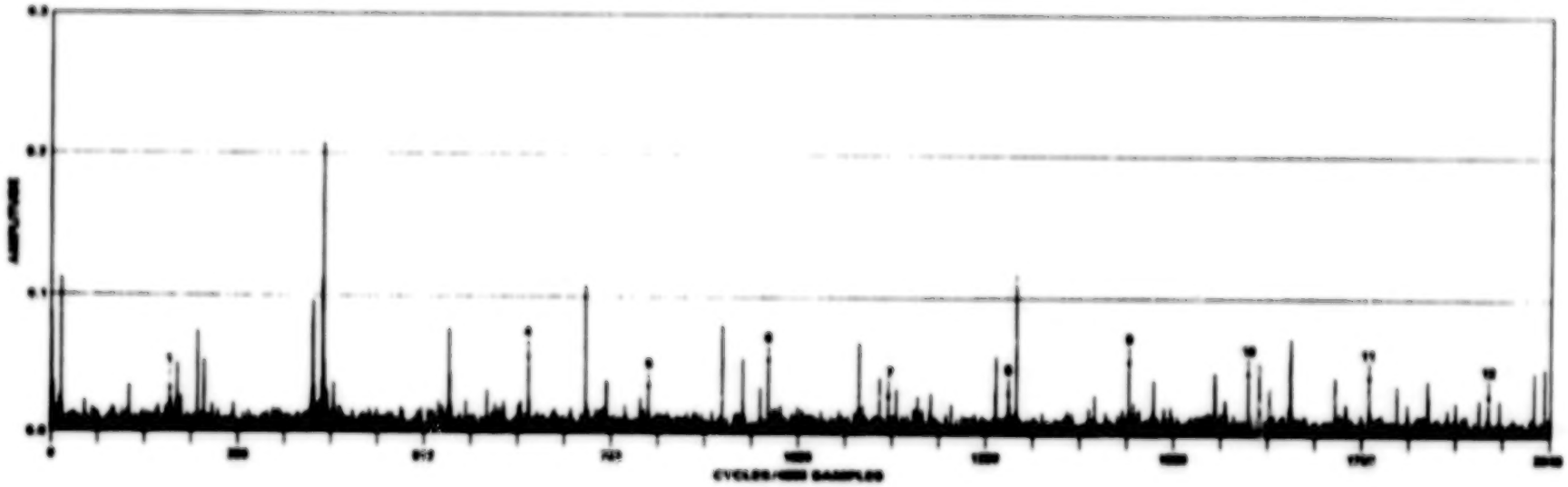

Note: 4096 samples correspond to 1.63158 milliseconds. Therefore the frequency scale can be read as cycles/1.63158 milliseconds.

Figure 4. Fourier Amplitudes of Resequenced Data. Scene ID 4007015081; North Carolina; September 24, 1982.

Table 1. Means and Standard Deviations of Selected Common MSS areas from Simultaneous Overpasses of Landsats 3 and 4. Scene ID 3175314591 (Landsat-3) and ID 4015915010 (Landsat-4); Vermont; December 22, 1982.

AREA	BAND 1		BAND 2		BAND 3		BAND 4	
	L-3	L-4	L-3	L-4	L-3	L-4	L-3	L-4
1	11.75	13.03	10.73	9.54	14.49	16.97	16.37	14.90
2	56.31	59.19	69.56	62.55	67.51	74.15	54.84	47.64
3	33.94	35.32	39.86	36.26	40.86	44.76	35.66	31.12
4	51.46	53.74	62.66	56.81	62.79	68.90	52.24	46.08
5	14.12	15.53	13.21	12.01	11.34	13.11	9.95	9.50
6	9.68	10.93	7.71	6.51	4.95	5.46	3.73	3.26
7	46.44	48.48	55.92	50.88	56.48	62.52	47.10	41.42
8	11.56	12.82	10.28	9.13	11.26	13.13	12.24	10.86
9	20.34	21.49	22.61	19.82	25.52	27.94	24.70	21.85

BAND MEANS

1	1.34	1.46	1.55	1.61	1.85	2.25	1.92	1.98
2	1.48	1.09	1.95	1.43	1.90	1.93	1.39	0.95
3	3.53	3.64	3.91	4.20	4.25	4.80	3.74	2.83
4	2.06	2.16	3.19	2.75	2.14	2.42	1.94	1.69
5	1.28	1.17	1.28	1.04	1.71	1.09	1.60	1.09
6	0.76	0.82	0.87	1.05	0.77	1.07	1.23	0.97
7	3.72	3.72	5.07	4.61	4.11	4.23	3.02	2.77
8	1.10	1.38	1.49	1.45	1.67	1.78	2.07	1.49
9	1.85	2.26	2.61	2.78	3.00	3.40	3.20	2.62

BAND STANDARD DEVIATIONS

Table 2. Relationship Between the Pixel Values of the Landsats 3 and 4 MSS Instruments Based on Image Data Values. Scene ID 3175314591 (Ladnsat-3) and ID 4015915010 (Landsat-4); Vermont; December 22, 1982.

BANDS	A	B	R^2
1	1.03	0.84	.99
2	0.91	-0.27	.99
3	1.09	0.58	.99
4	0.87	0.42	.99

(Landsat-4 Value) = A x (Landsat-3 Value) + B

Table 3. Relationship Between the Pixel Values of the Landsats 3 and 4 MSS Instruments Based on Rmax and Rmin Values.

	Landsat-3 (after 5/31/78)		Landsat-4 (after mid Aug 82)			
BANDS	Rmin at 0	Rmax at 127	Rmin at 0	Rmax at 127	A	B
1	0.04	2.59	0.02	2.30	1.12	1.11
2	0.03	1.79	0.04	1.80	1.00	-0.72
3	0.03	1.49	0.04	1.30	1.16	-1.01
4	0.03	3.83	0.01	4.00	0.97	-2.28
milliwatt cm - ^{2} steradian $^{-1}$						
(Landsat-4 value) = A x (Landsat-3 value) + B						

Table 4. Frequency Components, Scene ID 4007015081; North Carolina; September 24, 1982.

Observed Frequency (cycles/T)	Amplitude (Pixel value x 10^{-3})	Image Domain Period (Pixels)
14.1	113	11.6
172.8	51	18.3
201.0	75	4.4
• 210.0	54	3.5
359.6	97	5.1
373.8	112	3.6
386.2	37	2.7
546.2	77	3.0
733.1	108	2.1
761.5	39	2.8
920.0	80	2.6
948.1	56	4.7
1,107.8	68	4.2
1,135.0	42	13.8
1,293.8	58	9.7
1,322.0	117	14.5
1,508.8	41	4.8
• 1,592.5	46	3.6
1,653.0	55	11.2
1,695.6	72	2.9
• 1,756.1	43	3.6
1,840.0	37	4.3
1,882.4	41	2.0
2,027.0	48	2.7
2,041.0	51	2.2

Notes:
1. T = 1.63158 milliseconds.
2. Frequency values were estimated to the nearest tenth.
3. • are components that do not fit the harmonic components assumption
4. Amplitude values are 1/4 the peak-to-peak value of the corresponding sine waves.

SPECTRAL CHARACTERIZATION OF THE LANDSAT-4 MSS SENSORS

Brian L. Markham and John L. Barker
Earth Resources Branch
NASA/Goddard Space Flight Center
Greenbelt, MD 20771

INTRODUCTION

Two multispectral scanner subsystems (MSS) have been fabricated and tested by Hughes Aircraft Company for the NASA Landsat program. The intention was to provide continuity with the MSS sensors on Landsats 1-3. One MSS, designated the protoflight (PF) model, was integrated into the Landsat-4 spacecraft, which was launched on July 16, 1982. The second, designated the flight (F) model, has been integrated into the Landsat-4 backup satellite, which is scheduled for possible launch in 1985. Each MSS has four bands in the reflective portion of the electromagnetic spectrum: (1) a green band, nominally 500 to 600 nm; (2) a red band, 600 to 700 nm; (3) a near-IR band, 700 to 800 nm; and (4) a second near-IR band, 800 to 1100 nm. On previous Landsats, these bands were known as MSS-4, MSS-5, MSS-6, and MSS-7, respectively, because the three-band return-beam vidicon (RBV) camera system occupied bands 1, 2, and 3. With the absence of the RBV camera system on Landsat-4, this designation is obsolete, and the MSS bands are referred to as 1, 2, 3, and 4, respectively. Each band consists of an array of six channels (i.e., six detectors and six filters). Thus, there are a total of 24 channels (i.e., four bands with six channels per band) that are numbered sequentially from 1 to 24 as follows: band 1 (channels 1 through 6), band 2 (channels 7 through 12), band 3 (channels 13 through 18), and band 4 (channels 19 through 24).

The engineering test data that were collected included channel-by-channel spectral response curves, detailing the relative response of each channel as a function of wavelength. Because this response is measured through the system's optics, it includes the combined effects of optics, filters, and detectors on the spectral response. A description of the test procedure is included in Appendix A. For previous MSS's, these data were contained in generally unavailable contractor reports to NASA (Norwood et al., 1972; Felkel et al., 1977). The primary intent of this document is to make available to the Landsat user community data on the spectral characteristics of these two sensors, including a characterization of the variability within and differences between the two sensors. These data can be used by individual investigators to assess the sensors' utility for their applications.

A second objective is to provide, through simulation, an estimate of the potential contribution of spectral differences between channels to within-band striping. In the remainder of this report, this type of striping will be referred to as "spectral striping." This should not be confused with "radiometric striping," which results from gain or offset differences between

channels. Because spectral striping cannot be removed by uniform radiometric calibration, it limits the ability to remove banding from images.

One objective in placing an MSS on Landsat-4 was to provide continuity with the previous three Landsats. Thus, the Landsat-4 MSS's were designed, to the extent possible given the lower 705-km altitude of Landsat-4, to replicate the imagery of the previous MSS's. Therefore, a third objective of this document is to assess the extent to which the new MSS's match the previous MSS's in terms of spectral response.

METHODS

Relative spectral response (RSR) curves for each channel (six in each of four bands) of the Landsat-4 PF and F multispectral scanners, (Hughes Aircraft Company, unpublished reports, 1980; 1981) as well as the MSS's on Landsat 1, Landsat 2 (Norwood et al., 1972) and Landsat 3 (Felkel et al., 1977), were digitized at 10-nm intervals for bands 1, 2, and 3 and at 20-nm intervals for band 4. Two sets of curves were available for the PF scanner, one generated from data collected in June 1980 and one from data collected June 1981. The more recent set of curves was used to characterize the PF scanner.

The following attributes were computed from the digitized curves:

1. Lower-band edge (50-percent relative response point)

2. Upper-band edge (50-percent relative response point)

3. Lower-edge slope interval (width between lower 5- and 50-percent response points)

4. Upper-edge slope interval (width between upper 5- and 50-percent response points)

5. Positive spectral flatness (maximum positive percent deviation from mean response in central 70 percent of nominal bandpass)

6. Negative spectral flatness (maximum negative percent deviation from mean response in central 70 percent of nominal bandpass)

Although listed only under specifications for the filters (Table 1), these six characteristics were deemed appropriate for characterizing the overall relative spectral responses. In addition, the bandwidth (band edge to band edge) was calculated. For completeness, a characterization of the filter components for the PF and F models is included (Appendix B).

Each band was checked for anomalous channels (i.e., channels within the band that were significantly different from the rest). A modified F test (outlier test) was used for the screening (Grubbs, 1950) with an α-level of 0.01.

Two parameters were calculated for each of the seven spectral characteristics for each band of each MSS: (1) the band mean (the average value of the characteristic for the six channels in the band), and (2) the band standard deviation (equal to the sample standard deviation using each channel as an

observations. A statistical comparison between scanners of the band means and band standard deviations for each spectral characteristic was not possible because independent multiple measurements of each channel's spectral characteristics were not generally available. Two independent sets of measurements were available for the Landsat-4 PF scanner only. The approach used here was to consider an indicated difference between scanners in band mean or band standard deviation for a particular characteristic to be of consequence if it exceeded a specified value (threshold) determined from the differences between the two sets of PF relative spectral response measurements (Appendix C). The values used were:

1. 3 nm for means and 1.8 nm for standard deviations for band edges, widths, and slope intervals except as indicated below

2. 33 nm for means and 2.7 nm for standard deviations for band 4 upper-band edge, width, and upper-edge slope interval

3. 4-percent means and 0.9-percent standard deviations for positive and 6-percent means and 1.5-percent standard deviations for negative spectral flatness in bands 1 through 3

4. 19-percent means and 2.4-percent standard deviations for positive and 12-percent means and 2.5-percent standard deviations for negative spectral flatness in band 4

A simulation procedure was established for assessing for each MSS the contribution of the channel-to-channel spectral differences to within-band target-dependent striping and for comparing the scanners' mean outputs to typical targets. Channel-by-channel digital MSS counts were simulated using field reflectance spectra.

Reflectance data of soil and soybeans collected with a Barnes Mark-II spectroreflectometer were used as input for the analysis. This instrument simultaneously samples incident sunlight and target-reflected light to provide target reflectance. Pertinent instrument characteristics over the spectral interval of 450 to 1150 nm are:

1. A sampling interval (filter position spacing) of 4 nm

2. An average spectral bandwidth of about 16 nm

3. Rms noise of about 0.5-percent reflectance with a 50-percent reflective target (0.2-percent with a 3-percent reflective target) at a 35-degree solar zenith angle.

One spectrum of a moist soil plot and one of a soybean plot having a full canopy cover collected on day 226 in 1978 were used in this study. In addition to being common agricultural targets, soil and soybeans were selected because they were spectrally different. The spectrum of soybeans is characteristic of green vegetation (Figure 1).

The simulation procedure involved the following steps:

1. Normalization of the relative spectral responses of the individual channels

2. Conversion of narrowband target reflectance data to simulated radiances at satellite altitude, using an atmospheric and irradiance model

3. Integration of narrowband radiances across each bandwidth, weighting by the normalized response coefficients (interpolated to match spectroreflectometer sample points)

4. Scaling the integrated radiances to match the output of the MSS

The procedure for normalizing the responses of the individual channels was designed to simulate the actual procedure that was used to calibrate the MSS channels during system testing. In the simulation program, the sensors "viewed" a spectrally flat target illuminated by a spectrally flat source, and correction factors were computed so that each channel gave the same output for this flat source. The calculation of a correction factor involved integrating the area under the RSR curve for the channel and dividing the result by the nominal bandwidth for the channel. A normalization factor was thus greater than one if the channel's bandwidth was effectively wider than nominal and less than one if narrower than nominal.

In the actual MSS calibration a spectrally nonuniform target (integrating sphere) is observed. Postprocessing of the data, where each channel's spectral response and the integrating sphere's spectral output are known, allows the integrating sphere to appear spectrally flat (General Electric Co., "MSS Standard Interface Document", unpublished, 1978).

Conversion of the narrowband field measured reflectances to satellite level radiances was facilitated by wavelength specific additive and multiplicative factors obtained from the use of the Turner and Spencer (1972) atmospheric model. Inputs to the model included 40-degree solar zenith angle, 20-km horizontal visibility, 100-percent target reflectance, background reflectance (average value for 50-percent soil/50-percent vegetated surface at a given wavelength), and 705-km satellite altitude. The use of the nominal Landsat 1-3 altitude of 918 km would not have changed the atmospheric model's output. The two model output parameters used for each wavelength input were target-contributed (beam) radiance and path radiance. To determine the total satellite level radiance for a particular target, the beam radiance (for 100-percent reflective target) was multiplied by the target reflectance and the path radiance was added to the product. The Turner and Spencer model considers only atmospheric scattering (haze), which is the most important atmospheric factor in the MSS bandpasses. However, because water absorption does attenuate light in the region, particularly between 900 and 950 nm, the radiances obtained by this model are expected to be somewhat high in band 4.

The narrowband simulated radiances were then summed across the individual channels, weighted by the normalized relative response coefficients. The integrated radiances were then scaled to match the digital counts of decompressed MSS data. Bands 1 through 3 were linearly scaled from 0 to 127.99 counts and band 4 from 0 to 63.99 counts, using the given nominal saturation radiances

of 2.48, 2.00, 1.76, and 4.60 mW cm^{-2} sr^{-1} for bands 1, 2, 3, 4, respectively, to determine the scaling factors.

The simulation procedure can be described by the following equation (1), which is applied individually to each channel on each scanner:

$$DN = SCFACT \times \sum_{i=a}^{b} ([REF_i \times BRAD_i] + PRAD_i) \times \frac{RESFAC_i}{NORFAC} \times WAVSPA \qquad (1)$$

where

DN = simulated digital number output for MSS channel (nontruncated counts)

SCFACT = scale factor for conversion of radiance to digital counts: Band 1, 51.61; band 2, 64.00; band 3, 72.73; band 4, 13.91 (counts/mW cm^{-2} sr^{-1})

REF_i = target reflectance at i

$BRAD_i$ = Turner model spectral beam radiance at i for 100-percent reflective target (mW cm^{-2} sr^{-1} μm^{-1})

$PRAD_i$ = Turner model spectral path radiance at i (mW cm^{-2} sr^{-1} μm^{-1})

$RESFAC_i$ = relative response factor of MSS channel at i

NORFAC = normalizing factor for MSS channel

WAVSPA = wavelength spacing between spectrometer filter positions (nominally 0.004 μm)

Throughout the simulation, perfect relative radiometric calibration within bands and perfect absolute radiometric calibration for all scanners has been assumed. Also, equivalent radiometric calibrations for all scanners have been assumed, i.e., a given digital count in a band on one scanner corresponds to the same radiance value as on all other scanners. Thus, in this simulation, output differences between scanners are due solely to differences in their relative spectral responses. This contrasts to the real situation where calibrations of each scanner are different and performed with some error. In real data, radiometric factors could hide or overshadow spectral factors.

The band mean outputs to soil and soybeans (averages of six channels) were used to compare differences between PF and F and between PF, F and the MSS's on Landsats 1 through 3. The maximum difference in output between channels within a band was used to compare the potentials for "spectral striping" among the scanners. Differences in means and maximum deviations were considered to be important if they exceeded:

1. 0.30 digital counts (approximate Rms quantization noise) and

2. The differences in Table C-3 of Appendix C (differences between outputs simulated with two sets of PF measurements)

RESULTS

Spectral Characterization of Landsat-4 Multispectral Scanners: Protoflight (PF) and Flight (F) Models

In most respects, the spectral responses of the PF and F (Figures 2 through 4) scanners are similar, and the following comments apply to both scanners unless otherwise noted:

Band 1 - No anomalous channels; relative spectral responses meet all filter specifications except flatness (Table 2).

Band 2 - PF channel 7 upper-band edge is 12 nm higher than the average of the other PF channels and is statistically an outlier (Figure 5); responses meet all filter specifications except flatness (Table 3).

Band 3 - No anomalous channels; all channels are slightly wide (2 to 4 nm) to the long wavlength side; otherwise, responses meet filter specifications except flatness (Table 4).

Band 4 - No anomalous channels, but upper-band edge varies by as much as 42 nm, resulting in width variations of up to 20 percent; system response upper-half power points below filter specifications because of silicon photodiode detector response; response flatness considerably below filter specifications (Table 5).

Besides the poorer uniformity of band 2 on the PF compared to the F as noted previously, the only other differences between the two scanners concerned the uniformity of the spectral flatness in bands 3 and 4, where the F is more uniform than the PF (Tables 6 through 9).

Comparison of PF and F Scanner Spectral Characteristics with Landsat 1, 2, and 3 Scanners

Meeting Filter Specifications. The relative spectral responses of previous MSS's failed to meet the filter specifications (Tables 6 through 9) in basically the same manner as those of the PF and F scanners (i.e., in the spectral flatness criteria). Although previous scanners met the band 3 upper-band edge specification, they occasionally failed elsewhere (e.g., the band 4 lower-band edge on the Landsat 3 MSS). Note that the filter specifications are only for comparison purposes; the overall response was not required to meet these specifications.

Anomalous Channels. Anomalous channels are not new to MSS scanners. Channel 6 (band 1) on the Landsat 1 (LS1) MSS was a statistical outlier on the basis of its spectral flatness (less flat). Channel 7 (band 2) on LS2 MSS was an outlier based on its upper-edge slope interval (wider).

Mean Characteristics. Because the PF and F scanners were essentially the same in terms of mean spectral response characteristics (Tables 6 through 9), they had a common set of differences from the LS1, LS2, and LS3 scanners. Because the characteristics of the LS1, LS2, and LS3 scanners were not consistent, the PF/F scanners differed from each one individually in dissimilar ways. The PF and F were different from all three previous scanners in the following ways:

Band 1 -	Upper-band edge higher (7 to 14 nm);	(Table 6)
	Bandwidth wider (8 to 13 nm)	(Figure 6)
Band 2 -	Upper-band edge lower (3 to 13 nm);	(Table 7)
	Upper-slope interval narrower (10 to 16 nm)	(Figure 7)
Band 3 -	Lower-band edge higher (4 to 11 nm);	
	Upper-band edge higher (11 to 21 nm);	(Table 8)
	Upper-slope interval narrower (17 to 21 nm).	(Figure 8)

In band 4 (Table 9, Figure 9), a number of large differences were apparent between the PF/F scanners and previous Landsats, particularly in regard to upper-band edge, bandwidth, and spectral flatness. The large magnitudes of these differences are believed to result from differences in test conditions or test equipment when the tests were conducted on the different scanners (Appendix C). This belief is based on the lesser differences between the PF model June 1980 measurements and the previous scanners than between the June 1981 PF measurements and the previous scanners (Figure 10).

Within-Band Variation. Previous Landsat MSS's displayed quite a range of within-band variability (Tables 6 through 9) in their spectral characteristics. For example, a factor of 4 difference in the standard deviation for a given characteristic between the best previous MSS (least variable) and the worst MSS (most variable) was not uncommon. Thus, in very few cases did the Landsat-4 MSS's differ from (fall outside the range of) all three previous scanners. However, for all spectral characteristics except those related to the band 4 upper-band edge (PF and F) and the band 2 upper-band edge (PF), the Landsat-4 MSS's were as uniform as the most uniform of the previous MSS's. The band 4 upper-band edge (PF and F), as well as the negative spectral flatness (PF), were less uniform than that of any previous MSS (Table 9), as was the band 2 upper-band edge (PF) and its related width (Table 7).

Simulated MSS Band Mean Outputs to Soybeans and Soils: PF, F, LS1, LS2, and LS3

PF Versus F. Because the PF and F have essentially the same mean spectral characteristics, they gave essentially the same simulated outputs to soil and soybeans targets (Table 10). The only difference occurred in band 3, where the F output to soybeans was higher than the PF. This difference resulted from the slighty shifted response of the F(704 to 814 nm), compared to the PF(701 to 813 nm), combined with the rapid increase in soybeans reflectance between 690 and 770 nm (Figure 8).

PF/F Versus LS1, LS2, and LS3. For the soybean target, differences in output between the PF and F scanners and previous scanners were apparent for bands 2, 3, and 4. Band 2 and 4 outputs were lower and band 3 output was higher than that for previous Landsats. The band 2 output was lower because the upper-band edge was lower than that of previous Landsats and because of the rapid increase in soybean reflected radiance from 690 to 770 nm (Figure 7). A contributing factor was the steeper upper slope of the PF and F. The elevated band 3 output resulted from the band being wider and shifted to longer wavelengths relative to previous MSS's. Thus, the proportion of the near-infrared high reflectance plateau of the vegetation included in the band was increased (Figure 7), which increased the output in the band.

The outputs in band 4 to soybeans on the PF and F models relative to LS1, LS2, and LS3 scanners were depressed because the response of the PF and F apparently extended to longer wavelengths and the radiance reflected from soybeans decreased with increasing wavelength (Figure 9). As mentioned earlier, because the extended responses in the PF and F are believed to be mainly spurious, the extent of depression of the output values is overestimated.

For the spectrally flatter soil target, the differences between scanner characteristics did not result in differences in mean outputs between the PF/F and the LS1, LS2, and LS3 scanners, except for the apparent difference in band 4.

Within-Band Variation in MSS Outputs to Soybeans and Soil: PF, F, LS1, LS2, and LS3

The within-band sensor output differences (Table 11) were larger for the PF than the F scanner in bands 2, 3, and 4 for the soybean target. The larger difference in band 2 of the PF compared to the F resulted from the anomalous channel on the PF with an upper-band edge of 708 nm, as opposed to the 696 nm norm for the rest of the band 2 channels. The band 3 and 4 differences were a result of the poorer uniformity of the PF than the F in spectral response, particularly flatness. For the soil target, differences between the PF and F in within-band sensor output differences were negligible.

The within-band sensor output differences of the PF and F for the soybean target were equal to or better than those of the most uniform previous Landsat, except for PF band 2 and PF/F band 4 (Table 11). The maximum difference in PF band 2 was of the same order as the difference observed in

the Landsat 2 MSS, which was the worst of the previous MSS's in that band. In band 4, the maximum within-band difference for the F model was of the same order as the Landsat 3 MSS, which was the worst of previous MSS's; the PF was somewhat worse.

The band 4 PF and F maximum within-band output differences to soil were not larger than those for previous Landsats by the criteria used. In terms of percentage of mean output, however, these differences were similar between soil and soybean targets. This indicates that the striping in band 4 would be primarily nontarget-dependent and would therefore be potentially removable.

Comparison of Simulated Data to Real Landsat Data

The simulated Landsat data were compared with actual Landsat 2 data collected under conditions similar to those simulated (37^{o} solar zenith angle, moderately clear, east-coast United States summer day) to determine if the simulated data were reasonable (Table 12). Except for band 4, the outputs of the simulated and actual soybean targets were in good agreement. The only targets characterized in the Landsat 2 scene that resembled bare soil were harvested wheat and oats. As might be expected, larger differences between simulated and actual were observed given the difference in the targets themselves. As noted earlier, the high values of simulated band 4, particularly for soybeans, probably resulted from the lack of modeling of atmospheric water absorption.

DISCUSSION

Differences in Mean Responses Between Scanners

The comparisons performed to determine how the PF and F differ from previous scanners in mean responses and outputs essentially indicate the ways in which the PF and F fall outside the range exhibited by the LS1, LS2, and LS3 MSS's. Note that if these comparisons were done with LS3 MSS's as compared to LS1 and LS2 MSS's, for example, a similar number of differences would be indicated. Thus, although the PF and F are different from previous scanners in selected ways, differences of this level are not unexpected or unprecedented, but are typical of the differences between existing scanners. No greater problems are anticipated in comparing data from the LS4 scanners (e.g., as in a change detection algorithm) than between LS3 MSS and LS2 MSS data. In addition, it is encouraging that the PF and F scanners are so similar in response.

Differences in Within-Band Variation Between Scanners

Target-dependent output differences between channels place a fundamental limit on the ability to discriminate between targets, producing "spectral striping." Exclusive of band 4, where the apparent output differences appear to be nontarget-dependent, the PF band 2 is the only case in which one of the LS4 scanners is poor in "spectral striping" potential for the targets evaluated. This "spectral striping," simulated to be 6.2 percent for a soybean target, occurs in a band that is important for vegetation discrimination. This may have an impact on data utility for this type of application.

Previous studies have assessed the magnitude of the spectral striping problem for the MSS's on Landsats 1 through 3 in a manner somewhat similar to this study (Slater, 1979; Duggin and Ellis, 1980). Except for band 4, the relative magnitudes of the within-band stripings between scanners are similar between studies (e.g., Landsat 1 is the most variable in band 1, Landsat 2 is the most variable in band 2, and Landsat 3 is the most variable in band 3).

However, the relative magnitudes of the striping as simulated here are different from those of previous studies because these studies:

1. Assumed constant irradiance across the bandpasses

2. Did not add a path radiance (haze) to the simulation

3. Used different reflectance spectra for the simulations

The first factor is primarily of concern in the wider bandpass of band 4 and tends to induce striping in this band. This results in the larger (0.8 to 1.7 percent) maximum intraband striping for this band in this study when compared to the work of Duggin and Ellis (0 to 0.6 percent). Because this is not target-dependent striping, however, it is potentially removable.

The second factor has the largest effect on bands 1 and 2 because the addition of a spectrally slowly varying haze reduces the relative magnitude of the interline striping. For example, using the data of Slater (1979), the percent difference in response between channels 7 and 8 on the Landsat 2 MSS is reduced from 14 percent when using reflectance to about 8 percent when using simulated radiances, including path radiance. The amount of this reduction depends, of course, on the level of haze.

The third factor is most important in band 2. A significant amount of variation occurs in the wavelength of onset and the steepness of the reflectance slope of vegetated targets in the wavelength interval of 690 to 800 nanometers. The spectra of an orange-tree leaf used by Slater (1979) nearly reaches its maximum reflectance at 730 nm, whereas the soybean canopy spectrum used here does not reach the same reflectance until 770 nanometers. This accounts for the 8-percent difference when using Slater's data as opposed to 4.5 percent when using the data of this study.

SUMMARY AND CONCLUSIONS

The Landsat-4 PF and F scanners were essentially identical in mean spectral response. Spectral differences between the PF and F model and previous scanners resulted in some differences between the simulated outputs to targets. The principal differences that affected the simulated sensor outputs from soybeans and/or soil were:

1. A lower upper-band edge and a narrower upper-slope interval on PF and F in band 2, resulting in lower sensor output from a soybean target than that of previous Landsat MSS's.

2. A higher lower-band edge and a higher upper-band edge on PF and F in band 3, resulting in higher sensor outputs from soybean targets than those of previous Landsats.

A higher upper-band edge and a wider bandwidth on PF and F in band 1 did not affect the outputs from soil or soybean targets. The differences between PF, F and previous scanners were usually small (i.e., differences between the PF or F and the most similar previous MSS were about the same as differences between previous MSS's). In general, therefore, these differences should not affect data utility more severely than the variability between prior Landsat MSS's.

One anomalous channel in the red band (2) on the PF scanner, with an upper-band edge 12 nm higher than those of the other channels in the band, has the greatest potential effect on the utility of Landsat-4 MSS data. This characteristic resulted in a potential within-band striping in simulated output to a vegetated target in band 2 of 6.2 percent, which was about the same as the highest observed for previous Landsat MSS's (5.4 percent). In band 4 on the PF and F scanners, the upper-band edge was also more variable than those of previous MSS's. Otherwise, the PF and F scanners were generally more uniform within bands than previous scanners.

ACKNOWLEDGEMENTS

The authors thank Inja Kim for her assistance in data entry and analysis and Jai Yuh (Santa Barbara Research Center) for his assistance in interpreting MSS test data. In addition, they thank Emmett Chappelle and Frank Wood for permission to use selected field spectral reflectance data.

REFERENCES

Duggin, M.J., and P.J. Ellis, 1980, "Limitations on the Spectral Discrimination of the Landsat MSS," Proc. 46th Annual Meeting Amer. Soc. of Photogrammetry, Falls Church, Virginia, pp. 329-334.

Felkel, E.O., K. Brinkman, R. Coon, and J. Stivers, 1977, "Five-Band Multi-Spectral Scanner--Final Report," Hughes Aircraft Co., Final Report for NASA contract NAS5-11255.

Grubbs, F.E., 1950, "Sample Criterion for Testing Outlier Observations," Annals of Mathematical Statistics, 21, pp. 27-58.

Norwood, V.T., L.R. Fernelia, and G.A. Tadler, 1972, "Multispectral Scanner System for ERTS--Four-Band Scanner System, Final Report," NASA CR-132758.

Slater, P.N., 1979, "A Re-examination of the Landsat MSS," Photogrammetric Engineering and Remote Sensing, 45(11) pp. 1479-1485.

Turner, R.E., and M.M. Spencer, 1972, "Atmospheric Model for Correction of Spacecraft Data," Proc. 8th International Symposium on Remote Sensing of Environment, Environmental Research Institute of Michigan, Ann Arbor, Michigan, pp. 895-933.

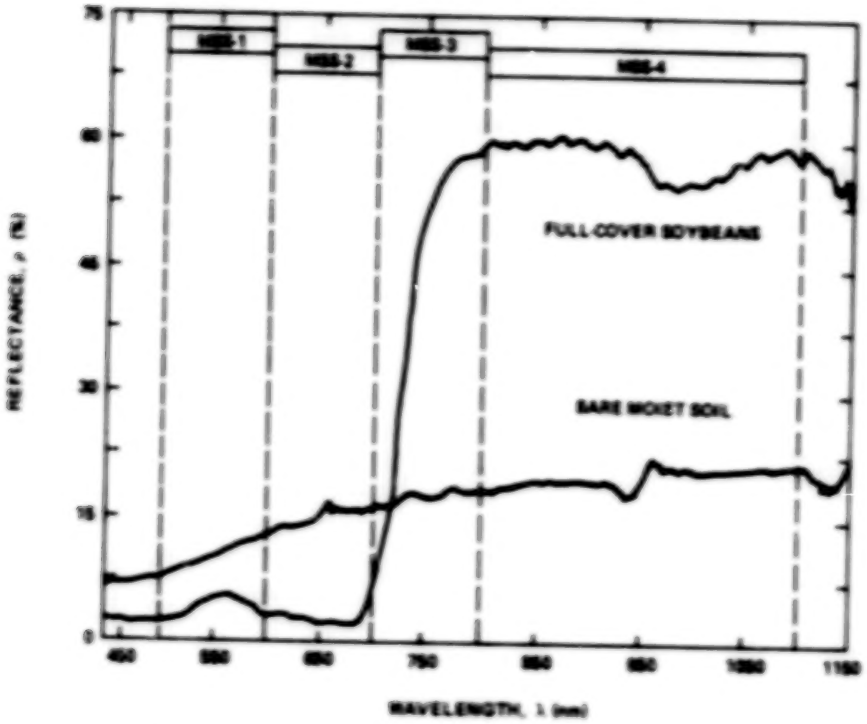

Figure 1. Reflectance spectra of soybeans and soil used for MSS output simulations.

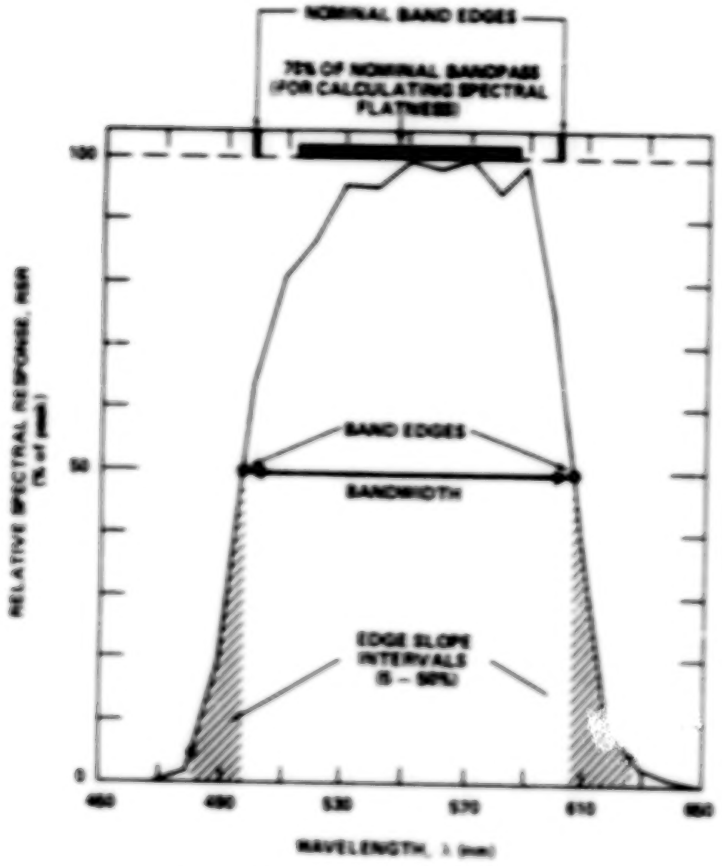

Figure 2. Key to Figures 3 and 4.

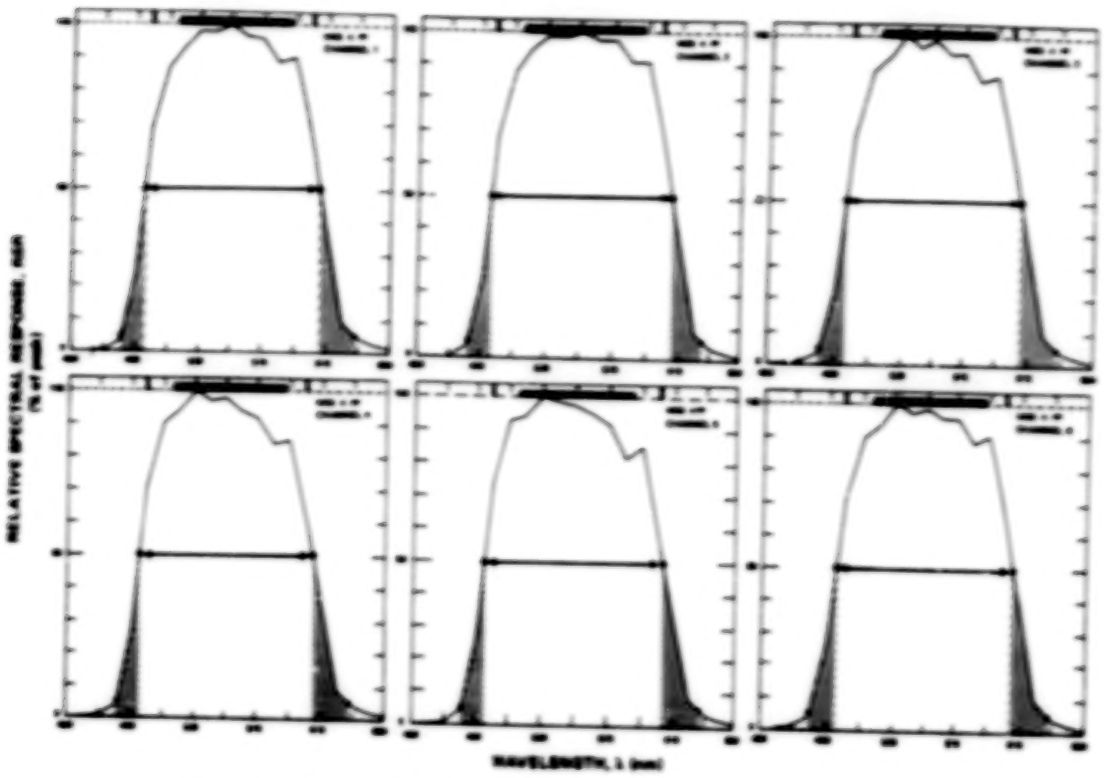

Figure 3a. Protoflight model MSS (Landsat-4) relative spectral response curves from IBM measurements (band 1).

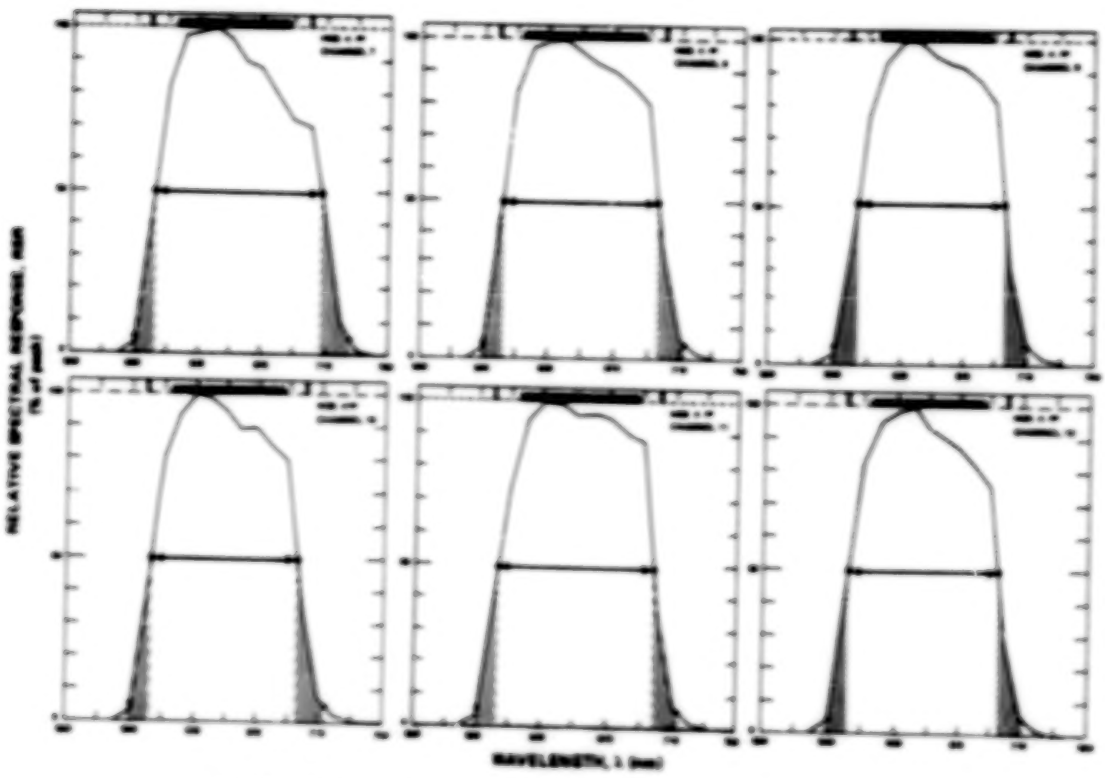

Figure 3b. Protoflight model MSS (Landsat-4) relative spectral response curves from IBM measurements (band 2).

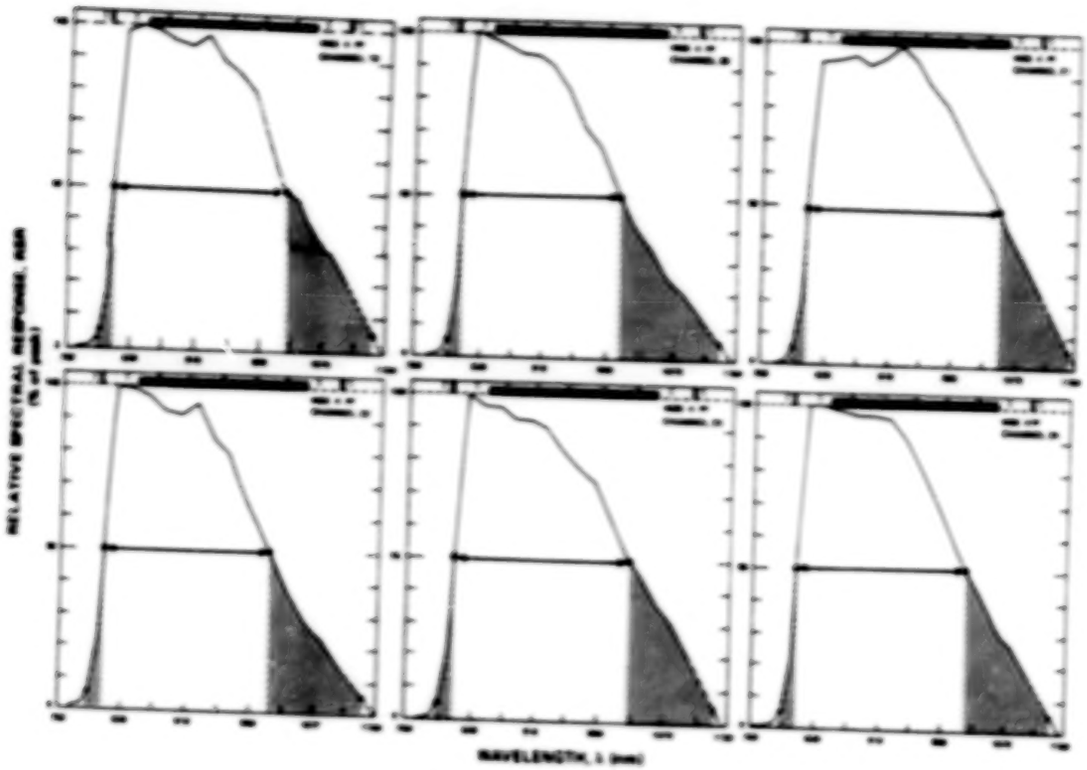

Figure 3c. Prototflight model MSS (Landsat-4) relative spectral response curves from IBEC measurements (band 3).

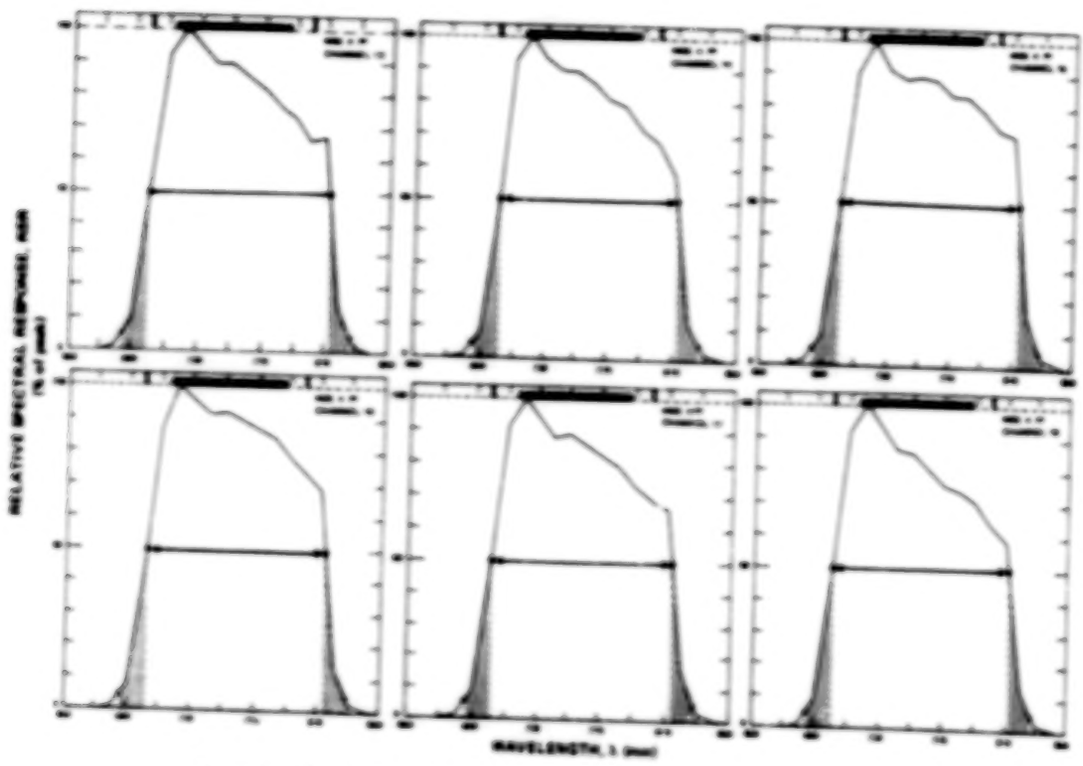

Figure 3d. Prototflight model MSS (Landsat-4) relative spectral response curves from IBEC measurements (band 4). Response measured to 1100 nm; dashed line indicates extrapolated response.

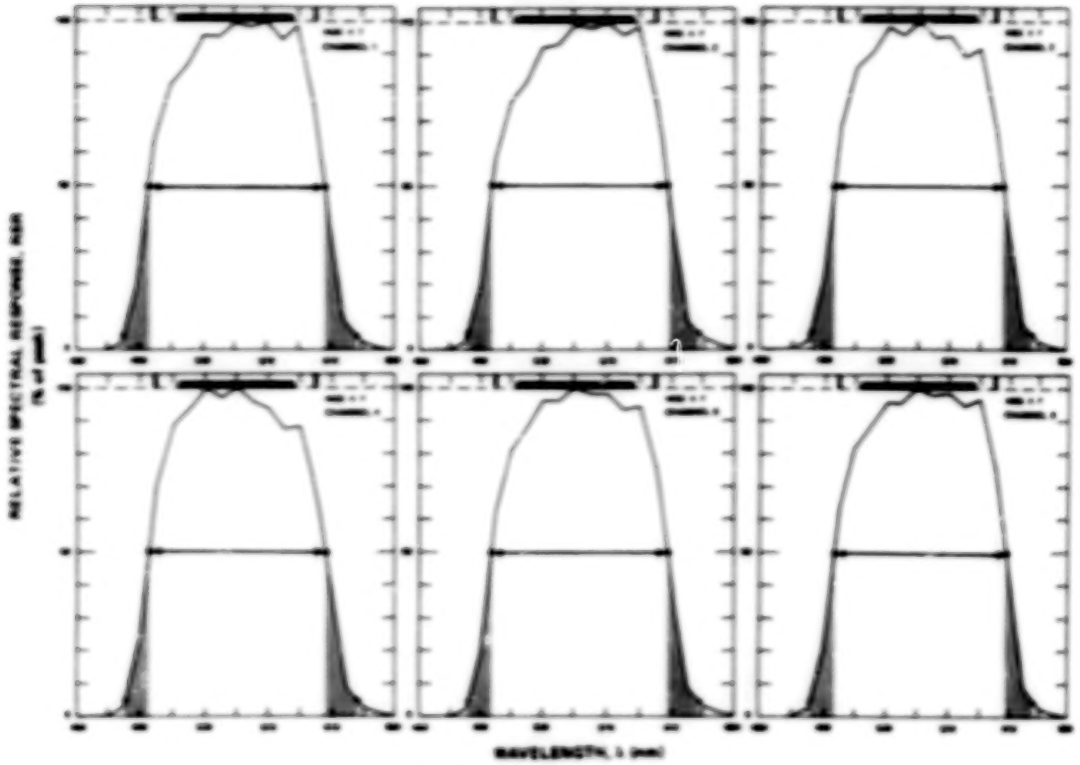

Figure 4a. Flight model MSS (Landsat-4 backup) relative spectral response curves (band 1).

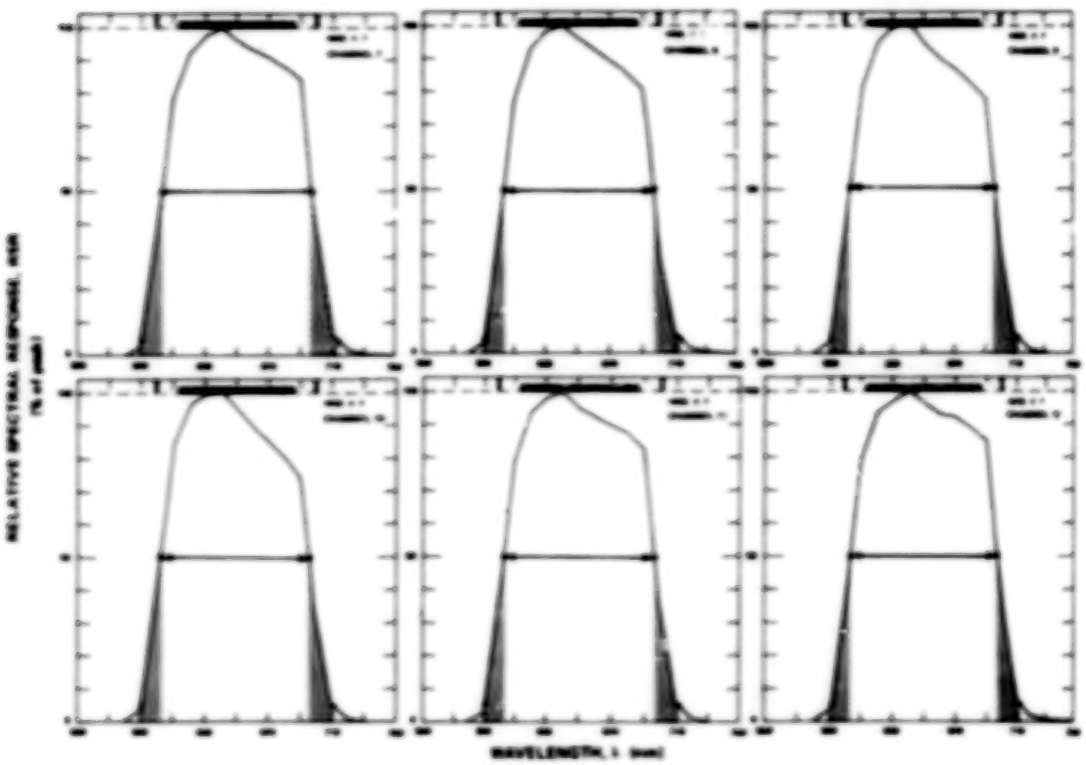

Figure 4b. Flight model MSS (Landsat-4 backup) relative spectral response curves (band 2).

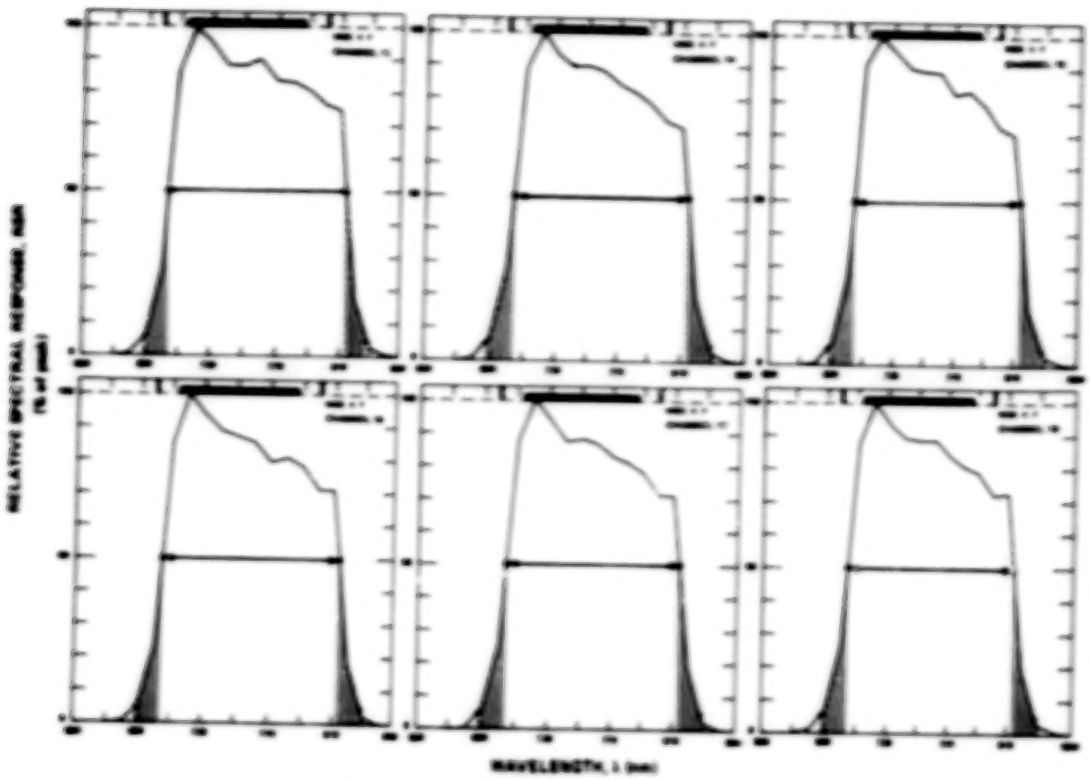

Figure 4c. Flight model MSS (Landsat-4 backup) relative spectral response curves (band 3).

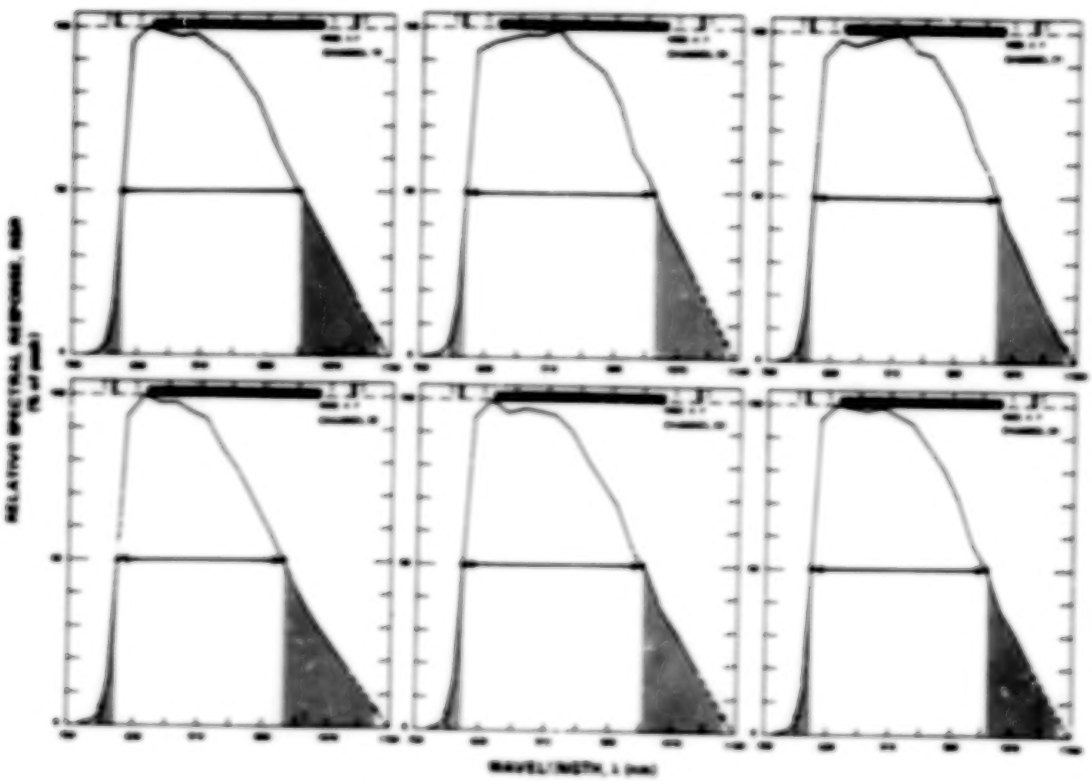

Figure 4d. Flight model MSS (Landsat-4 backup) relative spectral response curves (band 4). Response measured to 1100 nm; dashed line indicates extrapolated response.

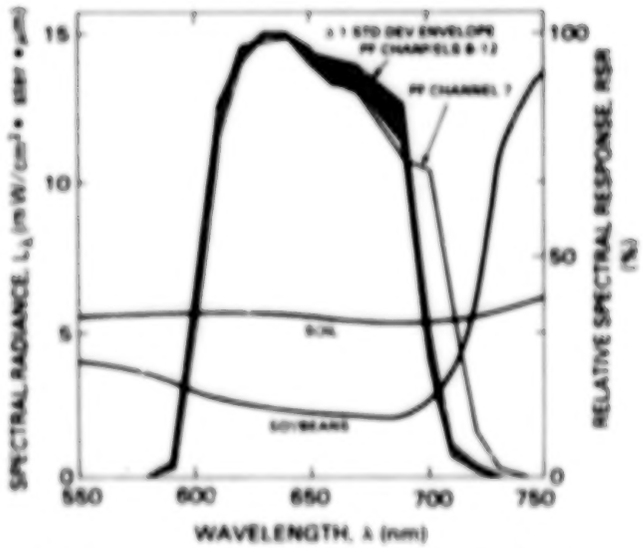

Figure 5. Protoflight model MSS (Landsat-4) band 2 (channels 7 through 12) relative spectral responses in relation to reflected radiances from soil and soybeans. Note anomalous response of channel 7 relative to channels 8 through 12.

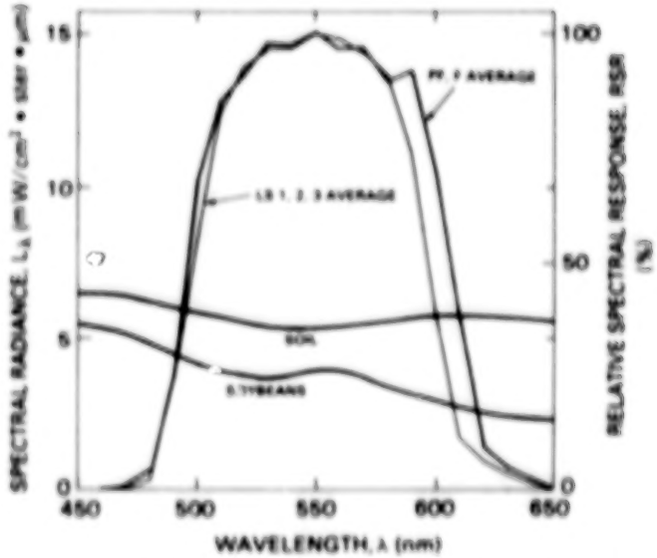

Figure 6. MSS band 1 relative spectral response averages for Landsat-4 (PF, 7) and for previous Landsats in relation to reflected radiances from soil and soybeans.

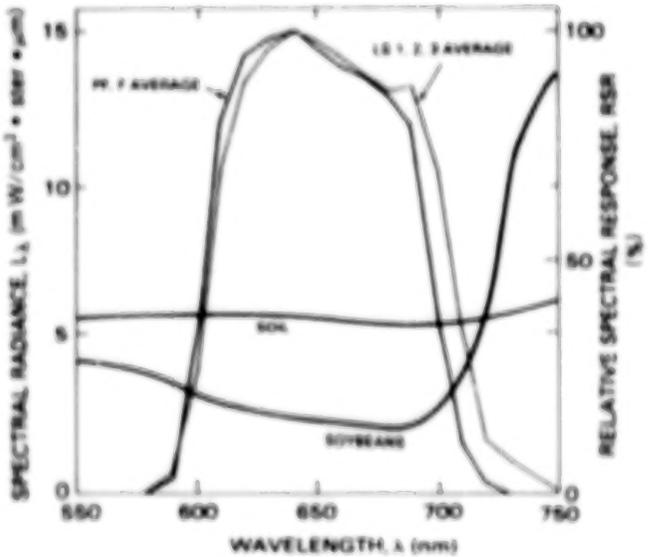

Figure 7. MSS band 2 relative spectral response averages for Landsat-4 (PF, 7) and for previous Landsats in relation to reflected radiances from soil and soybeans.

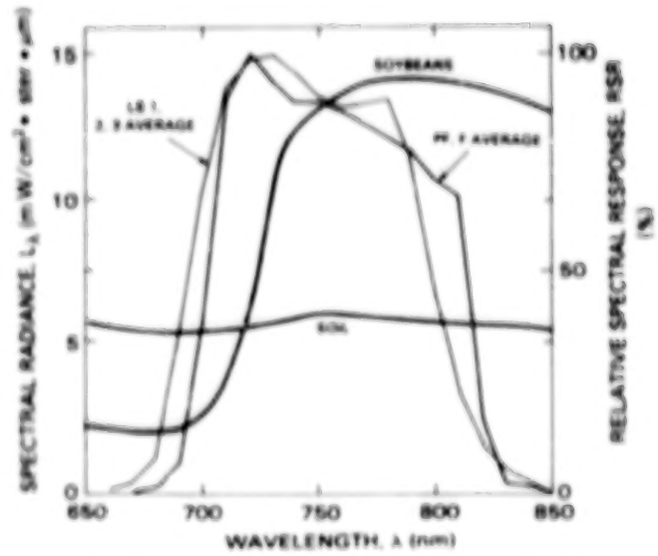

Figure 8. MSS band 3 relative spectral response averages for Landsat-4 (PF, 7) and for previous Landsats in relation to reflected radiances from soil and soybeans.

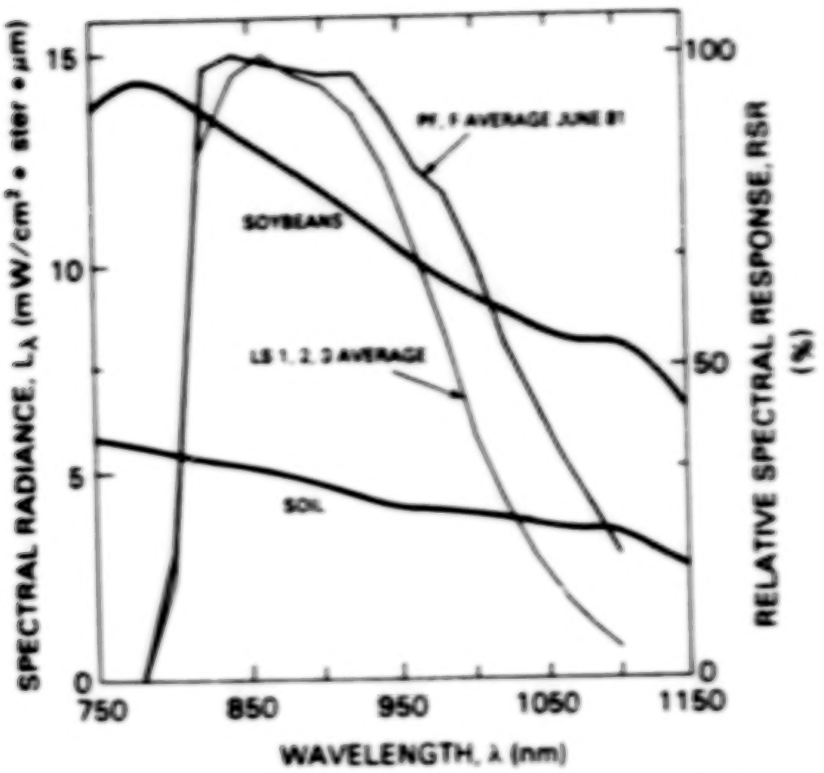

Figure 9. MSS band 4 relative spectral response average for Landsat-4 (PF, 1) and for previous Landsats in relation to reflected radiance from soil and soybeans (atmospheric water absorption not simulated).

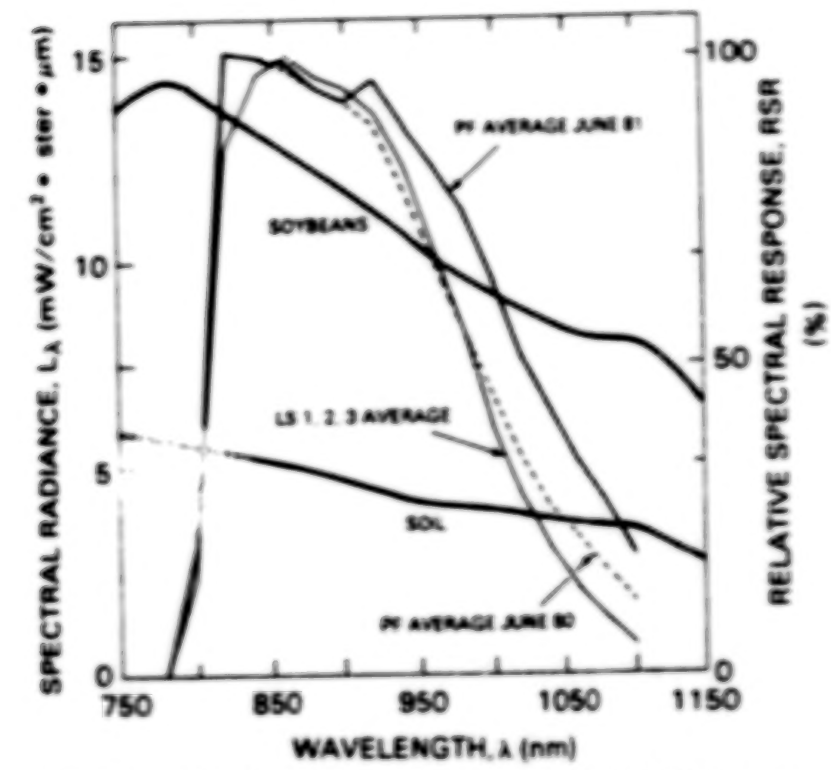

Figure 10. MSS band 4 relative spectral response for: (1) Landsat-4 PF measured June 1982, (2) Landsat-4 PF measured June 1981, and (3) Landsat 1-3 average in relation to reflected radiances from soil and soybeans (atmospheric water absorption not simulated). Note apparent large change in PF response above 900 nm between June 1982 and June 1981.

Table 1
Filter Specifications for Landsat Multispectral Scanners.

BAND	BAND EDGE (nm) HALF POWER POINTS LOWER	UPPER	BAND WIDTH (nm)	SLOPE INTERVAL (nm) FROM 5% TO 50% LOWER	UPPER	SPECTRAL FLATNESS (%) OVER CENTRAL 70% POSITIVE	NEGATIVE
1	500 ± 10	600 ± 10	—	<20	<40	<5.0	<5.0
2	600 ± 10	700 ± 10	—	<20	<45	<7.5	<7.5
3	700 ± 10	800 ± 10	—	<20	<50	<5.0	<5.0
4	800 ± 10	1100[a] ± 10	—	<35	—	<5.0	<5.0

a — UPPER BAND EDGE
NECESSARY FOR FLATNESS DETERMINATION

Table 2
Spectral Characterization of Landsat-4 MSS's by Channel: Band 1 (500 to 600 nm).

SCANNER	CHANNEL	BAND EDGE (nm) LOWER	UPPER	WIDTH[a] (nm)	SLOPE INTERVAL (nm) LOWER	UPPER	SPECTRAL FLATNESS POSITIVE	NEGATIVE
PROTO-FLIGHT	1	496	606	110	15	22	4.4	7.1[b]
	2	496	605	109	15	22	3.5	5.8[b]
	3	496	605	109	15	23	5.6[b]	9.2[b]
	4	495	604	109	15	24	6.0[b]	10.8[b]
	5	495	603	108	14	24	6.0[b]	13.1[b]
	6	495	606	110	15	22	4.8	7.8[b]
FLIGHT	1	497	607	110	15	21	4.4	12.3[b]
	2	498	607	109	16	20	6.2[b]	16.8[b]
	3	496	606	110	15	20	5.3[b]	6.8[b]
	4	496	606	110	15	21	4.9	8.8[b]
	5	497	607	110	16	21	4.8	11.5[b]
	6	497	607	111	16	19	4.6	11.1[b]

a— NO FILTER SPECIFICATION
b— FAILS TO MEET FILTER SPECIFICATIONS

Table 3
Spectral Characterization of Landsat-4 MSS's by Channel: Band 2 (600 to 700 nm).

SCANNER	CHANNEL	BAND EDGE (nm) LOWER	UPPER	WIDTH[a] (nm)	SLOPE INTERVAL (nm) LOWER	UPPER	SPECTRAL FLATNESS POSITIVE	NEGATIVE
PROTO-FLIGHT	7	603	708*	105*	12	19	8.2[b]	17.2[b]
	8	602	696	94	12	16	6.4	11.6[b]
	9	603	696	92	12	14	6.6	11.0[b]
	10	603	696	94	12	18	7.8[b]	11.1[b]
	11	604	698	94	13	17	4.5	11.7[b]
	12	602	695	93	12	15	8.2[b]	14.5[b]
FLIGHT	7	603	697	94	13	17	6.9	9.6[b]
	8	603	696	93	13	16	7.3	10.4[b]
	9	603	696	94	12	16	9.1[b]	13.3[b]
	10	602	696	93	12	14	9.1[b]	16.0[b]
	11	603	697	94	12	15	7.0	8.6[b]
	12	603	697	94	12	15	6.4	8.5[b]

a— NO FILTER SPECIFICATION
b— FAILS TO MEET FILTER SPECIFICATION
* —REJECTABLE AS OUTLIER: $\alpha = 0.01$

Table 4
Spectral Characterization of Landsat-4 MSS's by Channel: Band 3 (700 to 800 nm).

SCANNER	CHANNEL	BAND EDGE (nm) LOWER	UPPER	WIDTH[a] (nm)	SLOPE INTERVAL (nm) LOWER	UPPER	SPECTRAL FLATNESS POSITIVE	NEGATIVE
PROTO-FLIGHT	13	700	813[b]	113	16	14	13.7[b]	14.2[b]
	14	701	812[b]	110	16	15	11.6[b]	15.7[b]
	15	701	814[b]	113	15	14	12.9[b]	8.6[b]
	16	702	814[b]	111	15	14	7.8[b]	10.0[b]
	17	701	813[b]	112	15	15	13.0[b]	13.0[b]
	18	701	812[b]	111	15	16	18.5[b]	15.3[b]
FLIGHT	13	704	814[b]	110	16	14	11.8[b]	8.3[b]
	14	704	814[b]	110	17	14	12.2[b]	10.3[b]
	15	704	814[b]	110	17	14	11.8[b]	9.5[b]
	16	704	814[b]	110	14	14	14.4[b]	9.6[b]
	17	704	814[b]	110	16	14	13.6[b]	9.7[b]
	18	704	814[b]	110	17	14	12.0[b]	10.4[b]

a — NO FILTER SPECIFICATION
b — FAILS TO MEET FILTER SPECIFICATION

Table 5
Spectral Characterization of Landsat-4 MSS's by Channel: Band 4 (800 to 1100 nm).

SCANNER	CHANNEL	BAND EDGE (nm) LOWER	UPPER	WIDTH[a] (nm)	SLOPE INTERVAL (nm) LOWER	UPPER[a]	SPECTRAL FLATNESS POSITIVE	NEGATIVE
PROTO-FLIGHT	19	808	1025	217	23	110	25.5[b]	48.5[b]
	20	808	1006	199	23	120	38.7[b]	62.2[b]
	21	808	1049	241	24	94	19.5[b]	44.8[b]
	22	807	1012	205	23	117	34.9[b]	59.5[b]
	23	807	1025	218	23	108	31.1[b]	50.2[b]
	24	807	1018	211	23	112	29.3[b]	56.7[b]
FLIGHT	19	809	1030	221	23	104	24.0[b]	51.3[b]
	20	809	1048	239	23	92	17.6[b]	46.8[b]
	21	809	1047	238	23	93	16.9[b]	46.5[b]
	22	809	1014	206	23	119	33.4[b]	57.7[b]
	23	809	1034	226	23	103	24.9[b]	51.3[b]
	24	809	1040	231	22	98	21.1[b]	51.2[b]

a — NO FILTER SPECIFICATION
b — FAILS TO MEET FILTER SPECIFICATION

Table 6

Band 1 (500 to 600 nm) Spectral Characterization by Means and Standard Deviations: MSS-1, 2, 3, PF and F.

	SCANNER	BAND EDGE (nm) LOWER	BAND EDGE (nm) UPPER	WIDTH[a] (nm)	SLOPE INTERVAL (nm) LOWER	SLOPE INTERVAL (nm) UPPER	SPECTRAL FLATNESS POSITIVE	SPECTRAL FLATNESS NEGATIVE
MEANS	PF	495	606	109	15	23	5.1[b]	8.9[b]
	F	497	607	109	15	21	5.0	11.2[b]
	1*	501	599	98	15	27	7.1[b]	16.1[b]
	1**	499	597	98	15	27	6.1[b]	14.6[b]
	2	497	598	101	15	22	5.4[b]	14.1[b]
	3	497	593	96	16	22	5.4[b]	19.2[b]
STANDARD DEVIATIONS	PF	0.5	1.2	0.8	0.3	1.0	1.0	2.7
	F	0.8	0.8	0.5	0.6	0.7	0.6	3.4
	1*	6.5	4.1	3.5	1.6	5.6	2.4	6.4
	1**	5.3	3.0	3.5	1.8	5.4	0.4	5.8
	2	1.4	1.4	1.8	1.2	0.6	2.4	3.5
	3	3.7	2.5	3.8	3.2	3.4	1.5	7.8

*WITH OUTLIER CHANNEL INCLUDED
**WITH OUTLIER CHANNEL EXCLUDED

a — NO FILTER SPECIFICATION
b — FAILS TO MEET FILTER SPECIFICATION

BOXES INDICATE CHARACTERISTICS WHERE DIFFERENCES BETWEEN PF OR F AND ALL PREVIOUS SCANNERS (1,2,3) WERE GREATER THAN DIFFERENCES BETWEEN TWO SETS OF PF MEASUREMENTS.

Table 7

Band 2 (600 to 700 nm) Spectral Characterization by Means and Standard Deviations: MSS-1, 2, 3, PF and F.

	SCANNER	BAND EDGE (nm) LOWER	BAND EDGE (nm) UPPER	WIDTH[a] (nm)	SLOPE INTERVAL (nm) LOWER	SLOPE INTERVAL (nm) UPPER	SPECTRAL FLATNESS POSITIVE	SPECTRAL FLATNESS NEGATIVE
MEANS	PF*	603	696	95	12	16	7.0	12.9[b]
	PF**	603	696	93	12	16	6.7	12.0[b]
	F	603	697	94	12	15	7.6[b]	11.1[b]
	1	603	701	97	15	26	9.0[b]	13.3[b]
	2*	607	710	103	14	30	7.9[b]	18.0[b]
	2**	607	710	103	14	29	7.8[b]	16.8[b]
	3	606	705	100	14	31	7.2	17.2[b]
STANDARD DEVIATIONS	PF*	0.7	4.7	4.8	0.5	1.9	1.4	2.5
	PF**	0.8	0.8	0.6	0.5	1.4	1.5	1.4
	F	0.4	0.6	0.5	0.4	0.9	1.2	3.0
	1	3.5	2.2	2.8	1.7	3.4	3.4	2.8
	2*	0.6	0.8	1.0	1.2	3.6	1.1	4.5
	2**	0.6	0.9	1.1	1.2	1.0	1.2	3.8
	3	0.9	1.2	0.8	0.8	2.0	2.0	4.8

*WITH OUTLIER CHANNEL INCLUDED
**WITH OUTLIER CHANNEL EXCLUDED

a — NO FILTER SPECIFICATION
b — FAILS TO MEET FILTER SPECIFICATION

BOXES INDICATE CHARACTERISTICS WHERE DIFFERENCES BETWEEN PF OR F AND ALL PREVIOUS SCANNERS (1,2,3) WERE GREATER THAN DIFFERENCES BETWEEN TWO SETS OF PF MEASUREMENTS.

Table 8
Band 3 (700 to 800 nm) Spectral Characterization by Means and Standard Deviations: MSS-1, 2, 3, PF and F.

	SCANNER	BAND EDGE (nm) LOWER	BAND EDGE (nm) UPPER	WIDTH[a] (nm)	SLOPE INTERVAL (nm) LOWER	SLOPE INTERVAL (nm) UPPER	SPECTRAL FLATNESS POSITIVE	SPECTRAL FLATNESS NEGATIVE
	PF	701	813[b]	112	15	15	13.2[b]	12.8[b]
	F	704	814[b]	110	16	14	12.6[b]	9.6[b]
MEANS	1	694	800	105	19	35	7.2[b]	7.4[b]
	2	697	802	106	16	34	8.4[b]	7.9[b]
	3	693	793	100	19	32	9.9[b]	22.2[b]
	PF	0.7	0.9	1.1	0.3		2.9*	2.9*
	F	0.3	0.2	0.3	1.0		1.1*	0.8*
STANDARD DEVIATIONS	1	0.9	1.0	0.9	2.0	3.8	3.2	2.9
	2	1.1	2.3	2.1	0.6	2.7	3.0	1.9
	3	1.8	1.6	0.8	1.4	1.1	2.7	3.4

*PF, F DIFFERENCE EXCEEDS DIFFERENCE BETWEEN TWO SETS OF PF MEASUREMENTS

a — NO FILTER SPECIFICATION
b — FAILS TO MEET FILTER SPECIFICATION

BOXES INDICATE CHARACTERISTICS WHERE DIFFERENCES BETWEEN PF OR F AND ALL PREVIOUS SCANNERS (1,2,3) WERE GREATER THAN DIFFERENCES BETWEEN TWO SETS OF PF MEASUREMENTS.

Table 9
Band 4 (800 to 1100 nm) Spectral Characterization by Means and Standard Deviations: MSS-1, 2, 3, PF and F.

	SCANNER	BAND EDGE (nm) LOWER	BAND EDGE (nm) UPPER	WIDTH[a] (nm)	SLOPE INTERVAL (nm) LOWER	SLOPE INTERVAL (nm) UPPER[a]	SPECTRAL FLATNESS POSITIVE	SPECTRAL FLATNESS NEGATIVE
	PF	808	1023	215	23	110	29.8[b]	53.7[b]
	F	809	1036	227	23	101	23.0[b]	50.8[b]
MEANS	1	810	989	179	22	120	46.0[b]	74.5[b]
	2	807	990	183	23	118	45.4[b]	75.9[b]
	3	812[b]	979	167	24	108	56.4[b]	80.7[b]
	PF	0.5	14.9	14.6	0.2	9.2	6.8	6.8*
	F	0.1	12.5	12.5	0.4	9.9	6.0	4.1*
STANDARD DEVIATIONS	1	1.2	3.5	3.7	2.1	7.2	2.3	3.1
	2	2.0	4.0	5.3	0.8	2.7	4.7	1.1
	3	0.9	7.9	7.6	1.0	3.0	11.7	2.4

*PF, F DIFFERENCE EXCEEDS DIFFERENCE BETWEEN TWO SETS OF PF MEASUREMENTS

BOXES INDICATE CHARACTERISTICS WHERE DIFFERENCES BETWEEN PF OR F AND ALL PREVIOUS SCANNERS (1,2,3) WERE GREATER THAN DIFFERENCES BETWEEN TWO SETS OF PF MEASUREMENTS.

a — NO FILTER SPECIFICATION
b — FAILS TO MEET FILTER SPECIFICATION

Table 10
Simulated MSS Band Mean Outputs to Soybean and Soil Targets: MSS-1, 2, 3, PF and F.

TARGET	SENSOR SYSTEM	MEANS[a] (DIGITAL MSS COUNTS) BAND 1[b]	BAND 2[b]	BAND 3[b]	BAND 4[b]
SOYBEANS	LS4-PF	19.36	14.89 (14.76)[c]	80.82*	45.80
	LS4-F	19.25	14.72	82.81*	45.39
	LS1	19.46 (19.55)[c]	15.43	76.95	47.14
	LS2	19.58	16.24 (16.13)[c]	78.58	47.24
	LS3	19.77	15.36	73.93	47.55
SOIL	LS4-PF	28.39	34.75[d]	41.02	18.61
	LS4-F	28.39	34.75	41.05	18.48
	LS1	28.32[d]	34.73	41.04	19.02
	LS2	28.34	34.66[d]	41.05	19.07
	LS3	28.33	34.66	41.10	19.15

a — AT SATELLITE SENSOR RESPONSE, NADIR—LOOKING FOR 40° SOLAR ZENITH ANGLE AND 20 km VISIBILITY; UNITS ARE SIMULATED NON-TRUNCATED MSS DIGITAL COUNTS WITH MAXIMUM SPECIFIED RADIANCE SCALED TO 127.99 FOR BANDS 1, 2, 3 AND 63.99 FOR BAND 4.

b — LANDSAT-4 BANDS 1, 2, 3 AND 4 CORRESPOND TO BANDS 4, 5, 6 AND 7, RESPECTIVELY ON PREVIOUS LANDSATS.

c — MEAN IN PARENTHESES IS WITH OUTLIER CHANNEL EXCLUDED

d — EXCLUSION OF OUTLIER DID NOT CHANGE BAND MEAN

*PF, F DIFFERENCE EXCEEDS: (1) DIFFERENCE BETWEEN SIMULATIONS RUN WITH EACH SET OF PF MEASUREMENTS SEPARATELY AND (2) 0.30 DIGITAL COUNTS

BOXES INDICATE BANDS WHERE OUTPUT DIFFERENCES BETWEEN PF OR F AND ALL PREVIOUS SCANNERS (1,2,3) EXCEED: (1) AND (2) AS ABOVE.

Table 11
Simulated MSS Output Differences Between Channels within a Band (Maximum-Minimum) Resultant From Spectral Differences Between Channels: MSS-1, 2, 3, PF and F.

TARGET	SENSOR	DIGITAL COUNTS BAND 1	BAND 2	BAND 3	BAND 4	PERCENT BAND 1	BAND 2	BAND 3	BAND 4
SOYBEANS	LS4-PF	0.11	0.91*	2.23*	1.43*	0.6	6.2*	2.8*	3.1*
	LS4-F	0.17	0.10*	0.78*	1.04*	0.9	0.7*	0.5*	2.3*
	LS1	0.75	0.12	2.39	0.63	3.9	0.8	3.1	1.3
	LS2	0.16	0.77	3.63	0.39	0.8	4.8	4.6	0.8
	LS3	0.30	0.16	4.01	0.80	1.5	1.0	5.4	1.7
SOIL	LS4-PF	0.03	0.07	0.10	0.46	0.1	0.2	0.2	2.5
	LS4-F	0.01	0.06	0.02	0.32	0.1	0.2	0.1	1.8
	LS1	0.10	0.09	0.04	0.21	0.3	0.3	0.1	1.1
	LS2	0.06	0.03	0.06	0.12	0.2	0.1	0.2	0.6
	LS3	0.07	0.09	0.13	0.26	0.2	0.3	0.3	1.4

*PF, F DIFFERENCE EXCEEDS: (1) DIFFERENCE BETWEEN SIMULATIONS RUN WITH EACH SET OF PF MEASUREMENTS SEPARATELY AND (2) 0.30 DIGITAL COUNTS

BOXES INDICATE BANDS WHERE OUTPUT DIFFERENCES BETWEEN PF OR F AND ALL PREVIOUS SCANNERS EXCEED (1) AND (2) AS ABOVE; THIS CAN REPRESENT EITHER BETTER OR POORER PERFORMANCE

Table 12
Illustrative Landsat-2 MSS Observations* for Selected Targets for Comparison to Simulated Results†: Means and Standard Deviations.

TEST SITE CATEGORY	NUMBER OF PIXELS	MEANS (STANDARD DEVIATIONS) (DIGITAL MSS COUNTS) BAND 1 (4)	BAND 2 (5)	BAND 3 (6)	BAND 4 (7)
SOYBEANS	15	19.8 (1.4)	16.9 (1.1)	77.3 (7.3)	41.1 (3.8)
OATS (CUT)	24	23.6 (2.0)	27.2 (2.7)	40.8 (2.5)	18.4 (1.2)
WHEAT (CUT)	46	21.3 (2.5)	25.6 (2.7)	38.6 (4.9)	17.0 (2.8)

*SCENE 82905145015 (PATH 17 ROW 30)
JULY 15, 1977 NOMINAL SZA—38°
CENTER FIELD PIXELS, CENTRAL NEW YORK STATE

†IN GROUND PROCESSING OF ACTUAL MSS DATA, AFTER DECOMPRESSION, THE MSS DATA IS RESCALED USING SENSOR SPECIFIC SATURATION RADIANCES AND OFFSETS. AS SUCH THE SIMULATED OUTPUTS MAY NOT BE STRICTLY COMPARABLE TO CALIBRATED ACTUAL MSS DATA.

APPENDIX A

RELATIVE SPECTRAL RESPONSE MEASUREMENT PROCEDURE

The relative spectral responses of the protoflight and flight model MSS's were measured at Santa Barbara Research Center. The protoflight model RSR was measured in June 1980 and June 1981. The flight model RSR was first measured in March 1981, then the fiber optics assembly was replaced, and it was remeasured in June 1981. The earlier flight model measurements are considered inapplicable due to this optical change.

The instrumentation used to measure the relative spectral response of an MSS consisted of the following:

1. A tungsten-halogen light source

2. A plane diffraction grating monochromator

3. Two beam steering mirrors

4. A calibrated reference silicon photo diode

5. The MSS collimator

White light from the tungsten-halogen source impinged on the entrance slit of the monochromator. Within the monochromator dispersion was accomplished by means of a plane diffraction grating equipped with sine bar motion. A counter on the drive screw read wavelength directly in nanometers. The entrance and exit slits were adjusted to obtain 4 nanometer spectral resolution at any particular wavelength setting. Light exiting the monochromator impinged on a fiber optic bundle which transferred the light to the focal plane of the MSS collimator. The two beam steering mirrors located at this point chopped the light, alternately focusing it on the reference detector and letting it pass into the collimator. The collimator, optically aligned with the MSS, passed the light to the MSS, where the slit image completely overfilled all 24 channels simultaneously. The outputs from the reference detector and the MSS detectors were sampled at 10 nm intervals from 450 to 800 nm and 20 nm intervals from 800 to 1100 nm. The ratio of these two outputs, normalized to 100% maximum for each channel, was the relative spectral response.

APPENDIX B

PROTOFLIGHT AND FLIGHT MODEL FILTER CHARACTERISTICS

With the exception of the upper-band edge of band 4 (800 to 1100 nm), which is determined by the silicon photodiode response, the spectral filters are the primary components that determine the spectral response of the various channels. Tables B-1 and B-2 list the spectral response (transmission) characteristics of the filters only. These data were computed from curves supplied by Hughes Airfcraft Company (unpublished data, 1981) and subsequently digitized at 10-nm intervals for bands 1 through 3 and 20-nm intervals for band 4.

Technically, most of the band 1 filters, having negative deviations greater than 5 percent, failed the flatness criteria. However, because the flatness criteria were considered to be met if the sum of the positive and negative deviations did not exceed 10 percent, they passed. A similar situation existed for band 2; however, the sum of the positive and negative deviations typically slightly exceeded the specified 15 percent. Otherwise the filter specifications were met.

The band edges, widths, and slope intervals of the filters compared favorably to the total system response for bands 1, 2, and 4, being generally within 2 nanometers of each other. For band 3, the measured filter band edges were lower than the system response band edges. The upper-band edge of the system response was generally 10 nm greater than the filters, except for three channels, where the difference was 5 to 6 nanometers. Smaller differences with the same pattern existed for the lower-band edge. One unexplained observation was that filters 13, 15, and 18 on the F model, which were offset 4 nm relative to the other filters, did not show the same pattern for the total system response.

There are several possible explanations for this discrepancy. One is that there was a difference in the spectral calibration of the spectrometer used to measure the filter transmission coefficients and the monochromator used to measure the relative spectral responses (i.e., one or both were spectrally improperly calibrated). This possibility appears unlikely because the band 4 filters, which were measured with the same spectrometer at approximately the same time as the band 3 filters and whose lower-band edge corresponds approximately with the upper-band edge for band 3, showed little difference in their lower-band edge when compared to the relative system response lower-band edge (Figure B-1).

A second possibility is that the band 3 filters have been changing in their bandpass with time. The spectral characteristics of all the band 3 filters except for F 13, 15, and 18 were measured in December 1978. F 13, 15, and 18 were measured in November 1979. The relative spectral responses reported herein were measured in June 1981. When plotted versus time, a monotonic change is suggested (Figure B-1). When data from the first relative spectral response runs on the PF are included (June 1980), the curve shows a leveling-off trend. This suggests that the filters ceased to change after they were incorporated into the scanner. One explanation is that one or several layers of the many-layered interference filters were disturbed during storage or handling. The adsorption of water by interstitial voids or structural changes in the layers are possibilities. This multilayered structure principally determines the upper-band edge, whereas a color absorption filter primarily determines the lower-band edge. Thus, a

Table B-1
MSS Filter Spectral Characterization by Channel: PF for Landsat-4

Band	Channel	Band Edge (nm)		Width* (nm)	Slope Interval (nm)		Spectral Flatness		Maximum Transmission (%)
		Lower	Upper		Lower	Upper	Positive	Negative	
1	1	495	607	112	14	21	2.5	5.8†	93
	2	495	605	110	15	21	2.5	5.8†	93
	3	494	605	111	14	21	2.1	5.6†	93
	4	494	606	111	14	21	2.1	5.6†	93
	5	494	605	112	13	21	2.1	5.0	93
	6	493	604	111	13	22	1.7	4.9	93
2	7	603	710	107	12	16	3.2	13.1†	95
	8	601	697	96	13	16	3.3	12.1†	94
	9	602	697	95	13	16	3.3	13.8†	94
	10	602	698	96	12	17	2.8	13.1†	94
	11	602	697	95	12	18	3.3	13.2†	94
	12	602	697	95	13	17	3.3	13.8†	94
3	13	696	804	107	14	14	1.5	2.7	96
	14	697	804	107	15	13	1.4	2.9	96
	15	696	804	108	14	13	1.8	2.4	96
	16	697	804	107	15	13	1.1	2.2	94
	17	697	804	107	15	13	1.3	2.8	98
	18	697	804	108	14	13	2.1	3.1	98
4	19	806	–	–	24	–	2.4	3.0	96
	20	806	–	–	24	–	2.0	3.3	96
	21	806	–	–	24	–	1.8	4.6	96
	22	806	–	–	24	–	1.8	3.5	96
	23	806	–	–	24	–	2.4	2.9	96
	24	806	–	–	24	–	1.6	3.7	96

*No filter specification.
†Fails to meet filter specification.

Table B-2
MSS Filter Spectral Characterization by Channel: F for Landsat-4 Backup

Band	Channel	Band Edge (nm)		Width* (nm)	Slope Interval (nm)		Spectral Flatness		Maximum Transmission (%)
		Lower	Upper		Lower	Upper	Positive	Negative	
1	1	495	606	111	16	23	2.2	5.4†	94
	2	494	607	112	15	20	2.4	5.8†	93
	3	494	605	111	14	23	2.3	4.2	94
	4	494	605	111	14	24	3.6	5.8†	94
	5	495	605	111	14	21	2.6	5.7†	93
	6	494	606	112	15	21	2.1	5.6†	93
2	7	602	696	95	11	14	2.7	12.1†	94
	8	601	696	96	10	14	3.2	13.3†	94
	9	601	697	95	11	14	3.0	12.9†	94
	10	601	696	94	11	14	3.4	12.9†	95
	11	601	696	95	11	15	2.6	12.1†	94
	12	601	696	95	11	14	2.9	13.0†	94
3	13	701	808	108	17	12	2.1	2.1	98
	14	697	804	107	15	13	1.6	1.5	98
	15	701	808	107	17	12	1.3	1.8	96
	16	698	804	106	15	13	1.8	2.4	97
	17	698	804	106	16	13	2.0	2.3	97
	18	701	809	108	16	14	1.5	2.7	98
4	19	808	–	–	24	–	2.3	4.1	96
	20	806	–	–	24	–	2.1	4.2	97
	21	807	–	–	23	–	2.7	3.6	97
	22	808	–	–	24	–	2.0	4.4	95
	23	808	–	–	24	–	3.8	4.8	97
	24	808	–	–	24	–	3.2	5.9	96

*No filter specification.
†Fails to meet filter specification.

disturbance to the interference layer structure would more likely affect the upper-band edge, as was observed (Yuh, private communication).

When expressed as the sum of the positive and negative components, the spectral flatness criteria were always lower for the filters than for the entire system. This indicates that the principal effect of the detectors and optics is to degrade the flatness of the spectral response.

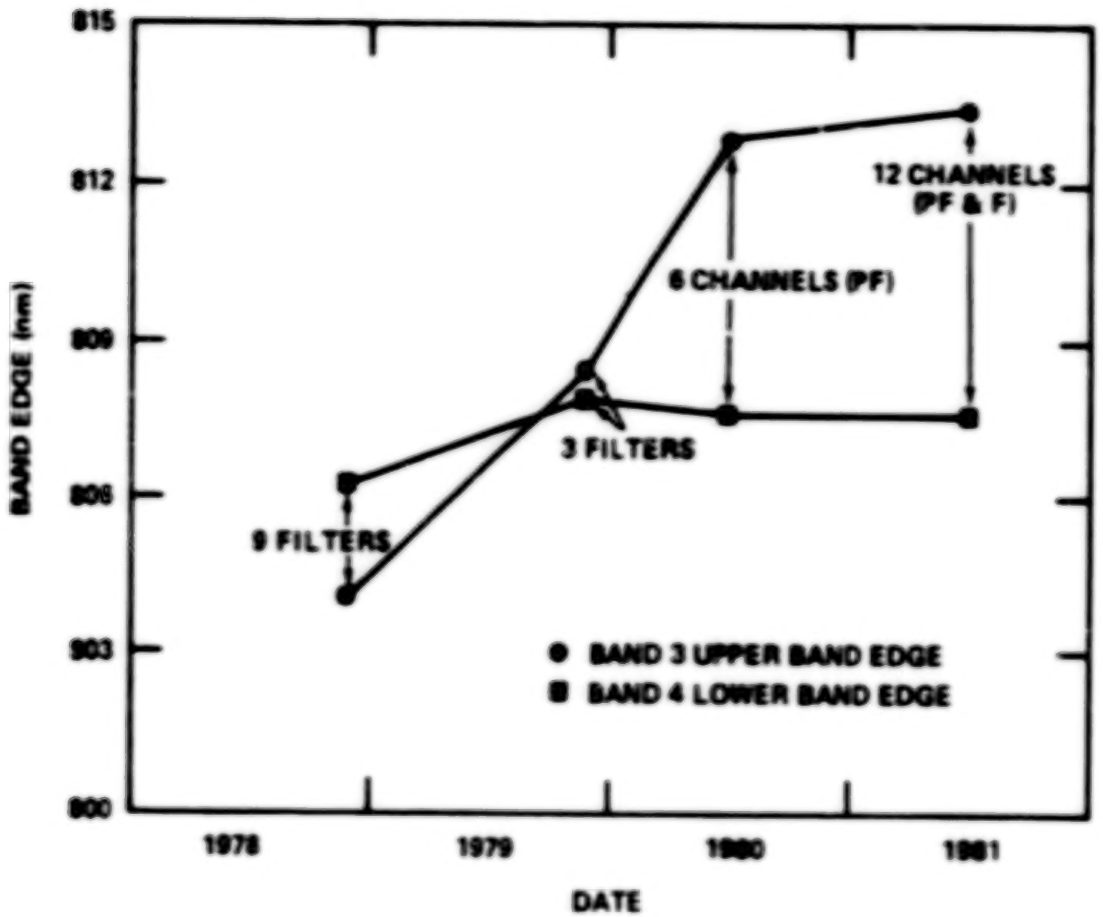

Figure B-1. Possible time dependence of upper-band edge for MSS-4 band 3 filters.

APPENDIX C

REPRODUCIBILITY OF RELATIVE SPECTRAL RESPONSE MEASUREMENTS

Only for the PF scanner was more than one set of relative spectral response (RSR) measurements available for the same unaltered scanner. The second set was collected in June 1980 (Table C-1), a year before the RSR measurements presented in the main text were acquired. The differences between the two sets of RSR measurements resulted from the composite effects of: (1) the stability of the alignment and calibration of the test equipment used to measure RSR, (2) the stability of the scanner spectral response itself, and (3) the reproducibility of the digitization of the RSR curves. Note that the June 1980 PF RSR curves were more difficult to digitize than the June 1981 curves.

Table C-2 lists the differences in the means and standard deviations of the PF RSR characteristics. Several explanations are suggested for the large band 4 mean upper-band edge (and flatness) differences that were measured: (1) a drift in the response of the reference photodiode used in measuring RSR, (2) poorer monochrometer-to-collimator alignment for the earlier tests, or (3) instrument operating temperature differences between the tests (Yuh, private communication).

The RSR parameters were categorized on the basis of their expected reproducibility, and a threshold difference for each category was established for use in comparing multispectral scanners. All the band edges (except for band 4 upper edge), widths (except for band 4) and slope intervals (except for band 4 upper slope) are primarily filter-determined and were deemed of similar reproducibility. Thresholds of 3-nm for means and 1.8 nm for standard deviations, (the maximum observed differences as shown in Table C-2) were established. The other categories that were established were:

1. The principally detector-determined characteristics of band 4 upper-band edge, width, and upper slope interval with thresholds of 33 nm for means and 2.7 nm for standard deviations

2. The positive spectral flatness for bands 1 thorugh 3 with thresholds of 4 percent for means and 0.9 percent for standard deviations

3. The negative spectral flatness for bands 1 through 3 with thresholds of 6 and 1.5 percent

4. The positive spectral flatness for band 4, 19 and 2.4 percent

5. The negative spectral flatness for band 4, 12 and 2.5 percent

Simulated outputs for soil and soybean targets were also generated by using the June 1980 data, and differences were computed between these outputs and the simulated outputs by using the June 1981 RSR data (Table C-3).

Table C-1
MSS Spectral Characteristics by Channel: PF for Landsat-4 (June 1982)

Channel	Band Edge (nm)		Width* (nm)	Slope Interval (nm)		Spectral Flatness (%)	
	Lower	Upper		Lower	Upper	Positive	Negative
1	498	607	110	17	22	10.6†	13.8†
2	497	606	109	17	22	9.7†	16.1†
3	498	606	109	16	21	9.1†	13.8†
4	497	607	110	17	21	7.5†	17.2†
5	497	605	109	19	23	7.2†	13.2†
6	498	607	108	17	22	11.1†	16.1†
7	604	713‡	110‡	13	15	5.0	12.4†
8	604	700	96	14	16	4.6	16.3†
9	604	696	92	14	18	3.1	17.5†
10	606	701	95	15	15	3.9	23.6†
11	603	700	97	13	16	3.4	17.2†
12	604	698	94	14	18	4.5	13.2†
13	702	813†	111	16	15	14.1†	13.8†
14	702	813†	109	12	14	15.2†	16.5†
15	702	814†	111	18	14	11.4†	12.0†
16	703	813†	109	12	15	10.4†	10.0†
17	702	814†	111	15	15	10.8†	12.5†
18	703	813†	110	18	15	14.1†	12.7†
19	808	991	183	23	139*	44.1†	44.7†
20	808	974	166	23	140*	61.1†	71.0†
21	808	1004	196	23	126*	37.8†	39.3†
22	808	992	185	24	133*	47.4†	47.2†
23	807	976	169	24	144*	60.8†	69.5†
24	807	1000	193	24	120*	43.8†	63.0†

* No filter specification.
† Fails to meet filter specification.
‡ Reportable as outlier: $\alpha = 0.01$.

Table C-2
Differences in Preflight Relative Spectral Responses between June 1980 and June 1981 Measurements

Band	Band Edge (nm)		Width (nm)	Slope Interval (nm)		Spectral Flatness (%)	
	Lower	Upper		Lower	Upper	Positive	Negative
Means							
1	-2.0	-1.7	+0.2	-2.5	+1.1	-4.2	-4.0
2	-1.2	-3.2	-2.0	-1.3	0.0	+2.9	-3.9
3	-1.6	0.0	+1.6	0.0	0.0	+0.6	-0.1
4	0.0	+33.0	+33.0	-0.3	-24.5	-19.4	-12.2
Standard Deviations							
1	-0.02	+0.40	+0.03	-0.67	+0.24	-0.4	+1.1
2	-0.34	-1.30	-1.34	-0.36	+0.45	+0.7	-1.5
3	+0.37	-0.03	+0.17	-1.77	+0.10	+0.9	+0.8
4	-0.17	+2.70	+2.30	-0.45	-1.10	-2.4	+2.5

Table C-3
Differences in Simulated MSS Outputs Using June 1980 Versus June 1981 Relative Spectral Response Data

Target	Band 1	Band 2	Band 3	Band 4
Means				
Soy	+0.16	+0.04	-0.89	-1.15
Soil	-0.02	+0.07	-0.04	-0.36
Maximum Differences Between Channels				
Soy	-0.02	-0.29	+1.09	+0.30
Soil	-0.01	-0.01	+0.03	+0.10

APPENDIX D
PROTOFLIGHT AND FLIGHT MODEL DIGITIZED RELATIVE SPECTRAL RESPONSES

Table D-1
Protoflight Digitized Relative Spectral Responses (June 1981)

Band 1							Band 2						
Wavelength	Channel						Wavelength	Channel					
(nanometers)	1	2	3	4	5	6	(nanometers)	7	8	9	10	11	12
450	0.	0.	0.	0.	0.	0.	550	0.	0.	0.	0.	0.	0.
460	0.	0.	0.	0.	0.	0.	560	0.	0.	0.	0.	0.	0.
470	1.	1.	1.	1.	1.	1.	570	0.	0.	0.	0.	0.	0.
480	3.	3.	3.	4.	4.	4.	580	0.	0.	0.	0.	0.	0.
490	23.	24.	24.	27.	28.	26.	590	3.	3.	2.	3.	2.	4.
500	68.	68.	68.	73.	74.	71.	600	39.	41.	35.	38.	36.	42.
510	87.	88.	89.	90.	93.	89.	610	82.	84.	79.	80.	74.	82.
520	93.	95.	93.	95.	94.	93.	620	97.	97.	94.	94.	95.	95.
530	98.	98.	100.	100.	100.	100.	630	98.	99.	100.	100.	100.	99.
540	98.	98.	96.	97.	99.	97.	640	100.	100.	100.	99.	99.	100.
550	100.	100.	98.	98.	98.	98.	650	97.	96.	95.	95.	96.	94.
560	97.	97.	95.	94.	95.	96.	660	89.	92.	93.	89.	97.	91.
570	96.	98.	95.	92.	92.	96.	670	88.	90.	91.	90.	95.	88.
580	89.	91.	86.	84.	82.	88.	680	81.	86.	86.	85.	91.	82.
590	90.	91.	88.	85.	85.	90.	690	72.	80.	81.	80.	88.	76.
600	68.	66.	65.	60.	58.	67.	700	70.	30.	28.	34.	37.	28.
610	38.	35.	37.	34.	32.	38.	710	44.	6.	5.	7.	8.	5.
620	9.	8.	9.	8.	8.	9.	720	12.	2.	2.	2.	1.	1.
630	4.	4.	4.	4.	4.	4.	730	2.	1.	1.	1.	0.	0.
640	2.	2.	2.	2.	2.	2.	740	0.	0.	0.	0.	0.	0.
650	1.	1.	1.	1.	1.	1.	750	0.	0.	0.	0.	0.	0.

Band 3							Band 4						
Wavelength	Channel						Wavelength	Channel					
(nanometers)	13	14	15	16	17	18	(nanometers)	19	20	21	22	23	24
650	0.	0.	0.	0.	0.	0.	740	0.	0.	0.	0.	0.	0.
660	0.	0.	0.	0.	0.	0.	760	0.	0.	0.	0.	0.	0.
670	0.	0.	0.	0.	0.	0.	780	1.	1.	1.	1.	1.	1.
680	1.	1.	1.	1.	1.	1.	800	18.	20.	18.	21.	21.	21.
690	10.	8.	9.	7.	8.	8.	820	98.	100.	94.	100.	100.	100.
700	50.	44.	46.	40.	47.	46.	840	100.	99.	95.	99.	97.	99.
710	92.	93.	90.	88.	92.	92.	860	98.	96.	97.	97.	96.	98.
720	100.	100.	100.	100.	100.	100.	880	95.	94.	94.	93.	93.	97.
730	95.	94.	91.	95.	94.	92.	900	94.	93.	96.	92.	93.	97.
740	89.	90.	88.	91.	88.	86.	920	97.	91.	100.	95.	90.	95.
750	89.	89.	89.	92.	90.	85.	940	90.	84.	96.	85.	84.	90.
760	85.	86.	88.	90.	86.	81.	960	84.	73.	88.	80.	78.	81.
770	82.	81.	83.	87.	83.	75.	980	80.	66.	82.	67.	75.	72.
780	77.	79.	83.	85.	80.	73.	1000	66.	54.	73.	56.	63.	60.
790	74.	72.	79.	79.	74.	70.	1020	51.	41.	63.	46.	52.	49.
800	66.	67.	73.	74.	69.	63.	1040	47.	34.	56.	36.	44.	41.
810	67.	58.	72.	69.	66.	58.	1060	39.	25.	43.	28.	36.	31.
820	13.	10.	15.	14.	16.	13.	1080	30.	20.	35.	23.	29.	26.
830	2.	2.	3.	2.	2.	2.	1100	21.	14.	25.	16.	19.	18.
840	0.	1.	1.	1.	1.	0.	1120*	11.	7.	15.	9.	10.	9.
850	0.	0.	1.	0.	0.	0.	1140*	3.	1.	6.	0.	2.	1.

*Extrapolated

Table D-2
Flight Digitized Relative Spectral Responses

Band 1							Band 2						
Wavelength	Channel						Wavelength	Channel					
(nanometers)	1	2	3	4	5	6	(nanometers)	7	8	9	10	11	12
450	0.	0.	0.	0.	0.	0.	550	0.	0.	0.	0.	0.	0.
460	0.	0.	0.	0.	0.	0.	560	0.	0.	0.	0.	0.	0.
470	0.	0.	1.	1.	1.	1.	570	0.	0.	0.	0.	0.	0.
480	2.	2.	3.	3.	3.	3.	580	0.	0.	0.	0.	0.	0.
490	21.	20.	23.	24.	21.	22.	590	3.	3.	3.	3.	3.	3.
500	63.	58.	67.	71.	63.	64.	600	36.	37.	38.	40.	38.	39.
510	81.	75.	86.	88.	81.	82.	610	77.	76.	81.	84.	79.	79.
520	87.	82.	91.	94.	88.	88.	620	92.	92.	94.	96.	94.	93.
530	96.	92.	98.	100.	96.	96.	630	97.	98.	99.	99.	98.	97.
540	95.	93.	96.	97.	96.	95.	640	100.	100.	100.	100.	100.	100.
550	100.	99.	100.	100.	100.	100.	650	96.	96.	94.	95.	95.	96.
560	98.	98.	95.	96.	98.	98.	660	93.	93.	89.	89.	92.	93.
570	100.	100.	96.	94.	98.	98.	670	91.	90.	86.	85.	90.	92.
580	95.	96.	89.	87.	93.	95.	680	88.	86.	82.	80.	88.	89.
590	99.	98.	92.	88.	94.	97.	690	84.	81.	77.	74.	83.	85.
600	76.	76.	68.	67.	75.	76.	700	37.	31.	34.	31.	34.	37.
610	40.	40.	36.	36.	39.	40.	710	7.	6.	6.	5.	6.	6.
620	9.	8.	8.	9.	9.	9.	720	2.	1.	1.	1.	1.	1.
630	4.	4.	3.	3.	4.	3.	730	0.	0.	0.	0.	0.	0.
640	2.	2.	1.	1.	2.	1.	740	0.	0.	0.	0.	0.	0.
650	1.	1.	0.	0.	1.	0.	750	0.	0.	0.	0.	0.	0.

Band 3							Band 4						
Wavelength	Channel						Wavelength	Channel					
(nanometers)	13	14	15	16	17	18	(nanometers)	19	20	21	22	23	24
650	0.	0.	0.	0.	0.	0.	740	0.	0.	0.	0.	0.	0.
660	0.	0.	0.	0.	0.	0.	760	0.	0.	0.	0.	0.	0.
670	0.	0.	0.	0.	0.	0.	780	1.	1.	1.	1.	1.	1.
680	1.	1.	1.	1.	1.	1.	800	15.	15.	15.	14.	15.	13.
690	6.	7.	7.	5.	6.	7.	820	95.	93.	92.	94.	95.	95.
700	25.	28.	27.	23.	26.	27.	840	100.	96.	98.	100.	100.	100.
710	85.	88.	91.	85.	88.	88.	860	99.	97.	96.	98.	96.	99.
720	100.	100.	100.	100.	100.	100.	880	97.	98.	97.	98.	98.	98.
730	95.	93.	95.	92.	94.	94.	900	98.	98.	99.	95.	97.	99.
740	88.	89.	90.	89.	85.	90.	920	95.	100.	100.	93.	96.	97.
750	88.	90.	89.	87.	88.	89.	940	91.	94.	95.	84.	91.	94.
760	90.	88.	89.	85.	87.	89.	960	85.	91.	93.	77.	82.	87.
770	84.	84.	82.	79.	83.	84.	980	78.	87.	86.	68.	76.	81.
780	83.	82.	83.	81.	81.	81.	1000	70.	77.	78.	58.	68.	71.
790	81.	78.	79.	78.	78.	79.	1020	54.	62.	65.	47.	55.	57.
800	76.	73.	72.	71.	71.	72.	1040	46.	55.	54.	37.	48.	50.
810	75.	71.	70.	71.	71.	73	1060	37.	42.	43.	30.	36.	37.
820	17.	19.	16.	18.	19.	20.	1080	27.	33.	34.	23.	29.	30.
830	2.	2.	2.	2.	2.	3.	1100	18.	24.	23.	16.	20.	21.
840	1.	0.	0.	1.	0.	1.	1120*	10.	14.	14.	9.	11.	12.
850	0.	0.	0.	0.	0.	0.	1140*	3.	5.	5.	3.	4.	4.

*Extrapolated

N85-20500

INVESTIGATION OF RADIOMETRIC PROPERTIES OF LANDSAT 4 MSS

Daniel P. Rice and William A. Malila
Environmental Research Institute of Michigan
Ann Arbor, Michigan 48107

INTRODUCTION

Background

The Landsat user community has been concerned about the continuity of Landsat multispectral scanner (MSS) data. Landsat-4 extends the decade of data availability afforded by the first three Landsat satellites. We believe that continuity should be thought of not only as being the continued availability of high quality Landsat MSS data, but also the consistent interpretability of signal amplitudes and spectral features extracted from MSS data. Hence, of interest are both the internal calibration between detectors within each spectral band, with related dynamic-range and signal-to-noise characteristics, and the radiometric calibration of the Landsat-4 MSS bands relative to the characteristics of the preceding Landsat sensors.

If detectors within a band are not perfectly calibrated with respect to each other (i.e., equalized), image banding results and extra variability or noise is introduced into the statistical descriptions (e.g., signatures) of signals from specific scene classes. Similarly, if the noise associated with each detector channel were to significantly exceed design specifications, the utility of the data collected by the system would be diminished. Also, reduced dynamic range could degrade data utility.

Furthermore, if the radiometric calibration of the Landsat-4 MSS bands were not to match well that of its predecessor or were to drift, algorithms, techniques and procedures with fixed coefficients or thresholds developed for use with Landsat 1, 2 and 3 MSS scanners would have to be modified accordingly.

Objectives

The objectives of this investigation are to address the following two topics, relative to characterization of Landsat-4 image data quality:

(a) Detector calibration: The calibration of the six Landsat detectors in each band will be studied in order to determine the magnitude of any calibration differences that remain after ground processing and, if needed, to provide information that would support corrective techniques.

(b) Satellite-to-satellite calibration: Calibration differences between Landsat-4 and previous Landsat satellites will be studied and, as needed, a method will be developed to adjust Landsat-4 multispectral scanner (MSS) signals, in all four spectral bands, to match the calibration of previous MSS sensors.

In addition, we will examine the overall quality and characteristics of Landsat-4 MSS data and make recommendations where possible that could improve the data quality.

APPROACH

An empirical approach involving several topics is being pursued to assess the quality of Landsat-4 MSS image data. Thus far, data from the several frames described in Section 3 have been obtained for analysis.

The first step was to compute and analyze signal statistics on a detector-by-detector basis for the six detectors in each of the four spectral bands on the "A" tapes. Means, variances and histograms of signal amplitudes were computed for the entire frame, for four 600-line segments and 12 subsegments, and for several diverse scene classes. Within-band means and variances were compared to search for evidence of detector "banding" effects. Histograms were examined to compare the quantization patterns (a result of radiometric look-up tables) found in the signal amplitudes, both for the entire scene and for the image subsegments. Digital display maps were produced from these scenes and examined visually for banding effects. The detector-based statistics and Variable X vs. Variable Y scatter plots also were examined qualitatively for dynamic range and other characteristics, relative to our experience with previous Landsats.

Another approach used for detecting banding effects was the Fast Fourier Transform (FFT) technique. FFT's were computed of a down-track profile for each band for each frame; these profiles were obtained by averaging all pixels in each scan line. Spatial frequencies at integer wavelengths (e.g., six scan lines) that are more pronounced than others at nearby frequencies are indicative of banding, and can give a quantitative measure of its magnitude.

FFT's also were computed for individual scan lines at selected locations in the frame. These results provided a mechanism for detecting and quantifying coherent noise effects in the image data, both amplitude and phase as well as between-band comparisons. This type of noise produces a pattern on images that appears as diagonal stripes.

The final topic addressed was satellite-to-satellite calibration. Landsat Path-Row locations and dates within the contiguous 48 states were identified where simultaneous coverage is possible by the Landsat 3 and Landsat 4 scanners. This possibility exists because of the 16-day and 18-day repeat coverage cycles of Landsat 4 and Landsat 3, respectively. Arrangements were made to have the Landsat-3 tape recorder turned on during those frames to acquire such data for subsequent analysis. The availability of simultaneous coverage eliminated several confounding effects from the analysis of relative radiometric calibration between these systems.

The method used to analyze Landsat 3 and 4 differences was to carefully extract polygons in each dataset that outline the same areas in both satellite images. Regression analysis of area mean statistics was used to determine the radiometric relationship and measure its accuracy. As a byproduct of this effort, the polygon positions themselves were used to measure the geometric consistency of data from the two satellites.

DESCRIPTION OF DATA SET

Table 1 below identifies the Landsat data used for the analyses reported herein.

Table 1

DESCRIPTION OF DATA SET

Geographic Location	Landsat	Path/Row	Date	Frame
Carolina (inland)	4	17/36	29 Sep 82	40075-15271
California (Imperial Valley)	4	39/37	23 Sep 82	40069-17433
N.Carolina (coast)	3	15/35	24 Sep 82	31664-15070
"	4	14/35	24 Sep 82	40070-15081
New England	3	14/30	22 Dec 82	31753-14591
"	4	13/30	22 Dec 82	40159-15010

Two Landsat 3/Landsat 4 pairs include one winter frame pair containing parts of Massachusetts, Vermont and New Hampshire, and one autumn frame pair containing the east coast of North Carolina.

In addition, two unpaired Landsat 4 frames (September 1982) were used for radiometric quality analysis. One of these is on the border of North and South Carolina, and is composed primarily of forests and pasture, with some agricultural fields. Dynamic range in this scene is limited,

possibly due to the limited scene classes, or to the presence of haze. The other frame covers the Imperial Valley of California at the border with Mexico, and contains the diverse scene classes of a highly productive agricultural area, a large inland lake (Salton Sea), desert or semi-desert areas, and mountains. This diversity is reflected in a substantial dynamic range of the data.

DATA ANALYSIS RESULTS

In this section we discuss several topics, including banding, quantization effects, coherent noise, relative calibration between Landsats 3 and 4, and geometric considerations. First, some general observations on Landsat 4 MSS quality are presented.

Qualitative Examination of Landsat 4 MSS Data

Data from the Landsat 3 and 4 MSS's were examined visually to see how well the two sensors correspond radiometrically. Figure 1 is an example of one such comparison for an agricultural area in North Carolina. The radiometric similarity is striking, a first suggestion that the two sensors are comparable.

Further evidence of this similarity was found in the examination of Landsat 4 data from Imperial Valley, California. In this scene, four distinct general scene classes were identified and scatterplots of Bands 2 and 3 were prepared for each class as well as for a comprehensive sample of the whole dataset. The distributions for the individual scene classes were marked on the comprehensive scatterplot, and this result is presented in Figure 2. From this figure four observations can be made:

1) Water is represented by low signals in all bands
2) Sand is bright in all bands
3) Clouds are so bright as to cause signal saturation (level 127), at the prevailing solar illumination angle
4) Agricultural data fills out a roughly triangular shape (a "tasseled cap")

All of these observations are generally true for Landsats 1-3 as well as Landsat 4.

DETECTOR BANDING AND QUANTIZATION EFFECTS

In order to determine whether banding effects exist in Landsat 4 MSS data after radiometric correction, photographic images and other displays of the data were examined. Banding effects were visually noted only in areas of nearly uniform signal such as water bodies. One such area, shown in Figure 3, is a high-reflectance area near Imperial Valley, California.

To measure the magnitude of this banding effect, two techniques were used. The first of these techniques was to tabulate the signal mean for each detector within five areas in the Imperial Valley scene. Table 2 presents this information. The largest difference found between detector

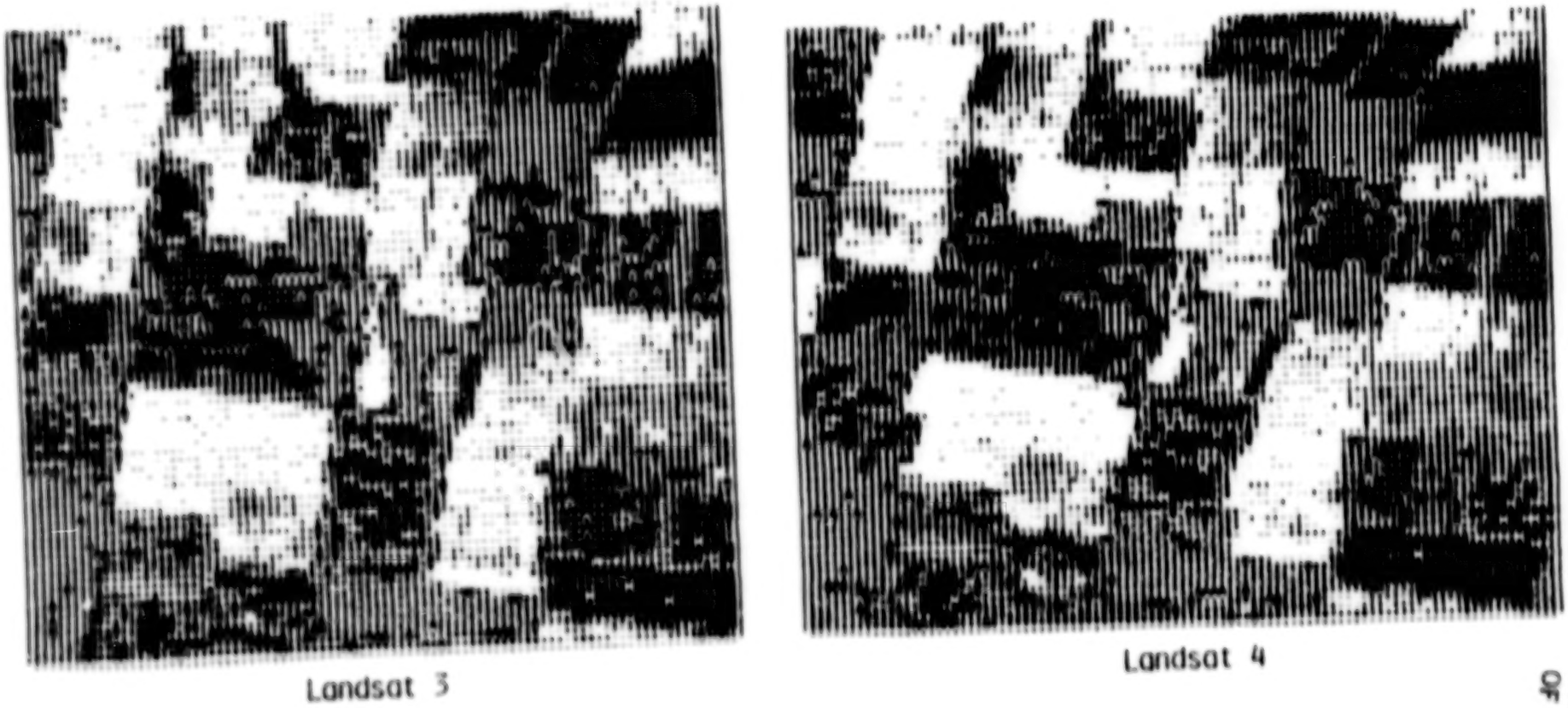

Landsat 3

Landsat 4

Figure 1. Qualitative Comparison of Landsat 3 and 4 MSS Data (North Carolina, Sept. 1982)

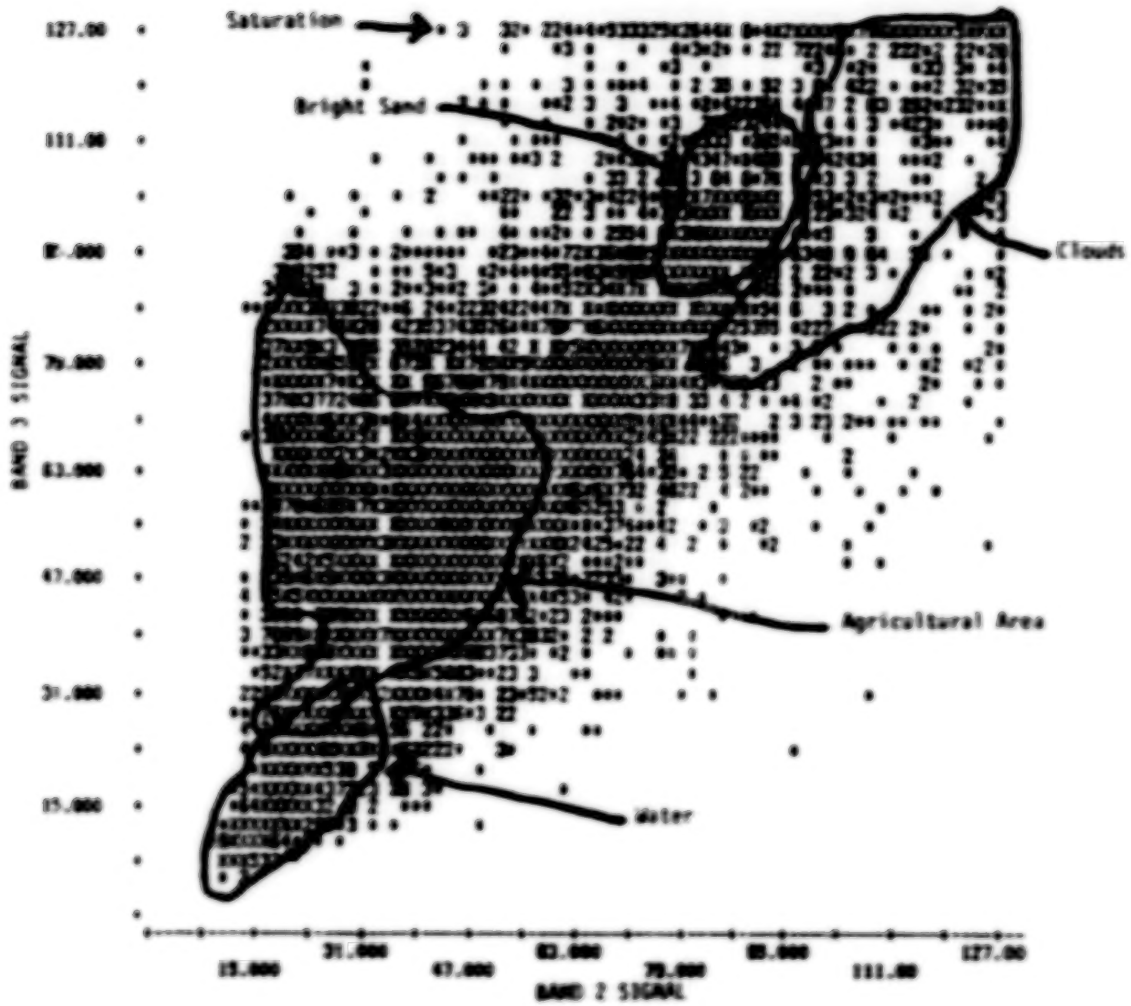

Figure 2. Spectral Distribution of Scene Classes from the Imperial Valley, California Scene

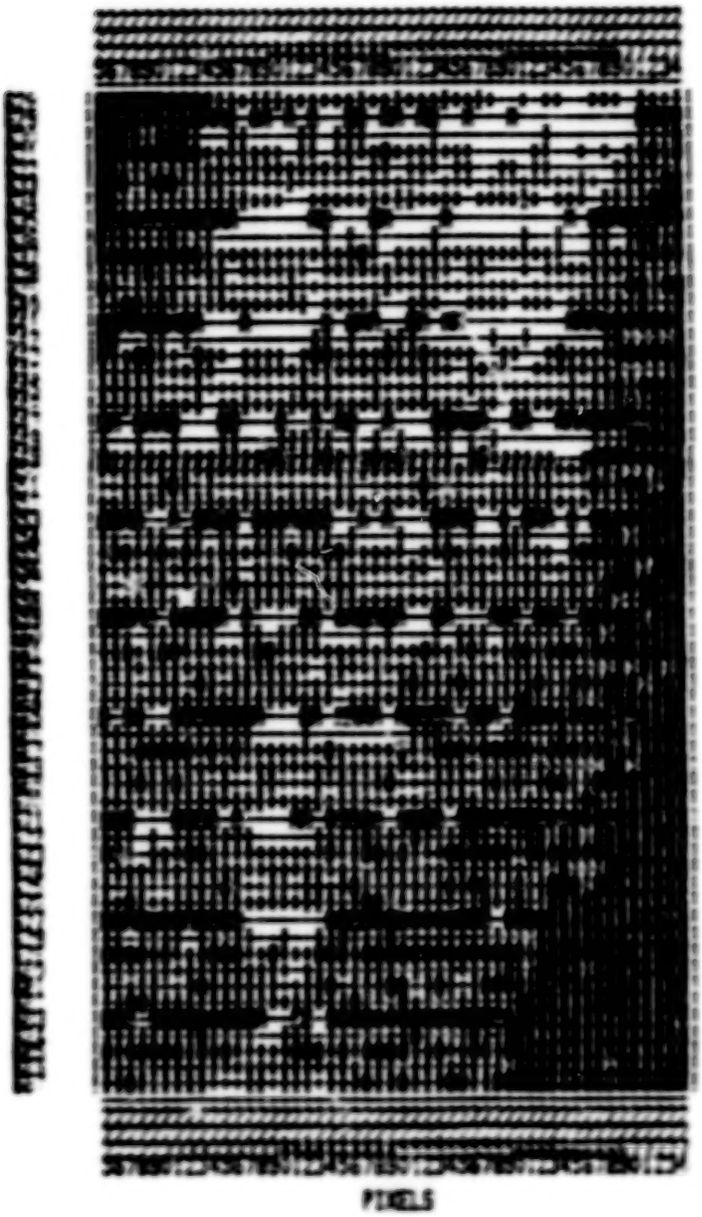

Figure 3. Example of the Detector Banding Effect (Bright Shallow Valley)

Table 2. Detector Averages for Five Areas in One Landsat 4 Frame (Imperial Valley, California)

		Landsat MSS Band				
Detector		1	2	3	4	
1		23.01	21.08	36.80	14.44	
2		23.29	21.00	36.91	14.41	
3		22.94	21.10	36.94	14.53	
4		23.23	21.04	37.31	14.62	Highlands
5		23.25	20.97	37.18	14.43	
6		23.31	21.03	37.15	14.70	
	σ =	.16	.05	.19	.12	
1		33.08	35.51	53.86	19.03	
2		33.38	35.78	54.18	19.09	
3		33.41	36.06	54.32	18.99	
4		33.32	36.10	54.22	18.80	Agricultural
5		33.31	35.86	53.60	18.81	
6		33.08	35.69	53.75	18.91	
	σ =	.15	.22	.29	.12	
1		62.23	76.10	84.14	25.73	
2		62.11	76.76	84.25	25.62	
3		62.10	76.08	84.54	25.84	
4		61.42	76.01	84.04	25.89	Sands
5		61.78	75.88	83.81	25.84	
6		61.99	76.23	83.88	25.63	
	σ =	.30	.31	.27	.12	
1		20.79	13.65	10.09	2.43	
2		21.02	13.69	9.88	2.35	
3		20.64	13.70	9.91	2.21	
4		20.73	13.52	9.59	2.27	Water
5		20.26	13.37	9.84	2.07	
6		20.81	13.90	10.22	2.30	
	σ =	.25	.18	.22	.12	
1		51.62	61.55	69.43	22.10	
2		51.77	61.82	69.17	22.27	
3		51.58	61.58	69.30	22.44	
4		52.16	61.68	69.52	22.53	Bright Shallow Valley
5		51.28	62.07	69.31	21.97	
6		51.67	61.79	69.56	22.05	
	σ =	.29	.19	.15	.22	

means was 0.88 of one count, and the RMS error was generally less than 0.3 counts, a very low error rate.

A more comprehensive estimate of residual banding error was made using Fourier analysis. Down-track FFT's were computed on scan line average signals on all bands of two Landsat frames*. An example of these FFT's is given in Figure 4. These FFT's were examined for response at a spatial wavelength of six pixels and the harmonics at three and two pixels. Disturbances were found at these wavelengths, that typically consisted of an upward spike with a modified pattern of response in the vicinity. By using the magnitude of the spikes, the average deviation from the mean of the six detectors was measured. The worst of these measurements, which occurred in the Carolina scene, was an average deviation of 0.27 of one count (with a measurement error of about 0.05 due to scene information). This result based on FFT analysis is very similar to the above result based on computing detector means.

The algorithm used at GSFC to achieve the above-reported residual banding error was examined to see if any further improvement seems possible. The algorithm carries out signal decompression (bands 1-3 only), calibration wedge normalization, and histogram detector equalization using a single transformation of received satellite samples to determine final count levels. A separate transformation is computed for 600-scan-line blocks, then is interpolated to each 200-scan-line block. Figure 5 shows an example of the resulting pattern of empty and full count level bins, a pattern which differs between detectors due to the correction. Examination of this pattern for a series of 200-scan-line blocks showed the expected gradual change from one block to the next, and indicated the correct working of the algorithm.

A very important limit on accuracy of this destriping algorithm is not one of measuring differences or determining corrections, but rather one of translating corrected values to nonfractional count levels. The theoretical RMS error of this truncation process is 0.29, which is similar to the error magnitudes reported above. That is, the current correction algorithm can't be improved much if any without dealing with the truncation error problem. Spreading the signals over the range 0-255 instead of 0-127 could reduce this error a little bit (per radiance unit).

However, the analog-to-digital conversion process in the satellite is another assignment to nonfractional values with the same 0.29 count RMS error, measured in the 6-bit numeric system used at the satellite. This effect can cause minor but irretrievable banding which is most notable in relatively uniform areas.

*40075-15271 29 Sep 82 Carolina; 40069-17433 23 Sep 82 California

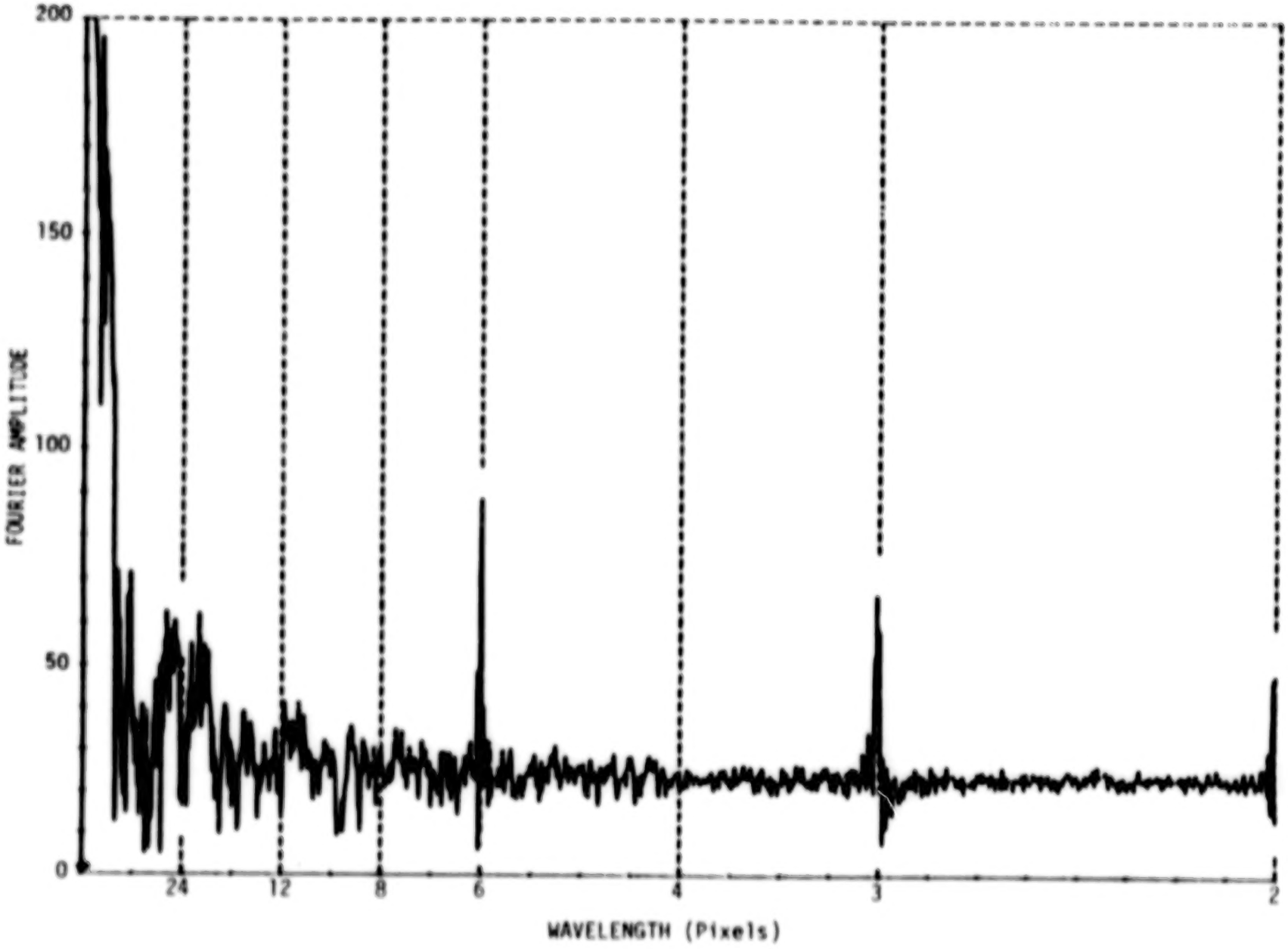

Figure 4. Fourier Transform of Down-Track Averages, Channel 1, Carolina Scene

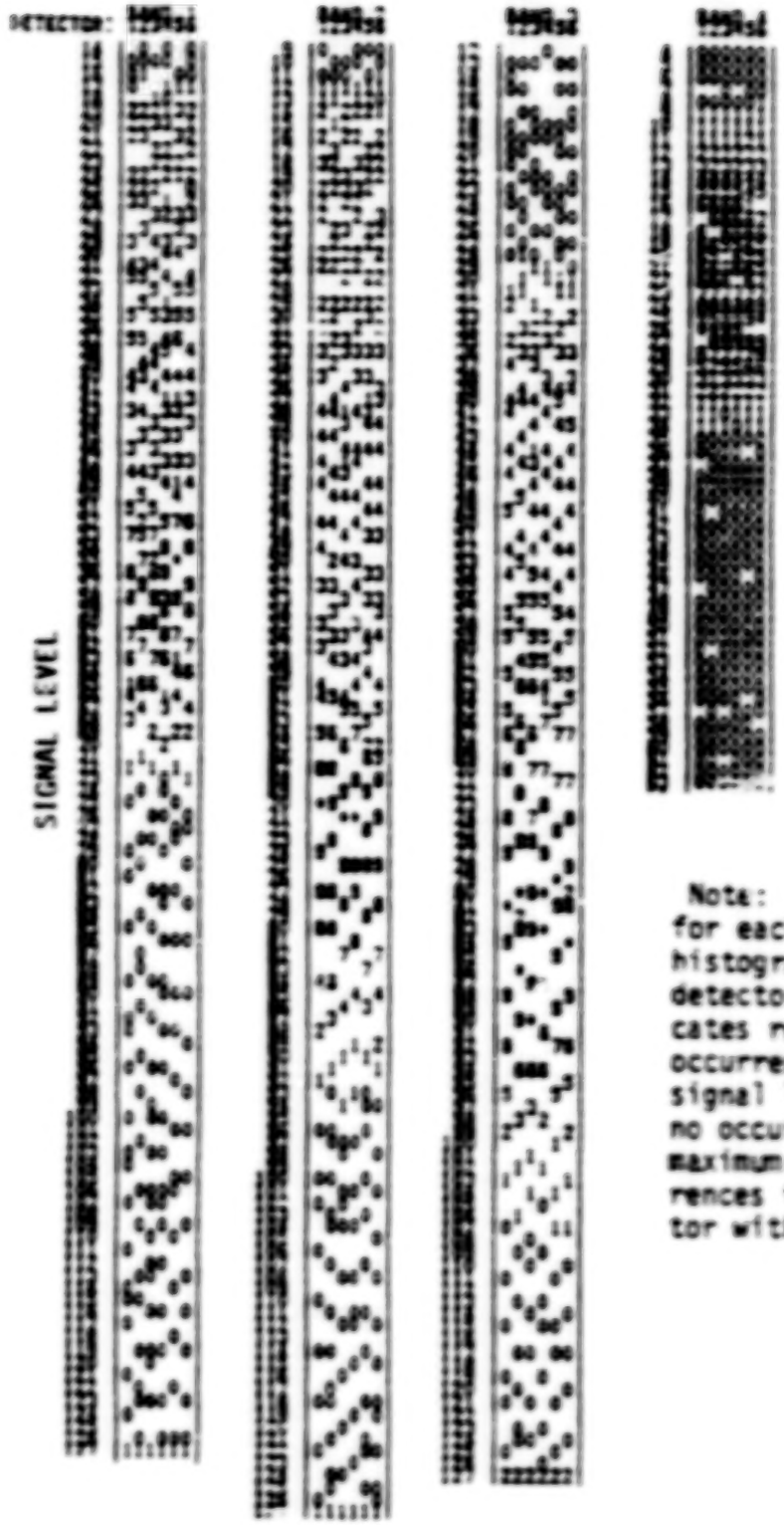

Note: Each of six columns for each band represents one histogram for a specific detector. Each digit indicates relative number of occurrences at a specific signal level (blank means no occurrences, * means maximum number of occurrences found for any detector within each band).

Figure 5. Example of Quantization Effects

THE COHERENT NOISE EFFECT

A careful examination of imagery from Landsat 4 MSS revealed a diagonal striping pattern, particularly in areas of nearly uniform radiance. An example of this pattern is presented in Figure 6.

A Fourier transform analysis of this noise pattern was carried out on selected scan lines distributed throughout two Landsat frames. As illustrated by Figure 7, it was found that the noise consisted of a dominant spatial wavelength of about 3.6 pixels along scan that was present in all bands. The frequency corresponding to the observed dominant wavelength is approximately 28 KHz. The wavelength was slightly different (3.57 compared to 3.59) for the two frames, but was consistent ($\pm$.001) within each frame. In one frame (South Carolina), two other wavelengths appeared somewhat consistently, namely the wavelengths of 2.02 and 4.63 pixels, but these and other smaller peaks in both frames were not analyzed in detail.

Figure 7 illustrates peaks at the principle wavelength, along with a number of additional peak that are minor and inconsistent. The magnitude of the sine-wave component at the primary peak was computed and tabulated for the group of scan lines that was processed. This information, presented in Table 3, shows that the magnitude of the noise did not exceed one count in the worst band (Band 1), and is a relatively minor source of error in spite of its nuisance effect on images of uniform areas. (The low value in Band 4 corresponds to the calibration in use prior to October 20, so should be approximately doubled. Questions of calibration are discussed in the next section.)

Satellite to Satellite Calibration

In order to ensure for the Landsat community a means to achieve consistent interpretability of Landsat data, it is necessary to calibrate one Landsat to another. This would mean that a specific signal value from two separate Landsat MSS sensors would correspond to the same target radiance. Algorithms developed using data from one Landsat could then be applicable to another. Below, we describe one such calibration that will make data from Landsat 4 match data from Landsat 3.

The basic approach was to find data taken by both satellites of the same targets at the same time, then to use regression analysis to form a calibration relationship. Due to the differing repeat cycles of Landsats 3 and 4 (18 and 16 days, respectively), simultaneous coverage of the same location by both satellites can occur every 144 days. Our investigation showed the locus of points in the contiguous US which can receive such coverage is a pair of tracks, one along the East Coast, and the other extending approximately from Los Angeles to Montana. We identified the time and place of all such potential coincidences, arranged for acquisition of several coincident datasets, and processed two frames pairs of such data thus far. These are:

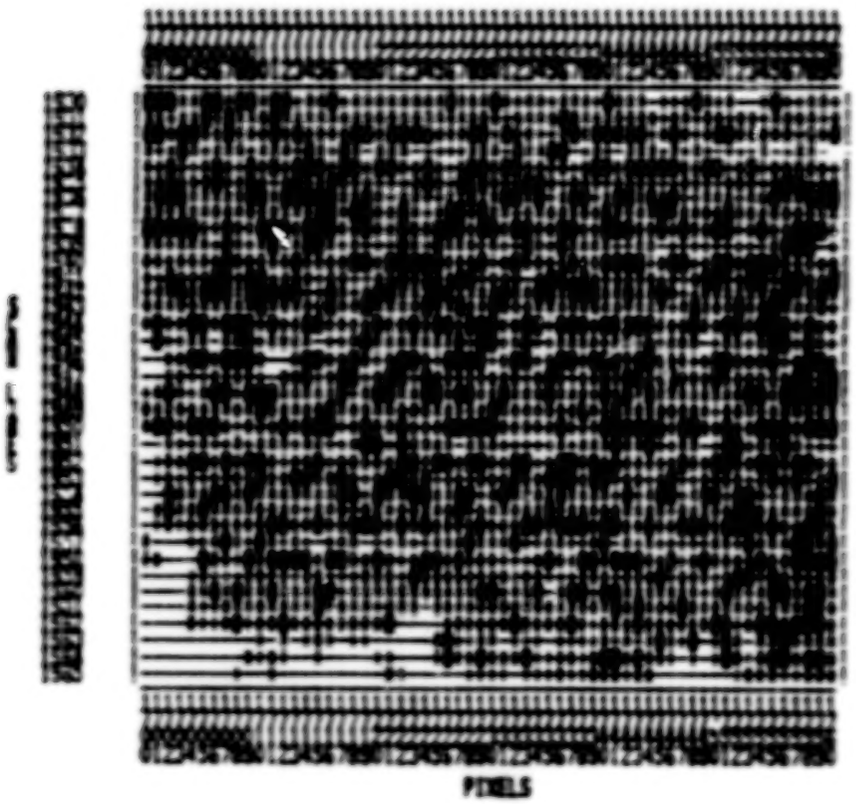

Figure 6. Example of Diagonal Striping (Coherent Noise) in South Carolina Scene, Water Area

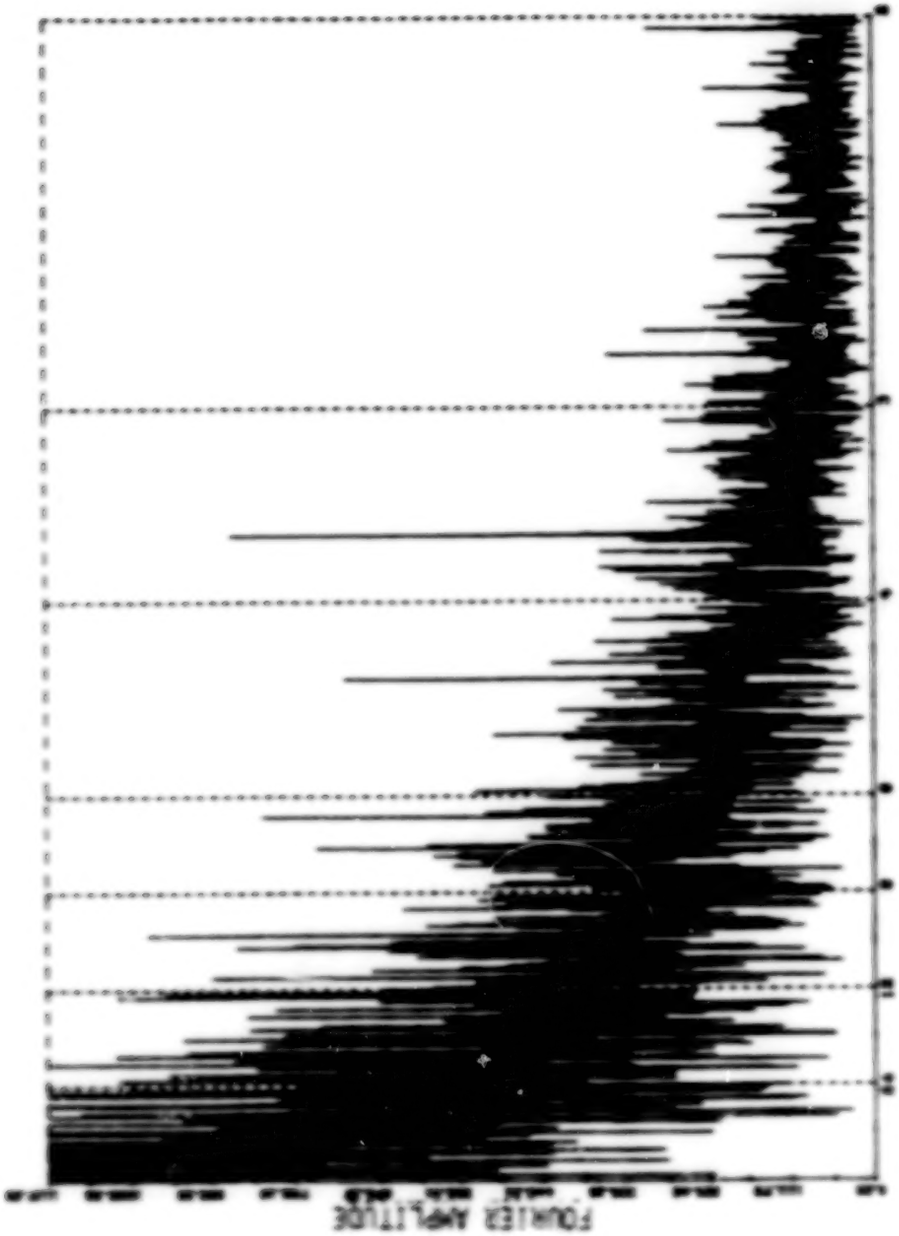

Figure 7. Along Scan Fourier Transform Showing Coherent Noise Peak at Wavelength 3.6 (South Carolina, Scan Line 2117, Band 3)

New England	22 Dec 82	40159-15010	13/30	31753-14591	14/30
Carolina coast	24 Sep 82	40070-15081	14/35	31664-15070	15/35

For the New England scene, the two overpasses differed in location by about 8 miles, representing a view angle difference of 1.2 degrees, which is 16% of the view angle difference between one side of the frame and the other. The difference in time of overpass was about 1.8 minutes, which indicates that targets on the ground were essentially unchanged between the passes (the change in sun angle would not have caused even a 1% change in the reflected radiance). Similarly the Carolina overpasses differed in location by about 9 miles and in time by 1.2 minutes.

To extract comparable measurements, relatively large and uniform polygonal areas were carefully identified and located in Landsat 4 data and in the matching Landsat 3 data. The fields were selected to provide as wide a spectral range as possible. After the polygonal area locations were verified, field mean statistics were extracted, and a linear regression was run in each band to determine a relation between the two satellites. The form of the relation used was:

[Landsat 3 signal] = gain*[Landsat 4 signal] + bias

In the New England frame, care was taken to spread the fields widely throughout the frame. This spatial spread, produced by assigning fields within uniformly spaced corridors, was done to determine whether view angle differences known to be present could cause significant error. Landsat 4 with its lower orbit has a view angle of about 2 degrees more than Landsat 3 at the end of a scan line if the view angle at scene center is the same. No statistically significant relationships with differential view angle were found, indicating that 2 degrees of view angle differences would not materially affect the results.

In all, 60 polygonal areas were selected in the New England frame pair, covering a total of about 8000 pixels. For the Carolina frame pair, 13 areas were selected. Relations were computed for each band and are presented in Table 4. As indicated by the statistics, and as illustrated in Figure 8, these relationships are very highly linear, implying that the two sensors themselves are also. Without the use of these relationships, an intermediate radiance level relates to signals up to 5 counts different between the two sensors. If published prelaunch information is used, about 3 counts of differences remain. Using the relationships introduced above, the signal level differences are reduced to less than 1 count.

In using these relationships it is important to track changes in standard Landsat processing that occur from time to time. One such change occurred on 20 October 1982, at which time the count levels for Band 4 were increased by a factor of 127/63.

As this paper is being prepared, another calibration change has been announced by NOAA, that takes effect 1 April 1983. The transformations discussed above relate to the post-October but pre-April calibration, and they must be converted in order to apply to the post-April calibration.

Table 3

AVERAGE MAGNITUDE OF COHERENT NOISE EFFECT

Band	Magnitude (counts)
1	.75 ±.11
2	.52 ±.09
3	.56 ±.10
4	.25 ±.05

Table 4

EMPIRICAL LANDSAT 4-TO-3 CALIBRATION COEFFICIENTS

Scene	Band	Gain	Offset	SE*	R^2
New England	1	1.018	-1.614	.52	.996
	2	1.112	0.018	.45	.999
	3	0.9096	-0.463	.53	.999
	4	1.148	-0.421	.53	.998
N. Carolina	1	0.962	-0.164	.41	.992
	2	1.096	0.499	.46	.998
	3	0.861	0.558	.67	.999
	4	1.145**	-0.546	.88	.999
[Prelaunch Calibration]	1	0.894	-1.00		
	2	1.000	0.722		
	3	0.863	0.870		
	4	1.026	2.34		

* SE = standard error in signal counts

** The N. Carolina scene was produced with the pre-October calibration but this number has been converted to the post-October calibration form as described in text.

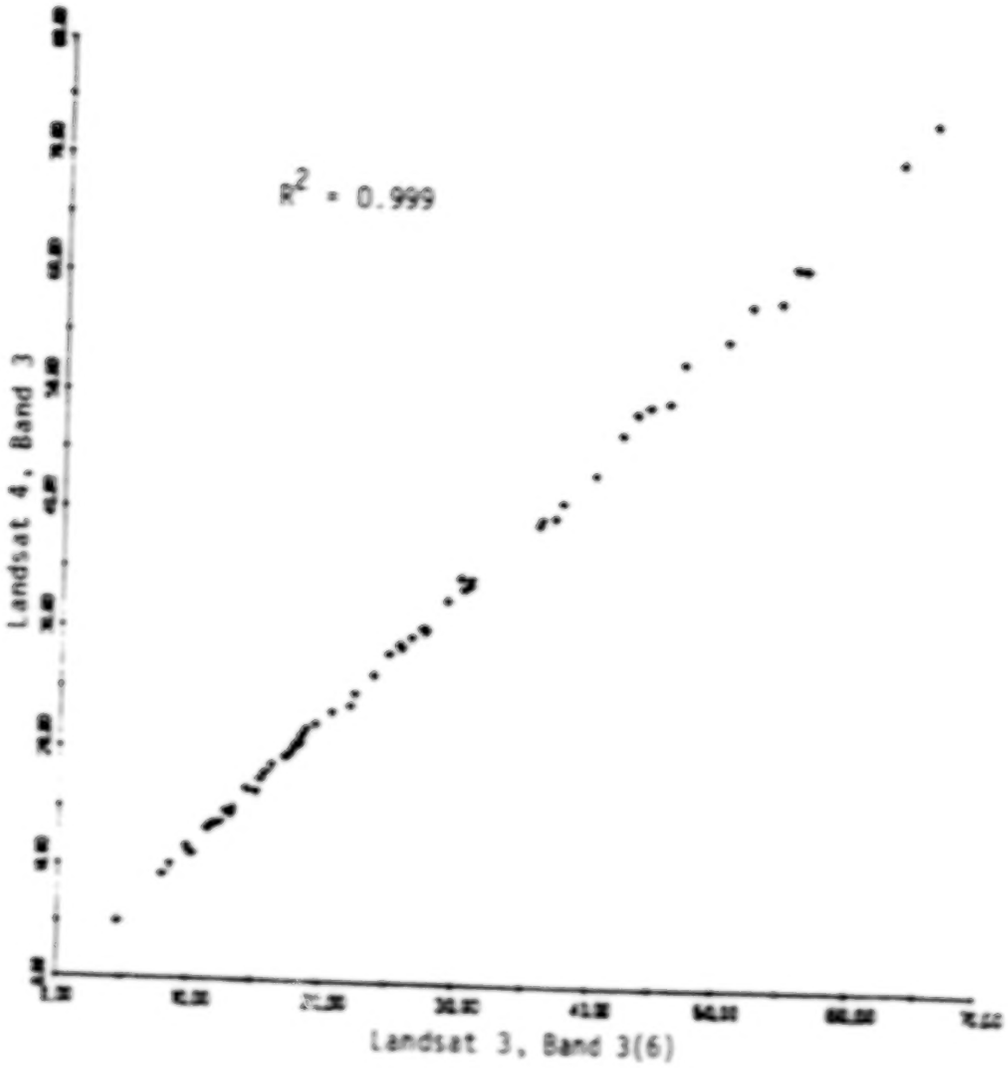

Figure 8. Linear Relationship Between Landsat 3 and 4 Signals in the New Englund Overpass Pair

In this paper we have attempted to indicate whenever we have converted pre-October statistics to the post-October form.

GEOMETRIC OBSERVATION

In carrying out the radiometric work described above, a significant geometric distortion was noted in the "A" tapes used in the analysis. This distortion is characterized by adjacent groups of 6 scan lines (one mirror sweep) displaced relative to one another, as illustrated in Figure 9. The magnitude of the displacement varied up to 6 pixels, and decreased to zero at the left side of the image, indicating that the distortion is a line length variation.

We found that this distortion was absent in scenes taken when the Thematic Mapper sensor was not operating.

We implemented a linear line stretch correction, based on the position of end-of-scan codes in each scan line, that we understand is equivalent to the correction used to produce the geometrically corrected "P" tapes. As Figure 9 shows, this correction restored the Connecticut River to its rightful contiguous banks.

Since accurately located polygonal area definitions were defined for the radiometric relationships discussed in the preceeding section, we were able to perform one simple test of geometric accuracy. Regression analysis was used to form a linear relation between the mean field location in Landsat 4 and that location in Landsat 3. The standard error of that relation is a measure of how geometrically consistent the two sensors are. It was found, based on the 60 well-dispersed fields in the New England site that the variation of pixel location was 1.8, and of scan line location was 0.8. Since it is felt that the polygons were located with a local accuracy of about 0.5 pixels, other error, such as nonlinear mirror sweep rates, could explain this result. (The polygons were located in data after the linear stretch correction was applied.)

CONCLUSIONS

The work above provides good evidence that Landsat 4 data is of the same high quality as previous Landsats, with a comparable dynamic range and target response, a good detector equalization procedure, and an accurate linear response to received radiance.

A linear relationship between Landsat 3 and 4 was determined that renders Landsat 4 signals to have the same radiance response as Landsat 3 signals.

Two artifacts, not noted in previous Landsats, were found and quantified. One is a geometric scan line length variation in Landsat "A" tapes, and was shown to be fairly well correctable. The other artifact is a coherent noise effect in all bands, having an amplitude of less than one count. This noise causes a minor diagonal stripping pattern on images of relatively uniform areas.

Figure 9. Line Length Variation in Landsat-4 MSS "A" Tapes

RADIOMETRIC CALIBRATION AND GEOCODED PRECISION PROCESSING OF LANDSAT-4 MULTISPECTRAL SCANNER PRODUCTS BY THE CANADA CENTRE FOR REMOTE SENSING

J. Murphy,
D. Bennett and
F. Guertin
Canada Centre for Remote Sensing

1.0 CCRS RADIOMETRIC CORRECTION METHOD

The radiometric correction process used by CCRS, as described by Ahern and Murphy (1978), may be divided into three stages.

a) a reference detector is chosen for each spectral band, and the corrections required to place the data from this detector on an absolute scale are calculated using the calibration wedge data, pre-launch calibration data and the maximum and minimum radiance values associated with the response of the band.

b) the relative differences between all other detectors in each band and the reference detector are calculated, using the means and standard deviations of the decompressed raw data values as calculated from the sums and the sums of the squares of the scene data values. (Excluded from the scene statistics are those pixels which cause any one detector to saturate, such that only that portion of the curve for which the response of all detectors within the band is essentially linear is used.)

c) finally, the absolute calibration of the reference detector is combined with the relative calibration of the other five detectors within the band, to provide an absolute calibration of all six detectors in each of the four bands.

Inherent in the technique is the assumption that the response of each detector is linear, that is, the voltage output varies in a linear fashion with the radiance input. Hence the calibration process may be represented by the equation:

$$V' = (V - a) / b \qquad (1)$$

where V' is the calibrated digital value, (0-255)
V is the uncalibrated decompressed digital value, (0-255)
b is the gain,
and a is the offset.

1.1 USE OF THE CALIBRATION WEDGE

Each calibration wedge for the selected reference detector is sampled at the six predefined locations, and the

histogram for each of the six samples is accumulated over the entire scene. Since one full scene contains 186 complete calibration wedges for each detector, the histogram is first used to isolate any outliers. This is accomplished by generating a smoothed histogram, where each of the histogram bins contains a count of all sample values falling within a window which is five digital values wide. The mean value is then calculated using only those samples which contribute to the smoothed histogram bin with the largest count.

The stability of the calibration wedge, and the choice of a reference detector for each band, are discussed further in Section 3.

The values of a and b in equation (1) are calculated using the formulae:

$$a = \sum_{i=1}^{6} C_i^{\circ} * V_i \qquad (2)$$

$$b = \sum_{i=1}^{6} D_i^{\circ} * V_i \qquad (3)$$

where the V_i's are the mean decompressed samples of the calibration wedge at the six locations.

NASA (Reference 1) supplied, before the launch of LANDSAT-4, tables for C_i' and D_i' in a band normalized form, and exemplified their generation and use (NASA, Reference 2). The pre-launch maximum and minimum radiance values to which the pre-launch C_i' and D_i' apply are shown, for each band, in Table 1.1 as RMAX and RMIN respectively.

However, the maximum radiance values for bands 1 and 3 were modified by NASA (Reference 3) using post-launch observations, and these are shown as RMAX' in Table 1.1. In order to obviate the necessity of changing the C_i' and D_i', multiplicative (M) and additive (A) modifiers to be used in the modified detector response equation (4) were supplied.

$$V' = (V - a)/M*b - A \qquad (4)$$

However, these modifiers include the effects of relative detector differences within the band, a process which is treated by CCRS completely independently from the absolute calibration. The C_i' and D_i' were therefore used in combination with the maximum and minimum radiance to give band normalized C_i° and D_i° appropriate to the revised RMAX'.

$$C_f' = C_f + RMIN * D_f \quad (5)$$

$$D_f' = (RMAX - RMIN) * D_f \quad (6)$$

From (6), $D_f = D_f'/(RMAX - RMIN)$ (7)

From (5) and (7), $C_f = C_f' - RMIN*(D_f'/(RMAX - RMIN))$ (8)

For RMAX' and RMIN'

$$C_f'' = C_f + RMIN' * D_f \quad (9)$$

$$C_f'' = C_f + RMIN' * D_f'/(RMAX - RMIN) \quad (9')$$

$$D_f'' = (RMAX' - RMIN') * D_f \quad (10)$$

From (7), $D_f'' = (RMAX' - RMIN') * D_f'/(RMAX - RMIN)$ (11)
From (8) and (9'),

$$C_f'' = C_f - (RMIN - RMIN') * D_f'/(RMAX - RMIN) \quad (12)$$

The C_f'' and D_f'' used by CCRS are shown in Table 1.4. For changes in maximum and minimum radiance values shown in Table 1.1, the C_f'' and D_f'' are related to C_f' and D_f' in the following way:

Bands 2 and 4 - No Change
Bands 1 and 3 - $C_f'' = C_f'$
Band 1 - $D_f'' = 0.919355*D_f'$
Band 3 - $D_f'' = 0.863014*D_f'$

In addition to supplying products calibrated using the values of RMAX' and RMIN' as discussed above, which CCRS terms the "CAL2" option, an alternative calibration, termed the "CAL3" option, can be supplied by CCRS, where the maximum and minimum radiance values are shown as RMAX" and RMIN" in Table 1.1.

The "CAL3" absolute gains and offsets are calculated from the "CAL2" absolute gains and offsets using the expressions:

$$a' = a - 255 * (RMIN' - RMIN'')/(RMAX' - RMIN') \quad (13)$$
$$b' = b * (RMAX'' - RMIN'')/(RMAX' - RMIN') \quad (14)$$

where a' and b' are the "CAL3" absolute offset and gain corresponding to the equivalent "CAL2" absolute offset and gain, a and b.

1.2 RELATIVE CALIBRATION

The relative correction of the individual detectors within each band is performed using information from the scene being viewed by the MSS, and this method has the advantage of using a calibration source with the spectrum of the scene rather than the very much redder spectrum of the calibration lamp. It has been shown (Strome et al., 1975) that the gain of one detector relative to the gain of the reference detector is equal to the ratio of the standard deviations of the data acquired with these detectors. Similarly, the difference in zero offset is equal to the difference between the mean of the data values acquired with one detector and the mean of the data values acquired with the reference detector. The mean and standard deviation can be calculated from the sum and the sum of the squares of the scene data values, which in turn, are calculated from the decompressed histogram of the raw data values. In order to ensure that the histograms correspond only to pixels with radiance values for which the response of each detector is linear, all those pixels which saturate any one detector within a band are removed from the histograms of EACH detector within that band. This process is performed for each band independently. This technique was shown by Murphy (1981) to reduce residual striping in scenes with very bright snow and clouds.

1.3 CREATION OF LOOK-UP TABLES

After combining the relative gains and offsets with the absolute gains and offsets of the reference detectors, a radiometric look-up table is created for each detector i by means of the equation:

$$L_i(N) = (1/b_i) * (V_i(N) - a_i) \qquad (15)$$

where L_i is the look-up table entry for each of the 64 possible data values N recorded by detector i; $V_i(N)$ is the decompressed data value corresponding to the compressed data value N; a_i and b_i are the absolute offset and gain of detector i. The decompression tables, obtained from those supplied by NASA (Reference 1) by expanding to a range of 0 to 255, are shown in Table 1.3.

1.4 CONVERSION OF DIGITAL VALUES TO SCENE RADIANCE

The scene radiance, R', (in watts/m^2sr) in each band can be calculated from the corrected linear digital value V', by means of the expression:

$$R' = A0 + V' * A1 \qquad (16)$$

where A0 and A1 for the CAL2 and CAL3 options are shown in Table 1.2.

1.5 TEST SCENES

A variety of test scenes was chosen, spanning the time period from late August 1982 to late January 1983, and each scene is identified in Table 1.5. The scenes were used for monitoring the calibration wedge, for studying the residual striping and for comparisons of LANDSAT-3 and LANDSAT-4 MSS data, as discussed in Sections 3, 4 and 5 respectively.

2.0 ABSOLUTE CALIBRATION OF TEST SCENE

The method outlined in Section 1 was used to calibrate a test scene recorded on December 9, 1982. First, however, the calwedge data was used for all six detectors in each band, and an absolute calibration for each was calculated as shown graphically in Figures 2.1 to 2.4 for bands 1 to 4 respectively. (Information obtained from these graphs was used in the choice of reference detectors, as described in Section 3.) The CAL3 gains and offsets are tabulated in Table 2.2.

Histograms for all six detectors in each band were accumulated, and are shown in Figures 2.5 to 2.8 for bands 1 to 4 respectively. From these were calculated the relative gains and offsets, shown in Table 2.1.

The CAL3 gains and offsets for all detectors in all bands were then derived, as shown in Table 2.3, by using the absolute gains and offsets for one reference detector in each band combined with the relative gains and offsets of all the other detectors. Comparison of the absolute gains and offsets in Tables 2.2 and 2.3 shows small differences, as discussed in Section 1.2.

3.0 STABILITY OF THE CALWEDGE

The stability of the calwedge is being monitored by CCRS for two major purposes. Firstly, it is advisable to select as reference detectors for absolute calibration purposes the detector within each band which is most reliable in terms of both long term stability and constancy within one scene. Secondly, any long term drift in the absolute calibration of the MSS sensor should be monitored for quality assessment purposes.

3.1 STABILITY WITHIN ONE SCENE

The calwedges from seven scenes in the time period from the end of September 1982 to the end of January 1983 were investigated. For all twenty-four detectors, the mean and standard deviation of each of the six calwedge samples were calculated using data from all 186 calwedges per detector in the full scene. The accumulation of the histograms for each calwedge sample showed the distribution of points to fall either equally in two adjacent bins, or predominantly in one bin with a few points in the closest bin on either side. The only exceptions were samples 5 and 6 for all six detectors in bands 1, 2 and 3, where points fell in up to six bins.

The calwedge sample statistics are shown in Figures 3.1 to 3.24 for each of detectors 1 to 24 respectively. The horizontal scale on the charts shows the sample numbers 1 to 6. For each sample number, the mean and standard deviation for the seven test samples are shown, where each test sample is shown slightly displaced to the right in order of time sequence. The vertical scale, showing the raw digital value in the range 0 to 63, is shown separately for samples 1 to 4 and samples 5 to 6. the relative locations for all six samples within the full calwedge are shown schematically in Figure 3.0.

3.2 STABILITY WITHIN ONE ORBIT

The latest test scenes used by CCRS were from the same orbit on January 20, 1983. Inspection of the plots of the last two sets of calwedge samples shows that the mean value, calculated over each of the test scenes, did not drift by more than one half of one digital level. This study will be continued by CCRS towards the end of the first year of LANDSAT-4 data reception.

3.3 STABILITY OVER A PERIOD OF TIME

Of the twenty-four detectors, sixteen are seen to record calwedge samples with random fluctuations with a spread of approximately one digital level over a period of five months. Detector 16 shows a spread of two digital values. Those detectors for which the calwedge samples are drifting, either up or down, are of some concern since this may represent a change in the gain of that detector. From early September 1982 to late January 1983, the calwedge samples for detectors 5, 10, 19, 21 and 23 have drifted down one level; for detectors 3 and 9 they have drifted up two levels; and for detector 7 they have drifted down two levels.

3.4 CHOICE OF REFERENCE DETECTORS

Reference detectors have been chosen by CCRS using information from three sources. Firstly, those detectors shown to have drifted by one or more levels were rejected as candidates. Secondly, the absolute calibration graphs shown in Figures 2.1 to 2.4 for bands 1 to 4 respectively were used to reject those detectors for which the absolute gain and offset were significantly different from those for the other detectors in the same band. Finally, information supplied by NASA (Reference 2) concerning calwedge data was incorporated into the following choice of reference detectors. (The detector number in the sequence 1 to 24 is shown in parentheses.)

Band 1, detector 2 (2)
Band 2, detector 5 (11)
Band 3, detector 4 (16)
Band 4, detector 4 (22)

4.0 RESIDUAL RADIOMETRIC STRIPING

A simple method to assess the radiometric striping in MSS images consists of selecting arbitrary subscenes, and for each band plotting as a function of the line number the radiometric intensity values averaged over a fixed number of pixels. In such profiles the residual striping appears as a repetitive pattern with a period of six lines which is added to the scene content. Because the scene data is averaged over a number of pixels, for example 100 pixels, variations from line to line due to scene content tend to be small and gradual, particularly over uniform areas such as large water bodies. A detailed discussion and evaluation of this striping assessment method is given by Murphy (1981).

Figures 4.1 and 4.2 show the striping profiles for two subscenes extracted from a LANDSAT-4 MSS scene acquired on August 28, 1983, (path 17, row 30). All the data is presented on a 256 digital counts scale. Figure 4.1 illustrates the striping before and after radiometric calibration for all four bands over a 60-line by 100-pixel subscene in Lake Ontario. For example in band 1, the striping in the uncorrected data is more than four digital levels (peak to peak) while after radiometric calibration it has been reduced to less than one level. The other profiles for calibrated data show residual striping less than two levels. It should be noted that in this subscene, the uncalibrated data presented very little striping in bands 3 and 4. Figure 4.2 contains the corresponding profiles for a subscene acquired over land. Except for the scene information content, the profiles exhibit similar striping characteristics.

5.0 COMPARISON OF LANDSAT-3 AND LANDSAT-4 DATA

Because LANDSAT-3 and LANDSAT-4 have 18-day and 16-day coverage cycles respectively, it is possible to acquire MSS data from two overlapping passes recorded within a few minutes of each other. For example, LANDSAT-3 path 19 and LANDSAT-4 path 18 show considerable overlap over Canada and MSS data were acquired from these two paths by the Prince Albert Station on December 9, 1982. Similarly, data was recorded from LANDSAT-3 path 43 and LANDSAT-4 path 40 on January 20, 1983. With such passes, it is possible to compare LANDSAT-4 MSS to LANDSAT-3 MSS data under identical atmospheric and scene content conditions.

So far the evaluation has been limited to LANDSAT-3 path 19 row 23 and LANDSAT-4 path 18 row 23. It consisted of comparing the raw data histograms for the full scenes. In each of the four bands the histograms have the same general shapes and show less than 1.5 digital level differences in their mean values.

Taking into account the offset between the orbits and the fact that the width of the LANDSAT-3 image is limited to 135 kilometres the overlap between these two images is reduced to 75 kilometres. A more detailed analysis will consist of comparing the histograms for only the portion of the scene which is present in both images.

6.0 MSS GEOMETRIC CORRECTION

For LANDSAT-1, 2, 3 and 4 MSS data CCRS is offering two types of geometric corrections: a priori system corrected products and precision processed geocoded products. The geocoded products are generated on the Digital Image Correction System (DICS) which first went into production in 1979 for LANDSAT-1, 2 and 3 MSS data and was upgraded in 1982 in order to process LANDSAT-4 MSS data. This section discusses the characteristics of the geocoded products and presents the geometric correction model used in DICS.

Section 7 contains results on the geodetic accuracy of geocoded products using LANDSAT-4 MSS data.

6.1 GEOCODED PRODUCTS DEFINITION

Geocoded products consist of remote sensing imagery which has been transformed to a cartographic projection, such as the Universal Transverse Mercator (UTM) projection, and is largely independent of the sensor characteristics and the orbital parameters of the platform. The imagery is corrected to a subpixel accuracy both in multitemporal registration and in absolute geodetic control (as represented by topographic maps). The products are offered in a subscene format derived from the quadrangle division system used for maps. Irrespective of the sensor scan line orientation the processed image lines are aligned to the projection grid, and the pixel spacing meshes conveniently with the grid itself.

Each MSS geocoded product offered by CCRS corresponds to four maps (2x2 sheets) at 1:50,000 scale, that is a 0.5^{o} Latitude by 1.0^{o} Longitude quadrangle in the National Topographic System (NTS) or roughly an area of 60 x 80 kilometres for southern Canada. The actual dimensions of each geocoded product are functions of the quadrangle latitude and quadrangle position within the UTM zone and are defined in terms of the smallest rectangle falling on a one-kilometre grid unit and encompassing an entire NTS 0.5^{o} x 1.0^{o} quadrangle. Except at the centre of a UTM zone, adjacent products present a one or two-kilometre common strip due to the fact that NTS quadrangles are non rectangular. Each product contains a 4-band MSS subscene in the UTM projection where each line of image data is parallel to the Easting direction of the UTM metric grid. The imagery data is resampled to a 50x50-metre grid registered on the one-kilometre UTM grid.

Because the pixel grid is congruent to the UTM grid and the geocoded product dimensions are defined by the NTS quadrangles, geocoded MSS products from LANDSAT-1, 2, 3 and 4 are always in registration and can be superimposed directly; for example, pixel (i,j) in a LANDSAT-4 product covers the same 50x50-metre area as pixel (i,j) from one of the earlier satellites.

This is particularly important given the fact that compared to the earlier missions, LANDSAT-4 follows a different swathing pattern due to a lower orbit.

Figure 6.1 shows as a shaded area a common geocoded product which is extracted from LANDSAT-3 path 17, row 28 and from LANDSAT-4 path 16, row 28. If a particular LANDSAT orbit does not cover completely a given geocoded product in the across track direction, the uncovered portion will contain zero-intensity pixels. There is no attempt to mosaic the data from adjacent orbits on DICS. More information on the definition of geocoded products can be found in Guertin (1981).

6.2 MSS GEOMETRIC CORRECTION MODEL

The geometric correction model implemented on DICS uses Ground Control Points (GCP) measured on maps or extracted from reference image chips and requires only a minimum of ancillary information from the satellite, namely, the time code and the swath length code. It does not model the position and attitude of the platform and represents the geometric correction to be applied as a sequence of three transformations, Figure 6.2.

A product transformation translates the Northing and Easting of any GCP location (N,E) measured on the map into (U,V), the corresponding pixel location in the geocoded product. The product transformation is an affine completely defined by the origin of the product coordinates and the product pixel size. Two bivariate correction functions map (U,V) the corrected pixel location into (X,Y) the systematically corrected pixel location. This second transformation is based on a two-dimensional least-squares estimation process using the GCP information. The GCPs can be measured manually by an operator or by digital correlation. Manual GCPs are digitized on maps at 1:50,000 scale or at 1:250,000 for the northern regions of Canada where larger scale map coverage is not complete. GCPs are located in the MSS imagery by magnifying the image up to 16 times using either a simple pixel repeat or a damped sinc function interpolator and by contrast stretching the radiometric values of the data in order to enhance the features of interest.

The third transformation is an a priori along scan correction which maps (X,Y) into (P,L) the uncorrected pixel and line numbers. It corrects for earth rotation, sensor delay (inter and fractional intra band offsets), swath length variation, mirror velocity variation, panoramic error and earth curvature. These corrections are based on the following information. The earth rotation correction is derived from the nominal orbital parameters of the satellite. The band and detector offsets are known from the pre-launch data. The swath length variations are obtained from the telemetry. The mirror velocity, panoramic error and earth curvature are treated as a single error which is derived experimentally for each satellite by measuring from a LANDSAT scene some 100 to 200 GCPs evenly distributed along the scan lines, following the technique developed by Shlien (1979). For all LANDSAT satellites the mirror profiles have been extracted using prairie scenes containing a regular road network and very little elevation changes.

Having removed most of the along scan systematic errors through the third transformation the least-squares fit is correcting primarily for position and attitude errors, for mapping, aligning and rescaling the imagery to the UTM grid and for any residual errors in the a priori model. Experiments conducted using the MSS imagery from earlier satellites have demonstrated that an absolute geodetic accuracy of 50 metres RMS or better can be achieved consistently over an entire LANDSAT frame using least-squares fit second-order polynomials based on 25 to 35

GCPs. The large number of GCPs contributes to the reduction of the errors associated with the maps, which is estimated at 15 to 30 metres RMS for 1:50,000 scale maps. It has been shown by Fleming (1980) that the overall absolute residual geodetic error can be reduced to 30 metres RMS by replacing in the model the map GCPs with higher accuracy geodetic control from aerial photographs.

7.0 GEOMETRIC ACCURACY OF LANDSAT-4 MSS PRODUCTS

During the past four years, MSS data from the first three LANDSAT missions have been corrected to a 50-metre accuracy. In order to assess the absolute geodetic accuracy of LANDSAT-4 MSS imagery corrected on DICS two studies were conducted: residual errors on GCPs used in the transformation were compared, and independent test GCPs were measured in LANDSAT-4 products.

While the same geometric correction model is applicable to all four satellites, mission specific parameters are required for the along scan correction transformation. In particular, compared to the earlier MSS data, the LANDSAT-4 MSS swath length corrections are more important. Not taking into account the anomaly that had developed on LANDSAT-3, earlier MSS data had swath length differences of only one pixel. They were due primarily to the fact that the MSS mirror active scan and the sensor sampling sequences are not synchronized. For LANDSAT-4 swath length variations as large as eight pixels have been observed on adjacent swaths. For example, Table 7.1 shows a case where the swath length varies on a swath to swath basis in the range of zero to seven pixels. Examples have also been found where the range was only two pixels. This suggests variations in the mirror active scan period for consecutive scans. On DICS, the swath length variations are corrected linearly across the entire scan such that all swaths have the same number of pixels.

After having measured the GCPs and having derived the least-squares fit transformation the accuracy of the transformation can be assessed by the residual errors between the measured GCP locations and the computed locations. Knowing the characteristics of the geometric distortions and the validity of the second-order polynomial fit this can serve as an indication of the image accuracy. Figure 7.1 shows as vectors the residual errors for 34 GCPs measured over an entire LANDSAT-4 scene (Ottawa, path 16, row 28, cycle 5). The largest along scan and across scan errors are 1.00 pixel and 0.57 line respectively. The residual error for the 34 GCPs is 39.7 metres RMS (The RMS error is assuming 28 degrees of freedom for the case of 34 observations).

Table 7.2 compares the GCP residual errors for LANDSAT-4 and for the earlier three satellites. For five LANDSAT-4 MSS scenes it shows the RMS errors for similar scenes obtained from the earlier LANDSAT satellites. The earlier scenes have been selected to cover approximately the same regions as LANDSAT-4 in order to minimize effects due to map accuracy, relief distortions and image content. The acquisition dates have not been taken into account. For the earlier LANDSATs, the RMS error averaged over 15 scenes is 35.1 metres with a standard deviation of 5.7 metres compared to 38.3 metres with a standard deviation of 3.0 metres for LANDSAT-4. While the earlier LANDSAT images extracted from the archive had been corrected over a period of three years, differences in the operational procedures could have contributed to the larger standard deviation. For each of the LANDSAT-4 images "LL" indicates the swath length variations observed in the image. Taking into account the small number of scenes it can be stated that using the same correction model LANDSAT-4 MSS can be corrected to about the same accuracy as the earlier satellites and that swath length variations do not contribute significantly to the product errors.

In the second evaluation of product accuracy, a LANDSAT-4 image was corrected based on 34 well-distributed GCPs, and 14 new GCPs from a different set were measured in a single geocoded product extracted from that image. The selected geocoded product covers NTS maps 31G3, 31G4, 31G5 and 31G6 which include Ottawa in the top left quadrant. The product is located in the bottom right corner of path 16 row 28 and the top right corner of path 16 row 29. In such cases the geometric correction model is estimated for a full LANDSAT scene consisting of the bottom half of the first frame (row 28) and the top half of the second frame (row 29). Table 7.3 shows the Northing and Easting errors for the test GCPs, and their means and standard deviations. Based on the 14 GCPs the absolute geodetic error for the entire geocoded product is estimated at 48.1 metres RMS. The RMS error on the 34 original GCPs is 39.7 metres. Since geometric correction models based on bivariate second order polynomials show larger distortions at the edges, it would be necessary to measure the residual errors over each geocoded product from the same input image in order to assess further the absolute geodetic accuracy.

8.0 CONCLUSION

This early report has described the methodology used by CCRS to perform radiometric calibration and precision geometric correction of standard LANDSAT-4 MSS products. It has shown how the same algorithms are used to radiometrically correct and to place on a calibrated radiance scale the data from all four LANDSAT satellites. To assess the reliability of absolute calibration, the report has discussed the minor variations observed in the LANDSAT-4 calibration data and has proposed the comparison of overlapping LANDSAT-3 and LANDSAT-4 scenes acquired at the same time.

After reviewing the concept of geocoded products, this document has shown that the geometric correction model developed to precision process the MSS data from the earlier LANDSAT satellites can generate LANDSAT-4 MSS geocoded products with comparable geodetic accuracy.

The results presented here are seen as preliminary and are expected to be refined and augmented as more LANDSAT-4 data are acquired and processed by CCRS production facilities over a longer period.

9.0 REFERENCES

Ahern F., Murphy, J. (1978) Radiometric Calibration and Correction of LANDSAT 1, 2 and 3 MSS Data, CCRS Research Report 78-4, November 1978.

Fleming, E.A., Guertin, F.E. (1980) Determination of the Geographical Position of Isolated Islands using the Digital Image Correction System for LANDSAT MSS Imagery, 14th Congress of the International Society for Photogrammetry, Hamburg.

Guertin, F.E., Shaw, E. (1981) Definition and Potential of Geocoded Satellite Imagery Products, 7th Canadian Symposium on Remote Sensing, Winnipeg, pp. 384-394.

Murphy, J. (1981) A Refined Destriping Procedure for LANDSAT MSS Data Products, 7th Canadian Symposium on Remote Sensing, Winnipeg, pp. 454-470.

NASA Ref. 1 (1982) LANDSAT-D to Ground Station Interface Description, Revision 5, October, GSFC 435-D-400.

NASA Ref. 2 (1982) LANDSAT-D Investigations Workshop (LIDQA), May 13-14.

NASA Ref. 3 (1982) Third LANDSAT Technical Working Group Meeting (LTWG), October.

Shlien, S. (1979) Geometric Correction Registration and Resampling of LANDSAT Imagery, Canadian Journal of Remote Sensing, May, pp. 74-89.

Strome, W.M. et al. (1975) Format Specifications for Canadian LANDSAT MSS System Corrected Computer Compatible Tape, CCRS Research Report 75-3.

TABLE 1.1 - MAXIMUM AND MINIMUM RADIANCE VALUES (MW/CM2SR)

CHANNEL	RMIN	RMAX	RMIN´	RMAX´	RMIN´´	RMAX´´
1	0.02	2.5	0.02	2.3	0.0	2.5
2	0.04	1.8	0.04	1.8	0.0	2.0
3	0.04	1.5	0.04	1.3	0.0	1.5
4	0.10	4.0	0 10	4.0	0.0	4.0

WHERE RMIN - NASA (CAL2) PRELAUNCH MINIMUM RADIANCE
RMAX - NASA (CAL2) PRELAUNCH MAXIMUM RADIANCE
RMIN´ - NASA (CAL2) POSTLAUNCH MINIMUM RADIANCE
RMAX´ - NASA (CAL2) POSTLAUNCH MAXIMUM RADIANCE
RMIN´´ - CAL3 MIMINUM RADIANCE
RMAX´´ - CAL3 MAXIMUM RADIANCE

TABLE 1.2 - A0 AND A1 COEFFICIENTS (W/M2SR)

CAL2 A0	CAL2 A1	CAL3 A0	CAL3 A1
2*10**-1	8941*10**-5	0	9804*10**-5
4*10**-1	6902*10**-5	0	7843*10**-5
4*10**-1	4941*10**-5	0	5882*10**-5
10*10**-1	15294*10**-5	0	15686*10**-5

WHERE
Absolute radiance value, R´ = A0 + A1 * V´
and V´ is the calibrated digital value.

TABLE 1.3 - DECOMPRESSION TABLES

DECOMPRESSION TABLES - BANDS 1 AND 3

0.0	1.8	3.6	5.4	7.2	9.0	11.0	13.0
14 8	16.6	18.6	20.6	22.6	24 6	26.8	29.0
31.2	33 6	36.2	38.8	42.0	45.0	48.0	51.0
54.6	58.0	61.6	65.0	68.8	72.8	77.0	81.0
85 0	88 8	92.6	96.2	99.8	103.6	108.0	113.2
118.8	124.0	129 0	134.4	139.8	146.0	151.8	157.8
163.6	169 6	175.4	181 0	186.6	192.2	198.0	204.0
210.0	216.2	222.4	228.6	234.8	241.0	247.2	254.0

DECOMPRESSION TABLES - BAND 2

0.0	1.6	3.2	5.0	6.8	8.8	10.6	12.4
14.4	16 4	18.4	20.6	22.6	24.6	26.8	29 0
31.2	33.6	36 2	38.8	42.0	45 0	48 0	51.0
54 6	58.0	61 6	65.0	68.8	72.8	77.0	81.0
85.0	88 6	92.2	95 8	99 4	103.0	107.4	112.8
118.4	123.6	128.6	134.0	139.6	145.6	151.4	157.4
163 2	169.2	175.0	180.6	186.2	192.2	198.0	204.0
210.0	216.2	222.4	228.6	234.8	241.0	247.2	254.0

Table 1.4 LANDSAT-4 Modified Ci"s & Di"s

```
OFFSETS (Ci's) :

      DATA ((CIM4(I,J),I=1,6),J=1,6)/
     +          -0.05044050, -0.02074160,  0.00846760,
     +           0.03403190,  0.51373140,  0.51495150,
     +          -0.04896130, -0.01938700,  0.00774700,
     +           0.03452340,  0.51237920,  0.51369880,
     +          -0.04889510, -0.01909270,  0.00701670,
     +           0.03240320,  0.51355590,  0.51501270,
     +          -0.04896040, -0.01941010,  0.00730540,
     +           0.03306180,  0.51314260,  0.51486010,
     +          -0.04955080, -0.02222870,  0.00953270,
     +           0.03481040,  0.51269500,  0.51474140,
     +          -0.04973960, -0.01888300,  0.00796110,
     +           0.03248670,  0.51322930,  0.51494550
     + /
      DATA ((CIM5(I,J),I=1,6),J=1,6)/
     +          -0.05344900, -0.01940160,  0.01122860,
     +           0.04251390,  0.50862710,  0.51188980,
     +          -0.05443910, -0.01916970,  0.01063320,
     +           0.03967680,  0.50986750,  0.51343050,
     +          -0.05335200, -0.01817020,  0.01165940,
     +           0.03866120,  0.50908450,  0.51211670,
     +          -0.05441640, -0.01823660,  0.01291340,
     +           0.04082070,  0.50803260,  0.51088560,
     +          -0.05380060, -0.01977140,  0.01027140,
     +           0.04085980,  0.50946330,  0.51297680,
     +          -0.05412580, -0.01990290,  0.00992610,
     +           0.04152150,  0.50942310,  0.51315740
     + /

      DATA ((CIM6(I,J),I=1,6),J=1,6)/
     +          -0.05704220, -0.02197540,  0.00842300
     +           0.03960200,  0.51324970,  0.51774330
     +          -0.05796830, -0.02231510,  0.00827520
     +           0.03914950,  0.51417110,  0.51868670
     +          -0.05926110, -0.02706710,  0.00411550
     +           0.03733270,  0.52006830,  0.52461070
     +          -0.06023280, -0.02476510,  0.00752620
     +           0.03826340,  0.51731030,  0.52189270
     +          -0.05873130, -0.02233320,  0.00803440
     +           0.03840670,  0.51492430,  0.51969320
     +          -0.05866450, -0.02347670,  0.00884060
     +           0.03874310,  0.51493910,  0.51961750
     + /
      DATA ((CIM7(I,J),I=1,6),J=1,6)/
     +          -0.08950200, -0.04144460, -0.00395170
     +           0.03990730,  0.54677160,  0.54822120
     +          -0.08913090, -0.04259440, -0.00207010
     +           0.03881090,  0.54638960,  0.54859710
     +          -0.08683630, -0.03995820, -0.00112650
     +           0.03891670,  0.54373020,  0.54527510
     +          -0.08828550, -0.04554920, -0.00276330
     +           0.04064930,  0.54713930,  0.54881220
     +          -0.08513990, -0.04295810, -0.00074280
     +           0.03921280,  0.54410990,  0.54554780
     +          -0.08418970, -0.04236670, -0.00032440
     +           0.03665530,  0.54427150,  0.54613470
     + /

GAINS (Di's) :

      DATA ((DIM4(I,J),I=1,6),J=1,6)/
     +           0.37384636,  0.32270623,  0.27240944,
     +           0.22838916, -0.59762305, -0.59972[illegible],
     +           0.38377613,  0.33113939,  0.28285027,
     +           0.23518577, -0.61530140, -0.61764640,
     +           0.37538711,  0.32348751,  0.27801971,
     +           0.23381069, -0.60408416, -0.60662195,
     +           0.38663017,  0.33364509,  0.28374274,
     +           0.23956043, -0.62124962, -0.62432872,
     +           0.38408816,  0.33555321,  0.27913222,
     +           0.23422909, -0.61468358, -0.61831871,
     +           0.38633607,  0.33124962,  0.28332677,
     +           0.23954269, -0.61869547, -0.62175573
     + /
      DATA ((DIM5(I,J),I=1,6),J=1,6)/
     +           0.37615660,  0.31510970,  0.26222080,
     +           0.21025470, -0.57911560, -0.58462580,
     +           0.37683800,  0.31672710,  0.26593290,
     +           0.21643300, -0.58492920, -0.59100160,
     +           0.37715130,  0.31684350,  0.26571010,
     +           0.21942420, -0.58696560, -0.59216330,
     +           0.38476210,  0.32179640,  0.26758440,
     +           0.21901600, -0.59409660, -0.59906200,
     +           0.36968810,  0.31262660,  0.26224960,
     +           0.21093770, -0.57481520, -0.58070670,
     +           0.38073110,  0.32173450,  0.27029510,
     +           0.21580960, -0.59107530, -0.59751480
     + /

      DATA ((DIM6(I,J),I=1,6),J=1,6)/
     +           0.34998028,  0.29512022,  0.24756368
     +           0.19878563, -0.54220993, -0.54923987,
     +           0.35163692,  0.29552634,  0.24794116,
     +           0.19981144, -0.54397333, -0.55104193,
     +           0.35757652,  0.30062272,  0.25227008
     +           0.20438063, -0.55933005, -0.56651939,
     +           0.36876274,  0.31112570,  0.25864600
     +           0.20868819, -0.56988652, -0.57733416,
     +           0.37168222,  0.31166160,  0.26158513
     +           0.21149782, -0.57427970, -0.58214667
     +           0.36461442,  0.30769303,  0.25519648
     +           0.20700799, -0.56358048, -0.57115126
     + /
      DATA ((DIM7(I,J),I=1,6),J=1,6)/
     +           0.41613790,  0.33807030,  0.27714460
     +           0.20591720, -0.61746820, -0.61982300
     +           0.43228070,  0.35363710,  0.29515370
     +           0.21606760, -0.64170430, -0.64543500
     +           0.41927050,  0.34173870,  0.27751450
     +           0.21128850, -0.62362830, -0.62618350
     +           0.44784980,  0.37277860,  0.29762140
     +           0.22136270, -0.66833770, -0.67127640
     +           0.47547810,  0.39588420,  0.31611370
     +           0.24066850, -0.71271490, -0.71543020
     +           0.45994920,  0.38326690,  0.30618120
     +           0.23874470, -0.69234530, -0.69579840
     + /
```

Table 1.5 Identification of Test Scenes

NASA SCENE IDENTIFICATION	PATH-ROW	ACQUISITION DATE
40043-152419	17-30	August 28, 1982
40048-171913	36-23	September 2, 1982
40068-151610	16-24	September 22, 1982
40098-170739	34-23	October 22, 1982
31695-17594	46-22	October 25, 1982
40101-173809	39-22	October 25, 1982
40131-17493	41-18	November 24, 1982
31726-17295	41-19	November 25, 1982
40146-15293	18-23	December 9, 1982
31740-15251	19-23	December 9, 1982
40169-171350	35-21	January 1, 1983
40188-17451	40-21	January 20, 1983
31782-17414	43-21	January 20, 1983
40188-17465	40-25	January 20, 1983
31782-17432	43-25	January 20, 1983
31782-17473	43-35	January 20, 1983

TABLE 2.1

RELATIVE GAINS AND OFFSETS, USING HISTOGRAMS

DETECTOR	BAND 1		BAND 2		BAND 3		BAND 4	
	GAIN	OFFSET	GAIN	OFFSET	GAIN	OFFSET	GAIN	OFFSET
1	0.9813	0.0856	0.9236	-0.7109	0.9474	0.0335	0.9611	0.3339
2	1.0000	0.0000 *	1.0458	-1.1507	0.9861	-0.1783	0.9795	0.0306
3	1.0379	1.2877	0.9313	-0.3736	1.0568	-0.8806	0.9696	-0.2955
4	1.0621	0.3233	0.9221	-0.0108	1.0000	0.0000 *	1.0000	0.0000 *
5	0.8356	0.9289	1.0000	0.0000 *	1.0246	-0.9032	0.9465	-0.1390
6	0.9601	0.3113	1.0225	-0.0948	0.9672	-0.2197	0.9676	-0.4966

TABLE 2.2

ABSOLUTE (CAL 3) GAINS AND OFFSETS, USING CALWEDGES

DETECTOR	BAND 1		BAND 2		BAND 3		BAND 4	
	GAIN	OFFSET	GAIN	OFFSET	GAIN	OFFSET	GAIN	OFFSET
1	0.8416	-0.7195	0.8241	-2.2747	0.8584	-1.9502	0.8974	-5.7692
2	0.8583	-0.6319 *	0.9379	-2.1670	0.8969	-2.8125	0.9060	-6.3150
3	0.8931	0.5993	0.8295	-2.2191	0.9693	-5.0502	0.9203	-5.5261
4	0.9148	-0.5279	0.8281	-1.3401	0.9154	-3.2833 *	0.9253	-6.4430*
5	0.7177	-1.0117	0.8745	-1.3472 *	0.9414	-3.3754	0.8884	-5.9598
6	0.8381	-0.9245	0.9126	-1.3563	0.8999	-3.1385	0.8873	-5.8561

TABLE 2.3

ABSOLUTE (CAL 3) GAINS AND OFFSETS

- COMBINING ABSOLUTE AND RELATIVE GAINS AND OFFSETS

DETECTOR	BAND 1		BAND 2		BAND 3		BAND 4	
	GAIN	OFFSET	GAIN	OFFSET	GAIN	OFFSET	GAIN	OFFSET
1	0.8422	-0.5343	0.8077	-1.9552	0.8672	-2.0770	0.8693	-5.8582
2	0.8583	-0.6319 *	0.9145	-2.5596	0.9072	-3.4160	0.9067	-6.2805
3	0.8909	0.6318	0.8144	-1.6292	0.9673	-4.3503	0.8971	-6.5426
4	0.9116	-0.5478	0.8064	-1.2530	0.9154	-3.2833*	0.9253	-6.4430*
5	0.7172	0.4008	0.8745	-1.3472 *	0.9379	-4.3474	0.8758	-6.2372
6	0.8240	-0.2954	0.8941	-1.4523	0.9036	-3.4608	0.8953	-6.7308

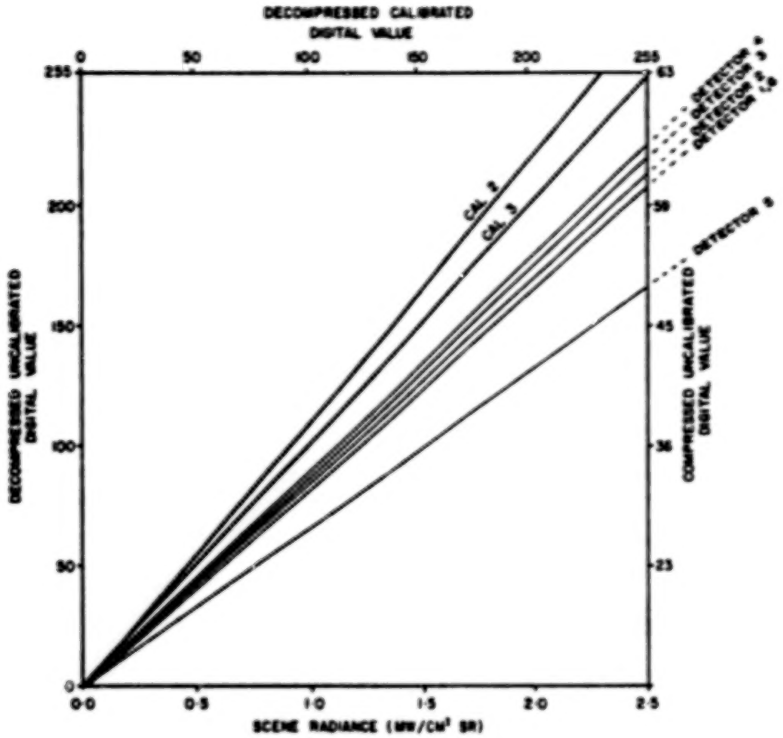

Relationship between Scene Radiance and Compressed, Decompressed and Calibrated Digital Values

Figure 2.1 ABSOLUTE CALIBRATION FOR BAND 1

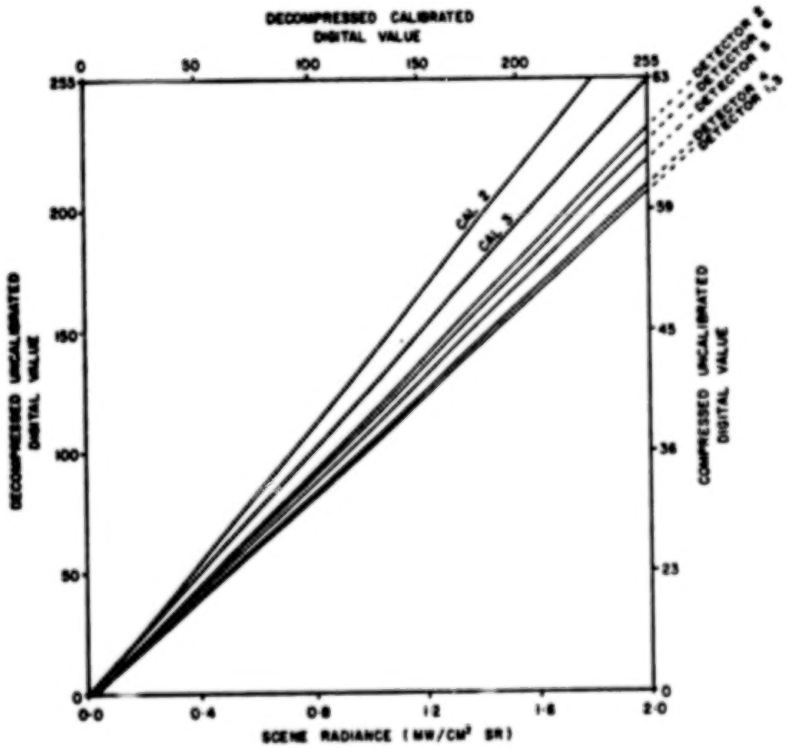

Relationship between Scene Radiance and Compressed Decompressed and Calibrated Digital Values

Figure 2.2 ABSOLUTE CALIBRATION FOR BAND 2

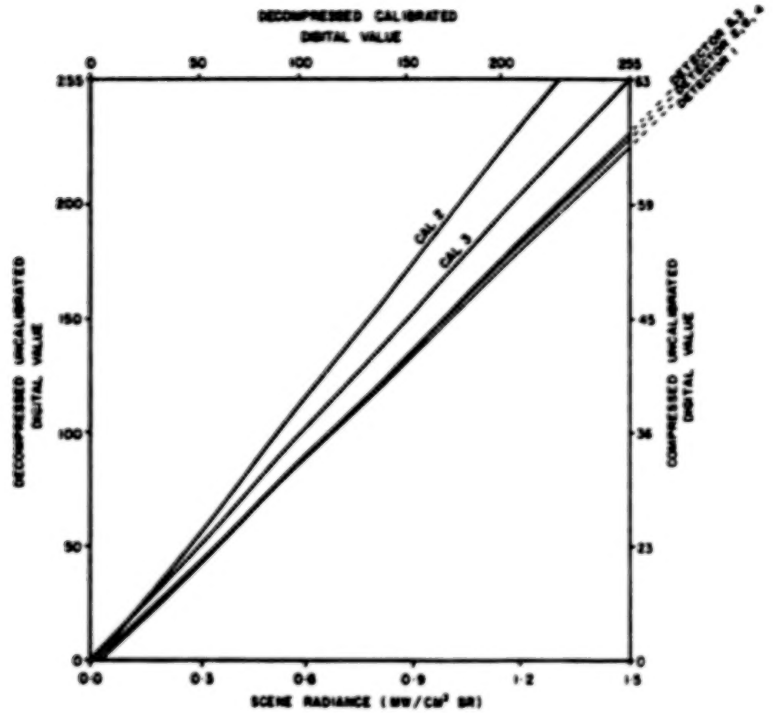

Relationship between Scene Radiance and Compressed Decompressed and Calibrated Digital Values

Figure 2.3 ABSOLUTE CALIBRATION FOR BAND 3

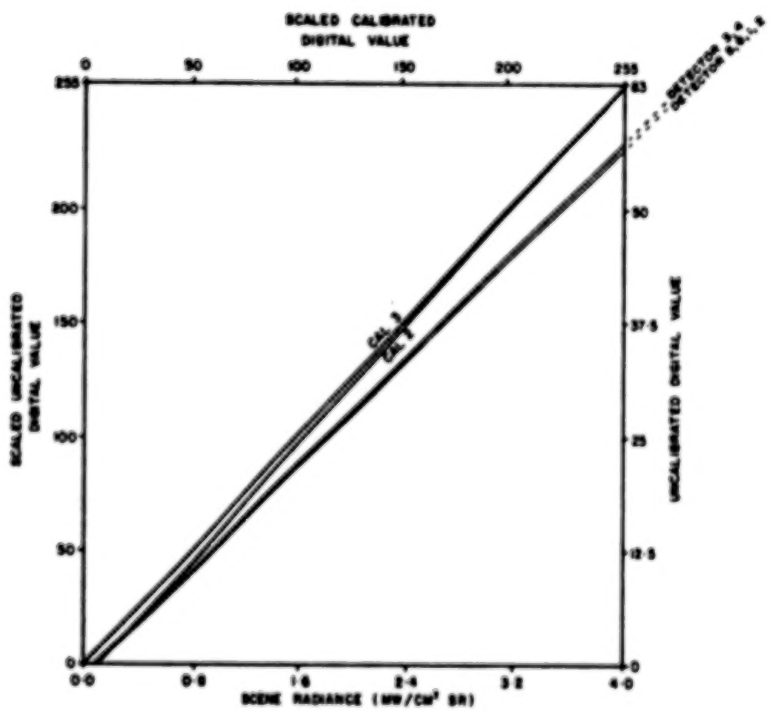

Relationship between Scene Radiance and Uncalibrated, Scaled Uncalibrated and Calibrated Digital Values

Figure 2.4 ABSOLUTE CALIBRATION FOR BAND 4

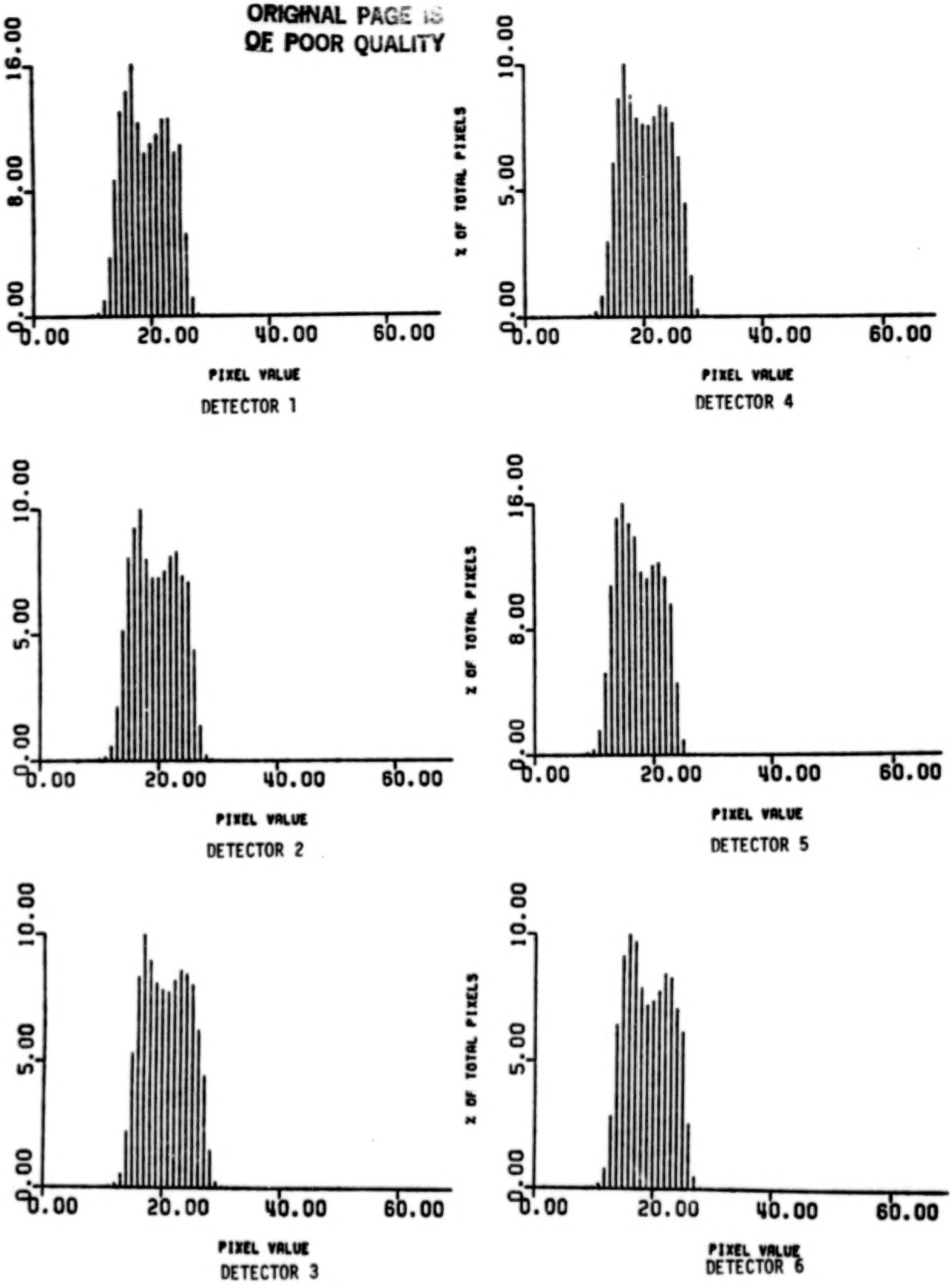

FIGURE 2.5 BAND 1 RAW DATA HISTOGRAMS

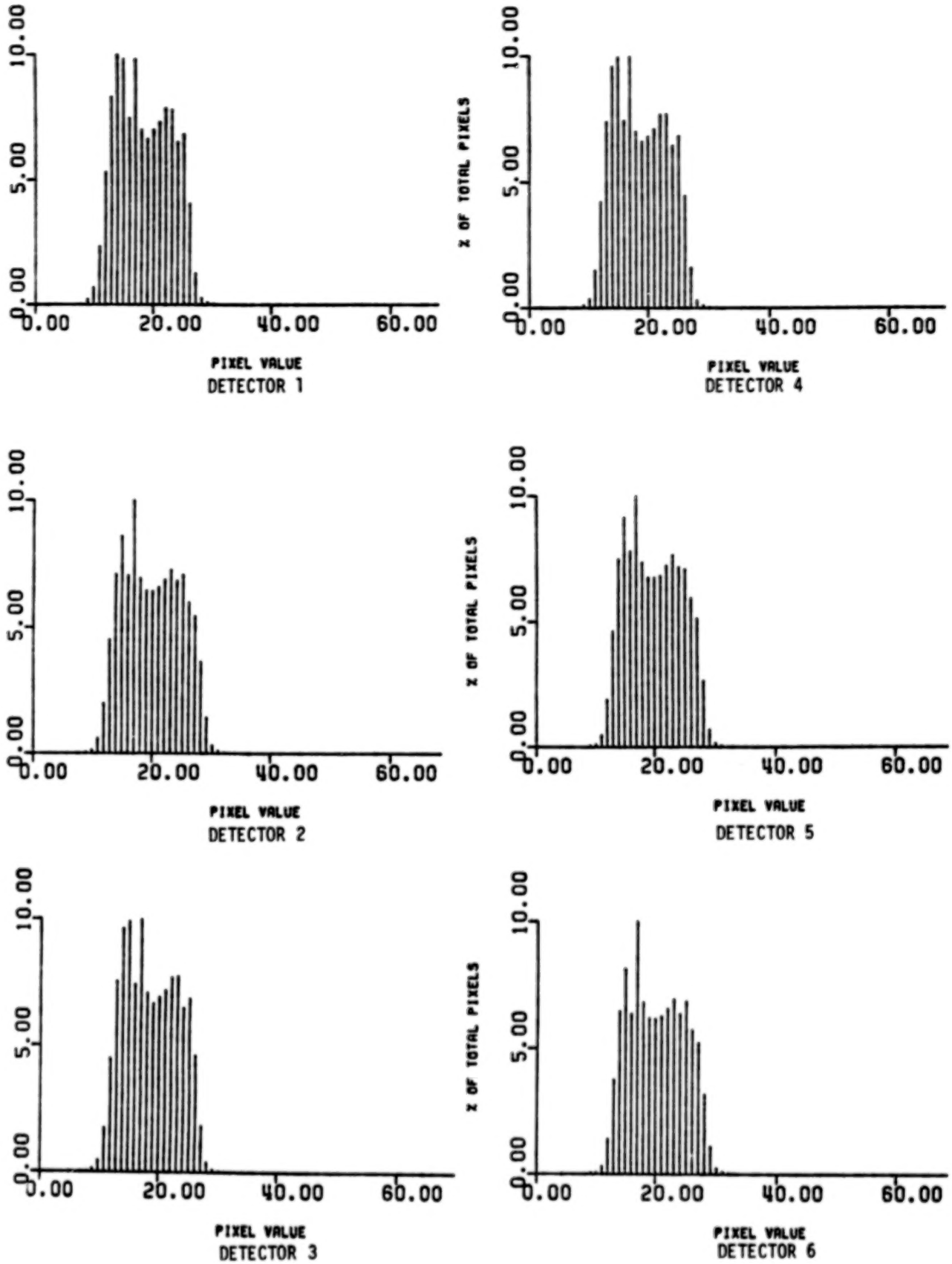

FIGURE 2.6 BAND 2 RAW DATA HISTOGRAMS

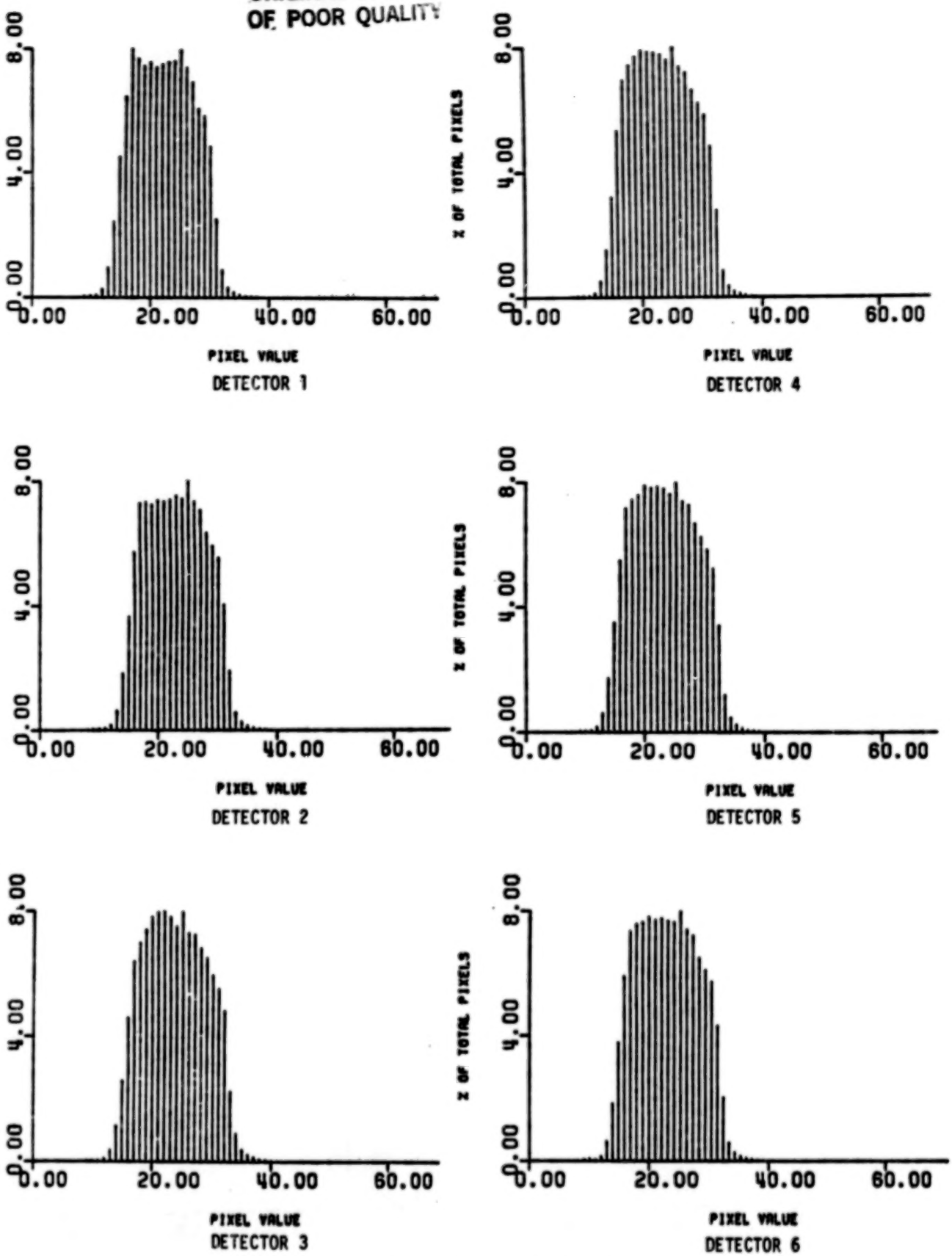

FIGURE 2.7 BAND 3 RAW DATA HISTOGRAMS

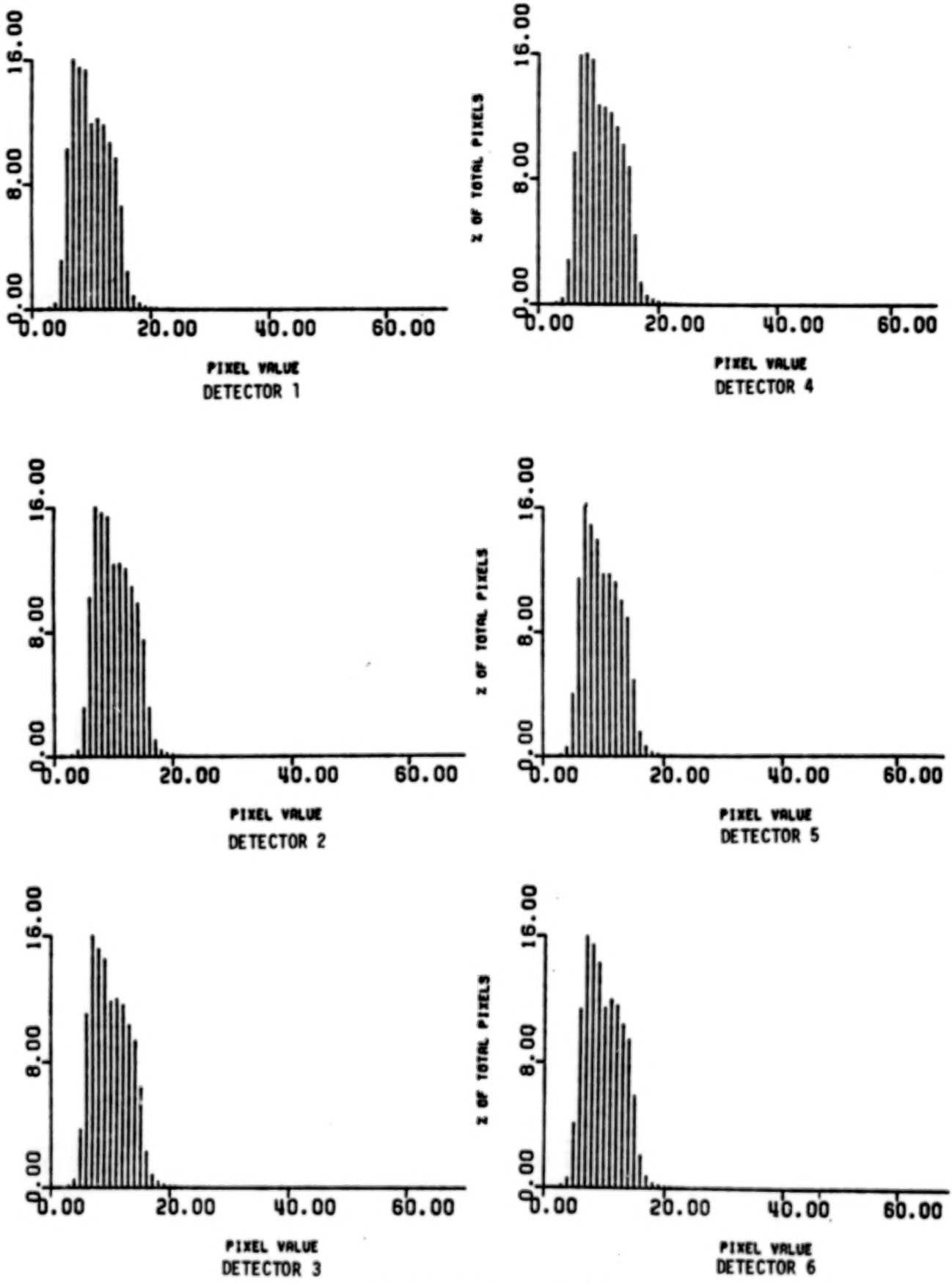

FIGURE 2.8 BAND 4 RAW DATA HISTOGRAMS

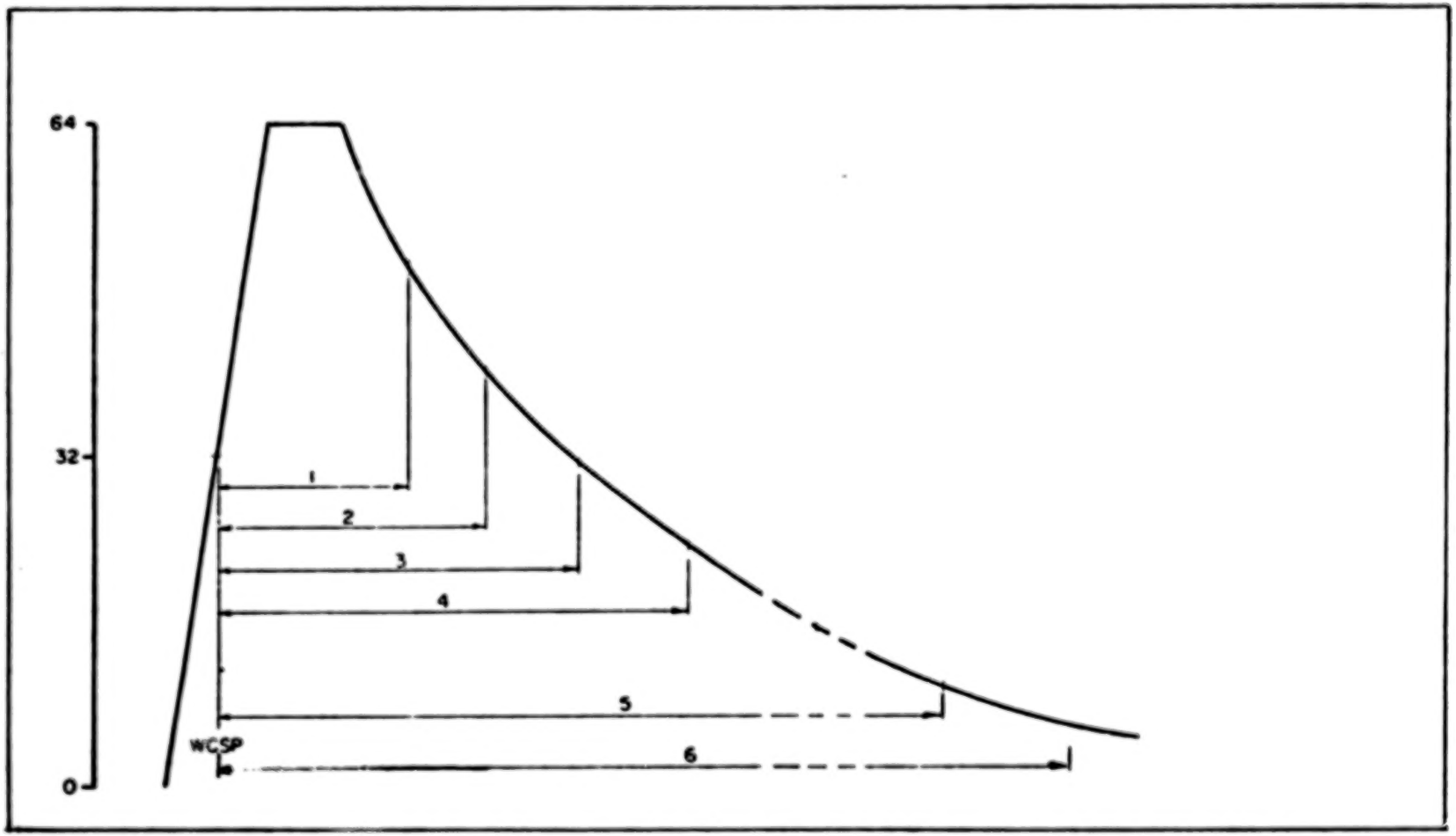

FIGURE 3.0 The calibration wedge. This is a schematic representation of a typical LANDSAT MSS calibration wedge showing the six sample locations relative to the word count start position (WCSP).

DETECTOR 1

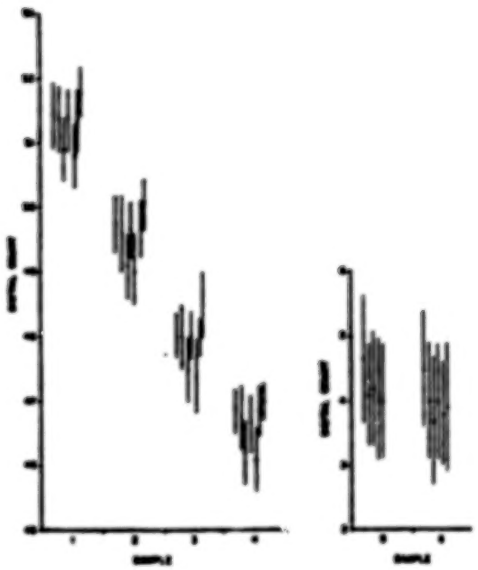

FIGURE 3-1

DETECTOR 2

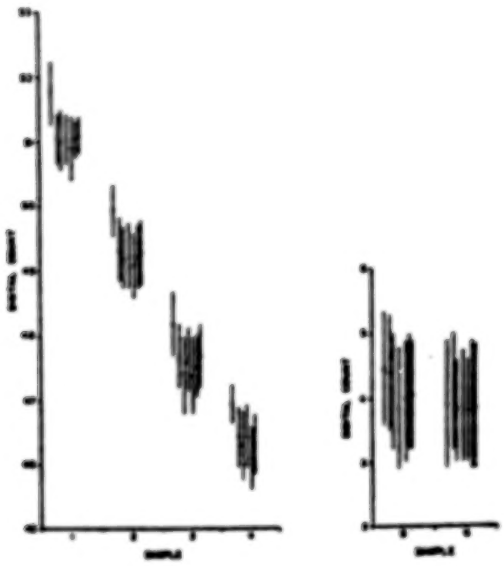

FIGURE 3-2

DETECTOR 3

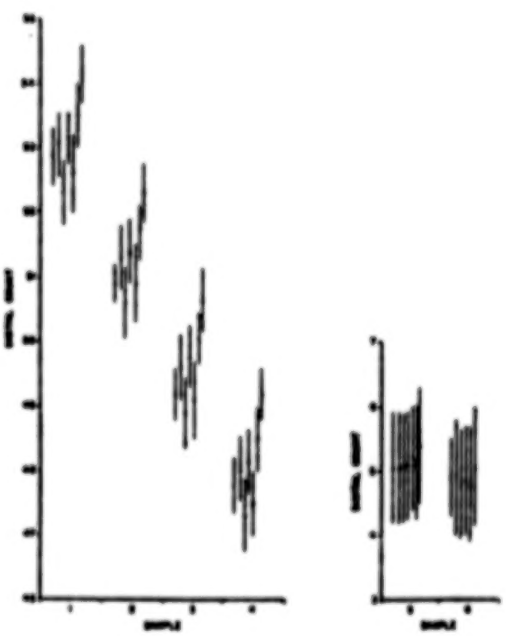

FIGURE 3-3

DETECTOR 4

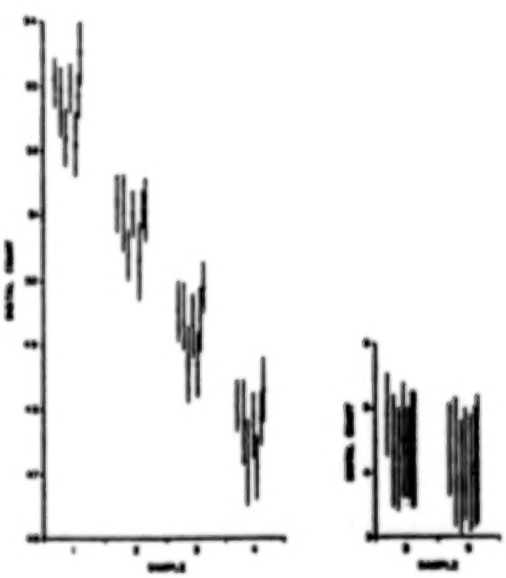

FIGURE 3-4

DETECTOR 5

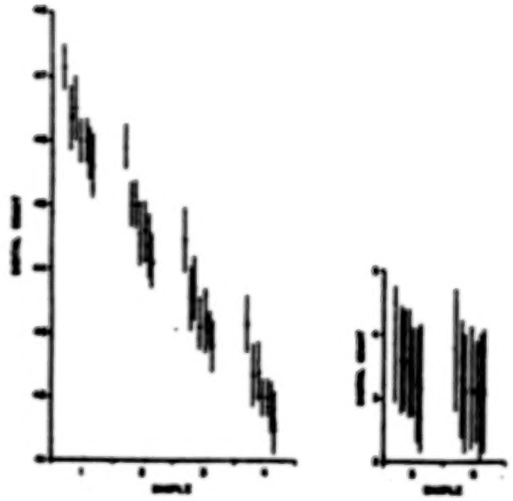

FIGURE 3.5

DETECTOR 6

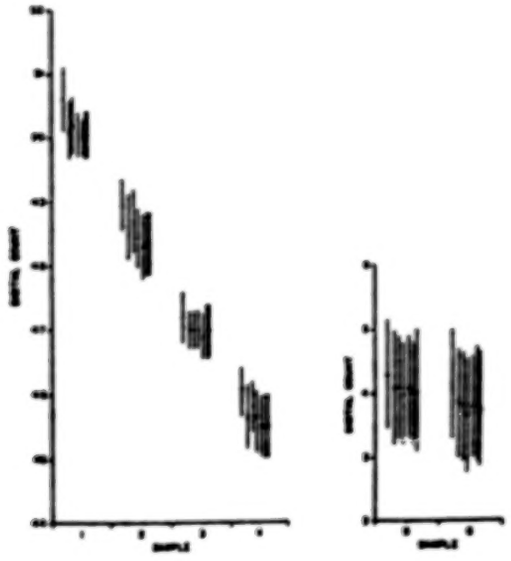

FIGURE 3.6

DETECTOR 7

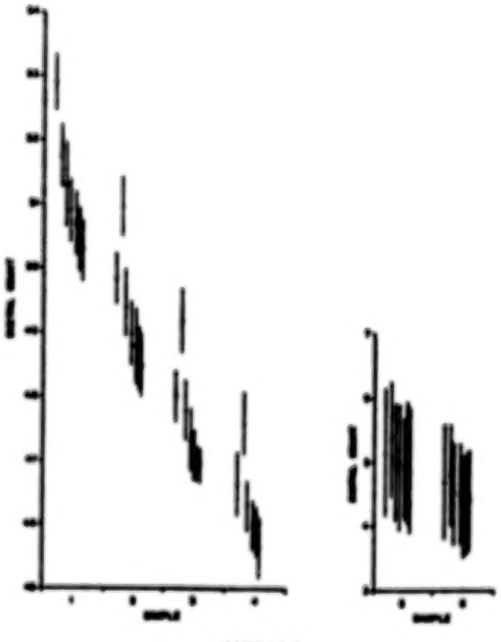

FIGURE 3.7

DETECTOR 8

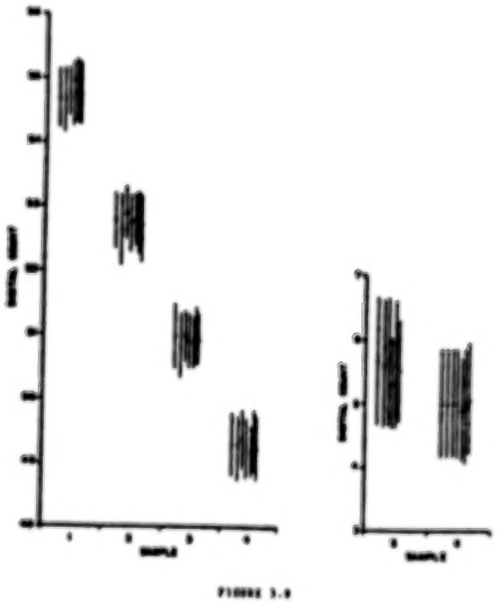

FIGURE 3.8

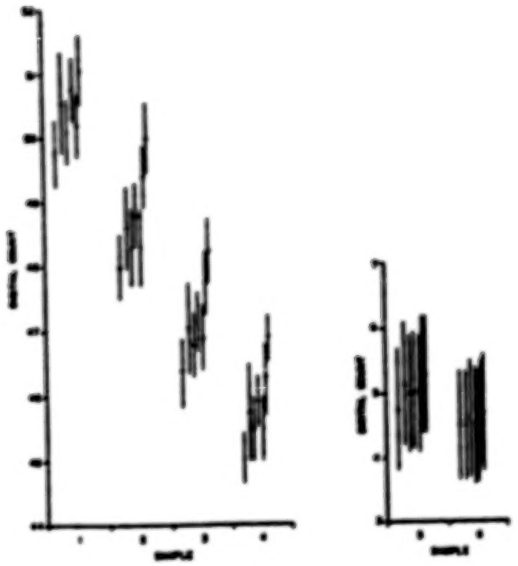

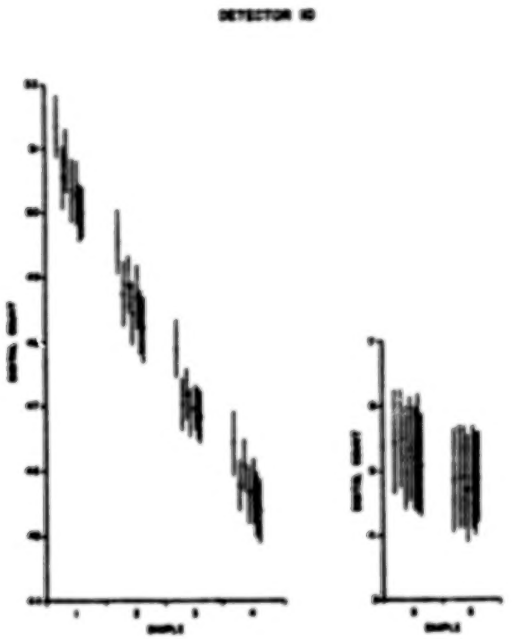

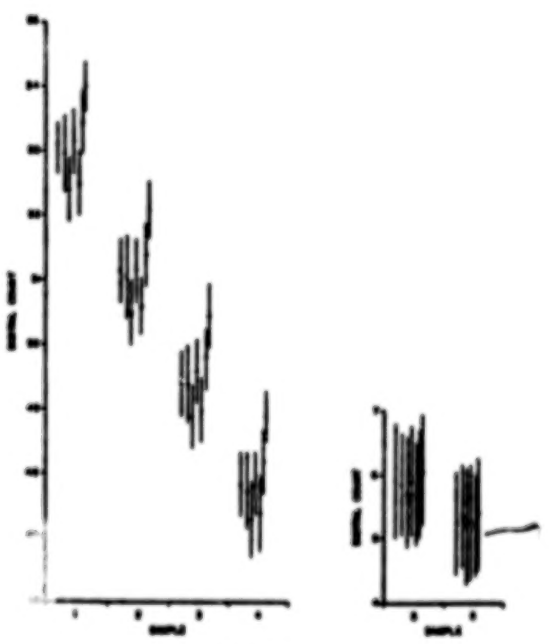

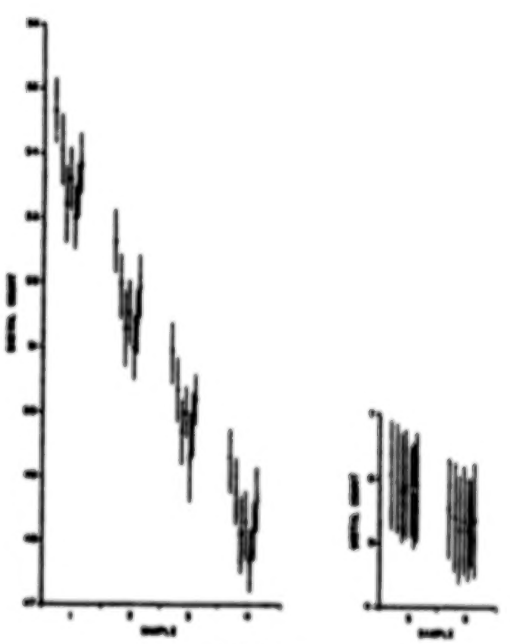

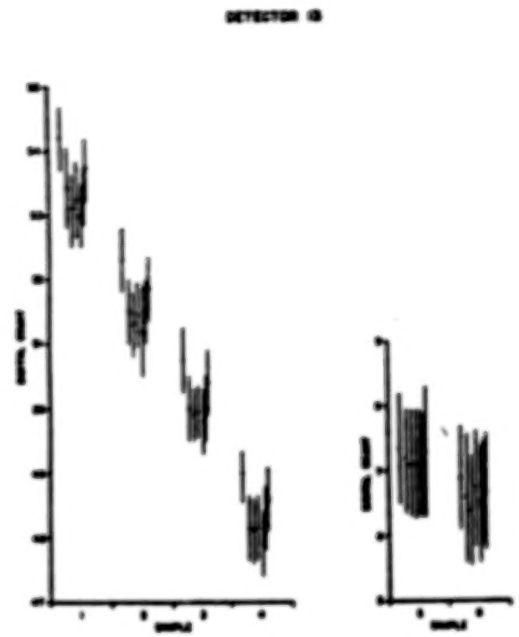

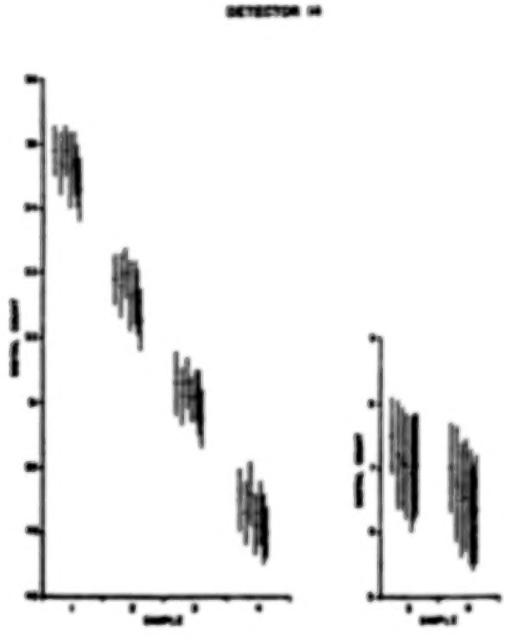

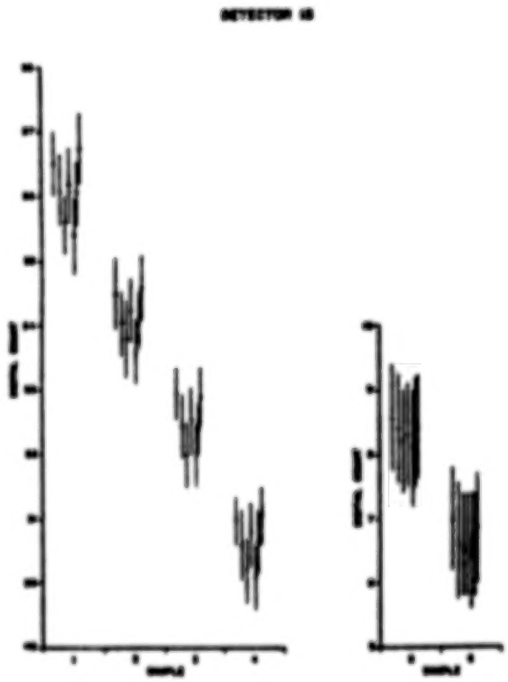

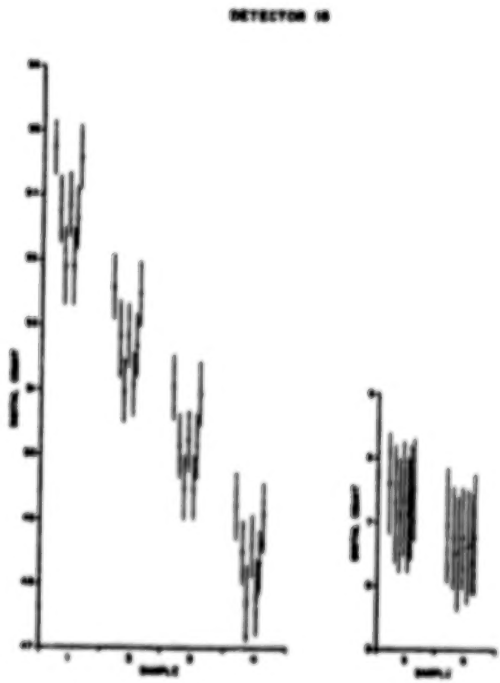

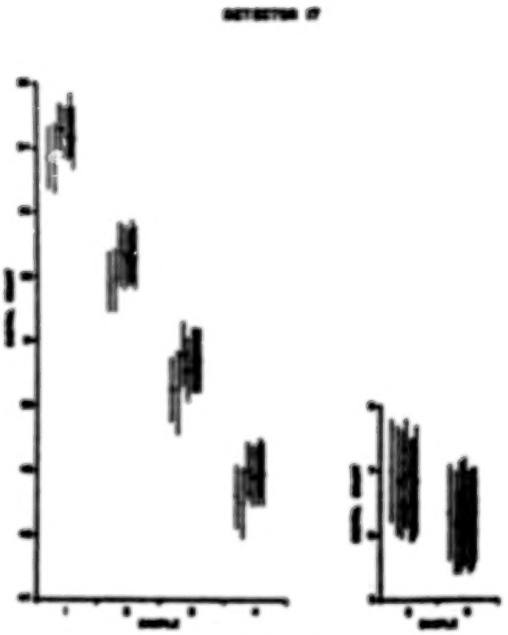

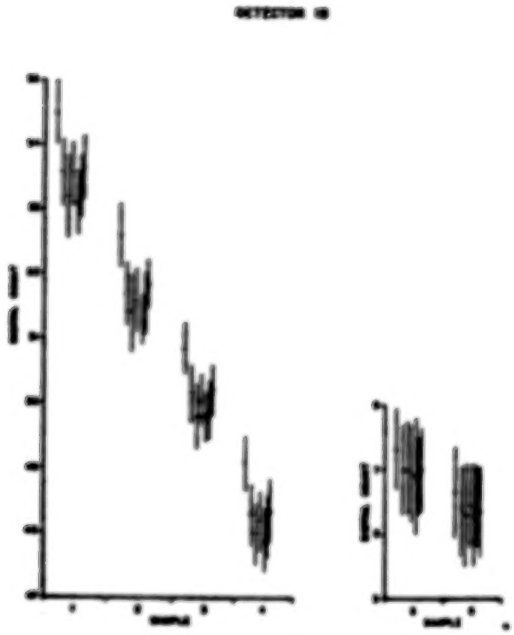

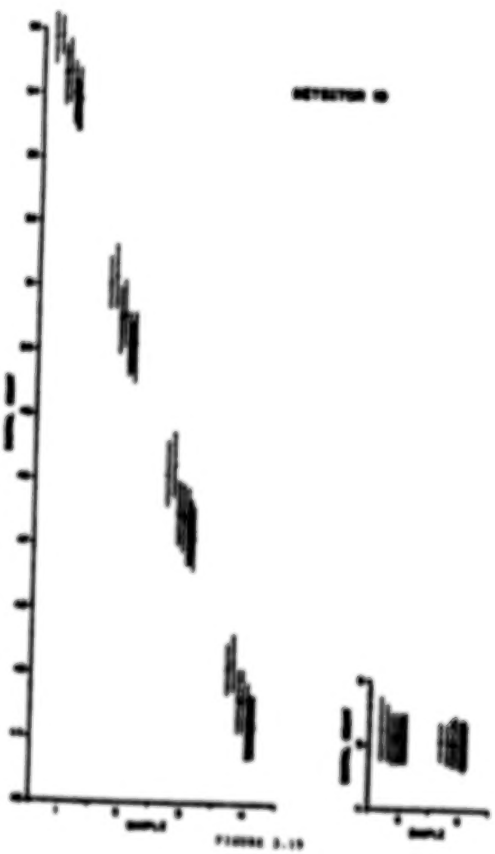

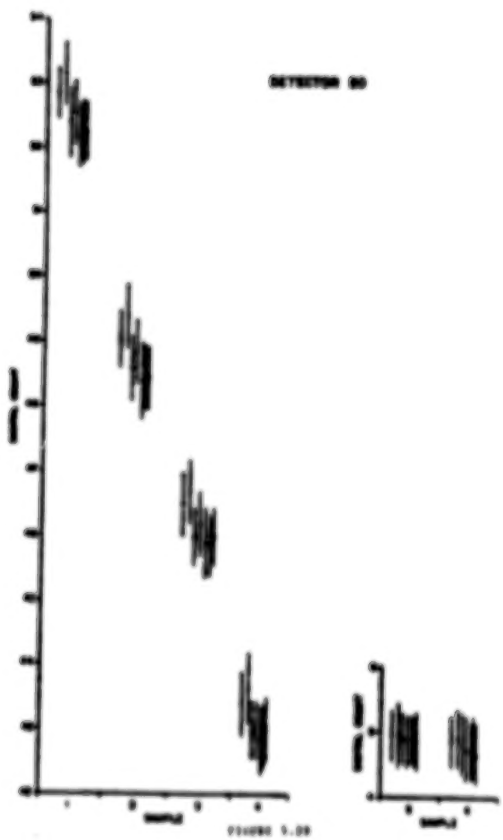

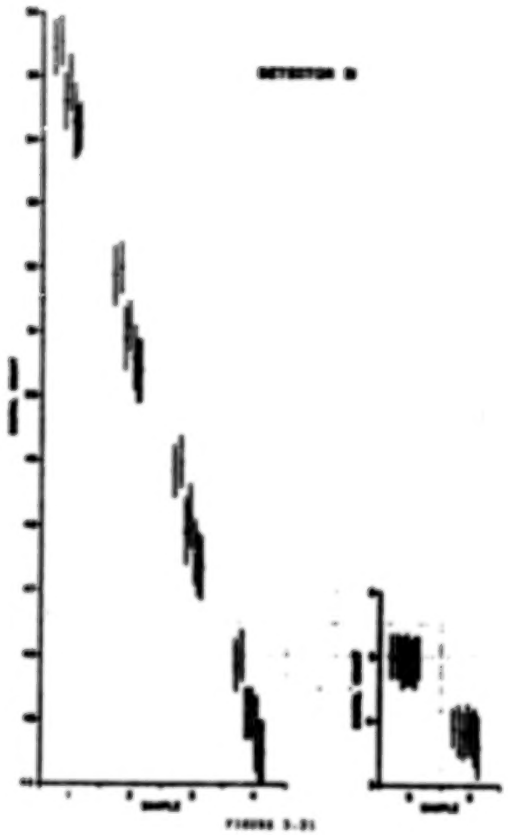

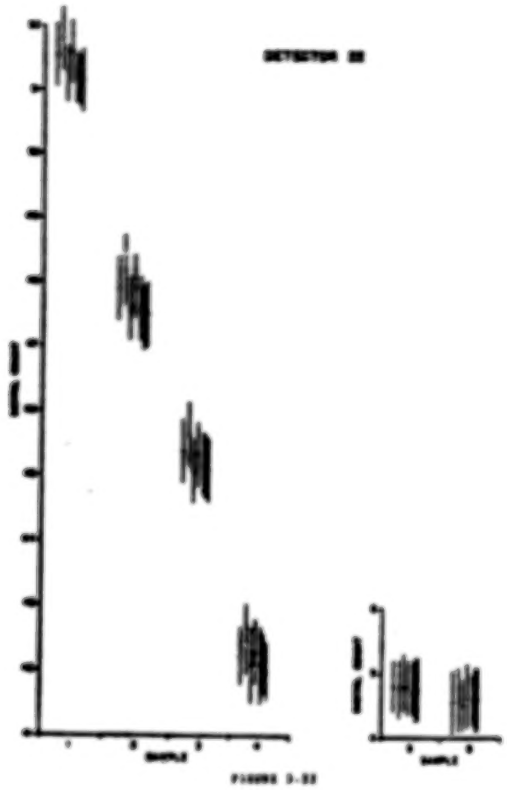

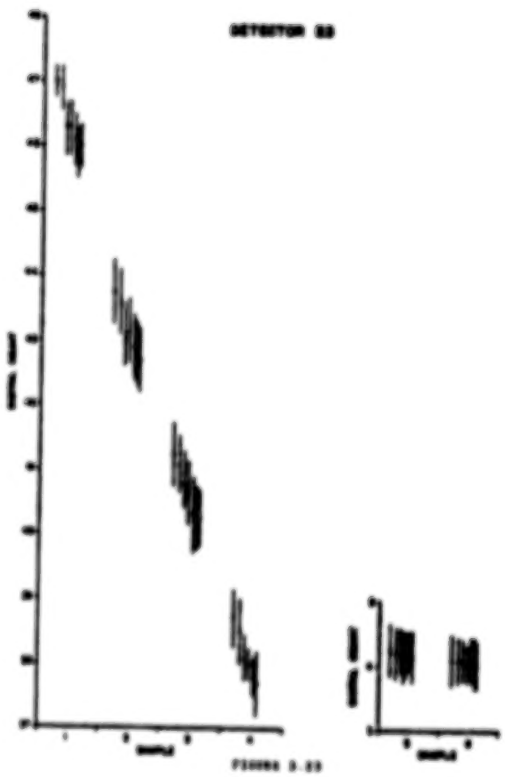

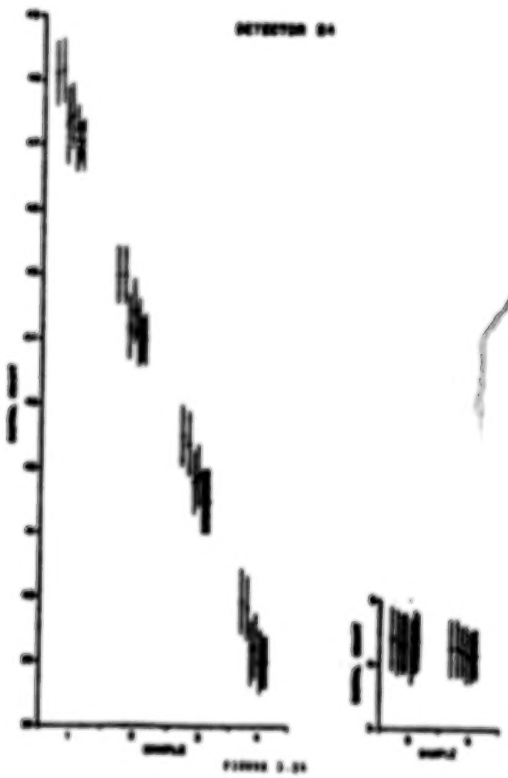

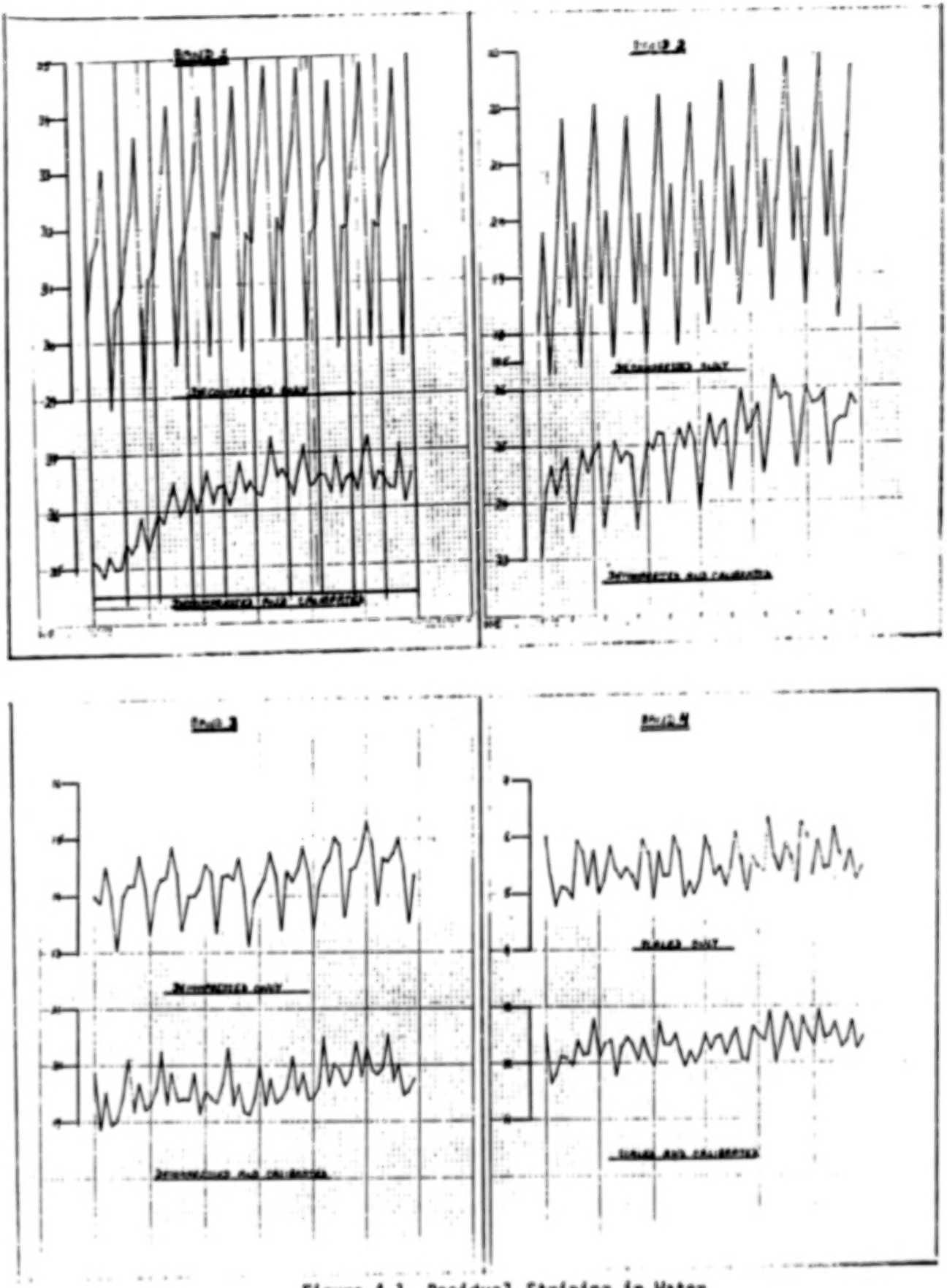

Figure 4.1 Residual Striping in Water

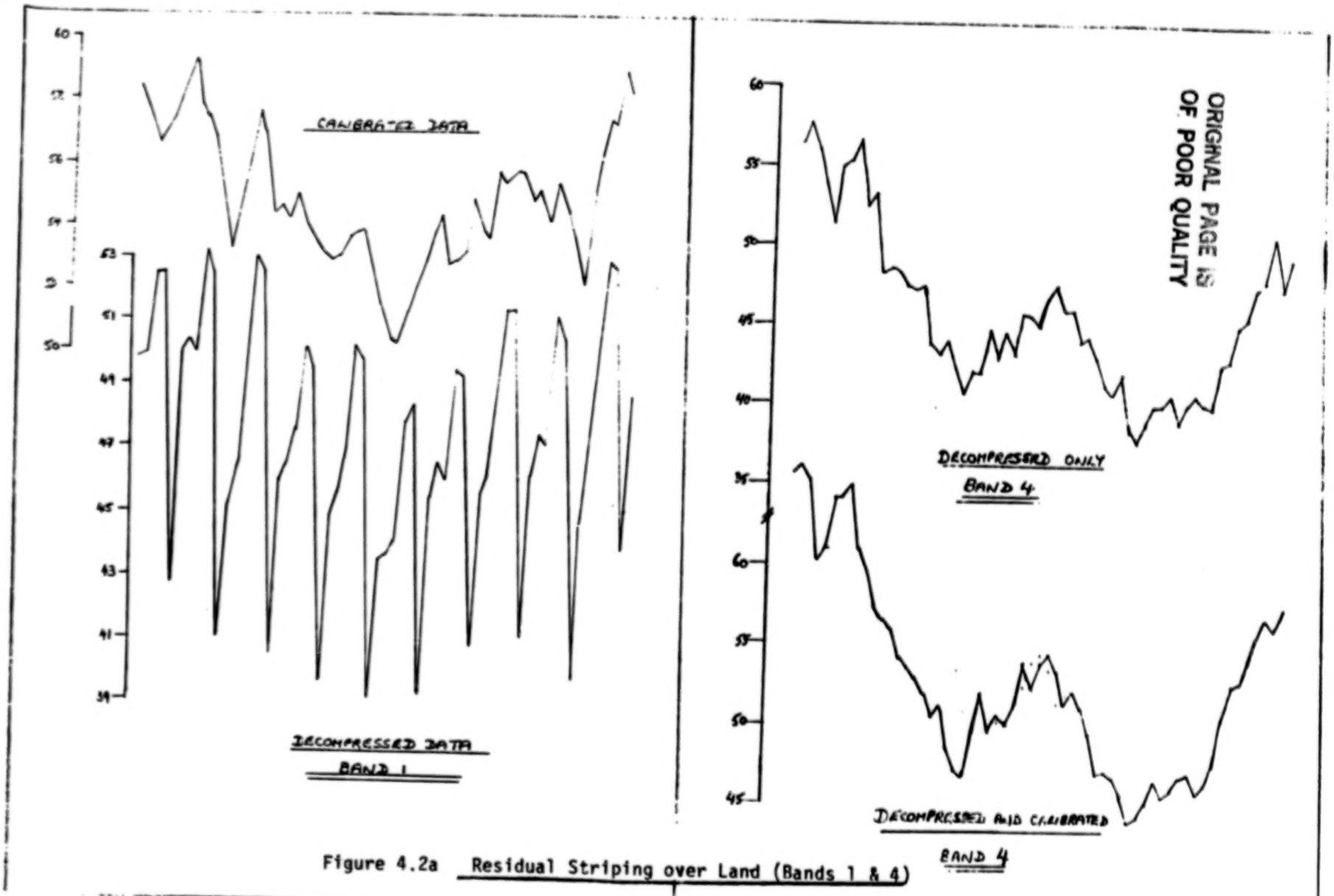

Figure 4.2a Residual Striping over Land (Bands 1 & 4)

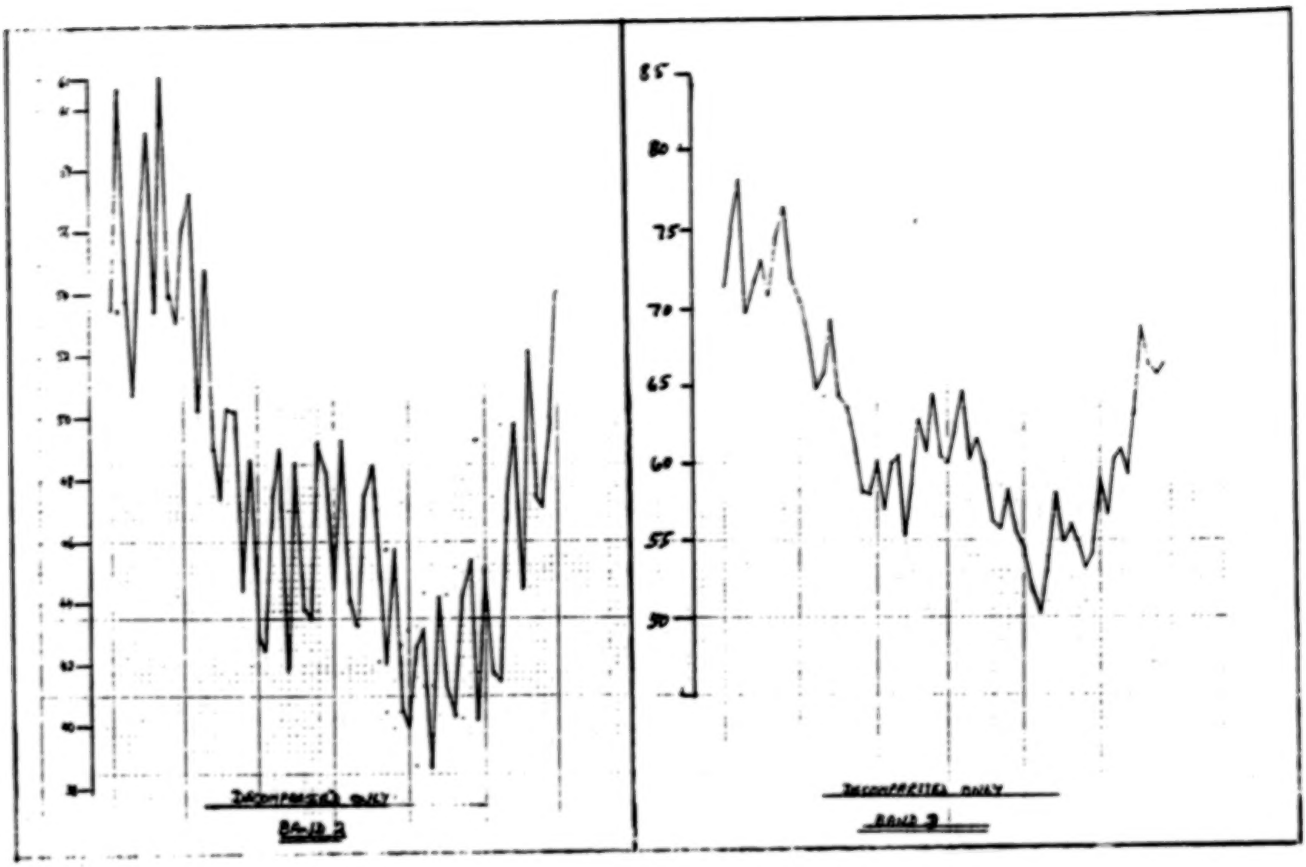

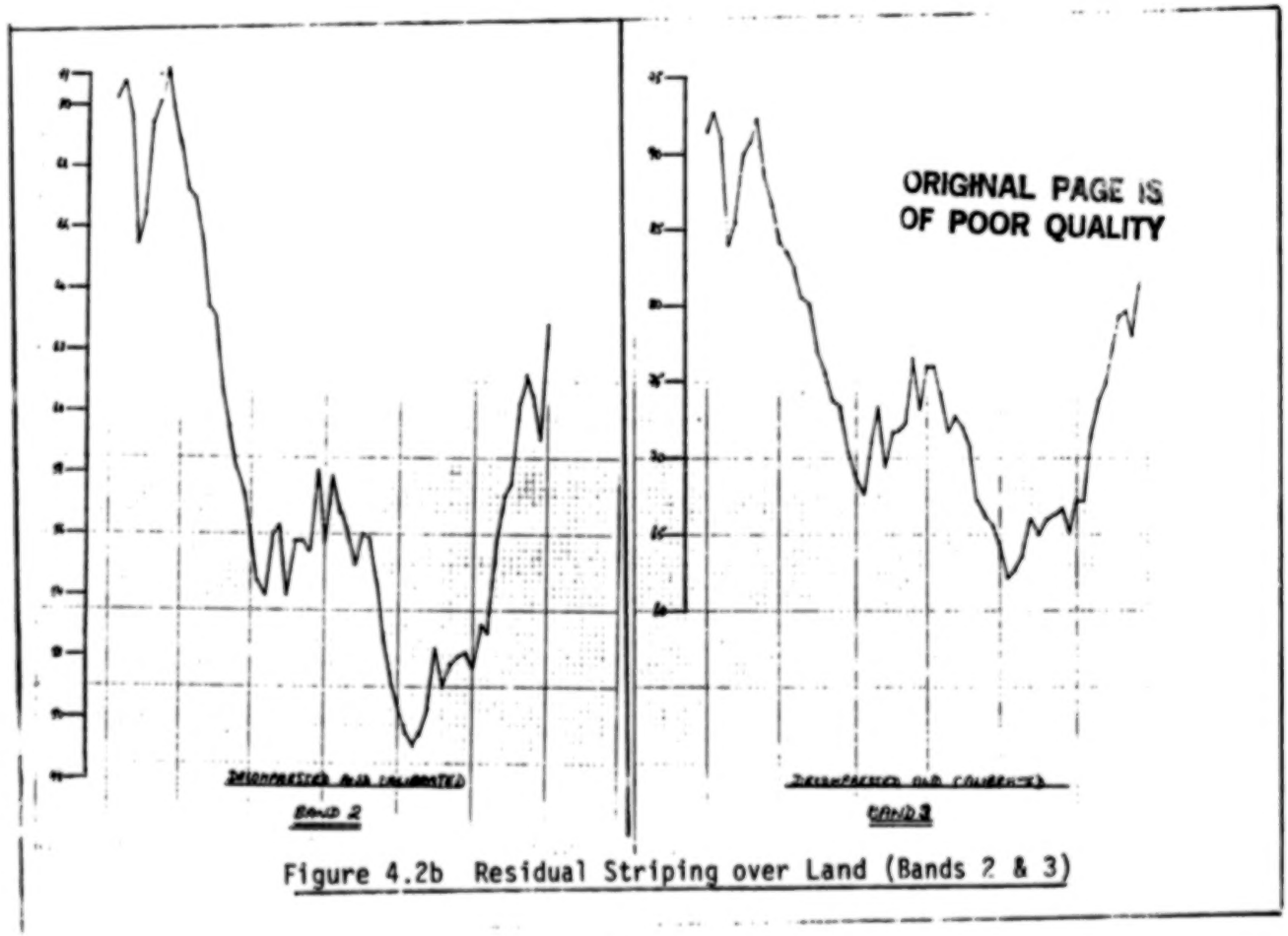

Figure 4.2b Residual Striping over Land (Bands 2 & 3)

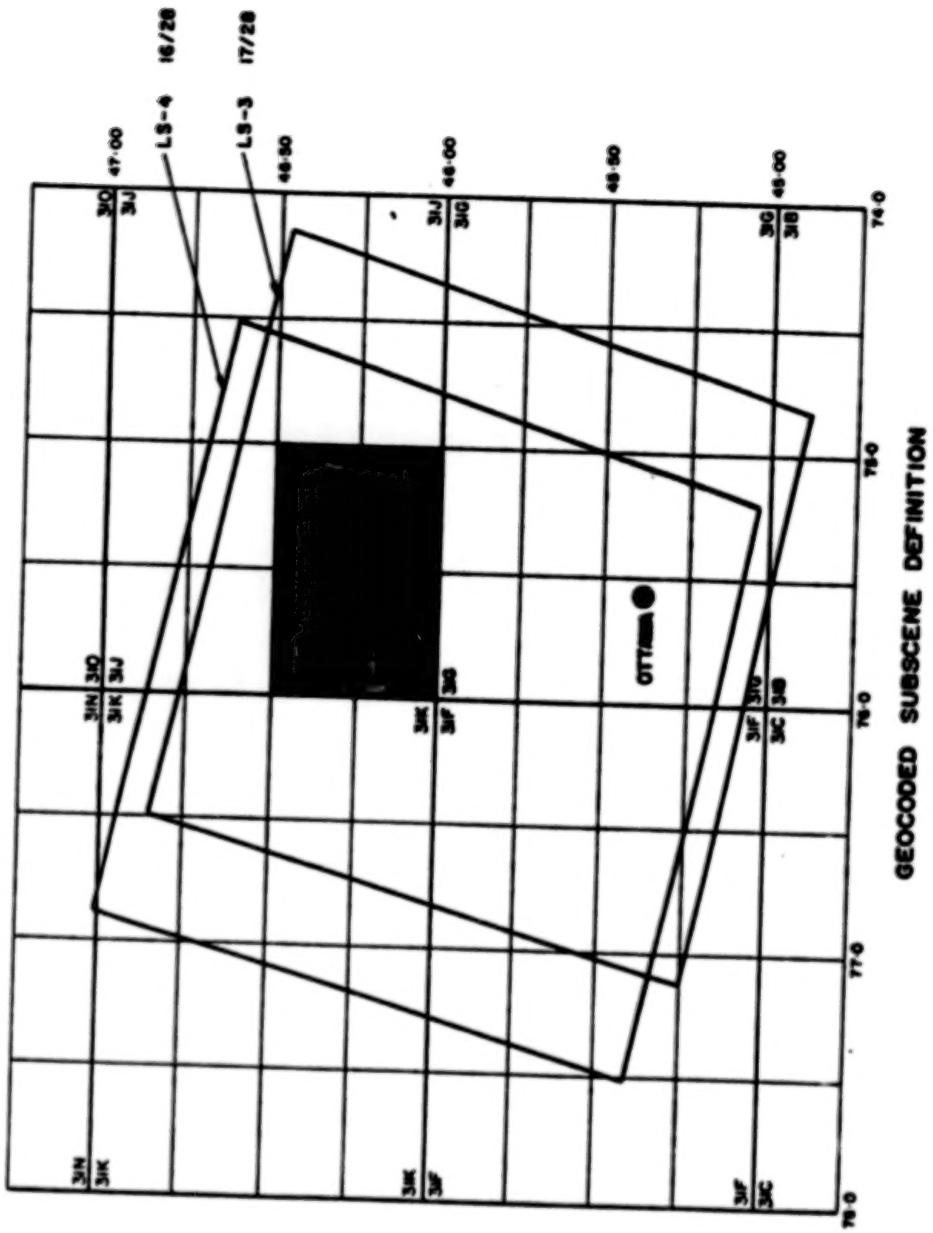

Figure 6.1

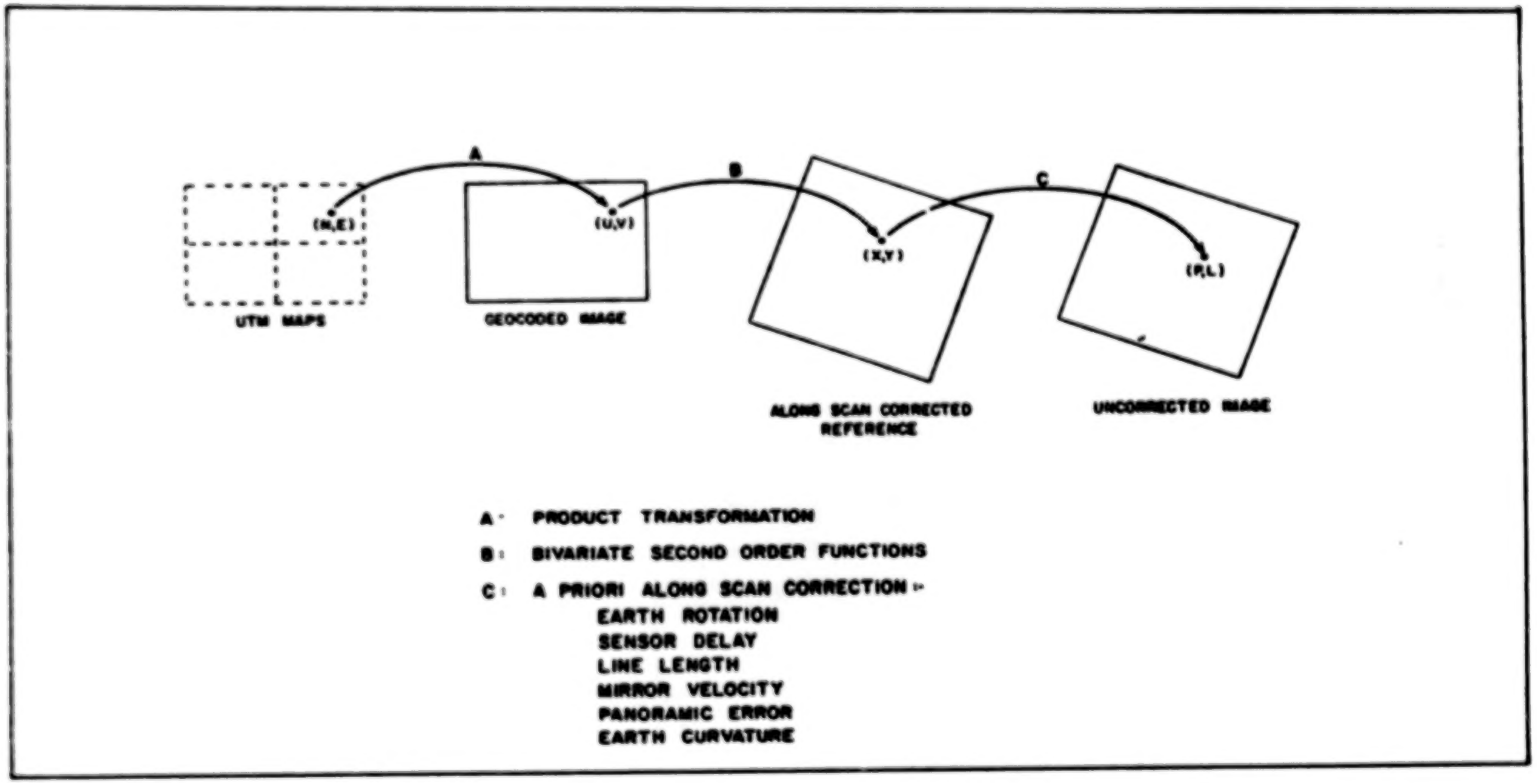

GEOMETRIC CORRECTION MODEL

Figure 6.2

Table 7.1

LINE LENGTH VARIATION

(LINE 25 TO LINE 30: +5 PIXELS)

13	5	19	3	25	5	31	3	37	5	43	2	49	4	61	2	67	7	73	2	79
109	1	115	5	121	2	127	3	133	6	139	2	145	6	151	2	157	4	163	3	169
199	6	205	1	211	7	217	3	223	5	229	3	235	4	241	2	247	5	253	3	259
289	5	295	4	307	1	313	6	319	2	325	5	337	2	343	5	349	2	355	5	361
391	6	397	4	403	2	409	7	415	1	421	5	427	3	433	4	439	3	445	6	451
487	5	493	2	499	4	505	3	511	6	517	2	523	6	529	2	535	3	541	5	547
577	5	583	1	589	7	595	2	601	4	607	5	613	0	619	7	625	2	631	5	637
667	4	673	6	679	2	685	5	691	2	697	5	703	4	709	5	715	2	721	5	727
757	1	763	5	769	3	775	5	781	3	787	7	793	0	799	6	805	3	811	2	817
847	3	853	5	859	2	865	5	871	3	877	2	883	6	889	2	895	6	901	3	907
937	2	943	4	955	2	961	6	967	2	973	5	979	3	985	4	991	1	997	7	1003
1039	5	1045	4	1051	5	1057	2	1063	5	1069	2	1075	4	1081	5	1087	2	1093	6	1099
1129	6	1135	1	1141	5	1147	3	1159	6	1165	1	1171	5	1177	2	1183	5	1189	3	1195
1225	7	1231	1	1237	6	1243	2	1249	4	1255	3	1261	5	1267	2	1273	6	1279	3	1285
1315	5	1321	3	1327	5	1333	1	1339	6	1345	2	1351	5	1357	4	1363	1	1369	6	1375
1405	6	1411	1	1417	5	1429	1	1435	6	1441	0	1447	5	1453	3	1459	5	1465	3	1471
1507	2	1513	5	1519	3	1525	4	1531	3	1537	6	1543	2	1549	5	1555	2	1561	3	1567
1597	2	1603	5	1609	1	1615	7	1621	2	1627	3	1633	5	1639	1	1645	6	1651	3	1657
1687	3	1693	4	1699	5	1705	1	1711	6	1717	2	1723	5	1729	4	1735	5	1741	1	1747
1777	5	1783	1	1789	5	1795	3	1801	5	1807	2	1813	6	1819	0	1825	6	1831	4	1837
1867	4	1873	3	1879	5	1885	2	1891	4	1903	2	1909	6	1915	2	1921	5	1927	2	1933
1963	2	1969	3	1975	5	1981	1	1987	6	1993	2	1999	4	2005	2	2011	5	2017	1	2023
2053	6	2059	2	2065	5	2071	3	2077	4	2083	2	2089	5	2095	3	2101	4	2107	5	2113
2143	5	2149	1	2155	5	2161	1	2167	5	2173	4	2179	3	2185	5	2191	1	2197	5	2203
2233	6																			

LANDSAT - 4

PATH 16 ROW 28 CYCLE 5

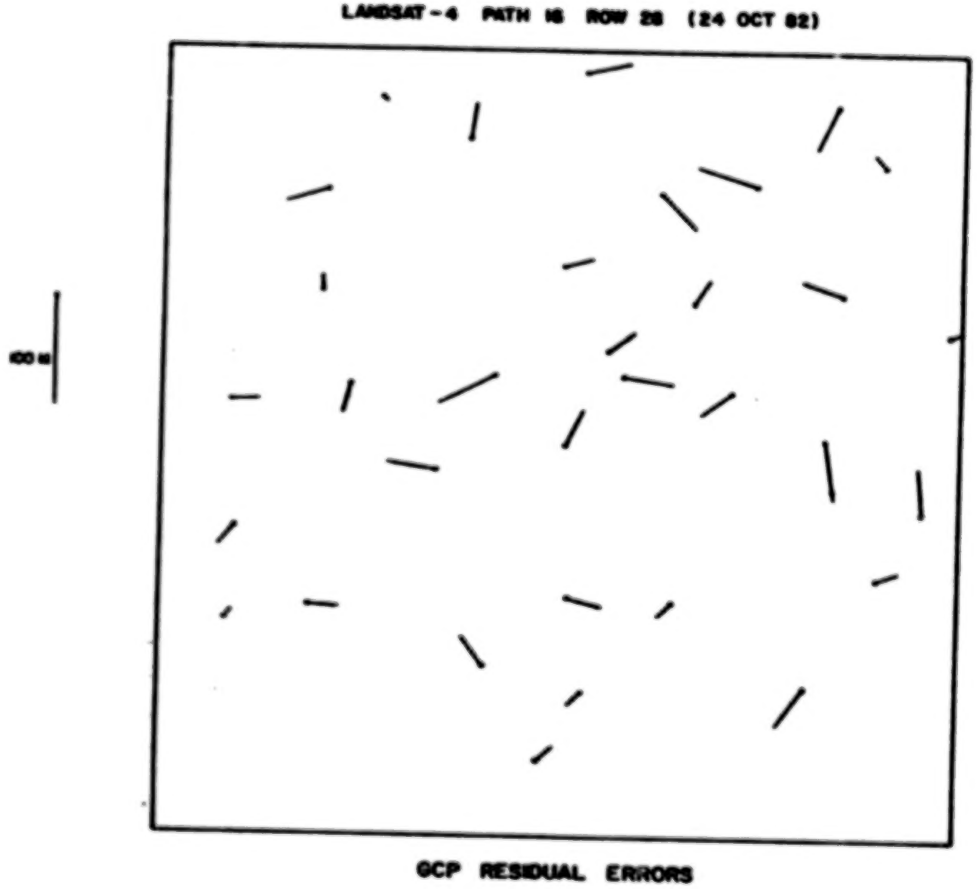

Figure 7.7

Table 7.2

GCP RESIDUAL ERRORS COMPARISON

LANDSAT-1, 2, 3		LANDSAT-4		
SAT/PATH/ROW/CYCLE	RMS (METRES)	PATH/ROW/CYCLE	RMS (METRES)	LL
2 / 17 /24 / 093	33.5	16 / 24 / 003	42.6	(0-8)
1 / 17 / 28 / 079	30.0	16 / 28 / 005	39.7	(0-7)
2 / 17 / 28 / 071	38.7			
2 / 17 / 28 / 089	34.1			
2 / 17 / 28 / 084	43.0			
2 / 17 / 28 / 133	46.1			
3 / 17 / 28 / 085	34.6			
2 / 37 / 21 / 046	31.8	35 / 21 / 009	34.9	(0-8)
2 / 39 / 23 / 091	40.5	36 / 23 / 004	37.3	(0-2)
2 / 39 / 23 / 092	35.8			
2 / 39 / 23 / 132	33.0			
3 / 39 / 23 / 009	24.8			
2 / 42 / 22 / 050	29.4	39 / 22 / 005	36.9	(0-2)
2 / 42 / 22 / 092	40.7			
2 / 42 / 22 / 131	30.6			
	MEAN = 35.1 S.D. = 5.7		MEAN = 38.3 S.D. = 3.0	

Table 7.3

LANDSAT-4 ABSOLUTE GEODETIC ERROR

PATH 16 ROW 28 CYCLE 005

GCP NO.	NORTHING ERROR (METRES)	EASTING ERROR (METRES)
1	-17	31
2	-47	4
3	23	-18
4	-15	12
5	40	38
6	18	-22
7	17	-1
8	32	-8
9	-30	33
10	-85	-10
11	-36	31
12	11	50
13	-10	-44
14	32	-54
MEAN	4.8	3.0
S.D.	36.0	31.4

LANDSAT SCENE-TO-SCENE REGISTRATION ACCURACY ASSESSMENT

James E. Anderson
NASA/Earth Resources Laboratory
Code HA20, Bldg. 1100
NSTL Station, MS 39529

I. OBJECTIVES

The NASA/NSTL/Earth Resources Laboratory (ERL) is a participant in the NASA sponsored Landsat Image Data Quality Assessment Program. As its commitment to the program, ERL is conducting a Scene-to-Scene Registration Accuracy Assessment.

The objectives of the study described in this paper were to evaluate the scene-to-scene registration performance of the MSS on Landsat-4 relative to Landsat 1 through 3 MSS systems, and to determine the temporal registration performance of Landsat-4 Thematic Mapper (TM) data sets. Since only one TM data set has been received to date, only the MSS portion of the study will be reported on.

II. TECHNICAL APPROACH

A. Scene-to-Scene Registration

The procedure for temporarily registering MSS digital data at ERL can be summarized as follows:

1. After designating a "base" and "map" data set, manually locate six to ten uniformly distributed points which are geographically common to both data sets. The scan line/elements of these points are stored on a computer disc file for subsequent use.

2. Generate an initial mapping equation based on the points located in (1). This equation defines the fundamental relationship between points located in the map data set and identical points in the base data set. In essence, it is used to calculate the position of a map pixel relative to the base data set.

3. Based on the initial mapping equations developed in (2), locate 100 to 200 additional common points through the use of auto-correlation software. This software locates points in the base data set, and predicts their location in the map data set by using the mapping equation developed in (2). Once the first point is located, a sliding window is moved around the point and the correlation between the data in the window and a similar window containing the point in the base data set is computed. The point at the center of the window with the highest correlation to the base data set is indicated as the "best match" and is saved for subsequent analysis. This procedure continues until all points chosen in the base data have been examined, i.e., correlated with map data set locations.

4. Iteratively edit the registration points located in (3), until a user defined RMS error is obtained. This step in necessary, since some points located by the auto-correlation software may be erroneous. Although the auto-correlation software can be "programmed" to eliminate questionable points, some are nonetheless retained. Thus, the editing step can eliminate points which, when examined in the context of the entire set of points, have abnormally large registration errors associated with them. As each point is deleted, mapping equations are recomputed, errors for the remaining points are recalculated, and the user is given the opportunity to delete another point or end the procedure.

5. Using the final mapping equations based on only the points retained after completing (4), register (resample) the map data set to the base data set, using a piecewise linear fit and bilinear sampling.

B. Evaluation of Registration Accuracy

In order to determine the relative performance of the scene-to-scene registration produced, the following procedure is followed:

1. Produce three electrostatic (black/white) plots for numerous subscenes areas within the overall data available. Two plots are from two channels of the original base data set, the third plot is derived from a single channel of the original map data set. The plots all have identical initial/final scan line and element values, and thus represent the same "geographic" area within the now registered, composite data set.

2. Simultaneously mount three plots from one subscene area on an x-y digitizer table. After initializing the digitizer to the plots (table coordinate to scan line/element coordinate coversion), manually find numerous points which can be unambiguously located on all three plots. Digitize the scan line/element coordinates from each plot for each point used. The resulting 3 coordinates pairs are stored. Continue the process for all subscenes areas.

3. Use digitized points from (2) to calculate temporal registration performance in terms of RMS error. A mathematical model has been developed defining the registration error, which is of the form

$$\sigma_x^2 = \frac{\sum_{i=1}^{n} \left(X_{mi} - \frac{(X_{b1i} - X_{b2i})^2}{2}\right)}{n} - 3/4 \sum_{i=1}^{n} \frac{(X_{b1i} - X_{b2i})^2}{n}$$

where: σ_x^2 = misregistration error (element direction)
X_{b1i} = element value, first base channel, i^{th} point
X_{b2i} = element value, second base channel, i^{th} point
X_{mi} = element value, first map channel, i^{th} point
n = number of points digitized from all plots

A similar formula exists for the scan line value (σ_y^2, etc.). From these values, RMS errors can be calculated.

III. Data Sources:

Three MSS data sets were used in this study as defined in Table 1.

Table 1: MSS DATA ANALYZED

SATELLITE	DATE	FORMAT
LANDSAT-2	1980	PM
LANDSAT-2	1981	PM
LANDSAT-4	1982	PM

The Landsat-2 1980 data set was used as the base data set throughout the analysis.

IV. Results and Conclusions:

Results of temporal registration of MSS data are presented in Table II.

Table II. RESULTS OF ANALYSIS OF LANDSAT MSS DATA

BASE DATA	PARAMETER OF INTEREST	LANDSAT-2 1981	LANDSAT-4 1982
Landsat-2 1980	Element Error - σ_x^2	20.416 m	40.320 m
	Scan Line Error - σ_y^2	26.701 m	26.951 m
	Registration RMS Error - σ_m^2	33.612 m (74)	48.498 m (65)
	Indicated RMS Error at Time of Mapping Equation Development	34.98 m (67)	39.87 m (69)

An F test to evaluate the null hypothesis

H_o: σ_m^2 (1980/1981) = σ_m^2 (1980/1982) versus the alternate hypothesis.

H_o: σ_m^2 (1980/1981) $\neq$ σ_m^2 (1980/1982)

resulted in F(CALC) = 1.44
F(TAB).01 = 1.41

such that the null hypothesis was rejected in favoe of the alternate hypothesis, i.e., the temporal registrations evaluated were not performed to the same resulting RMS registration error.

It is interesting to note that the 1980/1982 registration resulted in an element error which was nearly twice as large as that obtained in the 1980/1981 registration (40.320 vs. 20.416 meters). This occurred even though the scan line errors were nearly identical (26.951 vs. 26.701 meters).

Subsequent analysis indicates that the large element error encountered in the 1980/1982 temporal registration may be the result of less than adequate modeling of the Landsat-4 MSS scan mirror profile. More precise coefficients have been incorporated into ground processing software and the next MSS-4 data set collected over the study area will be used to test the effectiveness of the new values.

N85-20503

GEOMETRIC ACCURACY OF LANDSAT-4 MSS IMAGE DATA

R. Welch and E. Lynn Usery
Department of Geography
University of Georgia
Athens, GA 30602

INTRODUCTION

The Landsat-4 mission is presenting investigators with an opportunity to assess the mapping potential of satellite image data of improved geometric quality in digital formats. This paper focuses on the geometric characteristics of Landsat-4 multispectral scanner (MSS) data available in CCT-p formats (57 m pixels) from the EROS Data Center (EDC).

When compared to characteristics of the previous Landsat missions, the improved pointing accuracy and attitude stability of the Landsat-4 platform offer significant advantages for mapping purposes. For example, Landsat-1, -2, and -3 data were acquired from a platform with 0.7 degree pointing accuracy and an attitude stability of 10^{-2} deg/sec. The geometric distortion within these early MSS scenes was estimated to be $\pm$200 to $\pm$300 m root-mean-square vector error ($RMSE_{xy}$) and was probably caused by variations in the attitude of the satellite (Schoonmaker, 1974; Wong, 1975; Bahr, 1976). Wong (1975) and Bernstein (1976) demonstrated that distortions could be reduced to about $\pm$100 m with a first degree polynomial, and to a limiting rectification accuracy of about $\pm$50 m with 20 term polynomials, when a dense network of ground control points (GCPs) was available. Relief was not a significant factor in these studies.

The MSS sensor on Landsat-4 is identical to that utilized on Landsats-1, -2 and -3, but with an instantaneous field-of-view (IFOV) of 83 m as compared to the 79 m of the earlier missions. The multimission modular spacecraft (MMS) of the Landsat-4 system, on the other hand, is designed to meet specifications for a pointing accuracy of 0.01 degree (1σ) and an attitude stability of 10^{-6} deg/sec (1σ), which represent approximately 2 and 4 orders of magnitude improvement over the previous Landsat systems. Thus, from an altitude of 705 km, pointing should be to within about $\pm$120 m of the nadir

and attitude should not vary by more than 0.1 sec (or about 0.4 m ground distance) during the approximate 25 second time interval required to record a 185 x 185 km scene. Therefore, it should prove possible to fit Landsat-4 data to a reference map by applying relatively simple rectification procedures based on a few well-distributed control points. In fact, these pointing accuracy and attitude control specifications led to the development of geodetic error tolerances for the CCT-p data of $\pm$0.5 IFOV 90 percent of the time (Carr, 1982).

It is the objective of this paper to evaluate the errors in EDC CCT-p products for MSS data acquired over test areas in North Georgia. In addition, assessments will be made of the possibilities for rectifying the image data by applying polynomials to full- and subscene areas, and of the effects of sensor resolution, digitizing techniques (for GCPs) and terrain relief on geodetic accuracy.

STUDY AREA AND DATA SETS

The study area is centered on North Georgia and is covered by two Landsat-4 scenes corresponding to path 18, row 36 (P18R36) and path 19, row 36 (P19R36) in the Landsat-4 Worldwide Reference System (Figure 1). This region is characterized by a blend of urban and rural land use features with terrain relief varying from about 1000 m in the rugged southern Appalachians of Georgia, Tennessee and North Carolina, to less than 30 m in the southernmost portions of the study area near Athens, Georgia. Thus, these scenes are ideally suited for assessments of the impact of relief on rectification accuracy.

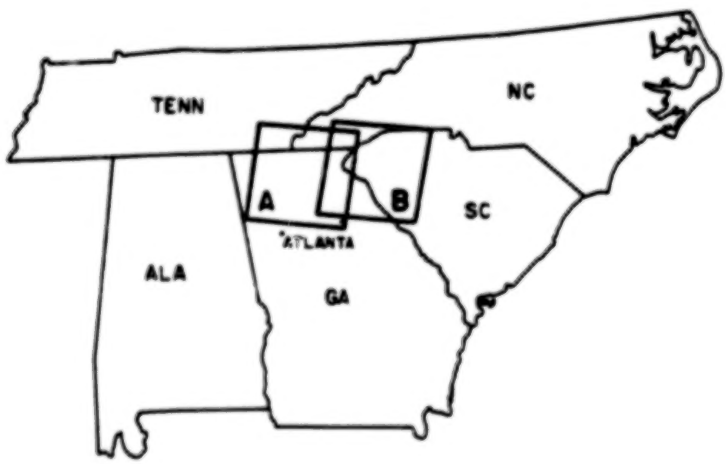

Fig. 1 Landsat-4 scenes from path 19, row 36 (A) and path 18, row 36 (B).

The specific Landsat-4 coverage which has been used to-date includes one MSS acquisition over each of the scene centers recorded on October 29 (P19R36) and December 9 (P18R36). Subscenes are centered on Blue Ridge, Georgia (P19R36) in the rugged North Georgia mountains and include data sets of 1024 x 1024 and 256 x 256 pixels. Terrain elevations in the area covered by the subscenes range from 400 to over 1000 m.

RECTIFICATION PROCEDURES

In order to implement rectification procedures, it was first necessary to locate a dense network of GCPs which could be correctly identified and precisely located on both the Landsat-4 image data and on 1:24,000 scale USGS topographic maps of the study areas. Image locations (in pixel and scan-line coordinates) of the GCPs were determined with the aid of an ERDAS 2400 interactive image processing system. Unfortunately, however, the limited spatial resolution of the MSS data poses a problem in identifying and locating features normally used as GCPs such as the intersections of roads, rivers and pipelines. For example, the center of a road intersection may be completely obscured by a pixel. Unless refinements are made to the location process, image coordinates can only be determined to about ± 1 data pixel, i.e. to about ± 60 m.

The image coordinates can be more precisely determined by reformatting/resampling image data to smaller pixels, which are then redisplayed on the CRT. Although rather tedious, this procedure does permit image coordinates to be determined to approximately one-half the dimension of the original data pixel, i.e. to ± 30 m in the case of the MSS.

Once provisional control points were located on the image data, their UTM map coordinates were manually digitized from 1:24,000 scale U.S. Geological Survey topographic quadrangles with an Altek Super Micro digitizing system (resolution $\pm .025$ mm). The errors in the maps and in the digitizing procedure influence the accuracy of the resulting rectifications and are estimated to have an $RMSE_{xy}$ value of approximately ± 10-15 m.

After the coordinates of the GCPs in image (pixel, scan-line) and map (Easting, Northing) space were determined, an accuracy validation procedure was undertaken to establish misidentified or suspect points. This procedure is referred to as a point-pair distance check and involves the computation and comparison of map and scaled image distances between all possible combinations of point-pairs (Figure 2). By performing distance checks, suspect points may be quickly identified. Once the suspect points have been eliminated, the point-pair distances are recomputed and the RMS difference in distance between the map and scaled image values determined. Linear regression of RMS distance differences against $RMSE_{xy}$ for the same data sets yielded correlation coefficients (r) of about +0.9. Thus, the RMS difference value is, for practical purposes, a surrogate measure of $RMSE_{xy}$ and serves as an indicator of the inherent geometric errors in the CCT-p data supplied by EDC.

An average RMS distance difference of ± 130 m was obtained for the MSS scenes of North Georgia, which is comparable to values reported by Bryant et al. (1983) for other geographic areas. Thus, it appears the geometric quality of the Landsat-4 MSS data is considerably better than those available from the Landsat-1, -2 and -3 missions.

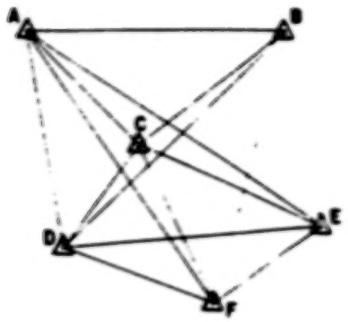

Fig. 2 Distance checks are performed between all possible point-pairs to validate the GCPs.

Probably the most direct method for the rectification of digital MSS data is by means of polynomials (Konecny, 1976; Figure 3). For example, early rectifications of Landsat MSS data by NASA involved the use of a computer program package known as the Digital Image Rectification System (DIRS) (Van Wie and Stein, 1975) which employs affine and polynomial transformation equations. DIRS is available from COSMIC, University of Georgia, and was subsequently obtained and modified to facilitate its use for the current studies. The DIRS procedures include the development of polynomial mapping functions of the general form:

$$z = c_0 + c_1x + c_2y + c_3x^2 + c_4xy + c_5y^2 + c_6x^3 + c_7x^2y + c_8xy^2 + c_9y^3 + \ldots$$

where x,y are the known image or map coordinates of GCPs.

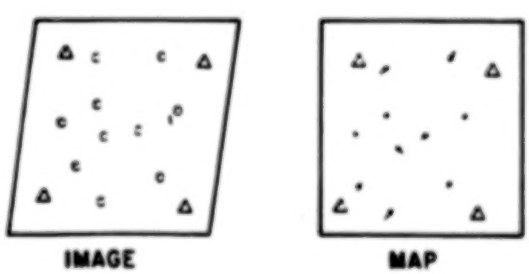

Fig. 3 Polynomials are employed to transform the image data to a map reference base. Error vectors at test points are used to calculate the $RMSE_{xy}$.

These functions may be used to solve (by the method of least-squares) for UTM Easting and Northing coordinates in terms of image pixel and scan-line coordinates. Correspondingly, the image coordinates may be determined by an inverse procedure. The minimum number of GCPs required to establish the unknown coefficients is dependent on the degree of the polynomials used in the rectification process. For example, 5th, 4th, 3rd, 2nd and 1st degree polynomials require a minimum of 21, 15, 10, 6, and 3 GCPs, respectively.

The pixel-by-pixel application of the polynomial mapping functions is computationally inefficient, thus, an interpolation grid of horizontal and vertical lines is established in the UTM coordinate system. Standard linear equations are used to compute the UTM coordinates of the grid intersections which are then transformed through the polynomial mapping functions to determine their corresponding image coordinates (pixel and scan-line). A regular lattice of output pixel locations is computed in the UTM system from the grid. The output image coordinates of these pixels are then determined by bilinear interpolation from the corners of each grid cell in the image space. Because the output pixels will not correspond to the input pixel locations, a resampling of the gray level values is necessary. DIRS permits nearest neighbor resampling for whole scenes and cubic convolution resampling for subscenes.

Rectification of Whole MSS Scenes

Over 100 GCPs were located in each of the two MSS scenes (P18R36, P19R36). From these GCPs, 42 well-distributed points were selected as control for the rectification of P19R36 and 21 points for P18R36. In order to provide an independent check of the rectification accuracies achieved, a total of 40 and 27 (withheld) test points were selected from the GCPs in P19R36 and P18R36, respectively. The distribution of control and test points for P19R36 is shown in Figure 4.

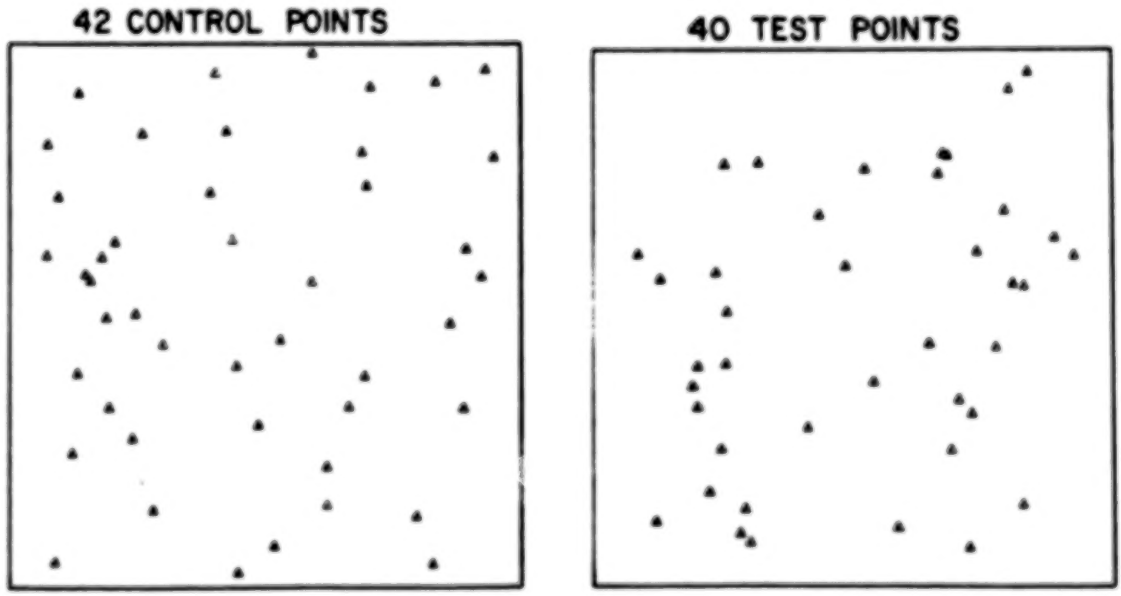

Fig. 4 Distribution of the control and test points for full scene rectification of P19R36.

For P19R36, the number of GCPs used in the rectification process was reduced in steps for polynomials of the 5th through 1st degree as shown in Figure 5 and Table 1. The $RMSE_{xy}$ value in each case was determined from the error vectors at the 40 withheld test points. These $RMSE_{xy}$ values were then plotted as a function of the number of GCPs used in the solutions of the different polynomials (Figure 6). It is evident from Figure 6 that a polynomial of the first degree based on 10 or more control points provides an $RMSE_{xy}$ of approximately $\pm$80 m and that the minimum $RMSE_{xy}$ of between $\pm$55 and 60 m can be obtained with a 3rd degree polynomial and 30 or more control points. Although the rectification experiments undertaken with P18R36 were not as comprehensive, comparable results were obtained for solutions of the first through 4th degree based on 21 GCPs (Table 1). Overall, rectifications with 2nd and 3rd degree polynomials and 20 or more control points yielded RMSEs of about $\pm$1 data pixel ($\pm$57 m), even in this rugged terrain.

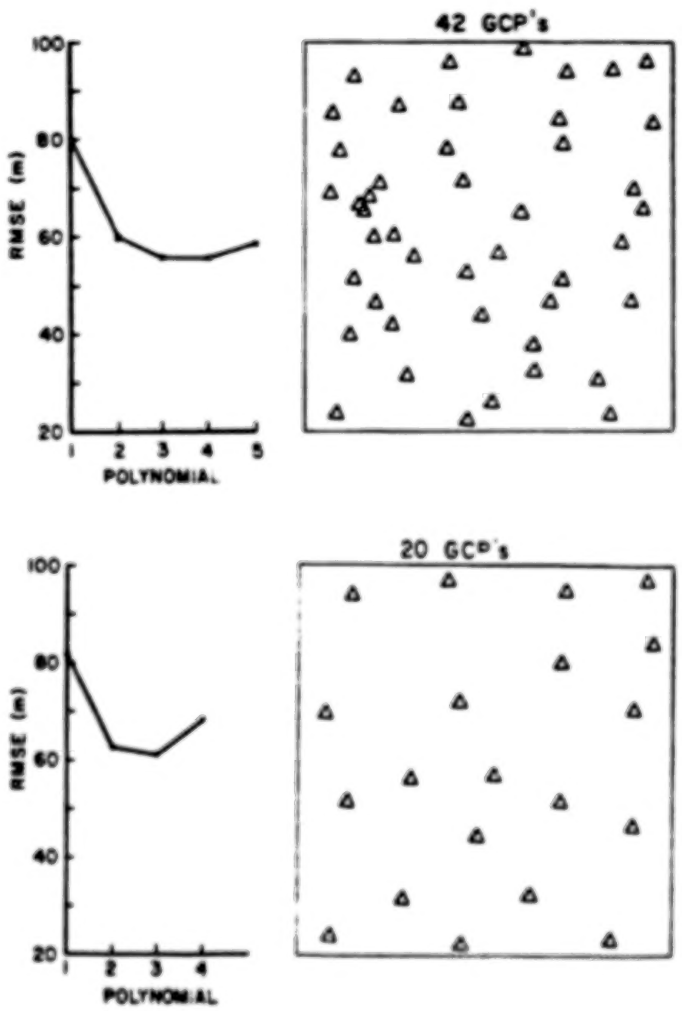

Fig. 5 $RMSE_{xy}$ at 40 test points as a function of the degree of polynomials used in the rectification process. The diagrams on the right show the distribution of the GCPs.

Table 1

$RMSE_{xy}$ FOR WHOLE SCENE RECTIFICATION

Number of control points used in the rectification	$RMSE_{xy}$ values (from 40 test points) for polynomials of degree 1-5.				
	5th	4th	3rd	2nd	1st
42	59m	56	56	60	80
30	69	61	57	60	82
21*	66	64	62	70	80
20		69	61	63	82
15			73	73	83
10				70	83
5					91

*from P18R36 @ 27 test points

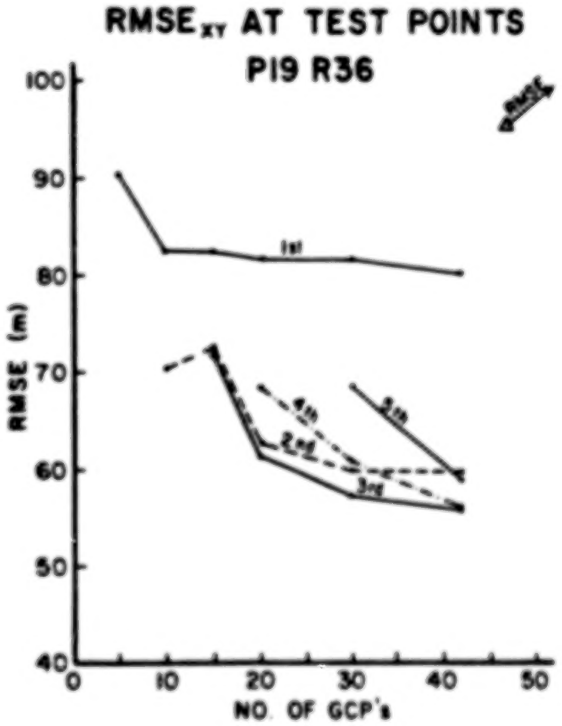

Fig. 6 $RMSE_{xy}$ as a function of the number of GCPs used to solve polynomials of the 1st through 5th degree.

Rectification of MSS Subscenes

Subscenes of 1024 x 1024 pixels and 256 x 256 pixels were also rectified to determine the number of GCPs and the degree of polynomial required to maximize the geometric accuracy within the areas displayed by high (1024 x 1024) and low (256 x 256) resolution CRT devices. Because a 256 x 256 pixel subscene roughly corresponds to the area covered by a USGS 1:24,000 scale quadrangle, these rectification studies also permit an assessment of the accuracies to which Landsat-4 MSS data can be registered to a relatively large scale topographic map.

The 1024 x 1024 pixel test area is centered on the town of Blue Ridge, Georgia, and the 256 x 256 pixel subscene corresponds to the USGS Blue Ridge 7 1/2 minute quadrangle. Rectification was accomplished using the previously described procedures. In the case of the 1024 x 1024 pixel area, 15 GCPs were employed to develop least squares solutions for polynomials of the 1st through 3rd degree. Accuracy was evaluated at 16 withheld test points, and minimum RMSEs of ±45 m were obtained with 1st and 2nd degree equations (Table 2). When the number of GCPs was reduced to 10 points, the $RMSE_{xy}$ increased to approximately ±60 m. The smaller 256 x 256 pixel subscene was rectified with a 1st order polynomial based on 5 GCPs and 3 withheld test points. The $RMSE_{xy}$ of ± 40 m indicates that subpixel accuracy is feasible for quadrangle-sized areas with limited control.

Table 2

$RMSE_{xy}$ VALUES FOR SUBSCENE AREAS

Number of GCPs	$RMSE_{xy}$ values for polynomials of degree 1-3.		
	3rd	2nd	1st
15*	55m	46	45
10*		60	61
5**			40

*1024 x 1024 pixels areas with 16 test points
**256 x 256 pixel areas with 3 test points

ERROR ANALYSES

Although of good geometric quality, the MSS data acquired from the EDC in CCT-p formats for this study has an $RMSE_{xy}$ error of about ±130 m. This value indicates the CCT-p data do not meet the pre-launch specifications for geodetic accuracy which states that 90 percent of the pixels will be correctly located to within ±0.5 IFOV (±41.5 m) in both the x and y directions. Based on this specification, the acceptable vector error ($RMSE_{xy}$) is ±59 m.

It must be noted that the two CCT-p scenes used in this study were not corrected to ground control as part of the EDC processing, and consequently

errors of approximately ±130 m are quite reasonable. As discussed below, by using adequate control the $RMSE_{xy}$ can be reduced to less than ±59 m. However, this requires significantly more processing than was performed on these scenes at the EDC.

The minimum $RMSE_{xy}$ of about ±55 m obtained for whole scenes after rectification with polynomials of the 2nd and 3rd degree is equivalent to about ±1 data pixel. This appears to be about the best result that can be expected for these test sites, given that the spatial resolution of the MSS prevents features from being located to better than about ±0.5 pixel, that errors in digitizing the UTM coordinates from 1:24,000 scale maps amount to approximately ±0.25 pixel, and that average displacements in the image data caused by terrain relief are greater than ±0.35 pixel. The typical RMSE values of ±55-60 m are compatible with national map accuracy standards for cartographic products of 1:200,000 scale and smaller.

CONCLUSION

Analyses of the Landsat-4 MSS image data of North Georgia provided by the EDC in CCT-p formats reveal that errors of approximately ±130 m in the raw data can be reduced to about ±55 m based on rectification procedures involving the use of 20-30 well-distributed GCPs and 2nd or 3rd degree polynomial equations. Higher order polynomials do not appear to improve the rectification accuracy. A subscene area of 256 x 256 pixels was rectified with a 1st degree polynomial to yield an $RMSE_{xy}$ value of ±40 m, indicating that USGS 1:24,000 scale quadrangle-sized areas of Landsat-4 data can be fitted to a map base with relatively few control points and simple equations.

The errors in the rectification process are caused by the spatial resolution of the MSS data (±0.5 pixel), by errors in the maps and GCP digitizing process (±0.25 pixel), and by displacements caused by terrain relief (>±0.35 pixel). Overall, due to the improved pointing and attitude control of the spacecraft, the geometric quality of the Landsat-4 MSS data appears much improved over that of Landsats -1, -2 and -3.

ACKNOWLEDGMENTS

These studies are being conducted as part of NASA contract number NAS5-27383.

REFERENCES

1. H. P. Bahr, "Geometrical Models for Satellite Scanner Imagery," Presented Paper, Commission III, XIII Congress of the International Society for Photogrammetry, Helsinki, Finland, 1976.

2. R. Bernstein, "Digital Image Processing of Earth Observation Sensor Data," IBM Journal of Research and Development, Vol. 20, 1976, pp. 40-57.

3. N. A. Bryant, A. L. Zobrist, F. C. Billingsley, S. Z. Friedman, B. Gokham, and T. L. Logan, "Evaluation of Landsat-4 Multispectral Scanner Ground Segment Performance," Abstracts, Landsat-4 Scientific Characterization Early Results Symposium, NASA Goddard Spaceflight Center, Greenbelt, Maryland, February 22-24, 1983.

4. J. Carr, "Multispectral Scanner (MSS) Geometric Correction Report (draft)," Landsat-D Science Office, NASA Goddard Spaceflight Center, Greenbelt, Maryland, July, 1982.

5. G. Konecny, "Mathematical Models and Procedures for the Geometric Restitution of Remote Sensing Imagery," Invited Paper, Commission III, XIII Congress of the International Society for Photogrammetry, Helsinki, Finland, 1976.

6. J. W. Schoonmaker, "Geometric Evaluation of MSS Images from ERTS-1," Proceedings of the 40th Annual Meeting of the American Society of Photogrammetry, St. Louis, 1974, pp. 582-588.

7. P. Van Wie and M. Stein, "A Landsat Digital Image Rectification System," NASA Goddard Spaceflight Center, Greenbelt, Maryland, 1975.

8. K. W. Wong, "Geometric and Cartographic Accuracy of ERTS-1 Imagery," Photogrammetric Engineering and Remote Sensing, Vol. 41, No. 5, 1975, pp. 621-635.

GEODETIC ACCURACY OF LANDSAT 4 MULTISPECTRAL SCANNER AND THEMATIC MAPPER DATA

J. M. Thormodsgard and D. J. DeVries

EROS Data Center, U.S. Geological Survey

INTRODUCTION

EROS Data Center is evaluating the geodetic accuracy of Landsat-4 data from both the Multispectral Scanner (MSS) and Thematic Mapper (TM) processing systems. Geodetic accuracy is a measure of the precision of Landsat data registration to the Earth's figure.

The assessment of the geometric accuracy of Landsat data generally requires locating ground control points (distinct features in an image) and calculating a surface fit, with the residuals (differences between the surface and the ground control points) indicating the accuracy. While this method provides the internal geometric consistency within a Landsat scene, it does not give the Landsat 4 user an appreciation of the geodetic accuracy or registration to the Earth's figure. This paper describes a geodetic accuracy assessment of several MSS and TM scenes, based on the geodetic referencing information supplied on a standard Landsat 4 computer compatible tape (CCT).

Landsat 4 data are geometrically corrected using all known sensor (detector array geometry, mirror scan), spacecraft (attitude and altitude variations), and terrestrial (Earth's rotation) geometric distortions to produce a system-corrected geometric product. Based on past performance of Landsat processing systems, this product can be expected to have good internal scene accuracy. However, geodetic (latitude and longitude) registration to the Earth's surface is significantly less accurate. A system-corrected scene has geodetic errors which are primarily translational; shifting the scene to a known geodetic location would result in a significantly improved geometric product.

To overcome the geodetic registration problem, a ground control point (GCP) library was developed for Landsats 2 and 3; the library is being edited and expanded for use with Landsat 4 data. This GCP library consists of 32- by 32-pixel areas extracted from individual Landsat scenes and referenced to a latitude and longitude location. These GCP's are then correlated with Landsat scenes to identify control points which further refine the geodetic accuracy of the Landsat data. This GCP-corrected product has small internal geometric errors and small geodetic errors depending on the distribution and number of GCP's which properly correlate with the Landsat scene.

In previous Landsat processing systems, no easy means of geodetically referencing the data was supplied on the standard CCT, and therefore the latitude and longitude of a pixel could not be calculated. The standard Landsat 4 CCT's have the information necessary to geodetically reference every pixel in the scene. The accuracy of the translation from geodetic location to pixel location depends on the precision of the geometric processing applied to the data; GCP-corrected data will be more accurate than system-corrected data. Therefore, measuring the accuracy of this translation results in an assessment of the geodetic accuracy of the data. The procedure is based on comparing the calculated image location, computed with the geodetic referencing algorithms given below, with the true image location visually located on a display device.

Geodetic Referencing Algorithms

Data provided on the standard Landsat 4 MSS and TM CCT's describe the rectangular map projection coordinate grid overlaying the image coordinate grid. To perform a translation from the map projection grid to the image grid, the angle of rotation between the two grid systems, and the coordinates of one location in both grid systems, are necessary. These values are contained in the header record of an MSS CCT and in the first ancillary record of a TM CCT, and consist of:

Map projection indicator,

Orientation angle of map projection,

WRS (World Reference System) scene center latitude and longitude,

WRS pixel offset from scene center.

The standard map projection applied to Landsat 4 MSS and TM data is the Space Oblique Mercator (SOM), although Universal Transverse Mercator (UTM) and Polar Stereographic (PS) map projections are available upon request, with PS being available for areas above 65°N. latitude and below 65°S. latitude.

A map projection grid at the orientation angle θ from the image grid at the WRS scene center ($\phi c, \lambda c$) is illustrated in Fig. 1. The WRS scene center is given in latitude and longitude, which can be converted to map projection coordinates. The vertical location or line coordinate of the WRS scene center is fixed while the sample coordinate can be computed given the WRS offset or horizontal shift in number of pixels giving the image coordinates ($Sc, \ell c$) at the WRS center. Thus, a simple translation of axes gives the image coordinates (s, ℓ) of a geodetic location (ϕ, λ):

$$\Delta s = \Delta x \cos\theta - \Delta y \sin\theta,$$

$$\Delta \ell = \Delta x \sin\theta + \Delta y \cos\theta,$$

$$s = s_c + \Delta s/\text{pixel size},$$

$$\ell = \ell_c - \Delta \ell/\text{pixel size}.$$

Where:

$\Delta x, \Delta y$ = displacement in projection coordinates (meters) between (ϕ, λ) and ($\phi c, \lambda c$), and

$\Delta s, \Delta \ell$ = displacement in image coordinates between (ϕ, λ) and ($\phi c, \lambda c$).

PROCEDURE

The latitude and longitude of a distinct feature on a 1:24,000-scale map are converted to line and sample coordinates using the geodetic referencing algorithms. An image subscene surrounding this calculated image location is displayed, the cursor is placed on the actual or true image location of the feature, and the pixel offsets from the calculated image location are computed. Maps are selected which result in an even distribution of 15 to 20 GCP locations throughout the image. Accuracy of the visual selection of the image locations is estimated to be 1.5 MSS pixels or 1.0 TM pixel.

RESULTS

Results of the testing and the geodetic accuracy of three MSS scenes and two TM scenes are presented on Figs. 2 through 6. The arrows represent the offset direction from the calculated image location of the GCP's to the actual image location. The table contains the latitude and longitude and the calculated and actual image location of the GCP's. The offset or difference between the calculated and actual image location, as well as the offset vector magnitude or pixel error, are presented. Note the pixel size for MSS is 57 m and 28.5 m for TM.

The two MSS scenes illustrated in Figs. 2 and 3 were system-corrected products with a root-mean-square (RMS) geodetic registration error of approximately 57 pixels or 3,200 m. The error is primarily a translational shift which is demonstrated by the high means and low standard deviations of the pixel offsets. An anomaly in the Washington, D.C., scene (Fig. 3) was the direction of the translational shift in the sample directon; all the other MSS and TM system-corrected scenes had the largest shift in the line (along-track) direction. Since Landsat's major positional error is in the along-track direction, the Washington, D.C., scene appears inconsistent.

The MSS GCP-corrected product (Fig. 4) had an RMS error of approximately 6 pixels or 325 m. There were only two GCP's out of 13 which correlated on this image; both points are located in the lower left corner of the image.

The TM system-corrected scenes (Figs. 5 and 6) had RMS errors of approximately 44 and 35 pixels or 1,250 and 1,000 m, respectively. As with the MSS data, the error is largely translational. A GCP-corrected TM product was not available to evaluate because a TM GCP library does not yet exist.

CONCLUSIONS

Conclusive statements concerning the geodetic accuracy of Landsat 4 data, based on such a small sampling of scenes, is impossible. However, the results provide a few interesting observations. For example, Landsat 4 MSS system-corrected errors were larger than were expected based on the authors' knowledge of the geometric accuracy of the data from Landsats 2 and 3. Also, the TM system-corrected scenes were more accurate than the MSS scenes by a factor of three. As the spacecraft platform for these two sensors is the same, this result cannot be explained, but a comparison of concurrently acquired MSS and TM data might clarify this situation. Finally, the single MSS GCP-corrected product evaluated had good geodetic accuracy considering the poor distribution of the two GCP's applied in the registration.

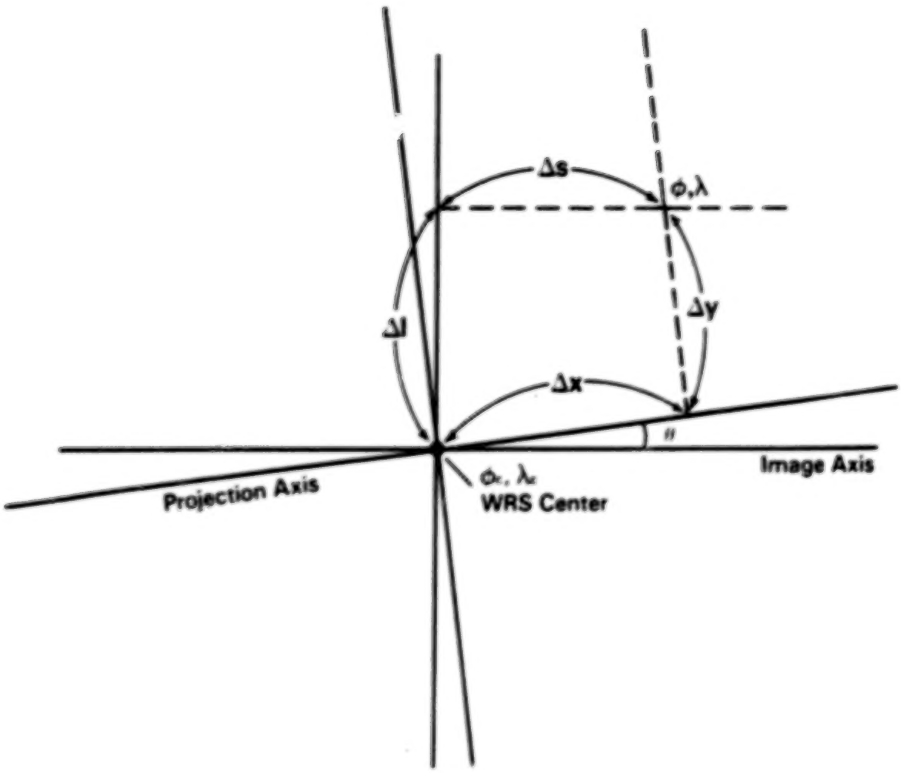

Fig. 1. Referencing a Landsat scene to the Earth's figure. The map projection grid at the orientation angle θ from the image grid at the WRS center.

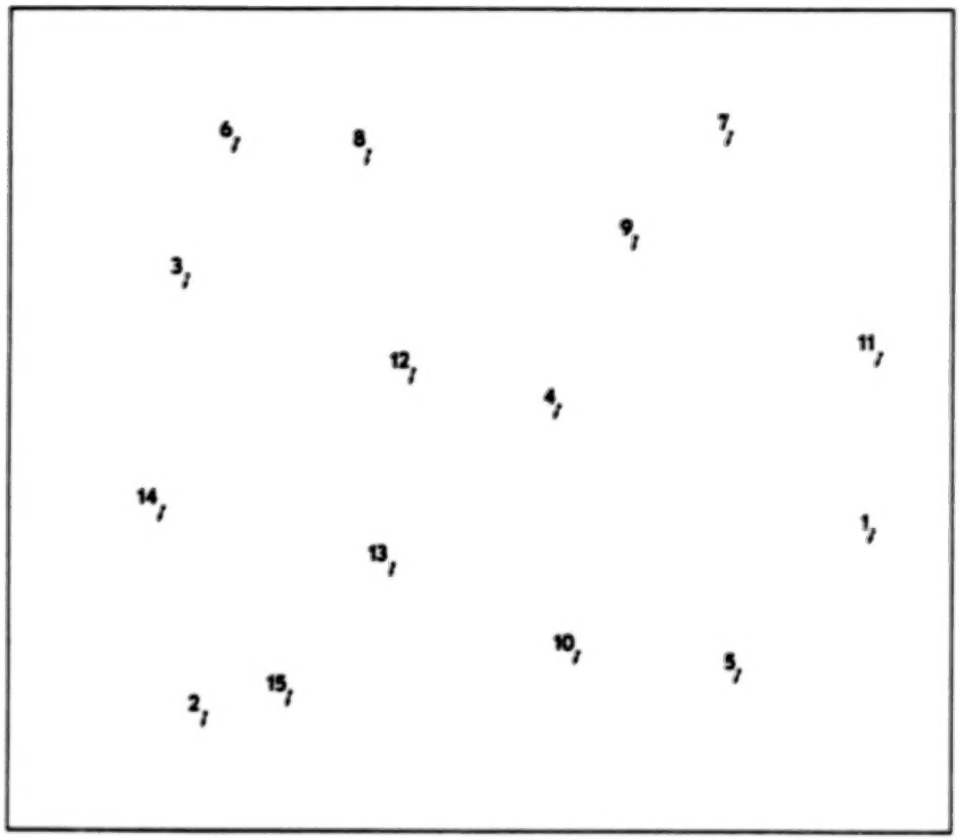

Point	Lat. DD	Lat. MM	Lat. SS	Long. DD	Long. MM	Long. SS	Calculated Line	Calculated Sample	Actual Line	Actual Sample	Offset Line	Offset Sample	Pixel Error
1	34	16	43	-117	27	2	1886	3251	1941	3234	-55	17	57.57
2	34	9	51	-119	3	35	2558	729	2608	711	-50	18	53.14
3	34	58	19	-118	56	23	976	658	1028	637	-52	21	56.08
4	34	36	50	-118	7	6	1437	2076	1491	2056	-54	20	57.58
5	34	3	56	-117	48	21	2397	2761	2451	2744	-54	17	56.61
6	35	12	34	-118	46	33	476	839	530	819	-54	20	57.58
7	35	3	35	-117	37	24	442	2704	499	2683	-57	21	60.75
8	35	8	31	-118	28	31	524	1334	581	1313	-57	21	60.75
9	34	54	20	-117	52	59	812	2348	869	2329	-57	19	60.08
10	34	9	41	-118	10	0	2317	2153	2369	2133	-52	20	55.71
11	34	36	10	-117	21	48	1241	3275	1299	3256	-58	19	61.03
12	34	43	41	-118	26	51	1310	1516	1364	1494	-54	22	58.31
13	34	22	44	-118	33	52	2011	1447	2063	1426	-52	21	56.08
14	34	33	23	-119	4	45	1810	571	1860	549	-50	22	54.63
15	34	10	39	-118	51	35	2478	1044	2530	1024	-52	20	55.71
MEAN =											53.9	19.9	
*STD. =											2.6	1.6	

RMS Error = 57.49 pixels

*Standard deviation from the mean

Fig. 2. MSS ground control points. Los Angeles, December 10, 1982, Path 41, Row 36, Scene ID 84014717565. System-corrected UTM projection.

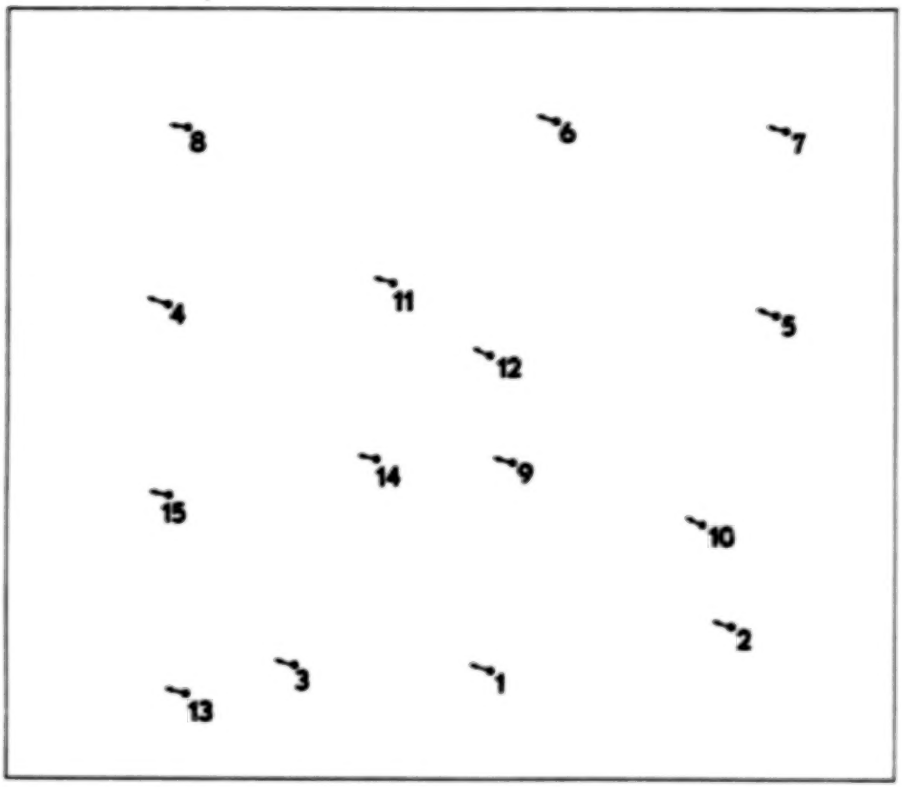

	LAT			LON			CALCULATED		ACTUAL		OFFSET		PIXEL
POINT	DD	MM	SS	DD	MM	SS	LINE	SAMPLE	LINE	SAMPLE	LINE	SAMPLE	ERROR
1	38	20	12	-76	50	31	2564	1923	2537	1865	17	58	60.44
2	38	19	32	-76	11	58	2391	2895	2370	2836	21	59	62.63
3	38	25	26	-77	21	15	2529	1120	2512	1068	17	52	54.71
4	39	10	10	-77	30	54	1143	621	1131	587	12	54	55.32
5	38	54	51	-75	56	39	1191	3057	1179	3007	12	50	51.42
6	39	22	57	-76	24	55	432	2183	419	2122	13	61	62.37
7	39	15	57	-75	49	37	485	3099	476	3046	9	53	53.76
8	39	30	12	-77	22	58	467	703	457	651	10	52	52.95
9	38	44	13	-76	41	5	1743	2015	1729	1963	14	52	53.85
10	38	32	22	-76	13	24	1989	2780	1976	2724	13	56	57.49
11	39	7	53	-76	55	9	1054	1524	1042	1468	12	56	57.27
12	38	57	20	-76	41	38	1328	1922	1314	1866	14	56	57.72
13	38	24	36	-77	38	7	2632	701	2613	649	19	52	55.36
14	38	47	35	-77	2	23	1735	1463	1721	1411	14	52	53.85
15	38	48	00	-77	35	36	1872	631	1858	573	14	58	59.67
									MEAN =		14.1	54.7	
									*STD. =		3.2	3.2	

RMS ERROR = 56.69 pixels

*Standard deviation from the mean

Fig. 3. MSS ground control points. Washington, D.C., November 2, 1982, Path 15, Row 33, Scene ID 84010915140. System-corrected UTM projection.

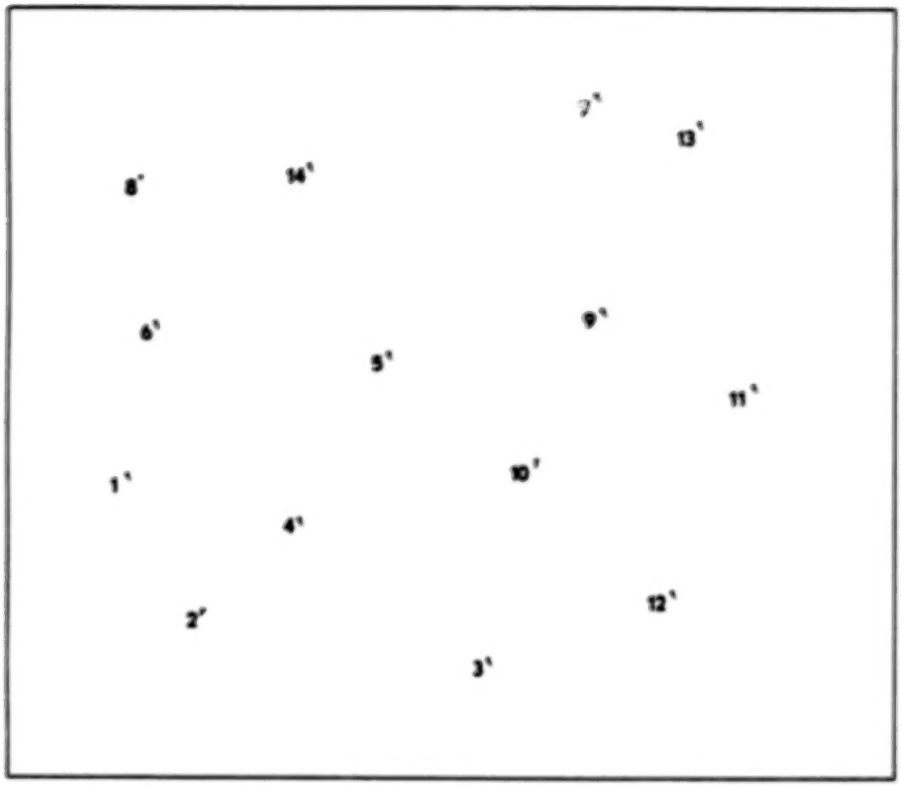

Point	Lat. DD	MM	SS	Long. DD	MM	SS	Calculated Line	Sample	Actual Line	Sample	Offset Line	Sample	Pixel Error
1	33	7	28	-87	2	9	1805	586	1807	592	-2	-6	6.32
2	32	50	35	-86	57	50	2326	792	2327	790	-1	2	2.24
3	32	39	19	-86	18	38	2507	1912	2510	1913	-3	-1	3.16
4	32	58	47	-86	41	18	1989	1194	1992	1197	-3	-3	4.24
5	33	16	58	-86	25	37	1336	1517	1342	1518	-6	-1	6.08
6	33	25	20	-86	58	7	1215	600	1219	600	-4	0	4.00
7	33	43	18	-85	48	59	324	2351	331	2354	-7	-3	7.62
8	33	42	36	-86	57	11	659	533	659	533	0	0	0.00
9	33	16	53	-85	53	26	1188	2381	1194	2387	-6	-6	8.49
10	33	1	12	-86	6	13	1750	2126	1754	2125	-4	1	4.12
11	33	5	9	-85	32	49	1464	3001	1468	3003	-4	-2	4.47
12	32	42	53	-85	50	34	2261	2650	2263	2653	-2	-3	3.61
13	33	37	20	-85	34	39	446	2768	455	2770	-9	-2	9.22
14	33	40	50	-86	32	19	603	1207	611	1209	-8	-2	8.25
										MEAN =	4.2	2.3	
										*STD. =	2.7	1.9	

RMS Error = 5.73 pixels

*Standard deviation from the mean

Fig. 4. MSS ground control points. Central Alabama, December 7, 1982, Path 20, Row 37, Scene ID 84014415472. GCP-corrected SOM projection.

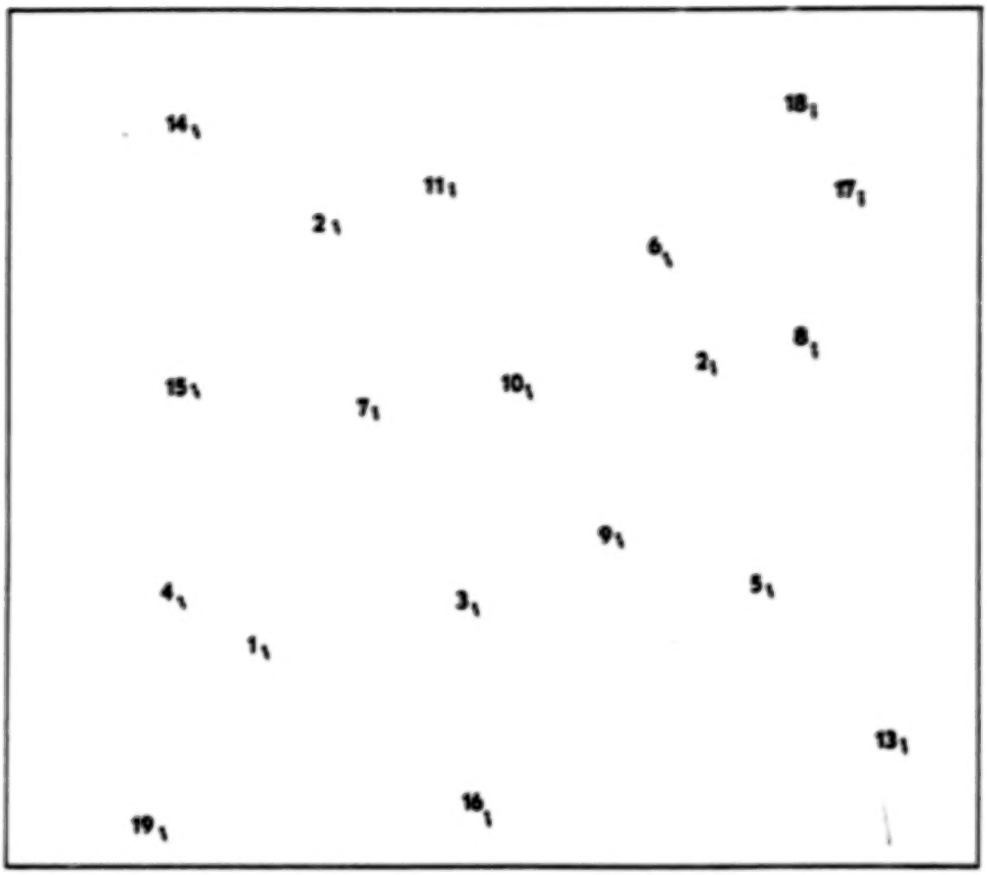

Point	Lat. DD	Lat. MM	Lat. SS	Long. DD	Long. MM	Long. SS	Calculated Line	Calculated Sample	Actual Line	Actual Sample	Offset Line	Offset Sample	Pixel Error
1	45	44	3	-98	18	37	4468	1864	4505	1872	-38	- 8	38.88
2	46	28	31	-97	54	30	1546	2381	1582	2390	-38	- 9	37.11
3	45	44	0	-97	45	3	4166	3361	4200	3371	-34	-10	35.44
4	45	51	3	-98	29	48	4122	1276	4158	1284	-36	- 8	36.88
5	45	39	36	-96	58	40	4004	5487	4036	5496	-32	- 9	33.24
6	46	15	41	-97	5	38	1779	4679	1813	4689	-34	-10	35.44
7	46	6	36	-97	54	13	2812	2655	2846	2664	-34	- 9	35.17
8	46	3	6	-96	44	29	2374	5788	2406	5798	-32	-10	33.53
9	45	48	20	-97	21	6	3664	4370	3698	4379	-34	- 9	35.17
10	46	5	41	-97	30	30	2650	3718	2684	3725	-34	- 7	34.71
11	46	28	17	-97	35	39	1261	3188	1296	3195	-35	- 7	35.69
12	46	4	0	-97	1	55	2485	5005	2519	5014	-34	- 9	35.17
13	45	20	27	-96	44	21	5079	6394	5110	6402	-31	- 8	32.02
14	46	39	37	-98	13	41	883	1368	918	1375	-35	- 7	35.69
15	46	12	42	-98	21	28	2668	1372	2705	1379	-37	- 7	37.68
16	45	22	13	-97	50	13	5599	3418	5633	3426	-34	- 8	34.93
17	46	17	50	-96	32	56	1325	6089	1358	6098	-33	- 9	34.21
18	46	28	17	-96	38	48	701	5770	734	5779	-33	- 9	34.21
19	45	27	39	-98	39	35	5701	1133	5738	1141	-37	- 8	37.85
									MEAN =		34.3	8.5	
									*STD. =		1.7	1.0	

RMS Error = 35.35 pixels

*Standard deviation from the mean

Fig. 5. TM ground control points. Aberdeen, SD, September 24, 1982, Path 30, Row 28, Scene ID 40070-16442. System-corrected SOM projection.

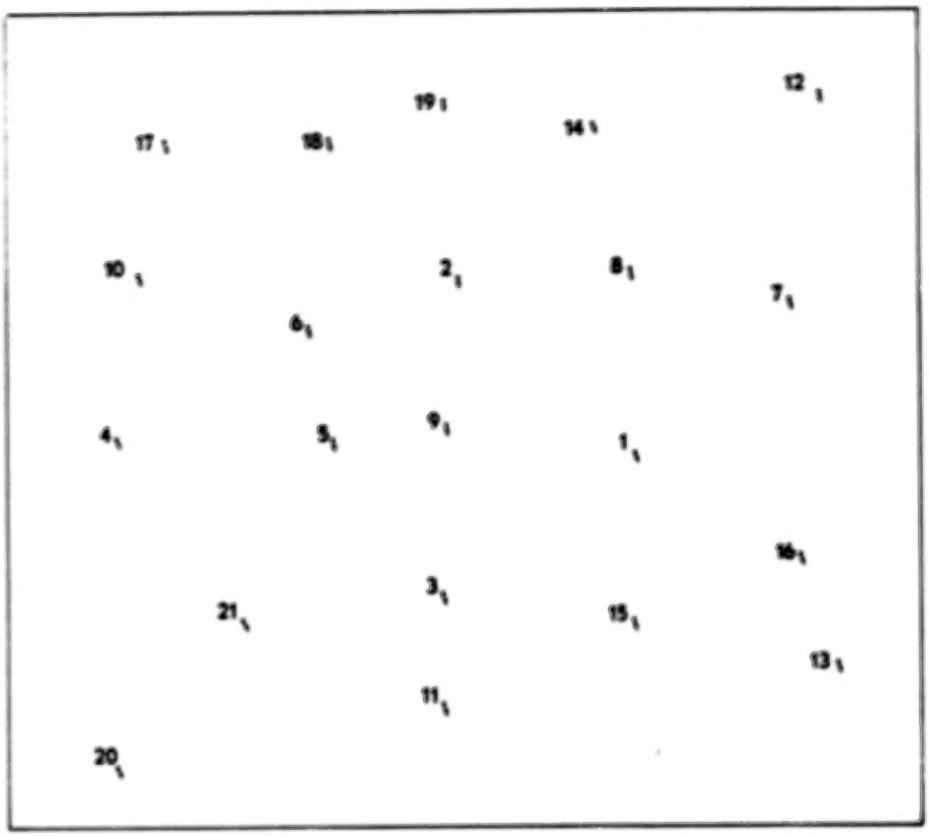

Point	Lat. DD	Lat. MM	Lat. SS	Long. DD	Long. MM	Long. SS	Calculated Line	Calculated Sample	Actual Line	Actual Sample	Offset Line	Offset Sample	Pixel Error
1	40	12	18	-89	54	40	3216	4771	3257	4781	-41	-10	42.20
2	40	35	49	-90	16	15	1920	3429	1963	3439	-43	-10	44.15
3	40	1	15	-90	27	3	4225	3320	4268	3331	-43	-11	44.38
4	40	25	1	-91	11	51	3112	847	3158	858	-46	-11	47.30
5	40	20	42	-90	39	11	3096	2493	3140	2503	-44	-10	45.12
6	40	33	24	-90	39	24	2287	2332	2331	2343	-44	-11	45.35
7	40	25	39	-89	27	26	2103	5931	2143	5941	-40	-10	41.23
8	40	32	32	-89	50	9	1884	4739	1926	4749	-42	-10	43.17
9	40	19	38	-90	21	31	3001	3369	3043	3380	-42	-11	43.42
10	40	42	51	-91	4	11	1905	1015	1951	1025	-46	-10	47.07
11	39	49	0	-90	30	26	5039	3302	5082	3312	-43	-10	44.15
12	40	47	34	-89	16	24	600	6185	641	6195	-41	-10	42.20
13	39	44	17	-89	31	2	4772	6282	4812	6294	-40	-12	41.78
14	40	49	40	-89	52	12	812	4425	854	4435	-42	-10	43.17
15	39	53	53	-89	59	40	4438	4754	4478	4765	-40	-11	41.48
16	39	57	33	-89	33	20	3950	6000	3990	6011	-40	-11	41.48
17	40	57	14	-90	56	26	918	1223	962	1235	-44	-12	45.61
18	40	53	22	-90	31	23	939	2482	985	2494	-46	-12	47.54
19	40	55	28	-90	12	21	630	3379	673	3388	-43	- 9	43.93
20	39	48	59	-91	18	44	5476	923	5522	932	-46	- 9	46.87
21	40	2	24	-90	55	25	4411	1914	4455	1925	-44	-11	45.35
									MEAN =		42.9		10.5
									*STD. =		2.1		0.9

RMS Error = 44.19 pixels

*Standard deviation from the mean

Fig. 6. TM ground control points. Galesburg, IL, October 16, 1982, Path 24, Row 32, Scene ID 40092-16092. System-corrected SOM projection.

N85-20505

GEOMETRIC ACCURACY ASSESSMENT OF LANDSAT-4 MULTISPECTRAL SCANNER (MSS) DATA

Marc L. Imhoff
William L. Alford

NASA/Goddard Space Flight Center
Greenbelt, Maryland

1.0 Introduction

One of the many objectives of the Landsat-4 program is the achievement of improvements in the geometric integrity of the MSS image data. Improvements are targeted for the spacecraft performance such as attitude and ephemeris control, pointing accuracy, and pointing stability, etc., as well as the performance of ground processing systems designed to generate the final image products. Especially important to the mission is the capability of producing consistently geometrically and geodetically accurate MSS image products for the user community. The Landsat-4 program is attempting to meet the following stringent self-imposed specifications for geometric performance of the MSS data.

geodetic accuracy . . . 0.5 sensor pixel or 41m (90 percent time)
temporal accuracy . . . 0.3 sensor pixel or 24.6m (90 percent time)
band-to-band accuracy . 0.2 sensor pixel or 16.4m (90 percent time)

A sensor pixel = 82x82m

The results reported here are the outcome of analyses performed on standard Landsat-4 MSS data output from the MSS Subsystem Image Processing System (MIPS). The analyses were designed to characterize the geometric performance of standard MSS data. As such only P-format geodetically corrected MSS digital image data were examined.

2.0 Objectives

The objectives of the analyses were to:

a. Characterize the geodetic accuracy of standard P-format MSS image data,

b. Characterize the temporal registration accuracy of standard P-format MSS image data, and

c. Characterize the band-to-band registration accuracy of standard P-format MSS image data.

3.0 Approach

Originally it was intended that the analyses include as many as 12 separate MSS data sets. However, technical problems with the functioning of the spacecraft fixed head star trackers caused delays in the refinement of the systematic geometric correction parameters which in turn seriously impacted the timely accumulation of suitable test data. As a result only 2 MSS scenes suitable for analysis existed at the time of this study.

The 2 scenes used in the analysis are Washington, DC, scene Day 109 (ID number 4010915140) and Washington, DC, scene Day 125 (ID number 4012515144). Both scenes were processed through MIPS in P-format using the Universal Transverse Mercator (UTM) projection. Both scenes were geodetically corrected.

Two methodologies were used for meeting the objectives. Geodetic accuracy was assessed by comparing the image data to map products while band-to-band registration accuracy and temporal registration accuracy were assessed using a cross-correlation approach. Since all of the data analyzed in this study were processed in P-format, the error measurements are presented in terms of a 57x57 m pixel.

3.1 Geodetic Accuracy Assessment

The Washington, DC, Day 109 data set was used for the analysis of geodetic accuracy. Geodetic verification points selected from US Geological Survey (USGS) topographic quadrangles were compared against the corresponding Landsat-4 MSS image feature locations as defined by the header record information provided on the CCT.

Over 30 geodetic verification points (GVP's) were defined for the Washington, DC, area. The points were selected using USGS 7.5 minute topographic quadrangles and Landsat 2-3 color composites. The GVP's were selected so that they were temporally stable, distributed evenly over the scene, and visible at the Landsat MSS spatial resolution and spectral composition. The points consisted primarily of road intersections, dams, and bridges.

Once selected, the GVP's were digitized at a precision level of 0.1 seconds (~3 meters) using a Talos digitizer. The GVP's were converted from latitude-longitude to UTM coordinates to conform to the MSS data projection format.

In order to compare the map-derived GVP's with the MSS data a modified Zoom transfer scope was set up in front of a DeAnza CRT display device. Matching for scale was accomplished by aligning a map grid pattern with a corresponding image grid created on the CRT through the Zoom transfer scope.

The scale factor between grids was calculated by measuring the raster size of the CRT unit and calculating the screen scale for a given magnification factor (4 times magnification in this analysis) based on the 57x57 m pixel size of the MSS data. Once the screen scale factor was calculated, a grid was constructed digitally on the CRT at measured intervals. Another grid for map registration was produced based on the CRT measurements but scaled to 1:24,000 to match the USGS 7.5 minute quadrangles.

The matching of grids not only allowed for accurate alignments in the x and y direction but also permitted adjustments to be made to the Zoom transfer scope to account for optical distortions such as x, y skew. Some pincushion effects could be seen, however, at the edges of the image as viewed through the scope. To alleviate that problem, alignments were made to match at the center of the image.

Once the Zoom transfer scope apparatus was aligned and scaled properly, the GVP's were entered into a software package developed for this analysis. The package (LOCATEG) is implemented on the IDIMS HP-3000 configuration. LOCATEG takes the Landsat header record information and user-defined scaling factors and converts the digitized GVP coordinates to line and element numbers conforming to the imagery. The Landsat MSS header record information used by LOCATEG to perform the transformation is as follows:

a. Image orientation beta angle--angle of offset between map projection grid (UTM, SOM, PS, etc.) and actual image line and pixel orientation,

b. WRS center latitude,

c. WRS center longitude,

d. WRS center line number, and

e. WRS center pixel number.

Once the transformation has been accomplished, image data surrounding each GVP can be displayed by user command. Alignment of the map sheet is then accomplished by matching surface features (road network, etc.) on the map with the image on the CRT. A cursor appears at the exact GVP location on the CRT unit. The location of the cursor can be adjusted using a track ball to the correct location as indicated by the map data (also viewed through the transfer scope). The computer then calculates the offsets in the x and y direction and is displayed in fractional pixels. Directional offsets can be ascertained by the sign (+ or -) of the error term. Error figures are also output in terms UTM northings and eastings or latitutde and longitude.

3.2 Band-to-Band and Temporal Registration

The method used to evaluate both band-to-band and temporal registration accuracy was cross-correlation. In both cases, a series of well-distributed control points selected from the GVP file provided the subsets or image chips used for correlation analysis.

For band-to-band registration accuracy assessment the cross-correlation technique using 28 image chips was applied to the Washington, DC, Day 109 data comparing band 1 to band 2, band 2 to band 3, and band 3 to band 4.

For temporal registration accuracy each band 1-4 from Washington, DC, Day 109 scene data was compared to bands 1-4 of Washington, DC, Day 125.

Subpixel measurement of correlations and offsets for both band-to-band and temporal registration was derived from a least squares surface fit to the correlation peak.

Almost no thresholding of measurements was implemented for the band-to-band and temporal registration analyses. Virtually all but the most erratic measurements were included in the analysis. Measurements were discarded only if they had extremely low correlations and if the offsets were several times larger than those yielded by comparisons with higher correlations.

4.0 Results and Discussion

4.1 Geodetic Accuracy Assessment

The Washington, DC, Day 109 MSS scene was used for the assessment of geodetic accuracy. The scene was processed in P-format UTM projection with a 57x57 m pixel size. Twenty control points were successfully correlated and used for the geodetic correction in the MIPS.

Using the Zoom transfer scope arrangement and the LOCATEG software, 12 GVP's scattered throughout the scene were successfully matched with the USGS topographic quadrangles (figure 1). Many GVP's were rejected due to problems in recognizing the verification point features on the MSS image.

A 4x expansion factor was used for the MSS data. Although this limited measurement precision to 0.25 pixel, it was necessary that an adequate feature area be represented on the CRT for an accurate image to map alignment in both the x and y direction. Mean offsets for both line and sample were positive although quite small (0.06 pixel and 0.08 pixel, respectively). The combined RMS registration error was well within specifications and measured as 0.43 pixel (24.51 m) (figure 2).

The measurement of subpixel accuracy proved to be somewhat difficult. Even a 4x expansion map to image alignment contained considerable latitude in measurement. Several senior analysts measuring error for the same GVP varied $\pm$.25 pixel in their interpretations of a best alignment. This was due predominantly to the lack of sharp edges and detail in the MSS imagery. The degree of precision of measurement of subpixel accuracy for geodetic registration is directly related to the ability of image data to define sharp edges. Even if this factor is alleviated problems will arise over the map information. Road burms, for example, that will contribute to a Landsat image feature may or may not be measured in the map representation of the road.

In general, however, the geodetic registration of the Washington, DC, scene proved to be excellent. In many cases the registration accuracy was so precise as to be beyond reasonable error detection simply due to the spatial resolution limitations of the MSS data.

4.2 Band-to-Band Registration

Cross-correlation analysis for band-to-band registration was performed on Washington, DC, scene Day 109 MSS data. Cross-correlation was performed on 28 image chips defined from the geodetic verifications points selected for the geodetic accuracy analysis. Three band combinations were examined:

a. Band 1 versus band 2,

b. Band 2 versus band 3, and

c. Band 3 versus band 4.

Band combinations such as band 1 versus band 4 were not attempted due to low natural correlations of the information content between them.

On the whole, band-to-band registration results were good. Registration between bands 1 and 2 yielded a combined RMS error of 0.173 pixels (14.2m) (figure 3). Registration between bands 3 and 4 yielded a combined RMS error of 0.167 pixels (13.7m) (figure 4). Registration accuracies for bands 1 versus 2 and 3 versus 4 were well within specifications. Band 2 versus band 3 yielded an RMS error of 0.464 (26.4m) (figure 5). The higher error for the band 2-band 3 comparison can be contributed to the differences in information content which make control feature matching difficult and yield lower overall correlations between the bands.

As expected, the offsets (error registration) between bands appeared to be random with a correlation between line and sample error measurements of all band-to-band comparisons of 0.332.

4.3 Temporal Registration Accuracy

Assessment of temporal registration accuracy was accomplished comparing Washington, DC, MSS scene Day 109 to Washington, DC, scene Day 125. The Washington, DC, Day 125 scene was corrected in the MIPS using 13 geodetic control points. Only 13 were used due to cloud cover which obscured some of the scene. The cloud cover problem also necessitated the rejection of some of the GVP's used in this analysis.

The comparison of the 2 scenes was made on a band-by-band basis using the cross-correlation technique described in the approach. Overall temporal registration accuracy appears to be quite good. A mean RSS for line and sample, all bands, was 0.313 pixels (17.8m). The offset errors were random with a correlation of 0.121 between line and sample error.

A band-by-band analysis of temporal registration showed that registration accuracies varied from band-to-band. Bands 1 and 2 showed RMS offset errors of 0.439 (25.0m) pixels and 0.541 pixels (30.8m), respectively (figures 6 and 7). Temporal registration errors for bands 3 and 4 were lower with RMS offset errors of 0.387 pixels (22.1m) and 0.342 pixels (19.5m), respectively (figures 8 and 9). The error measurements for bands 1 and 2 may be attributed to a lack of contrast in those bands which creates lower correlation peaks for the matched GVP features.

5.0 Conclusions

In conclusion, the geometric accuracies of Landsat-4 MSS data are excellent. The geodetic registrations accuracy appears very good. The Landsat data closely match the USGS map products with image-to-map offset errors of <.5 (57 x 57 m) pixels. The worst single case geodetic offset measured in this analysis was 0.80 (57 x 57) pixel which is 45.6 meters. The specification

calls for 0.5 sensor pixel (82 x 82 m) or 41 meters 90 percent of the time. The next worst case offset is .56 (57 x 57 m) pixel or 31.9 meters. The overall 90 percent error figure for geodetic registration error was computed to be 0.637 (57 x 57 m) pixel or 36.31 meters which is well within specifications.

Temporal registration accuracy was also quite good although results from this analysis do not meet specifications.

The specifications for temporal registration are 0.3 sensor (82 x 82 m) pixel or 24.6 m 90 percent of the time. Our results show that the 90 percent error figure for temporal registration is 0.68 (57 x 57 m) pixel or 38.8 meters. This large figure, however, may be explained in part as a result of the lack of thresholding in our analysis. This examination allowed for statistics (not erratics) with low correlations to be included in the calculations. The thresholding of the input measurements based on a minimum correlation may have decreased the error terms somewhat, although probably not enough to meet the specifications.

Band-to-band registration could be considered to meet specifications. The registration error between the bands having naturally higher correlations between information content (bands 1 and 2 and bands 3 and 4) proved to meet specifications 14.2m and 13.7m, respectively.

The measured band-to-band and temporal registration error as a result of this analysis is considerably below that required by most applications of the data. From a user standpoint therefore, the geometric registration of Landsat-4 data should be considered quite good.

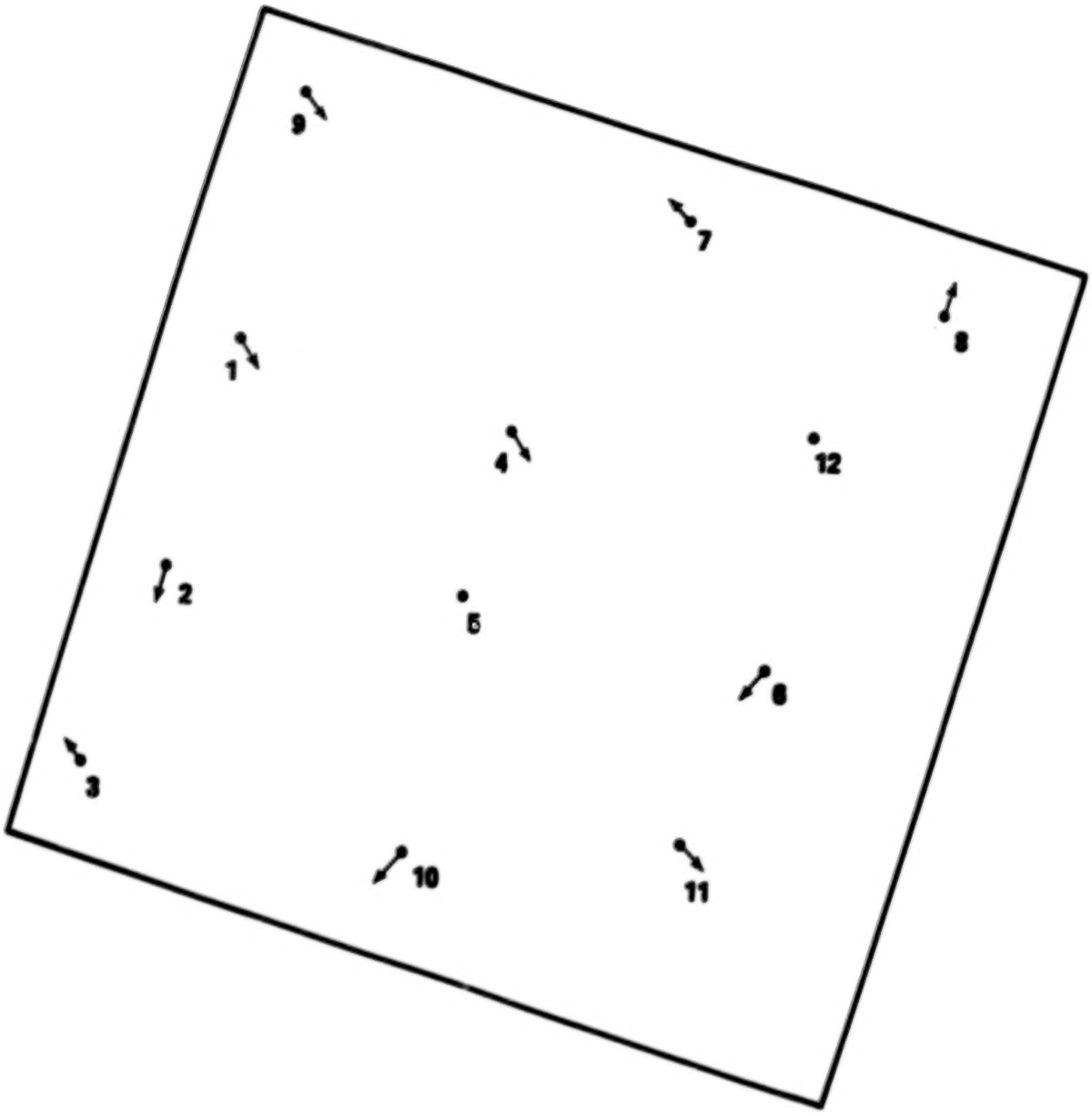

Figure 1. Geodetic Verification Points With Calculated Image Locations to Actual GVP Locations, Washington, DC MSS SCENE ID 4010915140, Day 109, UTM Projection

Verification Point	Calculated		Actual		Offset		Pixel Error
	Line	Sample	Line	Sample	Line	Sample	RSS
1	1276.00	543.50	1275.5	543.25	0.50	0.25	0.56
2	2647.75	105.75	2648.00	106.25	-0.25	-0.50	0.56
3	2089.25	280.50	2089.00	280.50	0.00	0.25	0.25
4	1211.50	1104.25	1211.25	1104.00	0.25	0.25	0.35
5	1777.75	1205.25	1777.75	1205.25	0.00	0.00	0.00
6	1463.75	2564.50	1463.50	2564.75	0.25	-0.25	0.35
7	61.25	1607.50	61.50	1607.75	-0.25	-0.25	0.35
8	105.25	2458.75	105.50	2458.25	-0.25	0.50	0.56
9	98.00	408.25	97.75	407.50	0.25	0.75	0.80
10	2618.25	1575.75	2618.00	1576.00	0.25	-0.25	0.35
11	783.50	2033.75	783.50	2033.75	0.00	0.00	0.00
12	2528.25	2539.00	2528.25	2538.75	0.00	0.25	0.25
				Mean Offsets	0.06	0.08	RMS Error = 0.43

Figure 2. Geodetic Accuracy Verification, Washington, DC MSS Scene ID 401091540, Day 109, P-tape UTM Projection.

	VERIFICATION POINT	CORRELATION	REFERENCE LINE	REFERENCE SAMPLE	SEARCH LINE	SEARCH SAMPLE	SEARCH + ERROR LINE	SEARCH + ERROR SAMPLE	ERRORS LINE	ERRORS SAMPLE
1	PT1	.7393	668.8	606.6	668.8	606.6	668.9	606.7	.04	.11
2	PT5	.8407	1276.0	543.6	1276.0	543.6	1276.1	543.7	.05	.10
3	PT11	.5129	2298.4	765.2	2298.4	765.2	2298.6	765.6	.28	.48
4	PT14	.3648	783.4	2033.6	783.4	2033.6	783.1	2033.4	-.31	-.26
5	PT19	.8527	1777.7	1205.3	1777.7	1205.3	1777.8	1205.3	.07	-.05
6	PT108	.8972	1598.7	1650.0	1598.7	1650.0	1598.8	1650.1	.06	.03
7	PT22	.8591	2618.2	1575.8	2618.2	1575.8	2618.3	1575.9	.04	.07
8	PT23	.7839	2964.6	1400.1	2964.6	1400.1	2964.5	1400.1	-.08	.03
9	PT7	.8863	212.9	1207.5	212.9	1207.5	212.9	1207.5	.01	-.02
10	PT13	.8828	447.2	1748.0	447.2	1748.0	447.2	1748.0	.04	-.01
11	PT26	.9117	1883.0	2952.2	1883.0	2952.2	1883.0	2952.3	.03	.12
12	PT27	.8883	2225.5	1587.5	2225.5	1587.5	2225.5	1587.5	.03	.01
13	PT71	.7505	1211.5	1104.4	1211.5	1104.4	1211.5	1104.3	-.05	-.08
14	PT29	.7069	2089.3	280.6	2089.3	280.6	2089.3	280.6	.08	-.03
15	PT30	.8904	1209.3	3168.5	1209.3	3168.5	1209.4	3168.6	.04	.08
16	PT34	.9374	2528.2	2539.0	2528.2	2539.0	2528.4	2539.0	.14	-.00
17	PT36	.6750	2647.8	105.8	2647.8	105.8	2647.9	106.1	.13	.28
18	PT46	.7610	2285.7	1036.6	2285.7	1036.6	2285.7	1036.5	.01	-.06
19	PT142	.7952	2166.5	2056.0	2166.5	2056.0	2166.4	2056.0	-.05	.05
20	PT32	.8591	221.2	3240.3	221.2	3240.3	221.3	3240.2	.02	-.01
21	MP1	.6865	98.0	408.2	98.0	408.2	98.0	407.9	-.03	-.20
22	MP14	.5941	1159.8	2147.8	1159.8	2147.8	1159.7	2147.7	-.07	-.04
23	MP13	.7329	724.0	1415.7	724.0	1415.7	723.9	1415.8	-.02	.13
24	MP17	.8811	1463.6	2564.5	1463.6	2564.5	1463.6	2564.5	-.05	-.04
25	MP15	.6927	367.1	2123.2	367.1	2123.2	367.1	2123.3	-.04	.16
26	MP16	.8414	1129.6	2642.3	1129.6	2642.3	1129.7	2642.4	.10	.07
27	MP10	.8630	105.2	2458.7	105.2	2458.7	105.3	2458.6	.08	-.10
28	MP4	.8383	3012.7	1946.0	3012.7	1946.0	3012.5	1946.0	-.12	-.07

AVERAGE ABSOLUTE ERROR 0.074 0.096

REFERENCE = BAND 1
SEARCH = BAND 2

RMS ERROR = 0.173

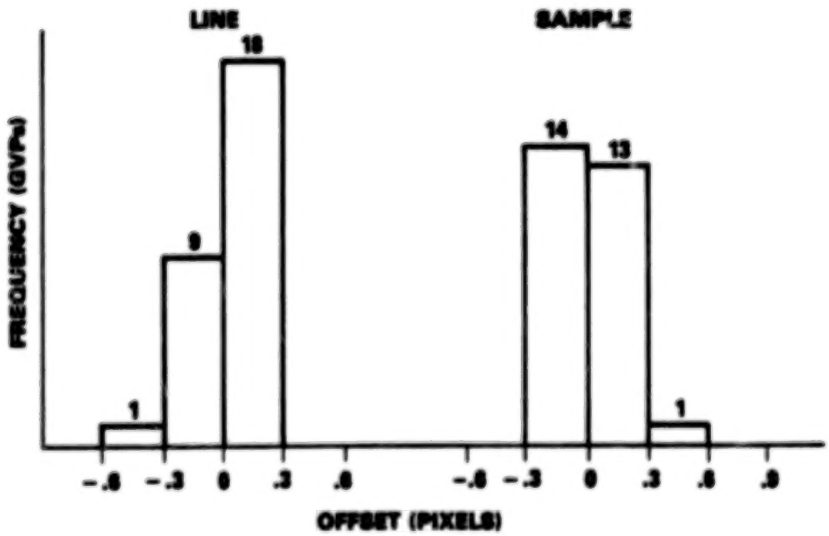

Figure 3. Band 1 to Band 2 Registration Accuracy, Washington, DC, Day 109.

	VERIFICATION POINT	CORRELATION	REFERENCE LINE	REFERENCE SAMPLE	SEARCH LINE	SEARCH SAMPLE	SEARCH + ERROR LINE	SEARCH + ERROR SAMPLE	ERRORS LINE	ERRORS SAMPLE
1	PT1	.8523	668.8	606.6	668.8	606.6	668.8	606.7	.02	.12
2	PT5	.8995	1276.0	543.6	1276.0	543.6	1275.9	543.8	-.12	.18
3	PT11	.5772	2298.4	765.2	2298.4	765.2	2298.1	765.1	-.26	-.05
4	PT14	.6292	783.4	2033.6	783.4	2033.6	783.5	2033.8	.10	.12
5	PT19	.8196	1777.7	1205.3	1777.7	1205.3	1777.6	1205.4	-.08	.05
6	PT108	.7150	1598.7	1650.0	1598.7	1650.0	1598.6	1650.0	-.11	-.00
7	PT22	.8247	2618.2	1575.8	2618.2	1575.8	2618.2	1575.8	.00	.02
8	PT23	.9726	2964.6	1400.1	2964.6	1400.1	2964.5	1400.2	-.08	.08
9	PT7	.8594	212.9	1207.5	212.9	1207.5	212.7	1207.5	-.20	.03
10	PT13	.8756	447.2	1748.0	447.2	1748.0	447.0	1747.9	-.12	-.08
11	PT26	.9754	1883.0	2952.2	1883.0	2952.2	1883.0	2952.4	.02	.20
12	PT27	.7383	2225.5	1587.5	2225.5	1587.5	2225.3	1587.6	-.13	.05
13	PT71	.8752	1211.5	1104.4	1211.5	1104.4	1211.5	1104.5	-.04	.18
14	PT29	.9252	2089.3	280.6	2089.3	280.6	2089.2	280.8	-.01	.13
15	PT30	.9491	1209.3	3168.5	1209.3	3168.5	1209.3	3168.7	-.04	.21
16	PT34	.8150	2528.2	2539.0	2528.2	2539.0	2528.1	2539.0	-.14	.04
17	PT36	.9052	2647.8	105.8	2647.8	105.8	2647.8	105.9	.05	.14
18	PT46	.7017	2285.7	1036.6	2285.7	1036.6	2285.5	1036.6	-.24	-.01
19	PT142	.9768	2166.5	2056.0	2166.5	2056.0	2166.6	2056.1	.08	.13
20	PT32	.7821	221.2	3240.3	221.2	3240.3	221.3	3240.5	.01	.24
21	MP1	.9263	98.0	408.2	98.0	408.2	98.0	408.3	-.00	.11
22	MP14	.9419	1159.8	2147.8	1159.8	2147.8	1159.7	2147.9	-.04	.08
23	MP13	.9213	724.0	1415.7	724.0	1415.7	723.9	1415.6	-.02	-.03
24	MP17	.9100	1463.6	2564.5	1463.6	2564.5	1463.5	2564.6	-.12	.03
25	MP15	.8913	367.1	2123.2	367.1	2123.2	367.0	2123.2	-.09	.01
26	MP16	.8439	1129.6	2642.3	1129.6	2642.3	1129.5	2642.2	-.10	-.09
27	MP10	.7866	105.2	2458.7	105.2	2458.7	105.0	2458.9	-.19	.17
28	MP4	.6574	3012.7	1946.0	3012.7	1946.0	3012.6	1946.3	-.08	.27
							AVERAGE ABSOLUTE ERROR		0.089	0.102

REFERENCE = BAND 3
SEARCH = BAND 4

RMS ERROR = 0.167

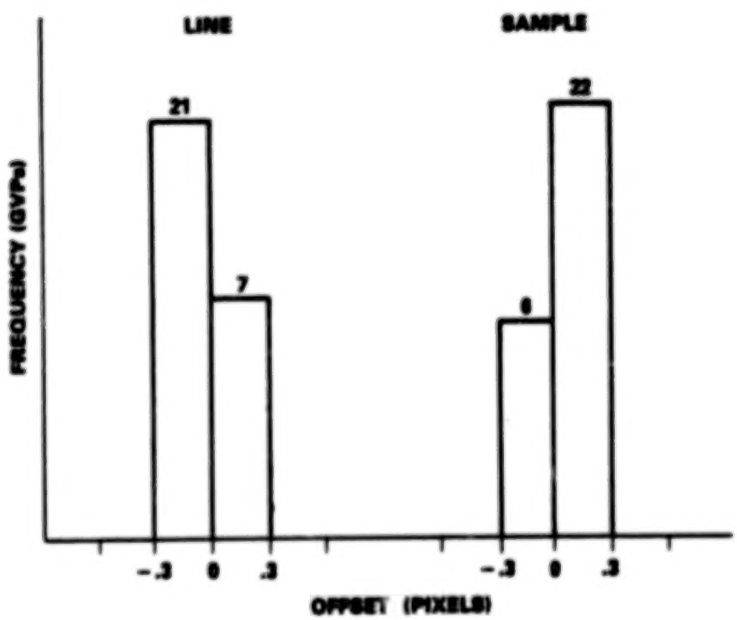

Figure 4. Band 3 to Band 4 Registration Accuracy, Washington, DC, Day 109.

	VERIFICATION POINT	CORRELATION	REFERENCE LINE	REFERENCE SAMPLE	SEARCH LINE	SEARCH SAMPLE	SEARCH + ERROR LINE	SEARCH + ERROR SAMPLE	ERRORS LINE	ERRORS SAMPLE
1	PT1	.2432	668.8	606.6	668.8	606.6	669.2	606.2	.41	-.48
2	PT5	.3790	1276.0	543.6	1276.0	543.6	1275.7	543.8	-.25	.18
3	PT11	.5714	2298.4	765.2	2298.4	765.2	2298.4	764.8	.04	-.37
4	PT14	.4992	783.4	2033.6	783.4	2033.6	783.4	2033.7	-.00	.01
5	PT19	.4319	1777.7	1205.3	1777.7	1205.3	1777.5	1205.1	-.21	-.20
6	PT10B	.5944	1598.7	1650.0	1598.7	1650.0	1598.6	1649.9	-.13	-.09
7	PT22	.4088	2618.2	1575.8	2618.2	1575.8	2618.4	1575.0	.12	-.80
8	PT23	.7109	2964.6	1400.1	2964.6	1400.1	2964.7	1400.0	.11	-.07
9	PT7	.2939	212.9	1207.5	212.9	1207.5	212.3	1207.1	-.57	-.38
10	PT13	.5818	447.2	1748.0	447.2	1748.0	447.1	1747.5	-.07	-.52
11	PT26	.8974	1883.0	2952.2	1883.0	2952.2	1883.2	2952.3	.19	.06
12	PT27	.5275	2225.5	1587.5	2225.5	1587.5	2225.4	1587.4	-.08	-.17
13	PT71	.3666	1211.5	1104.4	1211.5	1104.4	1211.7	1104.8	.22	.41
14	PT30	.8474	1209.3	3168.5	1209.3	3168.5	1209.4	3168.5	.06	.01
15	PT34	.3681	2528.2	2539.0	2528.2	2539.0	2527.8	2538.8	-.48	-.19
16	PT36	.1971	2647.8	105.8	2647.8	105.8	2648.5	105.4	.66	-.36
17	PT46	.6338	2285.7	1036.6	2285.7	1036.6	2285.4	1036.4	-.29	-.14
18	PT142	.8434	2166.5	2056.0	2166.5	2056.0	2166.6	2056.1	.14	.17
19	PT32	.7158	221.2	3240.3	221.2	3240.3	221.4	3240.4	.15	.15
20	HP1	.5337	98.0	408.2	98.0	408.2	98.0	408.1	-.02	-.09
21	HP14	.5633	1159.8	2147.8	1159.8	2147.8	1159.7	2147.5	-.06	-.27
22	HP17	.4561	1463.6	2564.5	1463.6	2564.5	1463.2	2563.8	-.49	-.74
23	HP15	.5299	367.1	2123.2	367.1	2123.2	367.1	2122.7	.04	-.50
24	HP16	.5789	1129.6	2642.3	1129.6	2642.3	1129.2	2641.5	-.41	-.83
25	HP10	.3695	105.2	2458.7	105.2	2458.7	105.0	2458.8	-.15	.09
26	HP4	.7147	3012.7	1946.0	3012.7	1946.0	3012.9	1946.2	.28	.16

AVERAGE ABSOLUTE ERROR 0.217 0.286

REFERENCE = BAND 2
SEARCH = BAND 3

RMS ERROR = 0.464

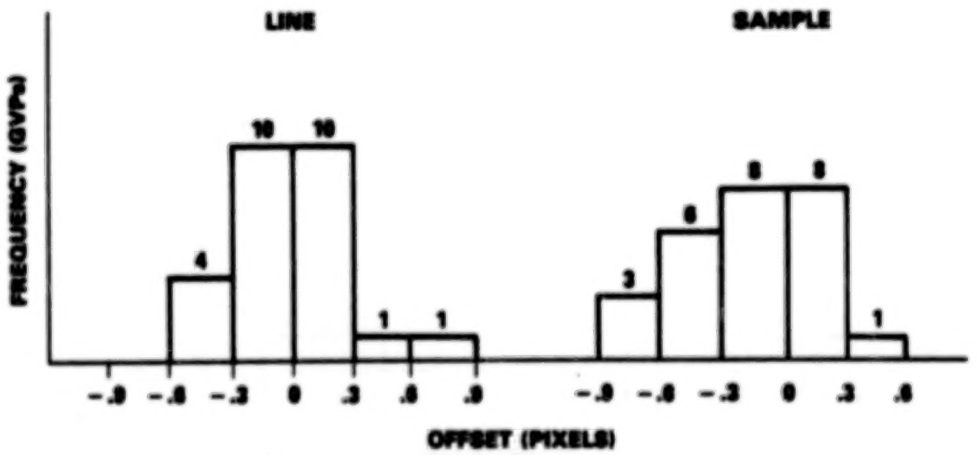

Figure 5. Band 2 to Band 3 Registration Accuracy, Washington, DC, Day 109.

	VERIFICATION POINT	CORRELATION	REFERENCE LINE	REFERENCE SAMPLE	SEARCH LINE	SEARCH SAMPLE	SEARCH + ERROR LINE	SEARCH + ERROR SAMPLE	ERRORS LINE	ERRORS SAMPLE
1	PT1	.6945	668.8	606.6	668.8	757.6	668.8	757.6	-.06	-.03
2	PT5	.8186	1276.0	543.6	1276.0	694.6	1275.9	694.7	-.05	.15
3	PT11	.3486	2298.4	765.2	2298.4	916.2	2298.3	916.7	-.09	.55
4	PT14	.2462	783.4	2033.6	783.4	2184.6	783.3	2183.7	-.11	-.89
5	PT19	.7437	1777.7	1205.3	1777.7	1356.3	1777.7	1356.4	.06	.04
6	PT22	.7468	2618.2	1575.8	2618.2	1726.8	2618.1	1726.5	-.11	-.27
7	PT23	.5748	2964.6	1400.1	2964.6	1551.1	2964.8	1551.0	.17	-.08
8	PT7	.6646	212.9	1207.5	212.9	1358.5	212.5	1358.8	-.32	.23
9	PT13	.7941	447.2	1748.0	447.2	1899.0	446.8	1899.0	-.39	-.02
10	PT27	.8435	2225.5	1587.5	2225.5	1738.5	2225.4	1738.4	-.12	-.10
11	PT71	.6629	1211.5	1104.4	1211.5	1255.4	1211.4	1255.7	-.16	.38
12	PT29	.6202	2089.3	280.6	2089.3	431.6	2089.1	431.4	-.15	-.24
13	PT30	.5560	1209.3	3168.5	1209.3	3319.5	1209.0	3318.8	-.39	-.65
14	PT34	.3743	2528.2	2539.0	2528.2	2690.0	2527.5	2689.8	-.75	-.21
15	PT36	.3262	2647.8	105.8	2647.8	256.8	2646.8	257.1	-.98	.32
16	PT46	.7205	2285.7	1036.6	2285.7	1187.6	2285.8	1187.8	.08	.27
17	PT142	.4795	2166.5	2056.0	2166.5	2207.0	2166.6	2206.6	.10	-.35
18	PT32	.7658	221.2	3240.3	221.2	3391.3	220.9	3391.0	-.33	-.26
19	HP1	.5602	98.0	408.2	98.0	559.2	97.9	558.8	-.13	-.32
20	HP14	.5974	1159.8	2147.8	1159.8	2298.8	1159.9	2298.8	.10	-.02
21	HP13	.7170	724.0	1415.7	724.0	1566.7	723.9	1567.0	-.09	.29
22	HP17	.7657	1463.6	2564.5	1463.6	2715.5	1463.6	2715.4	-.07	-.08
23	HP15	.6895	367.1	2123.2	367.1	2274.2	366.6	2274.2	-.51	.04
24	HP16	.7345	1129.6	2642.3	1129.6	2793.3	1129.5	2793.3	-.09	-.02
25	HP10	.6637	105.2	2458.7	105.2	2609.7	105.1	2609.8	-.11	.14
26	HP4	.6583	3012.7	1946.0	3012.7	2097.0	3012.6	2097.0	-.07	-.03

REFERENCE = WASH., DC DAY 109
SEARCH = WASH.,DC DAY 125

AVERAGE ABSOLUTE ERROR 0.215 0.230

RMS ERROR = 0.439

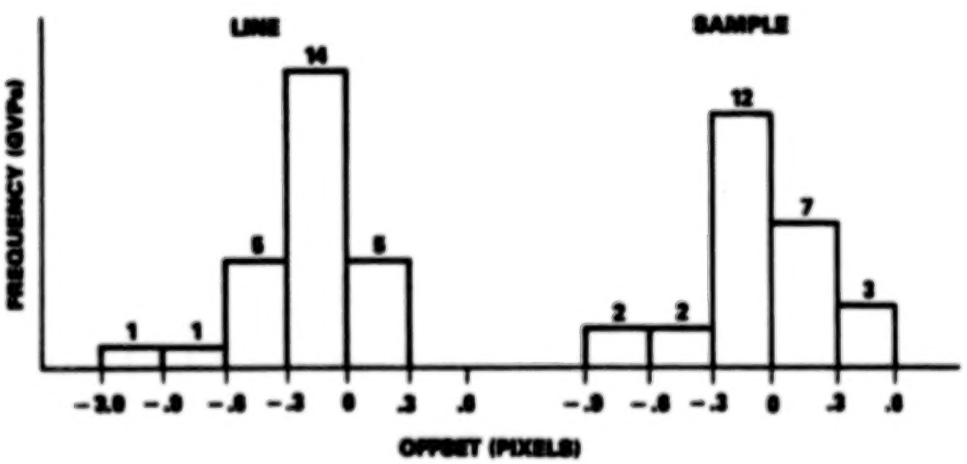

Figure 6. Temporal Registration Accuracy, Washington, DC, Day 109 and Day 125, Bands 1.

	VERIFICATION POINT	CORRELATION	REFERENCE LINE	REFERENCE SAMPLE	SEARCH LINE	SEARCH SAMPLE	SEARCH + ERROR LINE	SEARCH + ERROR SAMPLE	ERRORS LINE	ERRORS SAMPLE
1	PT1	.7932	668.8	606.6	668.8	757.6	668.8	757.9	-.01	.24
2	PT5	.8634	1276.0	543.6	1276.0	694.6	1275.9	694.6	-.09	.06
3	PT11	.6690	2298.4	765.2	2298.4	916.2	2298.3	916.4	-.10	.25
4	PT14	.2284	783.4	2033.6	783.4	2184.6	782.9	2184.6	-.49	-.04
5	PT19	.7798	1777.7	1205.3	1777.7	1356.3	1777.6	1356.4	-.04	.12
6	PT22	.8167	2618.2	1575.8	2618.2	1726.8	2618.2	1726.5	-.04	-.30
7	PT23	.8010	2964.6	1400.1	2964.6	1551.1	2964.7	1550.9	.11	-.17
8	PT7	.6092	212.9	1207.5	212.9	1358.5	212.5	1358.8	-.39	.28
9	PT13	.8607	447.2	1748.0	447.2	1897.0	446.8	1898.9	-.37	-.08
10	PT27	.8482	2225.5	1587.5	2225.5	1738.5	2225.4	1738.4	-.07	-.13
11	PT71	.7327	1211.5	1104.4	1211.5	1255.4	1211.4	1255.8	-.08	.42
12	PT29	.7183	2089.3	280.6	2089.3	431.6	2089.1	431.4	-.13	-.26
13	PT30	.6343	1209.3	3168.5	1209.3	3319.5	1208.8	3318.9	-.56	-.56
14	PT34	.4213	2528.2	2539.0	2528.2	2690.0	2527.4	2689.8	-.88	-.20
15	PT36	.4759	2647.8	105.8	2647.8	256.8	2647.2	256.7	-.65	-.14
16	PT46	.8154	2285.7	1036.6	2285.7	1187.6	2285.8	1187.3	.08	.26
17	PT142	.7229	2166.5	2056.0	2166.5	2207.0	2166.4	2206.8	-.14	-.20
18	PT32	.8349	221.2	3240.3	221.2	3391.3	220.9	3391.1	-.33	-.16
19	HP1	.4253	98.0	408.2	98.0	559.2	97.8	558.9	-.19	-.30
20	HP14	.6728	1159.8	2147.8	1159.8	2298.8	1159.9	2298.6	.15	-.21
21	HP13	.7393	724.0	1415.7	724.0	1566.7	724.0	1566.9	-.01	.24
22	HP17	.8527	1463.6	2564.5	1463.6	2715.5	1463.5	2715.5	-.15	-.06
23	HP15	.8093	367.1	2123.2	367.1	2274.2	366.9	2274.3	-.21	.15
24	HP16	.8197	1129.6	2642.3	1129.6	2793.3	1129.5	2793.3	-.07	-.02
25	HP10	.7213	105.2	2458.7	105.2	2609.7	105.1	2609.9	-.11	.23
26	HP4	.7883	3012.7	1946.0	3012.7	2097.0	3012.8	2097.0	.11	-.01

REFERENCE = WASH.,DC DAY 100
SEARCH = WASH.,DC DAY 125

AVERAGE ABSOLUTE ERROR 0.301 0.204
RMS ERROR = 0.541

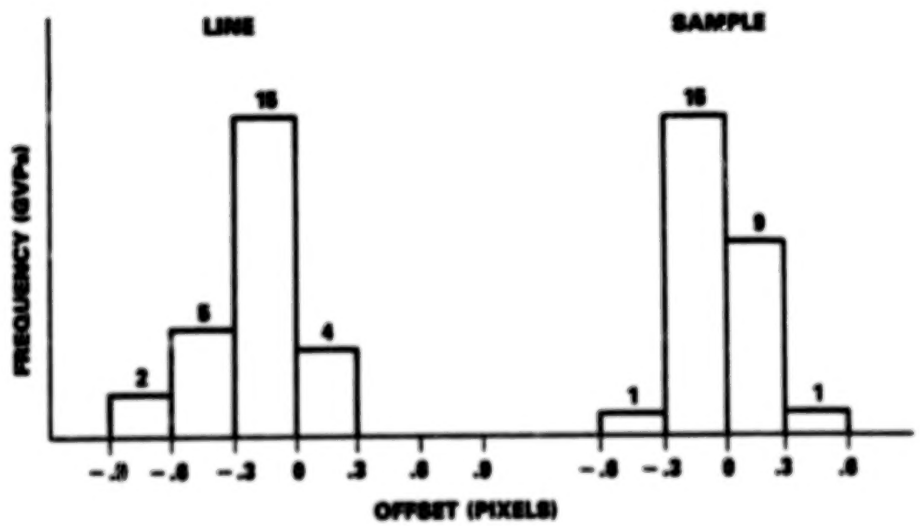

Figure 7. Temporal Registration Accuracy, Washington, DC, Day 109 and Day 125, Bands 2.

VERIFICATION POINT	CORRELATION	REFERENCE LINE	REFERENCE SAMPLE	SEARCH LINE	SEARCH SAMPLE	SEARCH + ERROR LINE	SEARCH + ERROR SAMPLE	ERRORS LINE	ERRORS SAMPLE
FT1	.7689	648.8	696.6	648.8	787.6	648.8	787.7	.01	.09
FT5	.9295	1276.0	543.6	1276.0	694.6	1275.9	694.7	-.10	.10
FT11	.6132	2298.4	765.2	2298.4	916.2	2298.3	916.5	-.07	.33
FT14	.8323	783.4	2033.6	783.4	2184.6	783.3	2184.7	-.10	.08
FT19	.3881	1777.7	1205.3	1777.7	1356.3	1777.6	1356.5	-.11	.16
FT103	.1996	1598.7	1650.0	1598.7	1801.0	1599.7	1800.8	.96	-.23
FT22	.7885	2618.2	1875.8	2618.2	1726.8	2618.2	1726.6	.01	-.24
FT23	.9356	2964.6	1400.1	2964.6	1551.1	2964.7	1550.9	.05	-.19
FT7	.8327	212.9	1207.5	212.9	1358.5	212.6	1358.5	-.24	-.02
FT18	.8464	447.2	1748.0	447.2	1899.0	447.0	1899.0	-.15	.05
FT26	.6965	1883.0	2952.2	1883.0	3103.2	1882.3	3103.0	-.70	-.23
FT27	.7781	2225.5	1587.5	2225.5	1738.5	2225.4	1738.6	-.05	.02
FT71	.8306	1211.5	1104.4	1211.5	1255.4	1211.7	1255.0	.14	.45
FT29	.8793	2089.3	280.6	2089.3	431.6	2089.3	431.4	.00	-.24
FT30	.7487	1209.3	3168.5	1209.3	3319.5	1208.8	3319.1	-.55	-.37
FT34	.3934	2528.2	2539.0	2528.2	2690.0	2528.2	2689.7	-.02	-.33
FT36	.3719	2647.8	105.8	2647.8	256.8	2647.0	257.0	-.84	.16
FT46	.7190	2285.7	1036.4	2285.7	1187.4	2286.1	1186.8	.32	.44
FT142	.9529	2144.5	2036.0	2144.5	2297.0	2144.4	2296.9	-.12	-.07
FT32	.7710	221.2	3240.3	221.2	3391.3	221.1	3391.2	-.12	-.06
HP1	.8885	98.0	408.2	98.0	559.2	97.8	558.9	-.18	-.22
HP14	.8604	1159.8	2147.8	1159.8	2298.8	1160.0	2298.9	.17	.15
HP18	.8904	724.0	1415.7	724.0	1566.7	723.8	1566.8	-.19	.17
HP17	.8865	1463.6	2564.5	1463.6	2715.5	1463.7	2715.6	.02	.07
HP15	.9809	367.1	2123.2	367.1	2274.2	366.9	2274.4	-.19	.20
HP16	.8286	1129.6	2642.3	1129.6	2793.3	1129.5	2793.3	-.05	-.01
HP10	.7912	105.2	2458.7	105.2	2609.7	105.2	2610.0	-.02	.31
HP4	.7254	3012.7	1946.0	3012.7	2097.0	3012.6	2097.0	-.05	.00
						AVERAGE ABSOLUTE ERROR		0.198	0.178

REFERENCE = WASH.,DC DAY 109
SEARCH = WASH.,DC DAY 125

RMS ERROR = 0.387

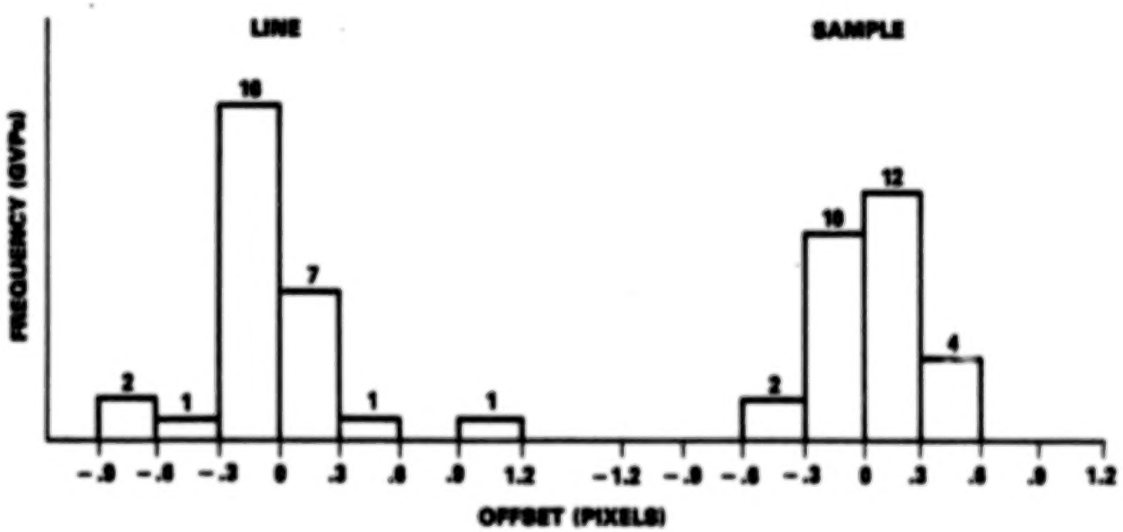

Figure 8. Temporal Registration Accuracy, Washington, DC, Day 109 and Day 125, Bands 3.

	VERIFICATION POINT	CORRELATION	REFERENCE LINE	REFERENCE SAMPLE	SEARCH LINE	SEARCH SAMPLE	SEARCH + ERROR LINE	SEARCH + ERROR SAMPLE	ERRORS LINE	ERRORS SAMPLE
1	PT1	.7897	668.8	606.6	668.8	757.6	668.8	757.7	.03	.08
2	PT5	.9385	1276.0	543.6	1276.0	694.6	1276.0	694.7	-.03	.12
3	PT11	.6502	2298.4	765.2	2298.4	916.2	2298.3	916.3	-.06	.12
4	PT14	.5338	783.4	2033.6	783.4	2184.6	783.2	2184.7	-.23	.08
5	PT19	.2585	1777.7	1205.3	1777.7	1356.3	1777.4	1356.5	-.34	.13
6	PT108	.2578	1598.7	1650.0	1598.7	1801.0	1598.9	1800.5	.21	-.59
7	PT22	.7598	2618.2	1575.8	2618.2	1726.8	2618.2	1726.6	-.07	-.21
8	PT23	.9515	2964.6	1400.1	2964.6	1551.1	2964.6	1551.0	.00	-.12
9	PT7	.5824	212.9	1207.5	212.9	1358.5	212.7	1358.6	-.11	.05
10	PT13	.7940	447.2	1748.0	447.2	1899.0	447.1	1899.1	-.11	.06
11	PT26	.6865	1883.0	2952.2	1883.0	3103.2	1882.4	3103.0	-.58	-.26
12	PT27	.7389	2225.5	1587.5	2225.5	1738.5	2225.3	1738.5	-.13	-.05
13	PT71	.8170	1211.5	1104.4	1211.5	1255.4	1211.7	1255.8	.17	.44
14	PT29	.8932	2089.3	280.6	2089.3	431.6	2089.2	431.4	-.00	-.23
15	PT30	.7921	1209.3	3168.5	1209.3	3319.5	1208.8	3319.2	-.56	-.25
16	PT34	.5003	2528.2	2539.0	2528.2	2690.0	2528.5	2689.7	.30	-.27
17	PT36	.5293	2647.8	105.8	2647.8	256.8	2647.1	256.9	-.70	.12
18	PT46	.7242	2285.7	1036.6	2285.7	1187.6	2286.0	1187.9	.28	.32
19	PT142	.9570	2166.5	2056.0	2166.5	2207.0	2166.0	2206.9	-.50	-.04
20	PT32	.6820	221.2	3240.3	221.2	3391.3	221.2	3391.2	-.05	-.06
21	HP1	.9018	98.0	408.2	98.0	559.2	97.7	558.9	-.26	-.24
22	HP14	.8900	1159.8	2147.8	1159.8	2298.8	1159.9	2299.0	.10	.18
23	HP13	.8774	724.0	1415.7	724.0	1566.7	723.8	1566.9	-.20	.22
24	HP17	.8863	1463.6	2564.5	1463.6	2715.5	1463.7	2715.6	.05	.05
25	HP15	.8722	367.1	2123.2	367.1	2274.2	367.0	2274.5	-.08	.28
26	HP16	.8294	1129.6	2642.3	1129.6	2793.3	1129.6	2793.3	.00	-.01
27	HP10	.8131	105.2	2458.7	105.2	2609.7	105.2	2609.8	.04	.15
28	HP4	.6112	3012.7	1946.0	3012.7	2097.0	3012.7	2097.0	.01	-.01

REFERENCE = WASH.,DC DAY 109
SEARCH = WASH.,DC DAY 125

AVERAGE ABSOLUTE ERROR 0.186 0.167
RMS ERROR = 0.342

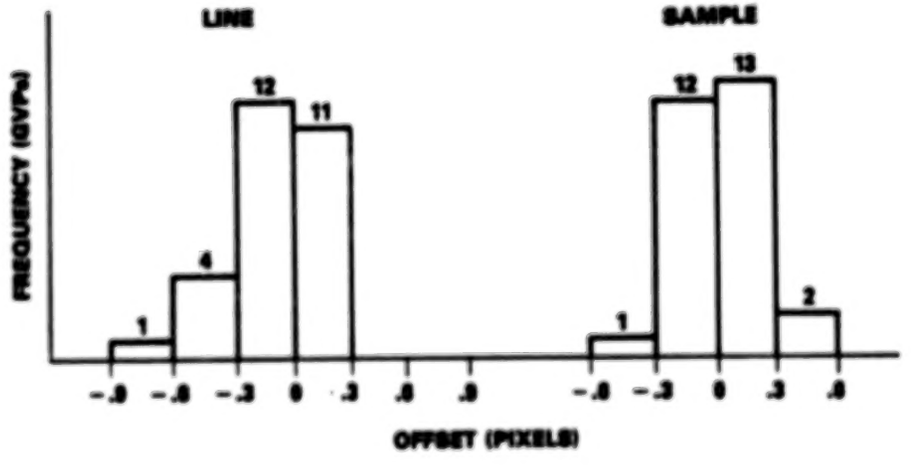

Figure 9. Temporal Registration Accuracy, Washington, DC, Day 109 and Day 125, Bands 4.

IMPACT OF LANDSAT MSS SENSOR DIFFERENCES ON CHANGE DETECTION ANALYSIS

William C. Likens
Robert C. Wrigley
NASA Ames Research Center
Moffett Field, California 94035

INTRODUCTION

The work presented has its origins in change detection work carried out at the Ames Research Center in 1981. At that time we co-registered a Landsat-1 and a Landsat-3 scene for the San Bernardino, California area and carried out image differencing as one means of identifying areas of land cover change (ref. 1). It was quickly noted that many spurious or false changes were being delineated in addition to real changes in the scene. These differences were found to be related to differences in the sensors, ground processing, atmosphere, and cover dependent sun angle effects. The data needed to be normalized in some manner to remove these effects. Contingency tables between the images were constructed in order to develop a transfer function relating digital values for individual points in one image to values for those same points in the other image. These functions for each band were used to normalize one date to the other. This normalization approach is very similar to the histogram equalization approach now used to remove detector striping from the Landsat-4 MSS data. Once normalized, real changes in scene features were more easily identifiable and most of the spurious changes were eliminated.

In the present study we sought to reverse the above approach by using change detection techniques to pinpoint differences between sensors. Alternately, the use of change detection techniques with Landsat-4 and earlier Landsat MSS sensors can be thought of as a user-oriented test of any insurmountable differences between the sensors when used for change detection. Scattergrams between co-registered scenes (a form of contingency analysis) are used to radiometrically compare data from the various MSS sensors.

MSS DATA SELECTION

Initially, three MSS scenes were acquired and compared for the San Francisco area. These data were not simultaneously imaged; the Landsat-3 scene was acquired four days earlier than the Landsat-4 scene and the Landsat-2 scene was almost exactly a year earlier to minimize cover type and seasonal changes. However, a search of the EROS Data Center's MSS data base indicated two orbits when data from both Landsat-4 and an earlier Landsat were

simultaneously recorded. Three scene pairs of simultaneous coverage were ordered for comparisons (Table 1). In all cases of same date coverage, the scene pairs were acquired within three minutes or less of each other. This is effectively simultaneous coverage. Any differences between scenes can then be assumed to be solely a function of sensor differences, as atmospheric effects, sun angle, and scene content will be identical between scenes. This assumption is made, but does not completely hold true in the case of the San Francisco data because the atmosphere is likely to have changed between dates. The time of acquisition in GMT is shown in the last five digits of the scene ID. All data were acquired in the EDIPS A-tape format (radiometric corrections only) rather than the P format (geometric correction) in order to prevent degradation of data characteristics through resampling. The Landsat-4 scene of southeast New Mexico was also ordered in the P-tape format in order to assess how well EDIPS geometric processing corrects for some geometric irregularities noted in the various Landsat-4 MSS data sets. Of the four Landsat-4 scenes, it appears probable that the Thematic Mapper sensor was turned on concurrently with the MSS in all but the San Francisco acquisition (which was acquired before West Coast TM data acquisition began).

Table 1. MSS Data Selection.

Location	Sensor	Date	Scene ID	Path, Row
San Francisco	4	10/12/82	84008818134	44,34
	3	10/08/82	83167818102	47,34
	2	10/04/81	82244718013	47,34
Southeast New Mexico	4	11/09/82	84011617005	32,37
	2	11/09/82	82284816571	34,37
Connecticut	4	12/22/82	84015915012	13,31
	3	12/22/82	83175314594	14,31
New Hampshire	4	12/22/82	84015915010	13,30
	3	12/22/82	82175314591	14,30

RADIOMETRIC ANALYSIS USING SCATTERGRAMS

The method of analysis was to co-register 512 by 512 pixel subwindows for all data pairs followed by scattergram generation and analysis. In all cases, the Landsat-4 data were used as the base to which other images were registered. Manually selected control points were acquired by visual examination of the data using a color video monitor. The control point pairs were input into a registration function that was used to register the data.

Scattergrams were generated between images for each band. These scattergrams plot the digital number (DN) found for each point in Landsat-4 against the DN recorded for that location in Landsat-2

or 3. Mode (maxima) values were derived from the scattergrams (y-axis modes for fixed x values as well as x-axis modes for fixed y values) and used to visually fit a linear regression (automated regression calculations were distorted by outliers). The regression line represents the relative radiometric transfer function relating Landsat-4 MSS to earlier MSS radiometry. Data values plotted in the scattergrams are those recorded on the A-tapes (dynamic range of band 4 previously scaled from 0 - 63, is now rescaled to 0 - 127 in all data processed since 1979). Nearest neighbor resampling, rather than bi-linear or cubic convolution, was used in the registration to preserve the radiometric integrity of the data. Root mean sqaure (RMS) errors of the registrations varied between .1 and 1.5 pixels. The relatively large errors resulted from a line length error in the Landsat-4 MSS (discussed later). A rigorous registration was not deemed necessary for the radiometric assessment; because although misregistrations will increase the scattergram variance, they are unlikely to affect the trend of mode values.

Table 2. MSS Radiometric Calibration Information.

	Landsat-2*		Landsat-3*		Landsat-4**	
	Radiance***					
Band	Min	Max	Min	Max	Min	Max
1	.08	2.63	.04	2.59	.02	2.3
2	.06	1.76	.03	1.79	.04	1.8
3	.06	1.52	.03	1.49	.04	1.3
4	.11	3.91	.03	3.83	.10	4.0

* reference 2.
** reference 3.
*** Radiance in the band in mW/cm**2*steradian

Radiometric calibration information is also available for each of the MSS sensors (ref. 2 and 3, and table 2). These can be used to predict the relative radiometric transfer functions between sensors. The predicted and actual transfer functions are listed in Tables 3, 4, and 5, and constitute the primary product of this study. The scattergram plots generated are shown in Figures 1 through 6.

CONCLUSIONS ON RADIOMETRY

The relative radiometric differences between Landsats -3 and -4 appear approximately the same as predicted by the calibration information. Comparisons of Landsats -2 and -3 (table 4), and -2 and -4 (table 3), however, show that the actual radiometry of Landsat-2 differs significantly from the calibration specifications. This may reflect drift in sensor sensitivity,

optical degradation of the scan mirror and telescope, or changes in the radiance minimum and maximum constants used in ground processing. Often, changes in sensor calibration are not well disseminated and are thus unavailable to data users.

Standard processing since 1979 has decompressed band 4 data for all MSS senors, resulting in a data range of 0 - 127. This has been true for data from all the Landsat satellites, except for Landsat-4 MSS data processed between launch and October 23, 1982. Histograms of all data acquired for this study show values in band 4 ranging above 63, indicating that the radiance maximum (Rmax) has been set to 127 for all sensors and not just in Landsat-4 data.

While radiometric values for Landsats-3 and -4 appear roughly the same as predicted by the calibration specifications, the San Francisco scene pair shows the high degree to which atmosphere can affect relative readings of features on different days. Atmospheric effects (up to 12 digital counts bias added to signal in band 1) in the Landsat-3 scene have caused features to saturate to a much greater degree than in the corresponding Landsat-4 scene, or in other scene pairs (table 5).

The saturation of Landsat-4 at relatively low radiance levels (compared to Landsats-1, -2, and -3) in bands 1 and 3 may result in loss of useful information for some data applications, including change detection.

OTHER OBSERVATIONS

While in the process of generating scattergrams, several geometric artifacts were noted (figures 7 and 8). All bands of each Landsat-4 image contained noise interference patterns. These patterns appeared to have two components; diagonal striping with a period of about 3.5 pixels, and concentric arcs with a period of 10 - 12 pixels. Over water areas, the noise was noted to have a magnitude of 2 digital counts in band 4.

Sweep offsets were noted in all but the San Francisco Landsat-4 scenes (example shown figure 9). The San Francisco scene was acquired before Thematic Mapper data acquisition began on the West Coast. All other scenes fall in a time period during which it is probable that TM and MSS were turned on concurrently, indicating the problem may be related to sensor interactions. The offsets result from varying line lengths, and are readily corrected by stretching all lines to a constant length using line length information imbedded in the right edge of the image. The problem occurs only in A-format tapes and is corrected during the geometric processing applied to generate P-tapes.

CONCLUSIONS

There appear to be no major problems preventing use of Landsat-4 MSS with previous MSS sensors for change detection, provided the interference noise can be removed or minimized. This noise may result in detection of spurious changes, as well as affect other uses of the data, including image classification. Analysis of dark (water and forests), rather than light, features will be most impacted because the noise will form a higher percentage of the total response at low DN values. The patterns are sweep dependent, and within a sweep it is not clear that they are completely systematic. The pattern is present even when TM is off. The problem was detected before launch (left uncorrected because of the cost of repair), and is caused by interference between the revised MSS power supply (the power bus on Landsat-4 is different than on previous Landsats) and the sensor's one kilohertz data quantitizer (ref. 4). The frequency of the interference is known to drift because of drift in power supply frequency (ref. 4). The identical problem has been identified in Landsat-D Prime and should be corrected.

Any data normalizations for change detection should be based upon the data, rather than solely upon calibration information. While the observed relative radiometric transfer function between Landsats-3 and -4 was approximately as predicted, there were still significant deviations (most noticable in band 3). Also, actual calibration specifications used in ground processing are not always made widely available, and published figures for Landsat-2 appear incorrect for recent data. The Landsat-4 specifications cited in this report (valid since August 1982) were not widely known until several months after their implementation. Normalizing based upon data content also can have the advantage of allowing simultaneous normalization of the atmosphere as well as the radiometry.

REFERENCES

1. Likens, W., K. Maw. 1982. Updating Landsat-Derived Land-Cover Maps Using Change Detection and Masking Techniques. Technical Papers of the American Society of Photogrammetry, 1982 Fall Convention, Ft. Lauderdale, Florida.

2. Robinove, C. J. 1982. Computation with Physical Values from Landsat Digital Data. Photogrammetric Engineering and Remote Sensing. Vol. 48, No. 5, pp. 781-784.

3. Singh, A. 1983. Landsat-4 MSS Radiometric Correction: Methods and Results. Landsat-4 Scientific Characterization Early Results Symposium (this volume). Goddard Space Flight Center, Greenbelt, MD.

4. Personal communication from Peter Malherbe, Electrical Engineer, General Electric.

Table 3. Digital values for selected radiances.
Landsat-2 vs.-4 (MSS)

	Predicted Corresponding Values		Observed Corresponding Values*			
			New Mexico		San Francisco	
	LS 2	LS 4	LS 2	LS4	LS 2	LS 4
Band 1	0 (.08mw/cm2ster)	5	0	0	0	2
	111 (2.3mw/cm2ster)	127	121	127	125	127
Band 2	0 (.06mw/cm2ster)	1	2	0	0	1
	127 (1.76mw/cm2ster)	124	127	120	127	107
Band 3	0 (.06mw/cm2ster)	2	1	0	0	1
	125 (1.3m2/cm2ster)	127	119	127	122	127
Band 4	0 (.11mw/cm2ster)	0	0	1	0	1
	127 (3.91mw/cm2ster)	125	127	115	127	115

*Derived from linear regression of modes.

Table 4. Digital values for selected radiances.
Landsat-2 vs.-3 (MSS)

	Predicted Corresponding Values		Observed Corresponding Values* San Francisco	
	LS 2	LS 3	LS 2	LS 3
Band 1	0 (.08mw/cm2ster)	2	0	0
	125 (2.59mw/cm2ster)	127	117	127
Band 2	0 (.06mw/cm2ster)	2	0	0
	127 (1.76mw/cm2ster)	125	120	127
Band 3	0 (.06mw/cm2ster)	3	0	0
	124 (1.49mw/cm2ster)	127	127	118
Band 4	0 (.11mw/cm2ster)	3	0	0
	124 (3.83mw/cm2ster)	127	120	127

*Derived from linear regression of modes.

Table 5. Digital values for selected radiances.
Landsat-3 vs.-4 (MSS)

	Predicted Corresponding Values		Observed Corresponding Values*					
			New Hampshire		Connecticut		San Francisco	
	LS 3	LS 4	LS 3	LS4	LS 3	LS 4	LS 3	LS 4
Band 1	0	1	0	0	0	0	0	2
	(.04mw/cm2ster)							
	112	127	119	127	115	127	127	120
	(2.3mw/cm2ster)							
Band 2	0	1	3	0	0	0	0	1
	(.04mw/cm2ster)							
	127	126	127	125	127	127	127	107
	(1.79mw/cm2ster)							
Band 3	1	0	1	0	0	0	0	0
	(.04mw/cm2ster)							
	110	127	119	127	115	127	113	127
	(1.3m2/cm2ster)							
Band 4	2	0	0	2	1	0	0	0
	(.10mw/cm2ster)							
	127	121	127	117	127	122	127	104
	(3.83mw/cm2ster)							

*Derived from linear regression of modes.

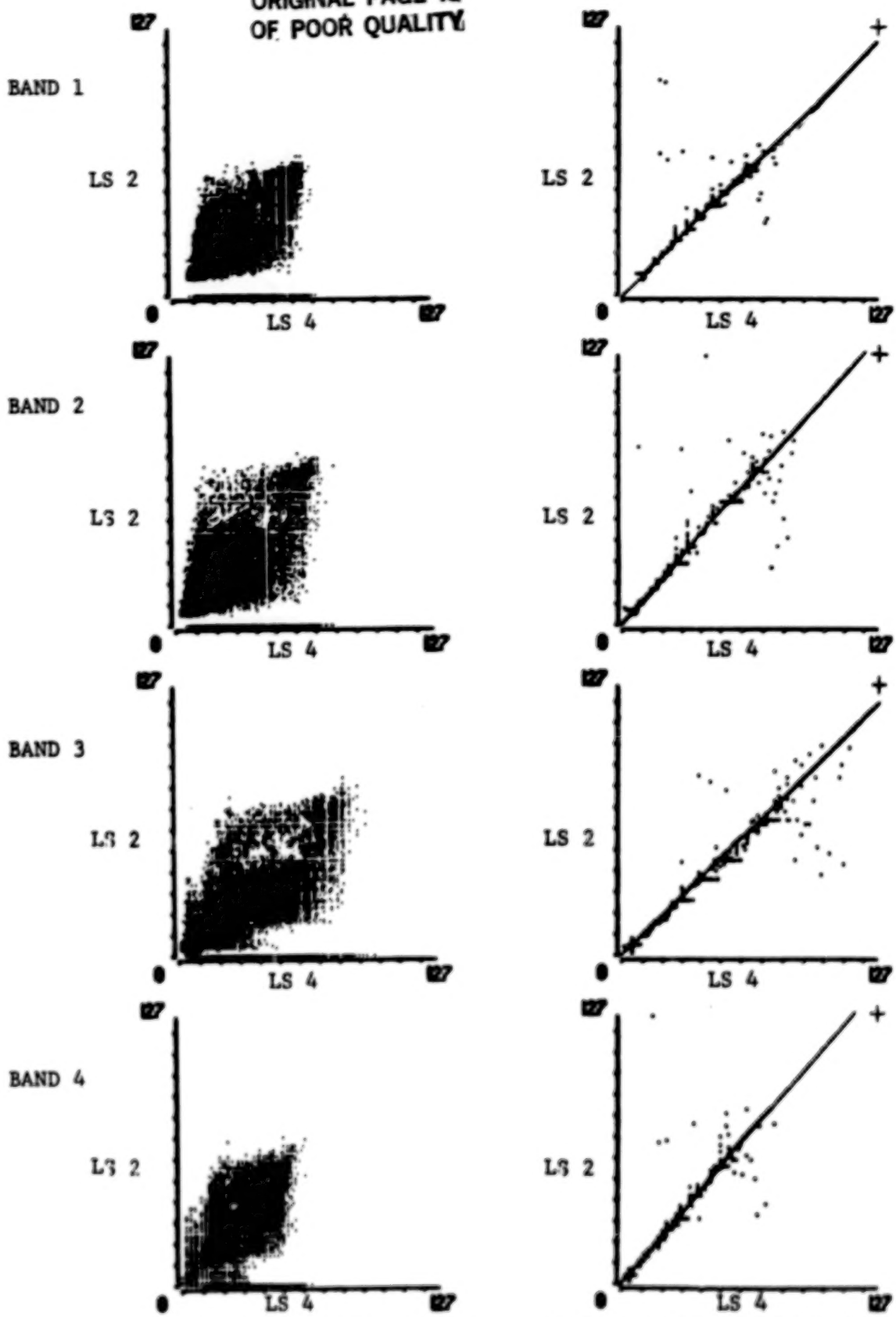

FIGURE 1. LANDSAT 2 vs. 4 MSS scattergrams (left) and maxima (right) for New Mexico scene pair acquired on Nov. 9, 1982.

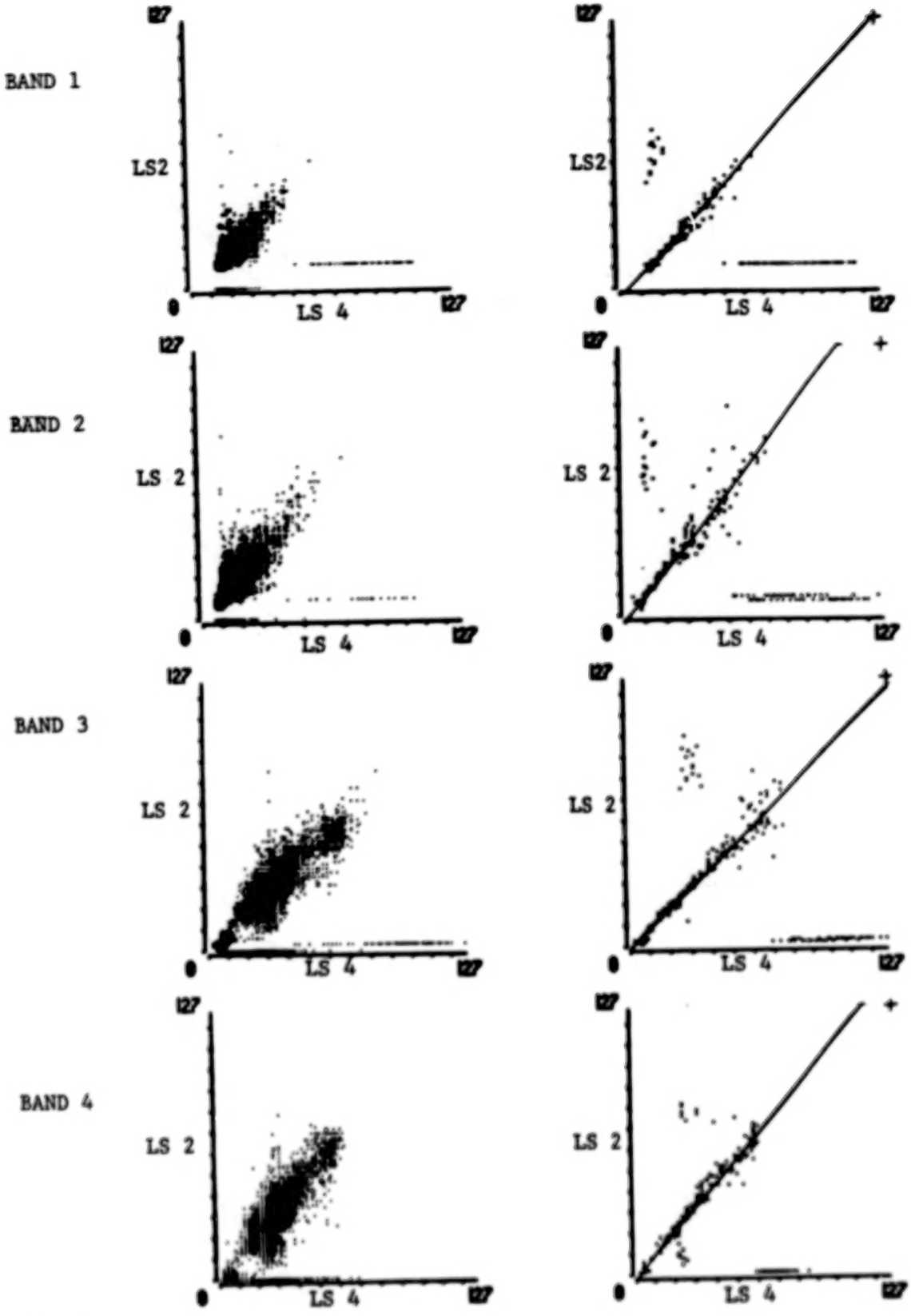

FIGURE 2. LANDSAT 2 (Oct 4, 1981) vs 4(Oct 12,1982) MSS spectral scattergrams (left) and maxima (right) for San Francisco scene pair.

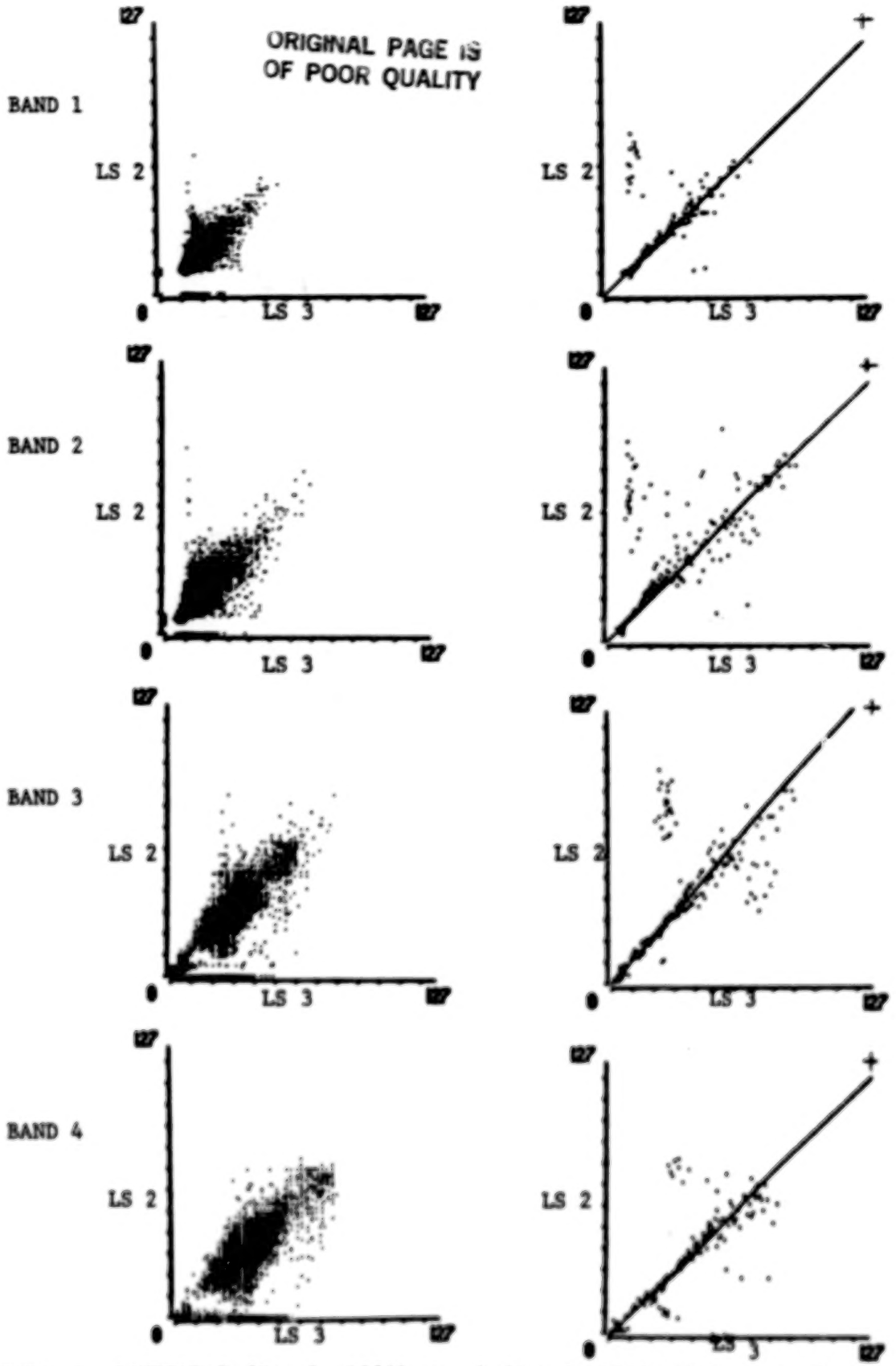

FIGURE 3. LANDSAT 2 (Oct 4, 1981) vs. 3 (Oct 8, 1982) MSS spectral scattergrams (left) and maxima (right) for San Francisco.

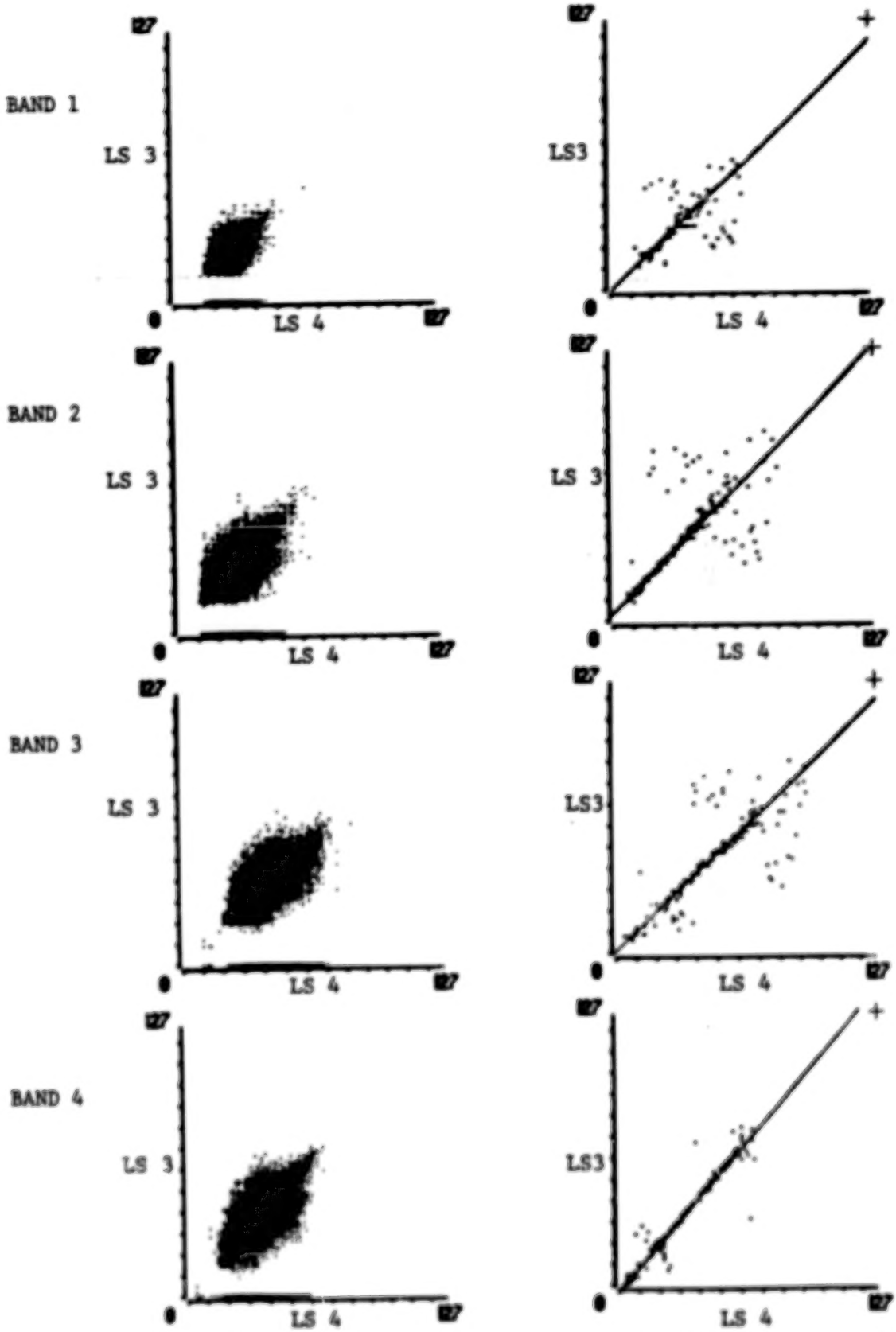

FIGURE 4 LANDSAT 3 vs 4 MSS spectral scattergrams (left) and maxima (right) for New Hampshire scene pair acquired on Dec. 22, 1982.

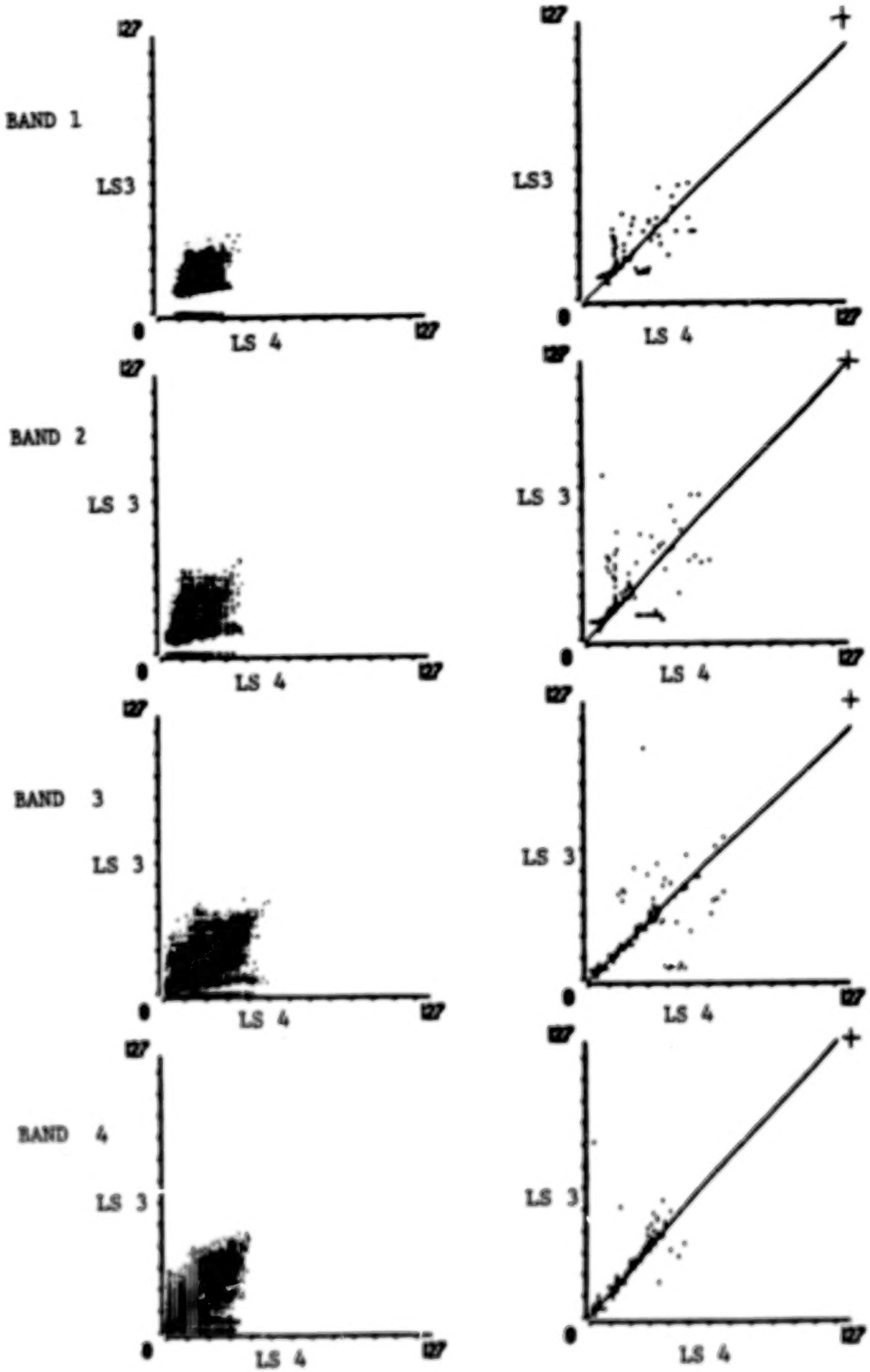

FIGURE 5. LANDSAT 3 vs 4 MSS scattergrams (left) and maxima (right) for Connecticut scene pair acquired on Dec. 22, 1982.

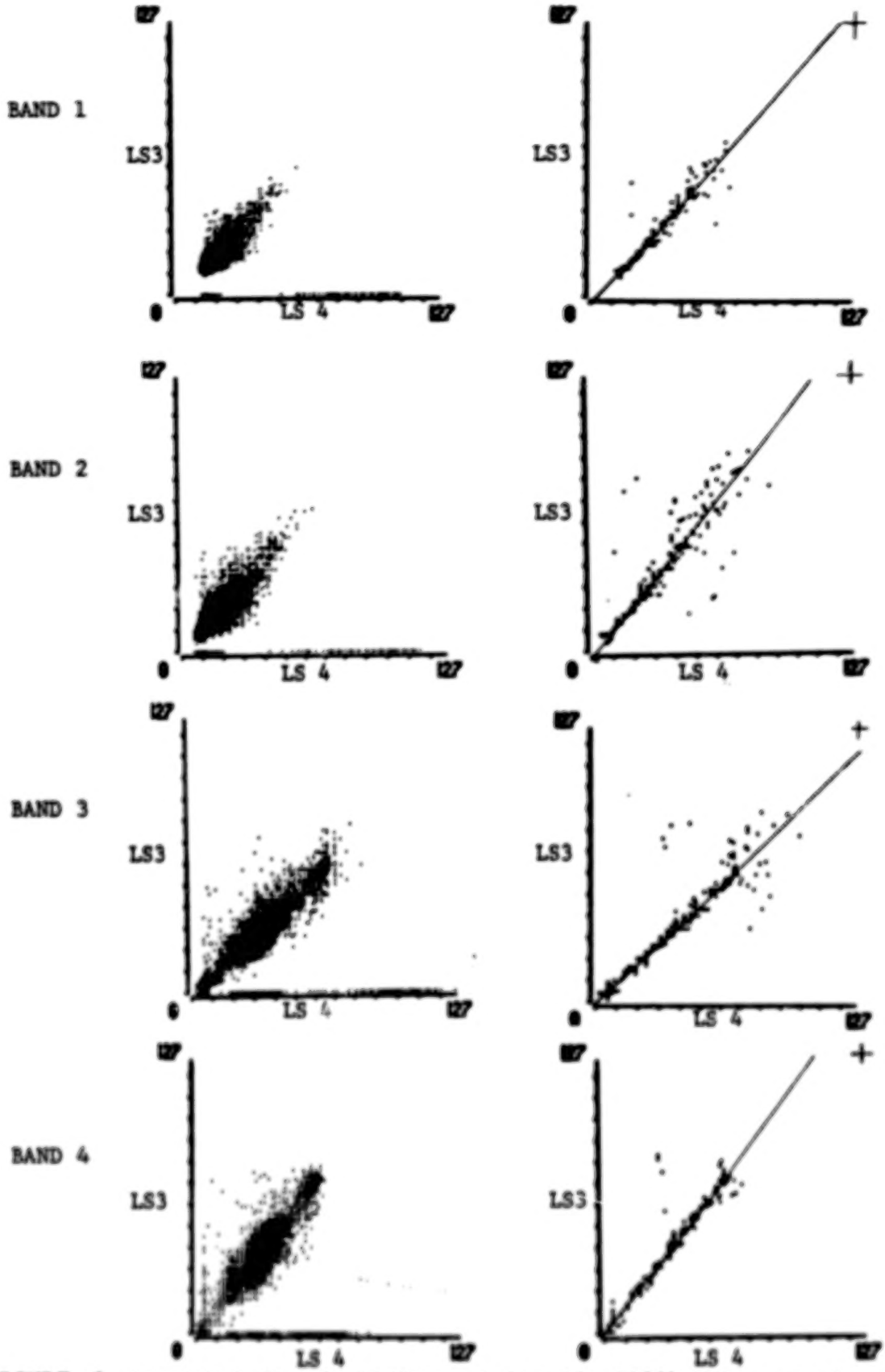

FIGURE 6. LANDSAT 3 (Oct 8, 1982) vs 4 (Oct 12, 1982) MSS spectral scattergrams (left) and maxima (right) for San Francisco.

FIGURE 7.
LANDSAT 4 MSS band 4 of Long Island subwindow of Conneticut scene. Enhanced to show interference patterns. The interference, shown here as black, is 2 digital counts brighter than the mean water value.

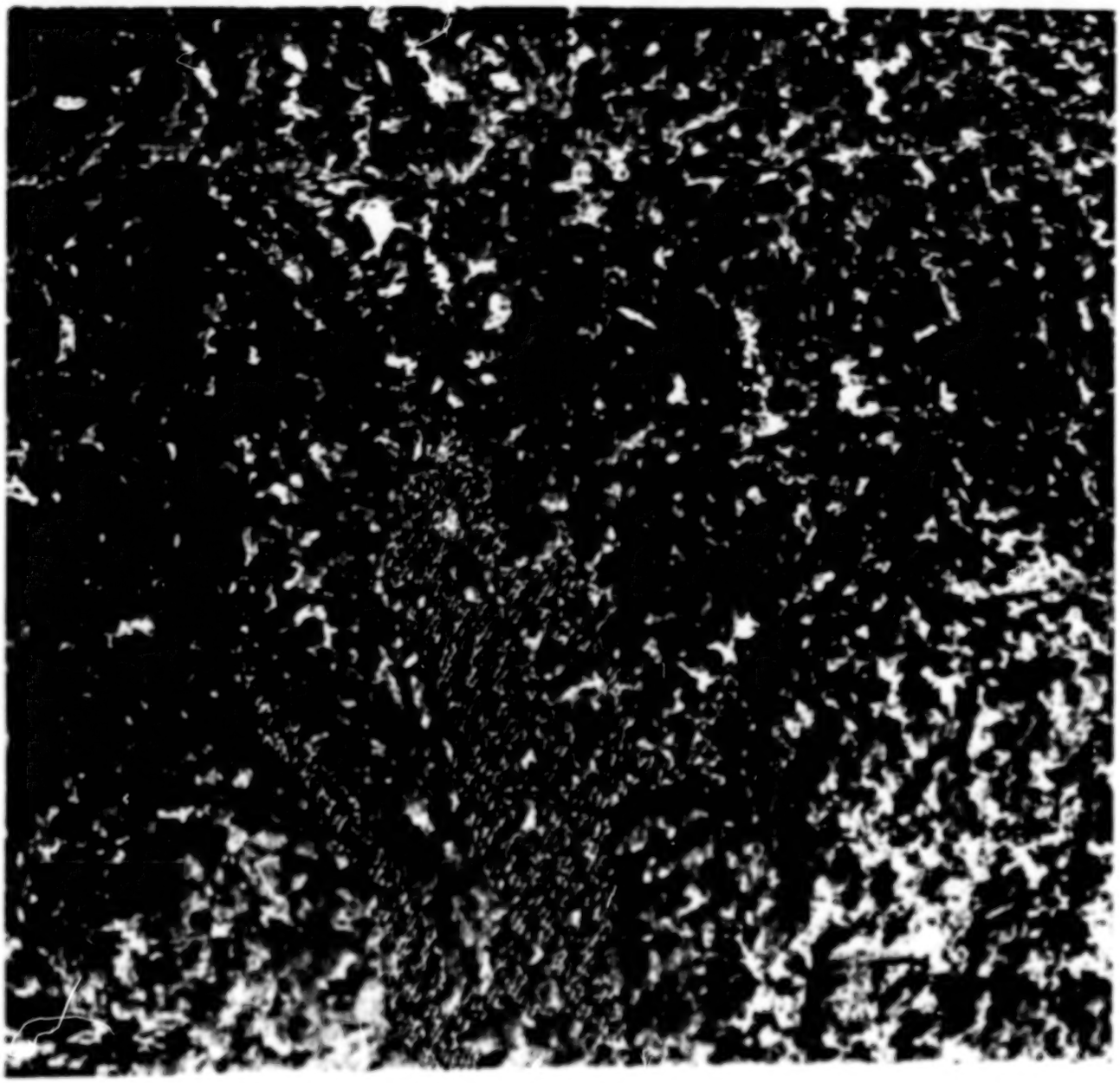

FIGURE 8.
LANDSAT 4 MSS band 4 subwindow from New Hampshire scene.
Enhanced to show interference patterns visible in
Quabbin Reservoir.

FIGURE 9. LANDSAT 4 MSS band 4 subwindow from southeast New Mexico showing sweep offset displacements along road.

LS-4 MSS GEOMETRIC CORRECTION: METHODS AND RESULTS

J. Brooks, Ph.D., E. Kimmer, Ph.D., J. Su

General Electric Space Division
Lanham Center Operations
4701 Forbes Boulevard, Lanham, MD 20706

ABSTRACT

An automated image registration system such as that developed for Landsat-4 can produce all of the information needed to verify and calibrate the software and to evaluate system performance. This paper describes methods and results of the effort that fine-tuned both software and data base and assessed geometric performance of the calibrated Landsat-4 system.

1. INTRODUCTION

LS-4 MSS Geometric Correction data are generated in a two step process. The first step utilizes models of the spacecraft-scanner-spinning earth system, with smoothed ephemeris and attitude data as input, to deduce systematic correction data. The systematic correction data therefore suffer from random system pointing and spacecraft location errors. If control points are available for the subject scene, the second step - automatic correlation of control point chips to control point neighborhoods - is performed to develop input to the MSS control point location error filter. The output of the filter is the state error vector, which is used to upgrade the systematic correction data to geodetic correction data. This online process is called the MSS Archive Generation process (MAG) because its output is the high density archival tape.

An important offline subsystem of the LS-4 MSS Image Generation Facility is the Control Point Library Build (CPLB) subsystem. This hardware and software complex is used to generate control point chips and support data for use in online upgrade of correction data. Control point chips that represent ground truth are called geodetic or supplemental, depending on whether they are used to establish the model surface (with the same filter that is used online) or are selected from the fully corrected imagery. Relative control points are designated in systematically corrected imagery, have no ground truth and can, therefore, be used only for temporal registration.

During the last six weeks before the NASA/NOAA turnover of the system, an extensive effort was carried out to fine-tune both software and data base and to evaluate the geometric performance of the calibrated system. The online processing and the CPLB process provided all the tools necessary for the verification, calibration (including initial scan profile correction) and evaluation of LS-4 geometric processing. In this presentation, we will describe the methods and results of that effort. Section 2 presents the system and methods. Section 3 is devoted to results.

2. TECHNICAL BACKGROUND

In this section we describe in greater detail the two processes outlined in the introduction. Because the concepts of systematic correction data (SCD) surface, geodetic correction data (GCD) surface and the MSS filter that links them are common to MAG and CPLB, those basic constructs are discussed first.

The MSS Filter and the Correction Data Surfaces

The correction surface is a vector field that relates a location in the corrected image to a location in raw image data. If the correction models are entirely systematic, using only attitude and ephemeris data as input, the surface is an SCD surface. The SCD surface for a particular World Reference System (WRS) frame is one of a family of surfaces that differ from one another only in the specifics of attitude and ephemeris data. The GCD surface is obtained from the SCD surface by addition of effects due to attitude and ephemeris biases (errors) which have been estimated using control point data. The MSS filter is the tool used to perform the estimation.

The MSS filter is a least squares filter which assumes a linear dependence of the spacecraft (S/C) on time. Six state vector components are estimated: along track bias, cross track bias, radial location bias, yaw bias, along track rate bias and cross track rate bias. The first bias combines the effects of along track location and pitch biases, while the second combines the effects of cross track location and roll biases. The six effects thus determined are equivalent to the linear mapping errors: along and cross track translations, cross track magnification, along track shear, along track magnification and cross track shear, respectively.

The input to the filter is the control point dislocation in systematically corrected image data, i.e. the difference between its known location on a map or in some other image and the location assigned to it in the current image by the SCD. The latter is determined in MAG by automatic correlation techniques, in CPLB by direct designation.

The output of the filter is the state error vector (S/C biases), the residual errors at each control point and the RMS values of these residual errors in the along track and cross track directions.

The state error vector is converted to a linear perturbation of the SCD surface by means of the measurement matrix. This is the matrix of partial derivatives of the SCD surface variables with respect to the state vector components, with time held constant. This matrix also plays a central role in the generation of the covariance matrix and the weighted measurement vector of the filter.

These, then, are the basic assumptions of Landsat-4 geometric correction techniques: as long as spacecraft and instrument behavior are within specification, any image of a WRS frame can be mapped to any other such image, or to the earth, using only the six state vector components in a linear perturbation of the SCD surface. We will show in Section 3 that these assumptions have been validated.

The MSS Archive Generation Process

Figure 2-1 is a schematic of MAG. Processed attitude and ephemeris data from the Payload Correction Subsystem are used in conjunction with systematic models to produce the SCD. These in turn are used to locate control point neighborhoods in the raw video data and to correct them systematically. Control point chips from the library are correlated to the neighborhoods to determine the dislocations at specific points in the imagery. The filter operates on the dislocations to produce the S/C biases and a report that includes the S/C biases, the covariance matrix and the information about residual error of the control points. MAG tnen utilizes the S/C biases and the measurement matrix to generate the GCD surface from the SCD surface by linear perturbation.

Note that it is not important to MAG whether the control point chips are from a SCD surface or a GCD surface.

Control Point Library Build

CPLB operates in one of two modes. When no ground truth is available, relative control points (RCP) are designated in systematically corrected imagery, screened for good auto-correlation characteristics and, if accepted, extracted and sent to the library with a location within the chip and a latitude and longitude based on the SCD center. This is illustrated in Figure 2-2.

In the second mode, illustrated in Figure 2-3, ground truth is available and is represented by a point on a map and an associated latitude and longitude obtained by digitization of the point with a sonic digitizer. The systematically corrected imagery is displayed and overlaid on the map by means of a Zoom Transfer Scope (ZTS). After map and imagery have been aligned, the point is designated with the cursor, the geodetic control point (GCP) chip is screened and extracted. The dislocation of the chip is determined, and saved with its SCD location.

When all GCP's have been extracted for the scene, the dislocations and locations are fed to the filter. The filter outputs are, as before, the S/C biases and the residuals at the control points. The residuals for each GCP are used to adjust the location in the chip so that the feature lies on the GCD surface.

Once the filter has been applied, supplemental control point chips (SCP) can be designated in the systematically corrected imagery and, using the S/C biases, their locations can be associated with a GCD latitude and longitude. Thus the GCP and the SCP both lie on the GCD surface and are distinguished only by label.

In preparation for Section 3 we call attention to the following:

1) RCP's used in MAG to upgrade the SCD of the parent tape should produce, through the filter, a null S/C state error vector and very small CP residual errors. This will be the basis for verification of the RCP loop.

2) SCP/GCP's used in MAG to upgrade the SCD of the parent tape should produce, through the filter, the same S/C biases produced in CPLB and very small CP residuals. This will be the basis for the verification of the GCP loop.

3) The residual errors of the GCP's in CPLB should be random with respect to cross track location. If they are not, the scan profile has not been represented correctly in the models. Any residual pattern should be removed by altering the systematic models.

4) The RMS residual error of the GCP after filtering is a good indication of the total error due to map error, digitization error, designation error and random image error. This will be the limiting factor in achieving geodetic registration accuracy.

Estimation of Performance

There are two physically different sources of error in registration of one image to another or to a map. These are the true random image error and the bias error due to establishing model parameters from noisy data.

The true random image error - due to high frequency jitter of spacecraft and instrument and other sources - can be estimated to within the correlation error by means of the variance of the residuals at the control points in MAG. This has been demonstrated both by simulation[1] and by analysis[2]. Hence any MAG registration (whether to RCPs or GCPs) provides an estimate (1σ) of the random error of registration.

Temporal registration error, t, is the RSS of the random error, $\mathcal{N}$, described above, and the bias, b_t, of the model surface produced in MAG. The particulars of temporal registration error are presented in Figure 2-4.

Geodetic registration error, as shown in Figure 2-5, is compounded of the temporal registration error and the bias, b_g, of the GCD surface relative to a map (or maps).

Note that the bias term is a function of the number of control points used in the model surface determination and should therefore be estimated for the number of GCP's used for a scene under operational conditions.

3. RESULTS

Verification

The ground processing system was verified for both temporal and geodetic registration. The basic method for both cases was to generate correction data for a scene using control points designated in the same scene. For temporal registration the registrant scene was its own reference scene (SCD surface), while for geodetic registration, control points from the registrant scene were used to generate a reference GCD surface.

Refering to Figure 3-1, the verification process starts with a high density tape of raw data (HDT-R) which is read by MAG. The raw data is radiometrically corrected and written to a high density archive tape (HDT-A). MAG also computes systematic correction data (SCD) which is appended to the HDT-A. Using ground control point chips, MAG has the option of updating the SCD to geodetic correction data (GCD). In the process of generating geodetic correction data MAG reports the filter state error vector (biases) and RMS residuals at the control points.

To verify the temporal registration process twenty relative control points (RCP's) were designated in the Washington scene of November 2, 1982 (W1). The RCP's were designated in systematically corrected imagery and a latitude and longitude was associated with each. This information was passed, along with the HDT-R, to MAG where all twenty control points correlated successfully. As noted in section 2, for relative control points correlated in the same scene from which they were extracted there should be no dislocations, and, therefore, a null state error vector should be produced by MAG. The results (Table 3-1) show that there were small residuals (possibly due in part from an assumption of symmetric correlation surfaces by the algorithm that estimates subpixel offsets) resulting in a non-zero state error vector. However, the state biases are small - on the order of one meter - and the temporal registration process (RCP loop) is verified.

To verify the geodetic registration process, twenty geodetic control points were designated in W1, using CPLB. This involved locating points in topographic maps, digitizing these points to obtain their latitude and longitudes, and then designating these points in systematically corrected imagery to extract control point chips. Designation produces cross and along track dislocations for each control point. These dislocations are filtered to produce a state error vector representing the geodetic error in the systematically corrected imagery. As discussed in section 2, control point residuals are used to change the feature location in the control point chip so that all the control point chips are consistent with the GCD surface computed in CPLB.

The control point chips were then used in MAG to generate an HDT-A with geodetic correction data. The steps in MAG parallel those in CPLB described above, except that the control point chips are correlated instead of being designated. Therefore, if the program is self consistent we expect the MAG filtered state error vector to be the same as for CPLB within the bias error due to establishing model parameters from noisy data. The results given in Table 3-2 show this to be true which verifies the geodetic registration process (GCP loop).

Calibration

System calibrations had to be completed before an accurate performance evaluation could be made. The system calibrations discussed here are of the mirror scan profile and control point outlier criteria.

The mirror scan profile errors can be measured from CPLB output. Figure 3-2 is a flowchart of the method used. The quantities of interest in the CPLB reports are the control point locations, and their residuals after filtering. In the absence of any scan profile modeling errors the residuals are expected to be random with respect to location. When the residuals were actually plotted versus location, significant systematic effects were found in the cross track direction, as shown in Figure 3-3. In this Figure results from three separate CPLB runs are plotted; two are for scene W1, and one for the Washington scene of November 18, 1982 (W2). The magnitude of the error is over three pixels from peak to trough. This non-linear error could not be modeled by the MAG filter and was corrected by updating the mirror scan profile based on the data in Figure 3-3.

After the update CPLB was run again for scene W1. The plot of residuals versus pixel location (Figure 3-4) shows that the residuals are now random with respect to cross track location, thereby verifying the scan profile correction.

The outlier criteria is used to eliminate control points with residuals larger than about 3 times the outlier criteria. We want to calibrate the value to ensure that we are eliminating true outliers without also rejecting valid control points. The flowchart for the calibration method is shown in Figure 3-5. HDT-R tapes were processed through MAG and geodetic correction data was generated by the filter. An HDT-A was created for use in later evaluation The information needed for the calibration was contained in the MAG report in the form of control point residuals. By examining the distribution of residuals obvious outliers that had not been rejected by the system were detected and based on their residual values new criteria were established. The processing was then repeated to verify the updated values.

The current outlier criteria values are shown in Table 3-3. It should be pointed out that only the MAG values have been calibrated. The CPLB values are based on a priori estimates of designation error and have not yet been calibrated.

Performance Evaluation

After completion of verification and calibration, the processing system evaluated its own performance using the system outputs described earlier.

Figure 3-6 is a flowchart of the procedure for temporal registration evaluation. An HDT-R of scene W2 was processed through MAG with W1 control points. Since the geodetic control points have been updated to SCP's in CPLB to be consistent with the GCD surface, MAG does not distinguish between these control points and RCP's which automatically lie on an SCD surface. Therefore, separate experiments can be run with RCP's and GCP's to determine the residual error incurred in MAG when fitting a surface (estimating a state error vector) consistent with the reference surface from CPLB.

The results of these experiments are shown in Table 3-4. The average of the cross and along track residuals are root sum squared with a theoretical estimate of the model bias error following the procedure in Section 2 to yield an estimate of the total registration error. This standard deviation error is then converted to a 90% error in IFOV units to compare it with the system specification of .3 IFOV, 90% percent of the time. With values in this case of .36 IFOV cross track and .29 IFOV along track the system is estimated to be close to or within specification. In actual production runs monitored, the results, shown in Table 3-5, are even better with average 90% errors of .29 IFOV cross track and .25 IFOV along track.

For geodetic performance evaluation, the model bias can be measured by designating control points in geodetically corrected imagery. This could not be done for temporal registration because the RCP's are selected from a COMTAL display and due to the consequent lack of knowledge about the exact feature center it cannot be located precisely on a map. The flowchart for the model bias measurement is shown in Figure 3-7. Starting with the HDT-A generated for W1 during the temporal registration evaluation (with W1 control points), CPLB is used to designate control points in geodetically corrected imagery. If the GCD surface generated in MAG agreed exactly with the reference GCD surface originally produced in CPLB then the measurement designation in CPLB will yield a null state error vector in the filter to within the designation errors.

The model bias was measured for both scene W1 and W2. Figure 3-8 displays the control point distribution for W1 on a 25 zone grid; a total of 32 evaluation points were designated. The along track and cross track designation offsets are listed in Table 3-6. The state error vector computed by the CPLB filter and the geodetic performance results for W1 are presented in Table 3-7. To get a standard deviation value for the model bias the shifts in the error vector were root sum squared with the RMS value of the internal distortions (radial and roll rate in the cross track direction; yaw and pitch rate in the along track direction). The total registration error is the root sum square of the temporal registration residual error and the model bias. The temporal registration residuals are taken from Table 3-4, and the total registration error is expressed in IFOV units 90% of the time to compare them with the system specification of .5 IFOV along track and cross track. The W1 results were .26 IFOV along track and .35 IFOV cross track. It should be kept in mind that this was an autocorrelation test since W1 was corrected with its own control points.

Scene W2 was partially cloud covered so only 14 evaluation control points were used to measure the model bias (See Figure 3-9 and Table 3-8). The registration error results shown in Table 3-9, are .43 IFOV along track and .63 IFOV cross track. This was a cross correlation test since W2 was corrected with W1 control points.

Based on these results and the fact that the model bias measured is conservatively high due to designation errors, it appears that the system is meeting or exceeding the specified performance.

REFERENCES

1. P. Arnold, CPLB Simulation Studies, Interim Report II, General Electric, Space Division, 1T81-LSD-SA&E-MEMO-149, October, 1982.

2. I. Levine, Private Communication.

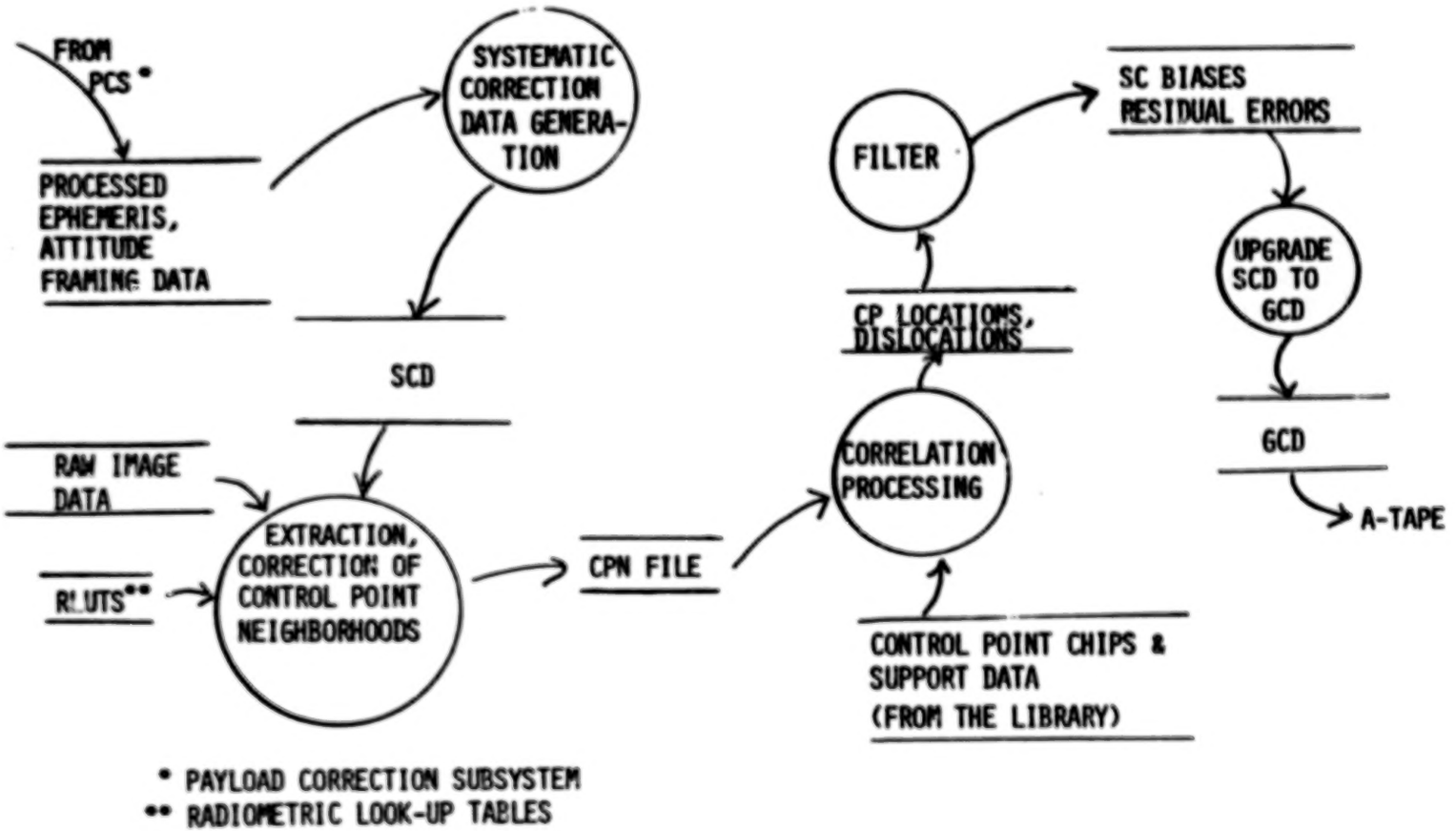

FIGURE 2-1 USE OF CONTROL POINTS IN ONLINE PROCESSING: THE MSS ARCHIVE GENERATION PROCESS (MAG)

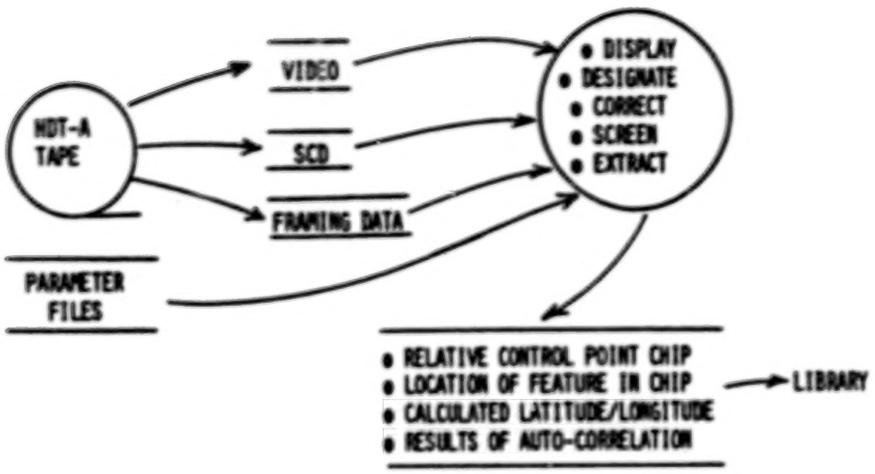

FIGURE 2-2 RELATIVE CONTROL POINTS GENERATED IN CPLB ARE ASSIGNED LOCATIONS BASED ON SCD - LIE ON SCD MODEL SURFACE.

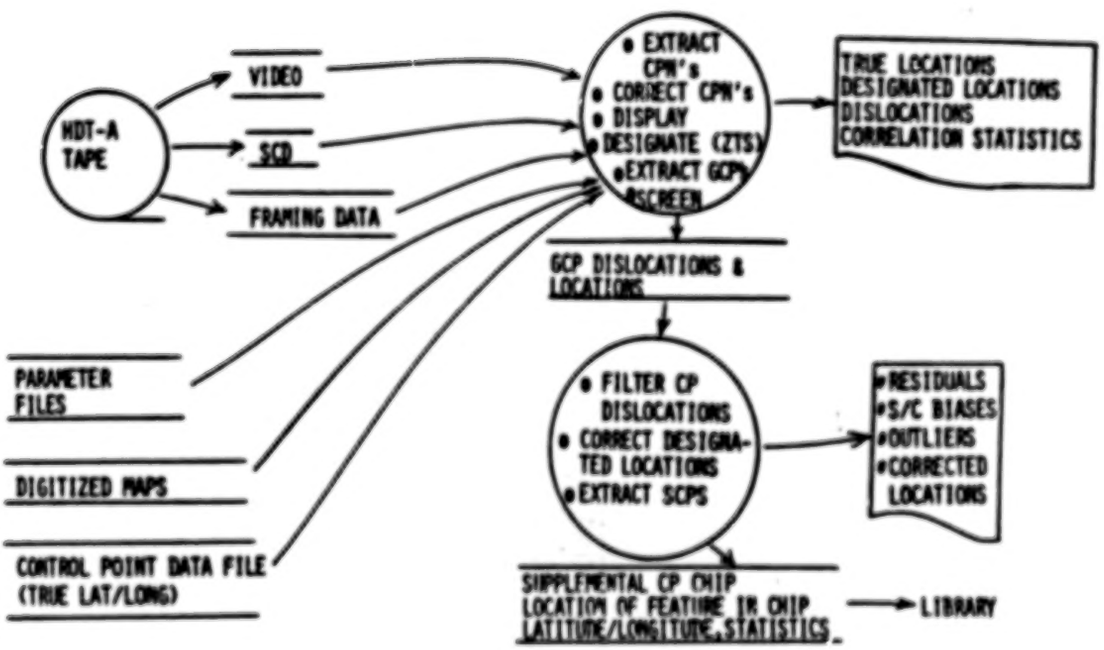

FIGURE 2-3 GEODETIC CONTROL POINTS DESIGNATED IN CPLB HAVE CORRECTED LOCATIONS IN THE CHIP BASED ON GCD

- DEFINITION: RSS OF η AND b_T (1σ)
- η ESTIMATED BY VARIANCE OF RESIDUAL ERROR IN MAG FOR SCP's OR RCP's
  IF ALL LINEAR DISTORTIONS ESTIMATED
  AND ADEQUATE NUMBER AND DISTRIBUTION OF CP's
- b_T: FUNCTION OF η AND NUMBER AND DISTRIBUTION OF CP's
- 1σ TEMPORAL REGISTRATION ERROR t (ESTIMATE)

  $t = (1 + 3/N)^{\frac{1}{2}}$
- $T = t(1.645/82.7)$ IFOV (90 PER CENT ERROR)

FIGURE 2-4 ESTIMATING 1σ TEMPORAL REGISTRATION ERROR FROM SYSTEM OUTPUTS

- DEFINITION: RSS OF t AND b_g
- b_g - MEASURES BIAS DUE TO NOISY DESIGNATION, MAP ERROR, DIGITIZATION ERROR
  - DEPENDS ON NUMBER AND DISTRIBUTION OF DESIGNATED GCP's
  - 1σ ESTIMATE GIVEN BY $\tau\sqrt{3/NGCP}$
  - τ ESTIMATED BY VARIANCE OF RESIDUALS IN CPLB
- t - INCLUDES RANDOM ERROR AND BIAS INTRODUCED IN MAG
- $g = (t^2 + \tau^2 \cdot 3/N)^{\frac{1}{2}}$ ESTIMATE OF 1σ ERROR
- $G = (g \cdot 1.645)/82.7$ IFOV ESTIMATE OF 90 PER CENT ERROR

FIGURE 2-5 ESTIMATING 1σ GEODETIC REGISTRATION ERROR FROM SYSTEM OUTPUTS

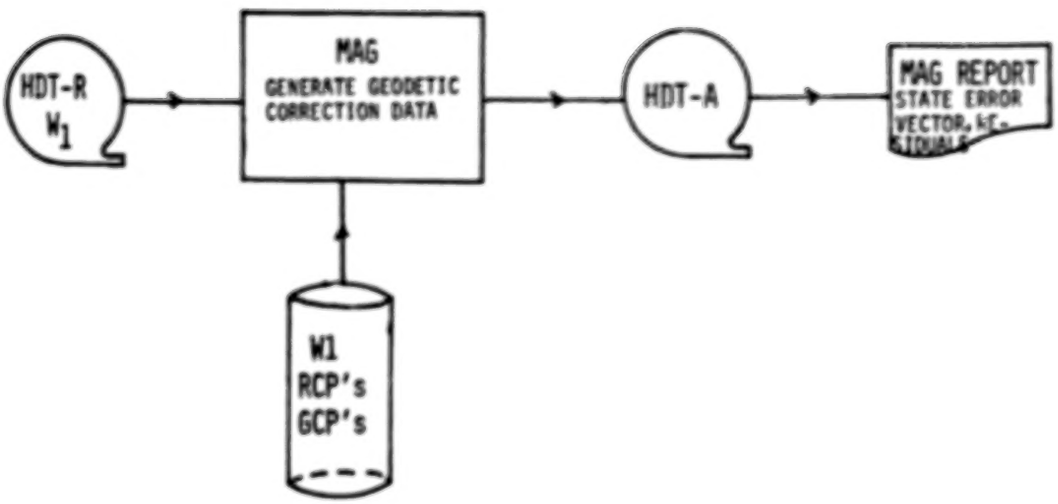

W1 = WASHINGTON SCENE NOVEMBER 2, 1982
RCP = RELATIVE CONTROL POINTS
GCP = GEODETIC CONTROL POINTS

FIGURE 3-1 VERIFICATION METHOD

TABLE 3-1
M1 CORRECTED WITH ITS OWN BCP's

STATE ERROR VECTOR (BIAS)	VALUE
ALONG TRACK POSITION	0.77 METERS
ALONG TRACK RATE	0.05 METERS/SEC
CROSS TRACK POSITION	1.60 METERS
CROSS TRACK RATE	0.07 METERS/SEC
ALTITUDE CHANGE	4.62 METERS
YAW	-3.30 μRAD

RESIDUAL	VALUE
ALONG TRACK	1.52 METERS
CROSS TRACK	1.27 METERS

TABLE 3-2
M1 CORRECTED WITH ITS OWN GCP's

STATE ERROR VECTOR (BIAS)	MAG	CPLB
ALONG TRACK POSITION	-375.71 METERS	-376.48 METERS
ALONG TRACK RATE	-22.67 METERS/SEC	-22.59 METERS/SEC
CROSS TRACK POSITION	547.30 METERS	552.11 METERS
CROSS TRACK RATE	-1.72 METERS/SEC	-1.85 METERS/SEC
ALTITUDE CHANGE	86.75 METERS	178.86 METERS
YAW	-693.21 URAD	-667.73 URAD

RESIDUAL	VALUE
ALONG TRACK	1.35 METERS
CROSS TRACK	4.31 METERS

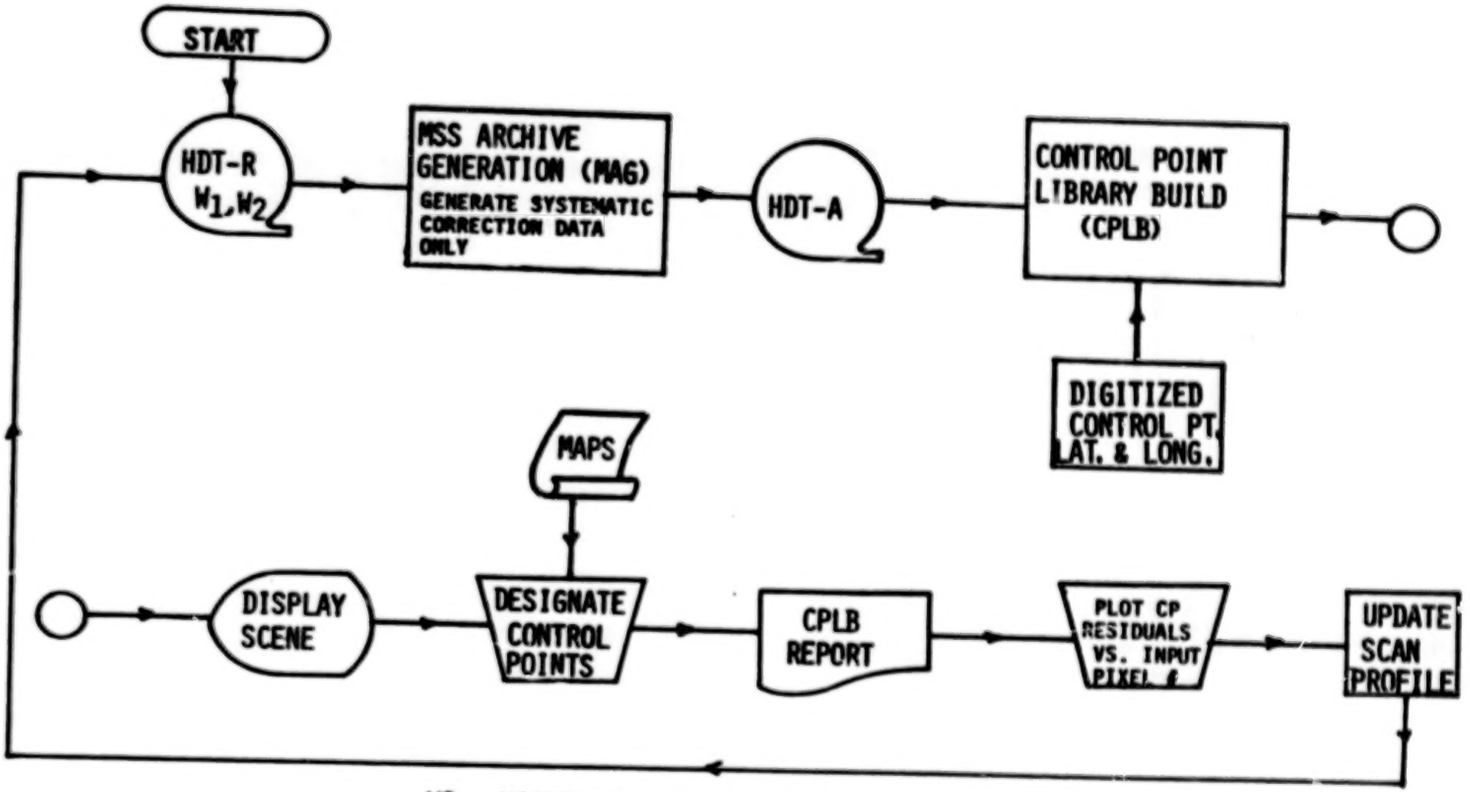

W2 = WASHINGTON SCENE NOVEMBER 18, 1982

FIGURE 3-2 MIRROR SCAN PROFILE CALIBRATION METHOD

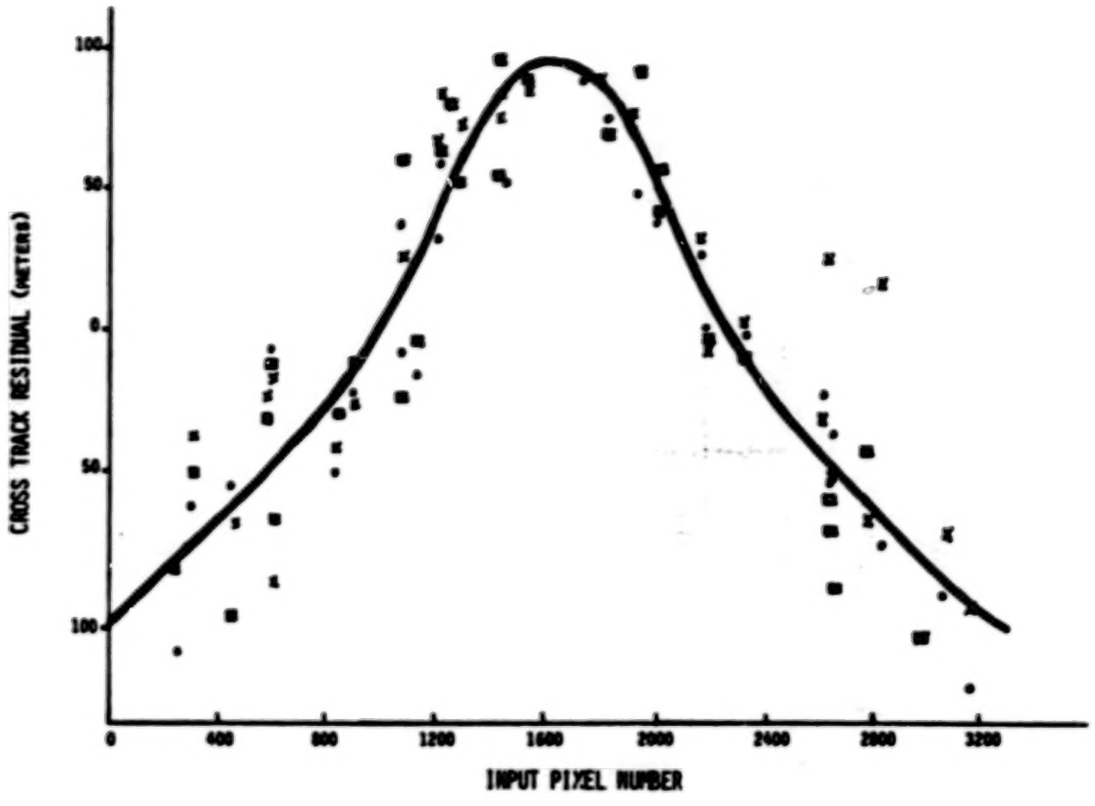

FIGURE 3-3 SCAN PROFILE DEFECT FROM GCP CROSS TRACK RESIDUALS VERSUS INPUT PIXEL NUMBER

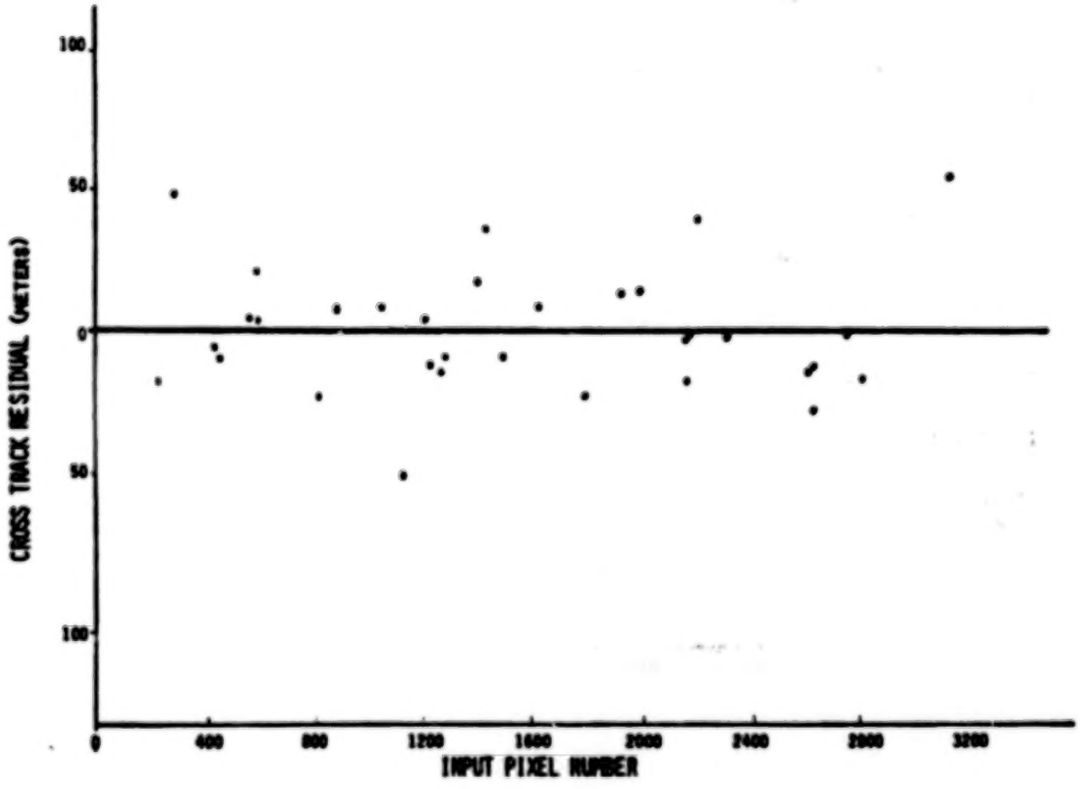

FIGURE 3-4 CROSS TRACK RESIDUAL VERSUS INPUT PIXEL NUMBER WITH CORRECTED SCAN PROFILE

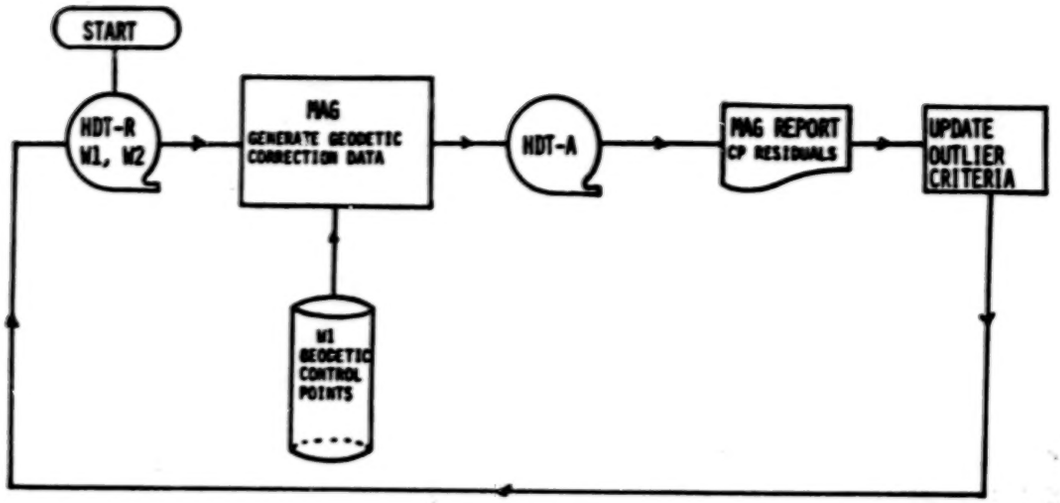

FIGURE 3-5 OUTLIER CRITERIA CALIBRATION METHOD

TABLE 3-3

OUTLIER CRITERIA VALUES

	CURRENT	
MAG:	CROSS TRACK NOISE -- 15 METERS	(1σ)
	ALONG TRACK NOISE -- 15 METERS	(1σ)
CPLB:	CROSS TRACK NOISE -- 35 METERS	(1σ)
	ALONG TRACK NOISE -- 42 METERS	(1σ)
	RECOMMENDED	
MAG:	CROSS TRACK NOISE -- 13 METERS	(1σ)
	ALONG TRACK NOISE -- 13 METERS	(1σ)
CPLB:	CHANGE AFTER MORE DATA IS AVAILABLE	

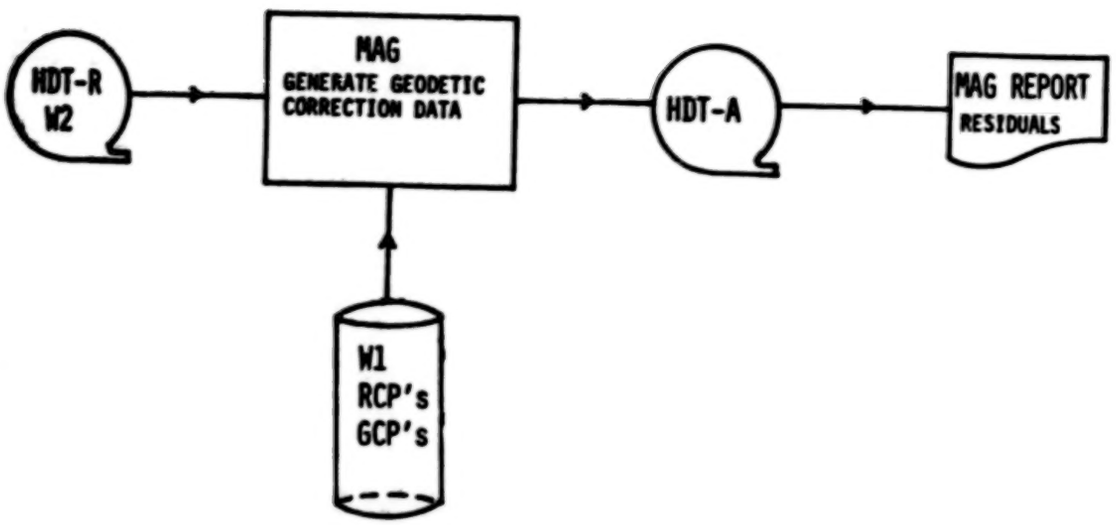

FIGURE 3-6 TEMPORAL REGISTRATION EVALUATION METHOD

TABLE 3-4

W2 CORRECTED WITH W1 CONTROL POINTS

	CROSS TRACK	ALONG TRACK
RESIDUALS USING W1 RCP's (16 RCP's)	20.6 METERS	12.2 METERS
RESIDUALS USING W1 GCP's (13 GCP's)	12.4 METERS	12.4 METERS
AVERAGE RESIDUALS	16.5 METERS	12.3 METERS
ASSUMED MODEL BIAS B (CALCULATED FOR 10 CP's)	8.0 METERS	8.0 METERS
90% TEMPORAL REGISTRATION ERROR = $(\text{AVERAGE RESIDUAL})^2 + (\text{BIAS})^2)^{1/2} * 1.645/82.7$	.36 IFOV	.29 IFOV

IFOV = 82.7 METERS

TABLE 3-5

RESULTS FROM PRODUCTION SYSTEM

- EXPECT RESIDUALS LESS THAN 0.3 IFOV PROVIDED ALL DISTORTIONS ARE ESTIMATED AND THERE ARE >10 WELL DISTRIBUTED CONTROL POINTS.

SCENE	NO. OF CP's	RESIDUALS CROSS TRACK (METERS)	RESIDUALS ALONG TRACK (METERS)
PATH ROW			
030 035	15	12.6	10.1
030 036	17	15.8	17.2
030 037	14	11.9	7.5
MEAN RESIDUAL		13.4	11.6
MEAN BIAS ($\sqrt{\frac{\pi}{2}}$)		5.9	5.1
90% TEMPORAL REGISTRATION ERROR		0.29 IFOV	0.25 IFOV

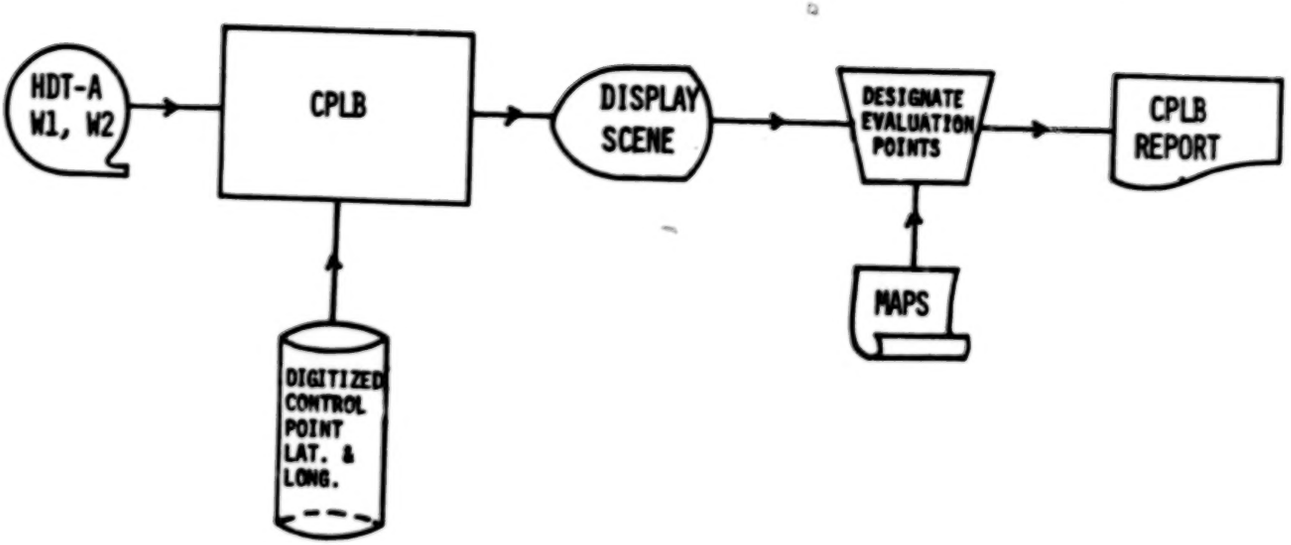

FIGURE 3-7 GEODETIC CORRECTION EVALUATION METHOD

TABLE 3-6

W1 - DESIGNATION OFFSETS

Control Point Number	Zone	Cross Track (82.7m pixels)	Along Track (82.7m pixels)
1	24	.12	.09
2	25	.29	.19
3	24	.46	.06
4	23	.26	.32
5	22	.10	.24
6	20	.48	.36
7	19	.17	.04
8	18	.00	.43
9	21	.19	.30
10	18	.26	.19
11	17	.39	.03
12	16	.16	.25
13	15	.54	.21
14	15	.06	.30
15	17	.30	.19
16	13	.22	.14
17	12	.20	.19
18	15	.48	.16
19	14	.12	.30
20	11	.32	.36
21	12	.13	.17
22	11	.12	.23
23	7	.28	.12
24	8	.04	.18
25	9	.37	.03
26	7	.04	.14
27	6	.30	.19
28	7	.29	.12
29	5	.97	.16
30	1	.01	.19
31	2	.30	.17
32	1	.04	.01

(1) 2	(2) 1	(3) 0	(4) 0	(5) 1
(6) 1	(7) 3	(8) 1	(9) 1	(10) 0
(11) 2	(12) 2	(13) 1	(14) 1	(15) 3
(16) 1	(17) 2	(18) 2	(19) 1	(20) 1
(21) 1	(22) 1	(23) 1	(24) 2	(25) 1

TOTAL OF 32 POINTS
ZONE NUMBER ( )

FIGURE 3-8 DISTRIBUTION OF MI EVALUATION POINTS

TABLE 3-7
RESULTS OF MI EVALUATION

STATE ERROR VECTOR	VALUE	RMS EFFECT IN IMAGE	TOTAL BIAS EFFECT (1σ)
ALONG TRACK SHIFT	5m	5m	ALONG TRACK DIRECTION
YAW BIAS	25μR	1m	5m
ALONG TRACK RATE	0.2m/sec	2m	
CROSS TRACK SHIFT	3m	3m	CROSS TRACK DIRECTION
RADIAL BIAS	59m	4m	5m
CROSS TRACK RATE	0.007m/sec	0m	

90% GEODETIC ERROR = $\{(\text{TEMPORAL REGISTRATION RESIDUAL})^2 + (\text{BIAS EFFECT})^2\}^{1/2} \cdot \frac{1.645}{82.7}$ IFOV

90% ALONG TRACK ERROR = $\{(12)^2 + (5)^2\}^{1/2} \cdot 1.645/82.7 = .26$ IFOV

90% CROSS TRACK ERROR = $\{(17)^2 + (5)^2\}^{1/2} \cdot 1.645/82.7 = .35$ IFOV

TABLE 3-8

M2 - DESIGNATION OFFSETS

Control Point Number	Zone	Cross Track (82.7m pixels)	Along Track (82.7m pixels)
1	24	.12	.14
2	24	.43	.02
3	18	.52	.43
4	21	.39	.30
5	13	.12	.14
6	14	.12	.14
7	12	.14	.12
8	12	.13	.17
9	11	.46	.48
10	9	.54	.23
11	7	.21	.11
12	6	.12	.07
13	1	.19	.19
14	2	.48	.17

(1) 1	(2) 1	(3) 0	(4) 0	(5) 0
(6) 1	(7) 1	(8) 0	(9) 1	(10) 0
(11) 1	(12) 2	(13) 1	(14) 1	(15) 0
(16) 0	(17) 0	(18) 1	(19) 0	(20) 0
(21) 1	(22) 0	(23) 0	(24) 2	(25) 0

TOTAL OF 14 POINTS
ZONE NUMBER ( )

FIGURE 3-9 DISTRIBUTION OF M2 EVALUATION POINTS

TABLE 3-9
RESULTS OF M2 EVALUATION

STATE ERROR VECTOR	VALUE	RMS EFFECT IN IMAGE	TOTAL BIAS EFFECT (1σ)
ALONG TRACK SHIFT	2m	2m	ALONG TRACK DIRECTION
YAW BIAS	278μr	16m	18m
ALONG TRACK RATE	1 m/sec	7m	
CROSS TRACK SHIFT	3m	3m	CROSS TRACK DIRECTION
RADIAL BIAS	340m	26m	27m
CROSS TRACK RATE	0.7m/sec	5m	

90% GEODETIC ERROR = $\{(\text{TEMPORAL REGISTRATION RESIDUAL})^2 + (\text{BIAS EFFECT})^2\}^{1/2} * \frac{1.645}{82.7}$ IFOV

90% ALONG TRACK ERROR = $\{(12)^2 + (18)^2\}^{1/2} \frac{1.645}{82.7} = .43$ IFOV

90% CROSS TRACK ERROR = $\{(17)^2 + (27)^2\}^{1/2} \frac{1.645}{82.7} = .63$ IFOV

Index of Authors

Index of Authors

Index of Authors

* Landsat-4 Science Investigations Summary, John L. Barker, ed., 2 volumes (NASA Conference Publication CP-2326) available through Government Printing Office, National Technical Information Service (NTIS). Accession Numbers N84-30359 and N84-30380 5285 Port Royal, Springfield, VA 22161, Phone 800-336-4700 or (703) 487-4650.

** Landsat-4 Science Characterization Early Results, John L. Barker, ed., 4 volumes NASA Conference Publication.

END

DATE

FILMED

MAY 14 1985